Univerzita Karlova

Přírodovědecká fakulta

Studijní program: Fyzikální chemie (P1404)

Studijní obor: 4XFYZCH (1404V000)

Mgr. Leonid Kaberov

Trojblokové kopolymery 2-oxazolinu s hydrofilními, lipofilními a fluorofilními bloky: od syntézy k hierarchickému samouspořádání

2-Oxazoline triblock copolymers with hydrophilic, lipophilic and fluorophilic blocks: from synthesis to hierarchical self-assembly

Doktorská dizertační práce

Školitel: RNDr. Petr Štěpánek, DrSc.

Ústav makromolekulární chemie AV ČR, v.v.i.

ÚSTAV
MAKROMOLEKULÁRNÍ
CHEMIE

Praha, 2018

Charles University

Faculty of Science

Study programme: Physical Chemistry (P1404)

Branch of study: 4XFYZCH (1404V000)

MSc. Leonid Kaberov

2-Oxazoline triblock copolymers with hydrophilic, lipophilic and fluorophilic blocks: from synthesis to hierarchical self-assembly

Trojblokové kopolymery 2-oxazolinu s hydrofilními, lipofilními a fluorofilními bloky: od syntézy k hierarchickému samouspořádání

Doctoral thesis

Supervisor: RNDr. Petr Štěpánek, DrSc.

Institute of Macromolecular Chemistry AS CR, v.v.i.

INSTITUTE OF MACROMOLECULAR CHEMISTRY

Prague, 2018

Prohlašuji, že jsem předkládanou závěrečnou práci zpracoval sam a že jsem uvedl všechny použité informační zdroje a literaturu. Předkládaná práce ani její část nebyla předložena k získání jiného nebo stejného akademického titulu.

I declare that I have written this thesis independently under the supervision of RNDr. Petr Štěpánek, DrSc. I did not submit this work, or a part of it, to obtain another university degree. To the best of my knowledge, I have cited all the sources I have used.

Prague, 22.05.2018   Leonid I. Kaberov

ACKNOWLEDGEMENTS

Table of Contents

Appendix

Manuscript M1

Manuscript M2

Manuscript M3

Manuscript M4

ABSTRACT

The focus of this research was on the study of di- and triblock poly(2-oxazoline) copolymers with fluorinated blocks. The synthesis and solution properties of novel copolymers combining hydrophilic, hydrophobic (lipophilic) and fluorophilic moieties into one segmented molecule were reported.

The simple synthetic approach which provides an easy way to attach a C_nF_{2n+1} terminal chain to a poly(2-methyl-2-oxazoline)–*block*–poly(2-*n*-octyl-2-oxazoline) copolymer was described. Small-angle neutron and x-ray scattering experiments unambiguously proved the existence of polymersomes, worm-like micelles and their aggregates in aqueous solution. It was shown that increasing content of fluorine in the poly(2-oxazoline) copolymers results in a morphological transition from bilayered or multi-layered vesicles to worm-like micelles.

The synthesis of poly(2-perfluoroalkyl-2-oxazoline)s is complicated by their extremely low activity in cationic ring-opening polymerization reaction (CROP), both in the initiation and in the propagation due to strong electron-withdrawing effect of perfluoroalkyl substituent. A detailed systematic study on synthetic approaches to increase the reactivity of 2-fluoroalkyl-2-oxazolines in CROP by the insertion of methyl and ethyl hydrocarbon spacers between the 2-oxazoline ring and the trifluoromethyl group was presented. New fluorine-containing 2-alkyl-2-oxazolines were synthesized. The kinetic studies showed the gradual increase of the polymerization rate with increasing of the hydrocarbon spacer length. The 2-(3,3,3-trifluoropropyl)-2-oxazoline (CF$_3$EtOx) was found to have similar reactivity as non-fluorinated 2-oxazolines, which allowed the synthesis of defined triblock copolymers.

This approach was further expanded for highly fluorinated 2-oxazolines. 2-(1H,1H,2H,2H-Perfluorooctyl)-2-oxazoline was synthesized via procedure supplemented by Grignard reaction. The kinetic study proved that the length of perfluoroalkyl substituent has no effect on the reactivity of 2-oxazolines with a double methylene spacer.

A number of fluorine-containing di- and triblock copolymers with 2-methyl-2-oxazoline (hydrophilic) and 2-*n*-octyl-2-oxazoline (hydrophobic) were synthesized. The effect of the fluorinated block on the aqueous self-assembly behaviour of the copolymers was studied by dynamic light scattering, transmission cryo-electron microscopy and small-angle neutron scattering experiments.

The described fluorine containing poly-2-oxazolines represent a potential platform for future utilization as ^{19}F magnetic resonance imaging contrast agents.

ABSTRAKT

Cílem tohoto výzkumu je studium kopolymerů dvou- a trojblokových poly(2-oxazolinů) s fluorovanými bloky. Byly popsány syntetické a roztokové vlastnosti nových kopolymerů kombinujících hydrofilní, hydrofobní (lipofilní) a fluorofilní části do jedné segmentované molekuly.

Byl popsán jednoduchý syntetický přístup, který poskytuje snadný způsob připojení koncového řetězce C_nF_{2n+1} ke kopolymeru poly(2-methyl-2-oxazolinu)-*blok*-poly(2-*n*-oktyl-2-oxazolinu). Experimenty s maloúhlovým rozptylem neutronů a rentgenovskeho záření jednoznačně prokázaly existenci vesiklů, červovitých micel a jejich agregátů ve vodném roztoku. Bylo prokázáno, že zvýšení obsahu fluoru v poly(2-oxazolinových) kopolymerech vede k morfologickému přechodu od dvouvrstvých nebo vícevrstvých vesiklů až do červovitých micel.

Syntéza poly(2-perfluoralkyl-2-oxazolinu) je komplikována jejich extrémně nízkou aktivitou v kationtové polymerizační reakci s otevřením cyklu (cationic ring-opening polymerization, CROP), a to jak při iniciaci, tak při propagaci kvůli silnému elektronovému odebíracímu efektu perfluoralkylového substituentu. Byla prezentována podrobná systematická studie o syntetických přístupech ke zvýšení reaktivity 2-fluoralkyl-2-oxazolinů v CROP vložením uhlovodíkového spaceru methyl nebo ethyl mezi 2-oxazolinovým cyklem a trifluormethylovou skupinu. Byly syntetizovány nové 2-alkyl-2-oxazoliny obsahující fluor. Kinetické studie prokázaly postupné zvyšování rychlosti polymerace se zvyšováním délky uhlovodíkoveho spaceru. Bylo zjištěno, že 2-(3,3,3-trifluorpropyl)-2-oxazolin (CF$_3$EtOx) má podobnou reaktivitu jako nefluorované 2-oxazoliny, což umožnilo syntézu definovaných trojblokových kopolymerů.

Tento přístup byl dále rozšířen o vysoce fluorované 2-oxazoliny. 2-(1H,1H,2H,2H-perfluorooktyl)-2-oxazolin byl syntetizován postupem doplněným Grignardovou reakcí. Kinetická studie ukázala, že délka perfluoralkylového substituentu nemá vliv na reaktivitu 2-oxazolinů s dvojitým methylenovým spacerem.

Byla syntetizována řada dvoj- a trojblokových kopolymerů obsahující fluor s 2-methyl-2-oxazolinem (hydrofilní) a 2-*n*-oktyl-2-oxazolinem (hydrofobní). Účinek fluorovaného bloku na chování vodných roztoků kopolymerů byl zkoumán dynamickým rozptylem světla, transmisní kryoelektronovou mikroskopií a maloúhlovým rozptylem neutronů.

Popsané poly-2-oxazoliny obsahující fluor představují potenciální platformu pro budoucí využití jako ^{19}F kontrastní činidla pro magnetickou rezonancí.

List of Symbols

β	Coherence factor
D	Repeat distance
$Đ$	Polydispersity
D_h	Hydrodynamic diameter
D_t	Translation diffusion coefficient
E	Energy
E_0 and E_S	Electric field strength of the incident and scattered irradiation
$G_2(\tau)$	Correlation function of the scattered light intensity
$g_2(\tau)$	Normalized correlation function of the scattered light intensity
$g_1(\tau)$	Correlation function of the scattered electric field
$I_S(q)$	Scattered intensity
$[I]_0$	Initial concentration of the initiator
$\mathbf{k_I}$ and $\mathbf{k_S}$	Wave vectors of the incident and scattered irradiation
k_i	Initiation rate constant
k_p	Propagation rate constant
k_B	Boltzmann constant
R_h	Hydrodynamic radius
M_n	Number average molar mass
M_w	Weight average molar mass
$[M]$	Concentration of the monomer
$P(q)$	Form factor
$[P^+]$	Concentration of living chains
q	Scattering vector
R_a	Radius of the vesicle interior
$S(q)$	Structure factor
t	Reaction time
t_i	Hydrophobic layer thickness
t_h	Hydrophilic layer thickness
θ	Scattering angle
η	Viscosity
λ	Wavelength in the medium

List of Abbreviations

CROP	Cationic ring-opening polymerization
Cryo-TEM	Transmission cryo-electron microscopy
CMC	Critical micelle concentration
DLS	Dynamic light scattering
HSAB theory	Theory of hard and soft Lewis acids and bases
LCST	Lower critical solution temperature
MRI	Magnetic resonance imaging
PdI	Polydispersity index
SAXS	Small angle X-ray scattering
SANS	Small angle neutron scattering
SEC	Size exclusion chromatography
SLD	Scattering length density
PAOx	Poly(2-alkyl-2-oxazoline) ("P" in front of monomer abbreviation means "poly")
n-BuOx	2-n-Butyl-2-oxazoline
CF_3MeOx	2-(2,2,2-Trifluoroethyl)-2-oxazoline
CF_3EtOx	2-(3,3,3-Trifluoropropyl)-2-oxazoline
DMSO	Dimethylsulfoxide
EHPOx	2-(1-Ethylheptyl)-2-oxazoline
EtOx	2-Ethyl-2-oxazoline
MeOx	2-Methyl-2-oxazoline
MeTos	Methyl p-toluenesulfonate
NonOx	2-n-Nonyl-2-oxazoline
ODFOx	2-(2,6-Difluorophenyl)-2-oxazoline
OctOx	2-n-Octyl-2-oxazoline
PhOx	2-Phenyl-2-oxazoline
n-PrOx	2-n-Propyl-2-oxazoline
R_f^6EtOx	2-(1H,1H,2H,2H-perfluorooctyl)-2-oxazoline

List of publications and contributions at conferences

The following manuscripts are included in the thesis:

1) <u>Kaberov L.I.</u>, Verbraeken B., Hruby M., Riabtseva A., Kovacik L., Kereïche S., Brus J., Stepanek P., Hoogenboom R., Filippov S.K.. Novel triphilic block copolymers based on poly(2-methyl-2-oxazoline)–*block*–poly(2-octyl-2-oxazoline) with different terminal perfluoroalkyl fragments: synthesis and self-assembly behaviour. *Eur. Polym. J.* **2017**, 88, 645–655. DOI: 10.1016/j.eurpolymj.2016.10.016.

2) Riabtseva A., <u>Kaberov L.I.</u>, Noirez L., Ryukhtin V., Nardin C., Verbraeken B., Hoogenboom R., Stepanek P., Filippov S.K.. Structural characterization of nanoparticles formed by fluorinated poly(2-oxazoline)-based polyphiles. *Eur. Polym. J.* **2018**, 99, 518-527. DOI: 10.1016/j.eurpolymj.2018.01.007.

3) <u>Kaberov L.I.</u>, Verbraeken B., Riabtseva A., Brus J., Talmon Y., Stepanek P., Hoogenboom R., Filippov S.K.. Fluorinated 2-alkyl-2-oxazolines of high reactivity: Spacer-length induced acceleration for Cationic Ring-Opening polymerization as basis for triphilic block copolymer synthesis. *ACS Macro Lett.* **2018**, 7, 7−10. DOI: 10.1021/acsmacrolett.7b00954

4) <u>Kaberov L.I.</u>, Verbraeken B., Riabtseva A., Brus J., Radulescu A., Talmon Y., Stepanek P., Hoogenboom R., Filippov S.K.. Fluorophilic-lipophilic-hydrophilic poly-2-oxazolines block copolymers: from synthesis to self-assembly. (**Submitted to *ACS Macromolecules*, 05.2018**)

Other manuscripts not included in the thesis:

1) Riabtseva A., <u>Kaberov L.I.</u>, Kucka J., Bogomolova A., Stepanek P., Filippov S.K. and Hruby M.. Polyelectrolyte pH-Responsive Protein-Containing Nanoparticles: The Physicochemical Supramolecular Approach. *Langmuir*, **2017**, 33 (3), 764–772. DOI: 10.1021/acs.langmuir.6b03778

2) Bogomolova A., <u>Kaberov L.I.</u>, Sedlacek O., Filippov S.K., Stepanek P., Kral V., Wang X.Y., Liu S.L., Ye X.D., Hruby M.. Double stimuli-responsive polymer systems: How to use crosstalk between pH- and thermosensitivity for drug depots. *Eur. Polym. J.* **2016**, *84*, 54–64. DOI: 10.1016/j.eurpolymj.2016.09.010.

3) Filippov S.K., Bogomolova A., <u>Kaberov L.I.</u>, Velychkivska N., Starovoytova L., Cernochova Z., Rogers S.E., Lau W.M., Khutoryanskiy V.V., and Cook M.T. Internal Nanoparticle Structure of Temperature-Responsive Self-Assembled PNIPAM-b-PEG-b-PNIPAM Triblock Copolymers in Aqueous Solutions: NMR, SANS, and Light Scattering Studies. *Langmuir*, **2016**, 32 (21), 5314–5323. DOI: 10.1021/acs.langmuir.6b00284.

Published conference contributions (selected):

Oral presentations

1) Kaberov L., Verbraeken B., Riabtseva A., Brus J., Štěpánek P., Hoogenboom R., Filippov S., Poly(2-oxazolines) triblock copolymers with mutually immiscible hydrophilic,

hydrophobic and fluorophilic blocks. 9th International Symposium Molecular Mobility and Order in Polymer Systems. St. Petersburg, Russian Federation, 2017.

2) Kaberov L., Verbraeken B., Riabtseva A., Brus J., Štěpánek P., Hoogenboom R., Filippov S.. Novel fluorinated 2-alkyl-2-oxazolines: three-fold increasing of reactivity in polymerization reaction. 254th ACS National Meeting & Exposition. Washington, USA, 2017.

Poster presentations

1) Filippov S., Kaberov L., Zhang X., Niebuur B.- J., Chytil P., Etrych T., Wieland F., Velychkivska N., Starovoytova L., Svergun D., Papadakis C., M.. HPMA-based drug delivery system and its interactions of human serum albumin: SAXS, ITC, and NMR study. 254th ACS National Meeting & Exposition. Washington, USA, 2017.

2) Kaberov L., Verbraeken B., Filippov S., Hrubý M., Riabtseva A., Kováčik L., Štěpánek P., Hoogenboom R.. Poly(2-oxazolines) triblock copolymers with mutually immiscible hydrophilic, hydrophobic and fluorophilic blocks. 252th ACS National Meeting & Exposition. Philadelphia, USA, 2016.

3) Kaberov L., Hrubý M., Bogomolova A., Pánek J., Štěpánek P., Filippov S.. Novel pH-sensitive nano-containers based on EUDRAGIT/Brij98 mixture for oral drug delivery. European Polymer Federation Congress 2015. Dresden, Germany, 2015.

1. THEORETICAL PART

1.1. Block-copolymers. Poly-2-oxazolines

Block copolymers include two or more homopolymer subunits linked by covalent bonds. Due to the long homopolymer units in their structure, block copolymers combine properties of individual homopolymers.[1]

The molecules composed of the fragments of different nature are prospective substances for preparing materials with tailored properties. By varying structure and nature of the blocks, one can produce copolymers, which are sensitive to external stimuli, such as temperature, pH, ionic strength of solution, *etc*. It is known, that di- and triblock copolymers based on hydrophilic and hydrophobic polymers[2] such as poly(ethylene oxide)[3], poly(ε-caprolactone)[3], poly(D, L)lactide[4], polyglycolide[5] exhibit surface activity, which allows to attribute them to non-ionic surfactants. Similarly to their low-molecular-weight (ionic) analogues, amphiphilic block copolymers are able to self-assemble in solvents that have an affinity to one of the blocks. The ratio between hydrophilic and hydrophobic parts has a great effect on the properties of the copolymers; increase of the length of hydrophobic block makes the copolymers insoluble in water. In contrast, an exceedingly large hydrophilic block may prevent the formation of micellar aggregates.

A major goal of recent research is the quest for the best monomers which will provide opportunity to create a plethora of different structures. The main requirements for such monomers are simplicity of synthesis, ability for controlled polymerization with narrow polydispersity of resulting polymers, and possibility for facile structure tuning. 2-Alkyl-2-oxazolines exhibit all of these characteristics, making them appealing candidates for this purpose.
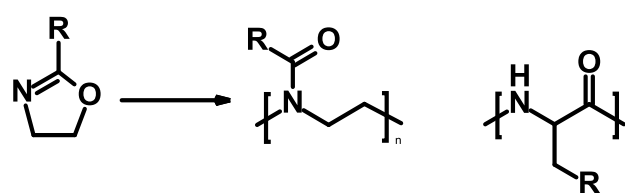
Figure 1. Structure of 2-substituted-2-oxazoline monomer, poly-2-oxazoline and the isomeric poly(amino acid).

As a result of their versatile properties, poly(2-alkyl/aryl-2-oxazoline)s (PAOx) and their derivatives received significant scientific attention.[6–8] Poly(2-oxazolines) have a good biocompatibility and immunogenicity due to the structure similar to poly(amino acids) and peptides (Figure 1).[9–11] It is known that poly(2-methyl-2-oxazoline) (PMeOx) and poly(2-ethyl-2-oxazoline) (PEtOx) exhibit "stealth" behaviour similar to poly(ethylene oxide).[12,13] PAOx are widely studied as materials for biomedical applications such as drug, protein, radionuclide or gene delivery[14–17] as well as for the preparation of non-fouling surfaces that resist non-specific adsorption of proteins, bacteria, and higher organisms.[18]

1.1.1 Cationic ring-opening polymerization of poly-2-oxazolines

Polymerization of 2-alkyl-2-oxazolines via the cationic ring-opening polymerization (CROP) mechanism was discovered in the 1960s.[19–22] This mechanism includes all of the common steps of chain-growth polymerization: initiation, propagation, and termination (Figure 2).
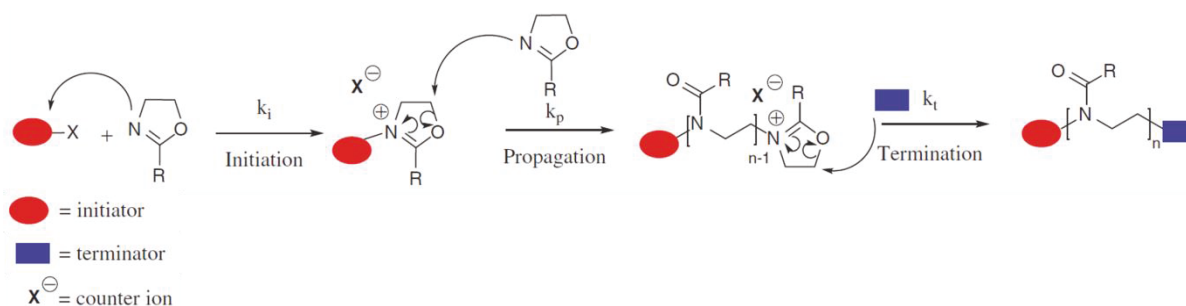
Figure 2. General simplified overview of the CROP of 2-oxazolines. Picture is taken from ref. [23].

In the absence of termination and chain transfer agents (moister and other nucleophilic impurities, chain transfer inducing functional groups), the CROP of 2-oxazolines can proceed as living polymerization. The living CROP of 2-oxazolines is ideally suited for the preparation of amphiphilic block copolymers because both hydrophilic and hydrophobic poly(2-oxazoline)s are readily accessible by varying the side-chain substituent of the monomer[10] and block copolymers can be easily prepared by sequential addition of the second monomer after full conversion of the first monomer. Besides, functional groups can be introduced during initiation and termination.[23] The application of the microwave synthesis described in the early works of Hoogenboom, significantly simplified the polymerization of 2-oxazolines and gave a new impetus for their development. [24–26]

A. Initiation
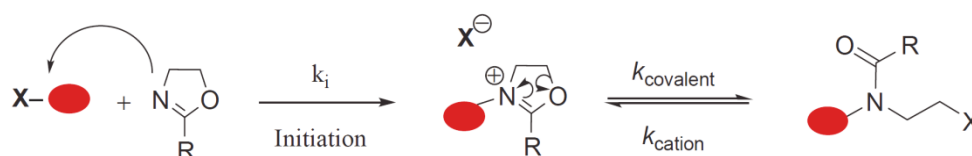
Figure 3. Initiation of the CROP of 2-oxazolines and the equilibrium between the cationic and covalent active species. Picture is taken from ref. [23].

The reaction starts from the nucleophilic attack of initiator by electron pair of nitrogen atom forming an oxazolinium cation (Figure 3). At room temperature the reaction is very slow, but some initiators demonstrate ability for slow initiation even with moderate heating. The fast and complete initiation is the first requirement for narrow molecular mass distribution of resulting polymers.

The most popular initiators for CROP are alkyl tosylates[27–29] and methyl triflate.[30,31] During the initiation, a counterion affects the equilibrium between an ionic form of active species and much less active covalent form.

B. Propagation

Propagation reaction can be divided into two steps (Figure 4). The first step is addition of the first monomer to the cationic active species formed during the initiation. This process is slow, which means that it determines the rate of a whole polymerization reaction (subject to full initiation).
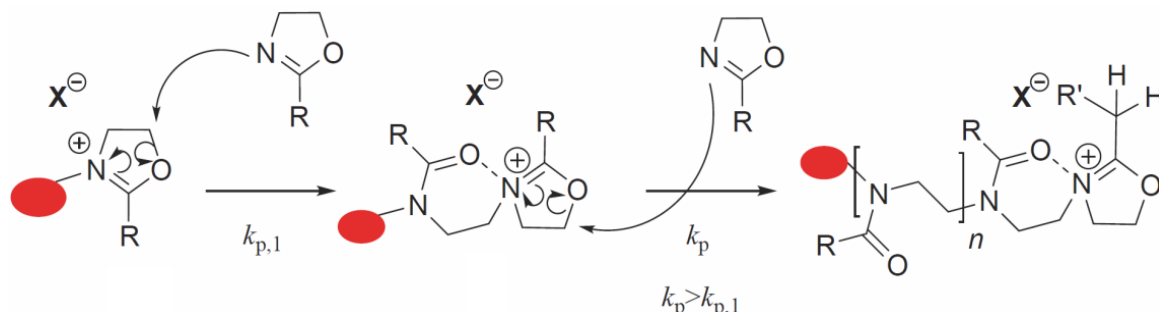
Figure 4. The mechanism of propagation for the CROP of 2-oxazolines. Picture is taken from ref. [23].

After the first step, the propagation rate constant k_p increases. This effect is attributed to the dipole-ion polarization effect of the neighbouring carbonyl group (Figure 4, middle), which leads to the stabilization of an intermediate and probably shifts the equilibrium towards cationic species. This equilibrium depends on various parameters, namely, concentration, temperature, and solvent. Moreover, the propagation rate grows with increasing percentage of cationic species, making them almost exclusively responsive for propagation. The prevalence of the cationic active centres is determined by the counterion stability. The nucleophilicity of the monomers also plays an important role on the equilibrium between cationic and covalent forms of active centres.

The rate of the ideal living polymerization (which implies the fast initiation and no side termination) is determined by the propagation rate, according to the first-order kinetics:

$$-\frac{d[M]}{dt} = k_p[P^+][M] \tag{1}$$

where $[M]$ is the concentration of monomer, $[P^+]$ is the concentration of living chains, and t is the reaction time. In case of fast initiation and lack of termination, the concentration of living chains could be equated to the initial concentration of the initiator $[I]_0$. Thereby, Equation 1 can be integrated and rewritten as

$$\ln\left(\frac{[M]_0}{[M]_t}\right) = k_p[I]_0 t \tag{2}$$

Following the dependence of the monomer concentration as a function of conversion time allows to obtain the k_p value from the slope of the linear first-order kinetic plot.

C. Chain-transfer reactions

The ideal living polymerization is characterized by a lack of side reactions. Although the chain-transfer reactions are known to occur for the CROP of 2-oxazolines, they are much

slower than propagation and, thus, the CROP of 2-oxazolines is still characterized by low dispersity for moderate polymerization degrees (below 200-300).
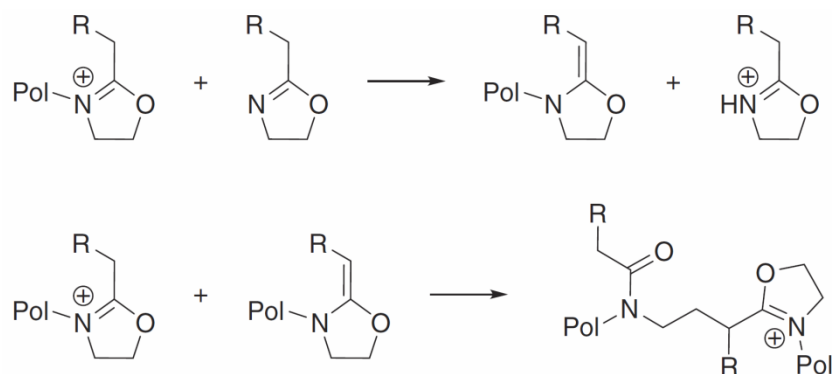
Figure 5. Chain-transfer reaction from a living polymer to the monomer via the so-called β-elimination (top). Coupling of a living polymer chain to an enamine-functionalized chain, which leads to chain coupling and the formation of a branching point (bottom). Picture is taken from ref. [23].

The main side reaction for CROP is the β-elimination, which produces proton initiated oxazolinium cation and enamine ether terminated (so called "dead") polymer chain (Figure 5). The obtained cation can induce a new growing chain, which will result in polymers with lower molecular weights. On the other hand, "dead" polymer chain can react with active cationic growing species resulting in chain coupling. The contribution of chain coupling reaction becomes significant at high conversion (>75%) that implies low reactivity of the enamine-caped chains.

D. Termination

As well as for initiation and propagation, the termination rate constant is affected by cationic-covalent equilibrium of active centres and nature of counterion. The termination conditions sometimes can be rather hard because of relative stability of cationic active centers.
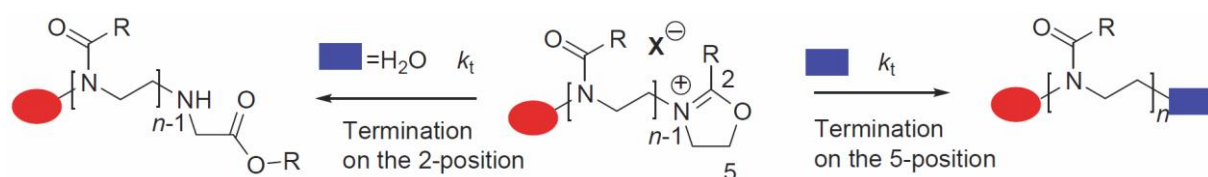
Figure 6. Termination mechanisms of the CROP of 2-oxazolines. (Left) Kinetically driven termination by attack of the terminating agent on the 2-position; (right) thermodynamically driven termination by the attack of the terminating agent on the 5-position. Picture is taken from ref [23].

The termination could proceed via two routes. The pathway of the termination can be explained using hard and soft Lewis acids and bases (HSAB) theory (Figure 6). Softer terminating agents (e.g. water) have the tendency to terminate through the kinetically controlled 2-position resulting in a secondary amine and ester containing end-group. The

thermodynamically controlled attack on the 5-position occurs in the case of harder terminating agents such as nitrogen based terminating agents, carboxylates, and methanolic potassium hydroxide.[32] The most common terminating agents are piperidine and a methanolic solution of potassium or sodium hydroxide due to the fast and reliable termination on the 5-position.

1.1.2   2-Oxazoline-based amphiphilic block copolymers

The synthesis of 2-oxazoline copolymers consisting of two blocks of different nature was described for the first time by Kobayashi et al.[33] The surface tension studies of aqueous solutions of the obtained polymers have proved their surfactant nature. The hydrophobicity of blocks could be tuned by varying the length and architecture of the substituent in the second position of 2-oxazoline monomer (Figure 7).[34,35]
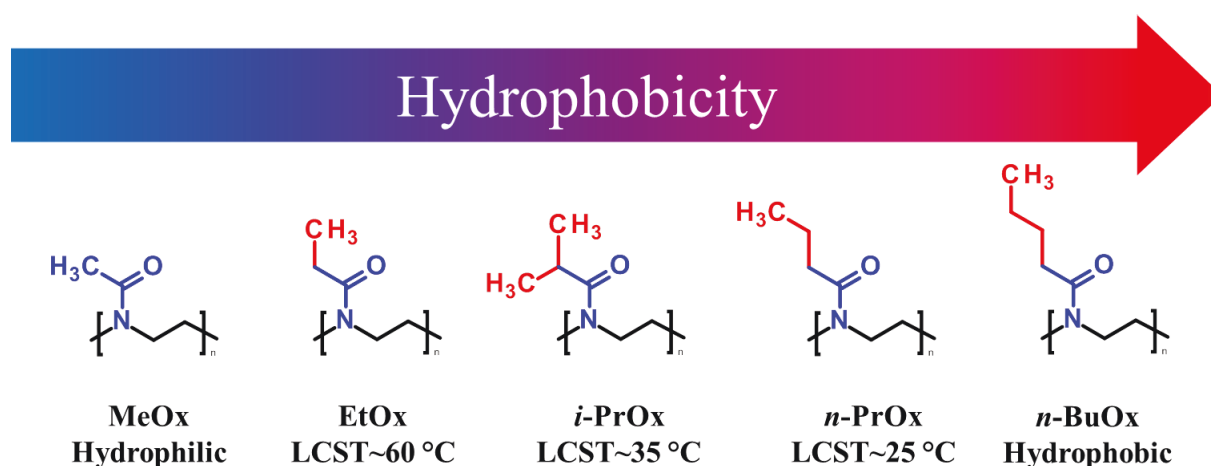
Figure 7. The increasing of hydrophobicity in homologue series of poly(2-alkyl-2-oxazolines).

Binder and Gruber reported the synthesis of a series of block copolymers with poly(2-methyl-2-oxazoline) (MeOx) as the hydrophilic block combined with a variety of hydrophobic 2-oxazolines to form the hydrophobic block.[36] These amphiphilic copolymers self-assemble in aqueous solution; the size of the aggregates increases with increase of molecular weight and mass fraction of the hydrophobic block.

Later, the self-assembly behaviour of the fluorescently labelled poly(2-methyl-2-oxazoline)-*block*-poly(2-*n*-nonyl-2-oxazoline) was described by Papadakis and co-workers using fluorescence correlation spectroscopy. The transition from the individual chains at low polymer concentrations ($<2\times10^{-5}$ M) to micelles at high polymer concentrations ($>10^{-2}$ M) was shown.

The solvent quality is also known to have an effect on the self-assembly of block copolymers. Hoogenboom and co-workers studied the behavior of series of poly(2-ethyl-2-oxazoline)-*block*-poly(2-*n*-nonyl-2-oxazoline) copolymers in water/ethanol mixtures.[37] A dynamic light scattering (DLS) study showed that the increase of ethanol content was accompanied by swelling of micelle corona formed by poly(2-ethyl-2-oxazolines) fragments, which, in turn, led to an increase of diameter of the whole micelle.

The architecture of linear block copolymers is not limited only by the diblock structure. Schubert et al. have conducted the study of tri- and tetra-block copolymers formed by MeOx, EtOx, 2-*n*-nonyl-2-oxazoline (NonOx), and 2-phenyl-2-oxazoline (PhOx).[38,39] The combination of DLS and atomic force microscopy demonstrated that the block order has a strong impact on the self-assembly behaviour of copolymers in solution: the triblock copolymers with hydrophobic block (PPhOx or PNonOx) in between two hydrophilic blocks form micelles of smaller diameter compared with copolymer of the same composition with outer hydrophobic block. A series of ABA and BAB copolymers composed of hydrophilic PMeOx (A-block) and thermoresponsive poly(2-*n*-propyl-2-oxazoline) (B-block) was prepared by Luxenhofer et al.[29] Resulting polymers revealed a temperature-induced self-assembly in aqueous solution. For these systems the blocks ratio affects a cloud point of solutions: the cloud point temperature increases with decreasing thermoresponsive block content.

The use of star-shaped initiators in CROP increases the number of available block copolymer structures. Jin described the synthesis of star-shaped PMeOx-*b*-PPhOx block copolymers using porphyrin-based initiator (Figure 8).[40] By varying the block order, it is possible to form either "classical" micelles with porphyrin in the core (inner PhOx block) or flower-like micelles (outer PhOx block) with porphyrin in the corona. The location of porphyrin in the corona also provides the pH-responsiveness of such flower-like micelles.
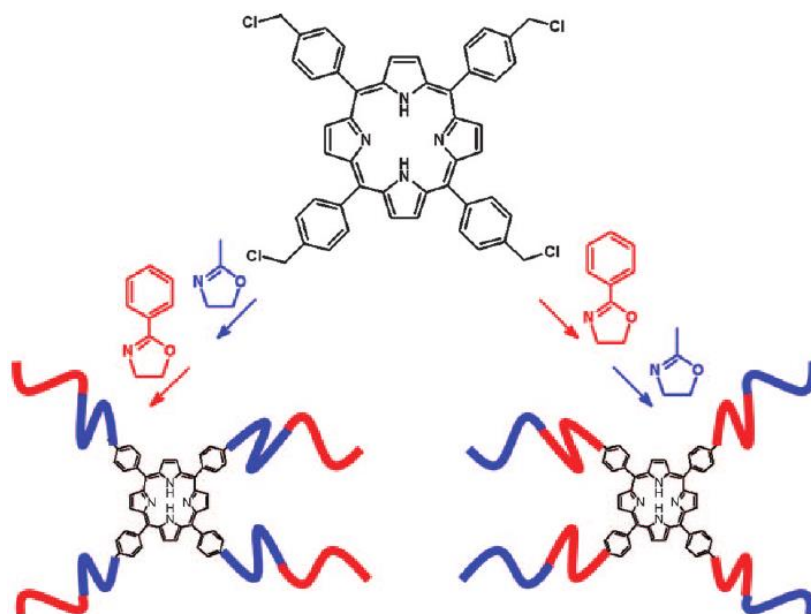
Figure 8. Synthesis of star-shaped block copolymers using porphyrin-based initiator. The picture is taken from ref. [10].

The amphiphilic behaviour of poly-2-oxazolines could be achieved even by insertion of long terminal alkyl fragments by initiation or/and termination of living CROP. Volet and Amiel reported the self-assembly of poly(2-methyl-2-oxazoline)s synthesized with a lipophilic initiator.[41] Winnik et al. demonstrated the formation of micellar aggregates in aqueous solutions for a series of poly(2-ethyl-2-oxazoline)s and poly (2-isopropyl-2-

oxazoline)s with terminal *n*-octadecyl chains and discussed their thermoresponsive behaviour.[42]

1.2. Fluorine containing polymers and block copolymers with fluorophilic blocks

The self-assembly of hydrophilic-hydrophobic block copolymers in solutions is already studied in detail.[43–47] Nowadays, there is a continuous quest for block copolymers that contain more than two thermodynamically immiscible moieties. One of the options is to combine hydrophilic, lipophilic and fluorophilic fragments in one polymer.

Perfluorohydrocarbons are components of many commercial intravascular oxygen carriers and tissue oxygenation fluids, such as Fluosol®, Perftoran®, Oxyfluor®, *etc*.[48] One of the main applications of perfluorinated substances is as contrast agents in ^{19}F Magnetic Resonance Imaging (MRI). The ^{19}F atoms have 100 % natural abundance, and their MRI sensitivity is 83 % that of ^{1}H atoms. Perfluorocarbons are immiscible with blood, but they could be injected as emulsions and since there are almost no endogenous fluorine atoms in body tissues (except for bones and teeth), the ^{19}F MRI allows imaging without significant background signal.[49–51] Perfluoroalkane chains are hydrophobic, but they are also lipophobic - alkanes and perfluoroalkanes are immiscible beginning from C_6. Moreover, perfluoroalkyl chains are much less flexible and polarizable in comparison with alkyl chains due to the larger fluorine atoms and high electron density, resulting in a greater ability to crystallize and form more ordered structures (Figure 9).[52]
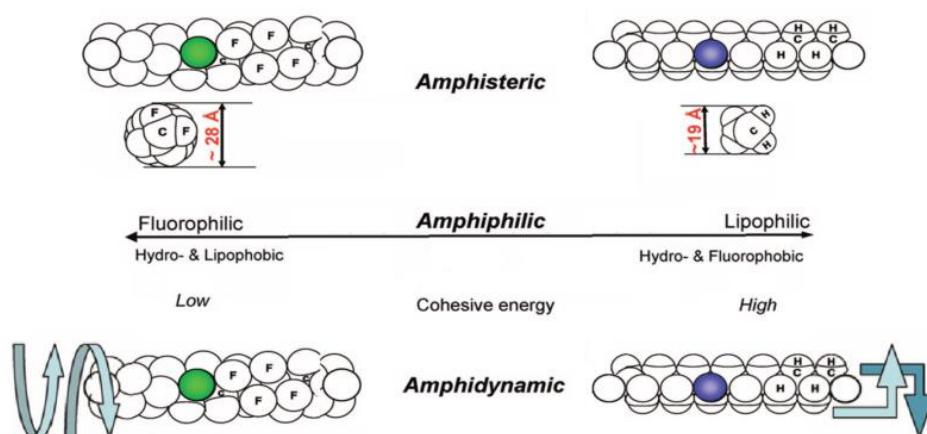
Figure 9. The difference in volume, affinity and flexibility between perfluoroalkyl and alkyl chains. Picture is taken from ref. [52].

One can expect that the insertion of perfluorinated fragments into amphiphilic block copolymers will promote additional complexity and decrease critical micelle concentrations due to their strong hydrophobic character and immiscibility with hydrocarbon hydrophobic domains. Indeed, in the work of Hillmyer and Lodge, miktoarm star block copolymers with poly(ethylene oxide), polyethylene, and poly(perfluoropropylene oxide) arms were found to form multicompartment micelles in dilute aqueous solution.[53] Depending on the relative

length of the blocks, discrete multicompartment micelles or wormlike structures with segmented cores were observed.

The investigation of multicompartment micelles formed by linear styrene-based ABC-triblock copolymers has been also reported by Laschewsky et.al..[54,55] The later researches of this group described self-assembly behavior of different compositions of triblock copolymers containing fluoroalkyl acrylate fragments (Figure 10).[56,57] It was shown that depending on the blocks order and preparation method one can obtain aggregates with structures from well known "core-shell-corona" to more complex structures with segmented hydrophobic core.[58,59]
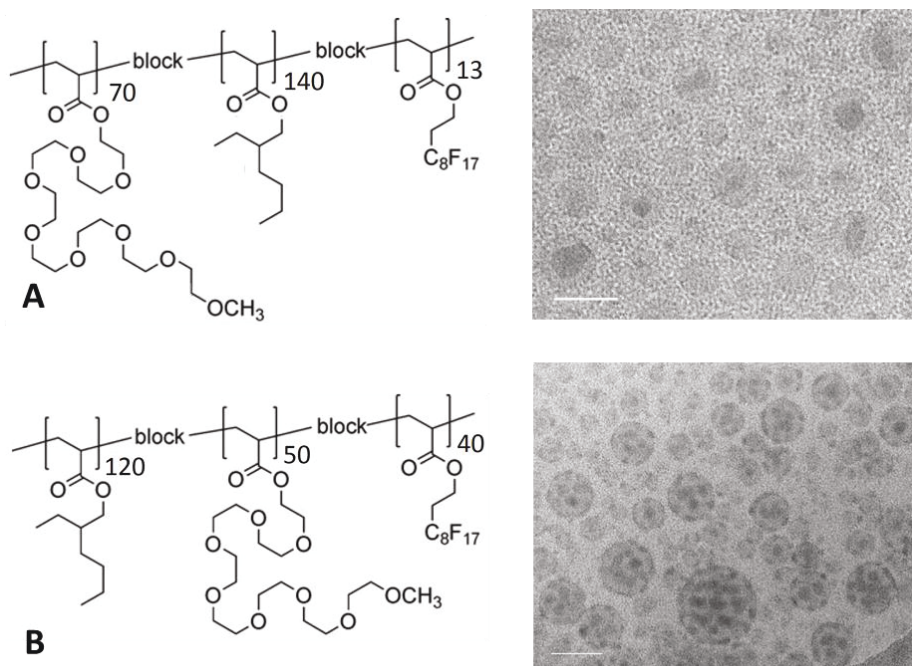
Figure 10. Structure of amphiphilic block copolymers with hydrophilic, lipophilic and fluorophilic blocks with different block order and cryo-TEM image of aggregates they formed in 0.5 wt. % aqueous dispersion (scale bar=50 nm). Picture is taken from ref. [59].

1.3. Fluorine containing poly-2-oxazolines

While the synthesis and the self-assembly behaviour of di- and triblock PAOx containing hydrophilic and hydrophobic blocks were widely studied, there is not much information about triblock PAOx that contain fluorinated moieties. The synthesis of fluorophilic poly(2-oxazoline)s suffers from the extremely low reactivity of fluorinated 2-oxazolines in the CROP, representing the main hurdle and challenge for the synthesis of aliphatic fluorophilic poly(2-oxazoline)s. As it was shown, the CROP of 2-alkyl-2-oxazolines normally proceeds via ionic propagation centers.[23] However, the presence of a strong electron-withdrawing perfluoroalkyl substituent in the 2-position of the 2-oxazoline ring extremely decreases the reactivity of the monomer and facilitates the transition of the active centres into the less reactive covalent form.[60,61] The synthesis of such perfluoroalkyl poly(2-oxazoline)s with more than 10 monomeric units requires usage of highly reactive initiators, high temperature and long reaction times.[62]

Nevertheless, several examples of fluorine containing 2-oxazoline based polymers are known. Schubert et.al. had overcome the low activity by using mono- and difluoro-2-phenyl-2-oxazolines.[63] In later work, the detailed study of the polymerization kinetics of fluorinated 2-phenyl-2-oxazolines was conducted.[64] It was also found that the amphiphilic ABC triblock copolymers with poly(2-(2,6-difluorophenyl)-2-oxazoline) (ODFOx, fluorophilic) and poly(2-(1-ethylheptyl)-2-oxazoline) (EHPOx, lipophilic) blocks was found to form multicompartment structures in aqueous milieu (Figure 11).[65]
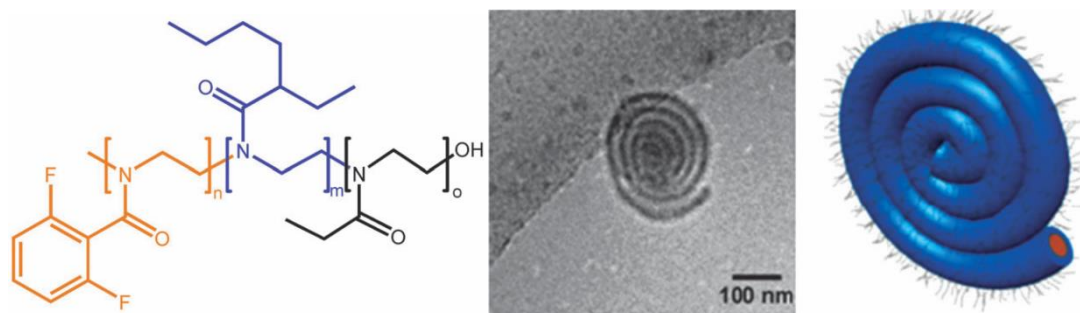
Figure 11. Left: the chemical structure of the poly(ODFOx$_{23}$-b-EHPOx$_{28}$-b-EtOx$_{49}$) triblock terpolymer. Middle: cryo-TEM picture of a spiral-like micellar aggregate from this terpolymer in water. Right: schematic representation of a potential spiral-like aggregate. Picture is taken from the ref. [65].

The synthesis of amphiphilic block copolymers of 2-fluoroalkylethyl-2-oxazoline and 2-methyl-2-oxazoline was described by Jordan and co-workers.[31] Small-angle neutron scattering and Transmission Electron Microscopy (TEM) study proved the formation of elongated micelles in aqueous solution for these copolymers. It was also demonstrated that mixing this copolymer with PMeOx-*b*-PNonOx results in coexistence of micelles with lipophilic and fluorophilic core due to incompatibility of lipophilic and fluorophilic blocks.

1.4. Characterization methods

1.4.1. Dynamic light scattering (DLS)

The method of Dynamic Light Scattering (DLS) (also known as photon correlation spectroscopy and quasi-elastic light scattering) is based on the fluctuations of the intensity of scattered light. There are many reasons for fluctuation of scattering light intensity. Pure liquids scatter light due to density or compressibility fluctuation. This scattering is very weak and depends on temperature of a liquid, its viscosity and other parameters. The presence of impurities or solute results in much stronger intensity of the scattered light, that is due to local fluctuations in concentration of the solute.

Solutions of nanoparticles or polymers scatter light in the most efficient way. The time-averaged intensity of the scattered light of polymer solution depends on polymer concentration, molecular weight, *etc*. The presence of particles in solution could be also manifested as rapid fluctuations of the scattered intensity in time. Such fluctuations occur due to the Brownian motion of the particles in solution. Indeed, due to continuous thermal motion of particles their number in a scattering volume is continuously alternating. The higher is the

value of the translational diffusion coefficient D_t, the faster fluctuations of the scattered intensity in time. This phenomenon is the basis of DLS experiment. It is possible to obtain a translational diffusion coefficient value by analyzing the time fluctuations of the scattered light intensity. The autocorrelation function mathematical apparatus is used for quantitative analysis of the time fluctuations.

The autocorrelation function $G_2(\tau)$ describes the correlation of scattered intensity by comparing the intensity value in initial moment $I(t)$ with the intensity at delay time τ:

$$G_2(\tau) = <I(t)I(t+\tau)> = \int_0^\infty I(t)I(t+\tau)dt \tag{3}$$

The correlation function $G_2(\tau)$ should be further normalized ($g_2(\tau)$) and converted to the autocorrelation function $g_1(\tau)$ related to time autocorrelation function of electric field strength by Siegert's relation[66]:

$$g_2(\tau) = 1 + \beta|g_1(\tau)|^2 \tag{4}$$

where β is the coherence factor determined by the geometry of the detection. For the hard spheres

$$g_1(\tau) = e^{-\frac{\tau}{t_c}} \tag{5}$$

where t_c is the relaxation time of the correlation function, which is related to translational diffusion coefficient D_t as

$$\frac{1}{t_c} = D_t q^2 \tag{6}$$

Taking into account equations (5) and (6), the equation (4) can be rewritten as

$$g_2(\tau) = 1 + \beta e^{-\left(\frac{2\tau}{t_c}\right)} \tag{7}$$

For dilute solution of small non-interacting spheres the hydrodynamic radius R_h can be calculated from the translational diffusion coefficient via the Stokes-Einstein equation

$$D_t = \frac{k_B T}{6\pi\eta R_h} \tag{8}$$

where k_B is the Boltzmann constant, T is the absolute temperature and η is the solvent viscosity.

1.4.2. Small-angle X-ray and neutron scattering (SAXS and SANS)

X-rays and neutrons have much lower wavelength value (0.1–1 nm) in comparison with wavelength of the visible light used in DLS (400–700 nm). Thereby, the SAXS and SANS are

often used for characterization of the nanoparticles internal structure with submicron dimensions.

In contrast with visible light, the scattering of X-rays occurs on the atoms electrons, whereas neutrons are scattered by atomic nuclei. Nevertheless, the mathematical description of a scattering event for visible light, X-rays and neutrons is the same.

When the irradiation passes through a sample it can be absorbed, i.e. converted into heat, fluorescence, etc., scattered, or transmitted without interaction. When the incident wave with the electric field strength E_0 interacts with an atom in the sample, it generates secondary spherical wave with the electric field strength E_S (Figure 12). The k_I is the wave vector of the incident irradiation with magnitude $|k_I|=2\pi/\lambda$. It is assumed that the scattering process is "quasielastic", so the magnitude of scattered radiation propagation vector k_S is also $2\pi/\lambda$.[67]
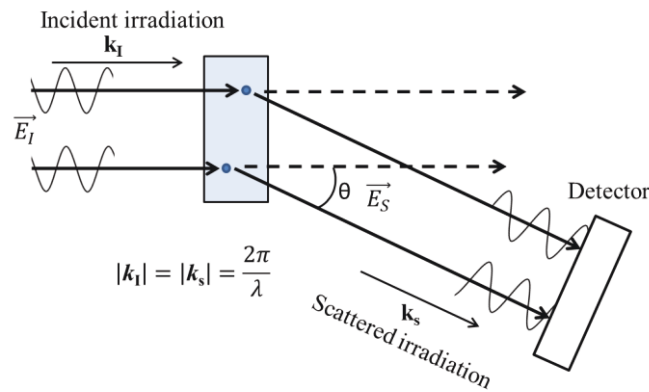
Figure 12. Typical scheme of scattering experiment.

Secondary spherical waves scattered at the same angle interfere producing an averaged interference pattern, which depends on the observation angle θ and the distribution of scattering centres.

Any detector registers not electric filed strength, but scattered intensity, which is related to E_S by

$$I_S(q) = \langle |E_S(q)|^2 \rangle \tag{9}$$

where q is the scattering vector

$$q = \frac{4\pi}{\lambda} \cdot \sin\frac{\theta}{2} \tag{10}$$

The scattering from the solution of non-interacting particles is the ensemble average of the secondary spherical waves from all atoms inside of the nanoparticle. The scattered intensity as a function of q is characteristic for the particle shape and called form factor $P(q)$.[68] In case of concentrated samples or strongly interacting diluted nanoparticles , the total scattering pattern contains also the contribution of interparticle interference, which called the structure factor $S(q)$. Thereby, the scattering intensity from the ensemble of identical particles could be presented as

$$I_S(q) = K \cdot P(q) \cdot S(q) \tag{11}$$

where K is the constant which includes experimental and material parameters.

For diluted solutions of identical particles $S(q) = 1$ and the scattering intensity is proportional to the sum of particles form factors

$$I_S(q) \sim N \cdot P(q) \tag{12}$$

Also, if the particles are different in size (polydisperse samples) or in shape (polymorphous samples) the form factors of all particles are summed up resulting in the average form factor.

$$I_s(q) \sim \sum_{i=1}^{N} P_i(q) \tag{13}$$

The analysis of experimental $P(q)$ is based on its comparison with known theoretical models, such as hard and hollow spheres, rod, random coil, *etc.* The model for the form factor of complex objects (such as polymer micelle, vesicle, *etc.*) could be obtained as a combination of simple models.[69] Also, the additional information about the sample (for example from chemical structure or microscopy) is required for adequate scattering data interpretation.

2. AIMS OF THE THESIS

The principal goal of this work is the synthesis and systematic investigation of novel 2-oxazoline triblock copolymers with thermodynamically immiscible hydrophilic, hydrophobic and fluorophilic blocks. Such systems are promising in the context of mimicking the biological systems since they are able to form micellar aggregates with a multicompartment hydrophobic core consisting of several domains of different nature, similar to multi-domain proteins and cell organelles. The presence of fluorinated fragments opens up the possibility for using them as contrast agents for MRI.
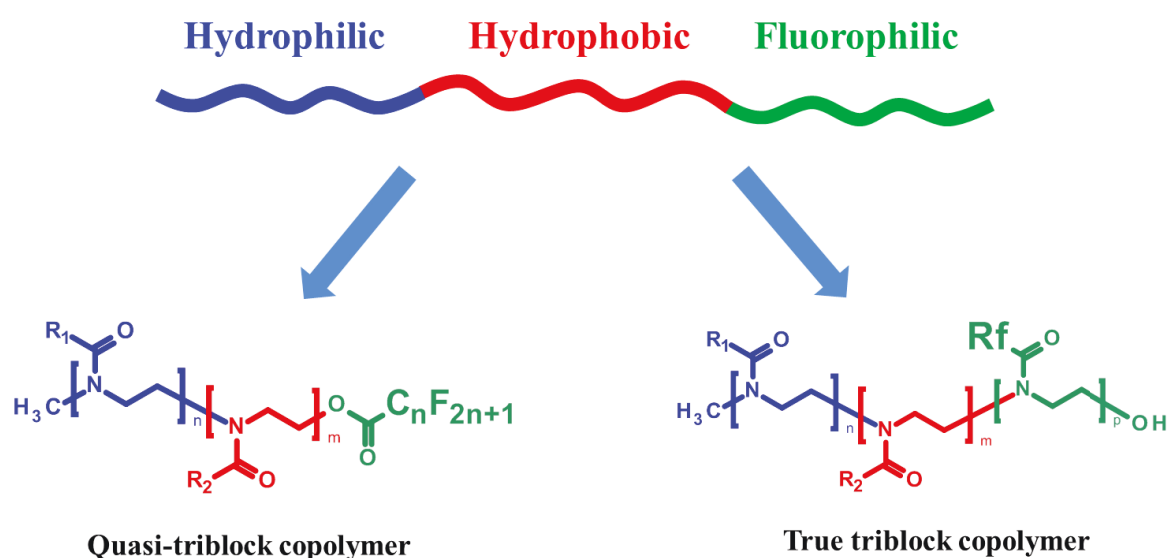
Figure 13. Structures of investigated copolymers ($R_f = C_nF_{n+1}$).

The work aims to address the following problems:

1. To facilitate the synthesis of model "quasi-triblock" systems (Figure 13, left) using insertion of perfluoroalkyl fragments into poly(2-oxazoline) diblock copolymers with hydrophilic and hydrophobic blocks during the termination of Cationic Ring-Opening Polymerization (CROP) (terminator-based functionalization). Study the effect of fluoroalkyl chains of various length on the copolymer self-assembly behaviour.

2. Synthesis of "true-triblock" copolymers with polymerizable fluorophilic block (Figure 13, right). Optimization of the synthesis of 2-fluoroalkyl-2-oxazolines and investigation of their reactivity in CROP.

3. Study of self-assembly behaviour of 2-oxazoline "true-triblock" copolymers by various physico-chemical methods such as dynamic light scattering, small angle X-ray and neutron scattering and cryo-transmission electron microscopy.

3. EXPERIMENTAL

3.1. Dynamic light scattering (DLS)

Dynamic light scattering (DLS) was performed to characterize the copolymers in dilute solutions. For this purpose, the hydrodynamic diameter of the particles, D_h, and the scattering intensity were measured at a scattering angle of $\theta = 173°$ with a Zetasizer Nano-ZS instrument, model ZEN3600 (Malvern Instruments, UK). The DTS (Nano) program was used to evaluate the data. It provides intensity-, volume-, and number-weighted D_h distribution functions.

Aqueous solutions of polymers were prepared via direct dissolving or using solvent exchange method. The last one was carried out as follows, the sample of polymer was dissolved in 1 mL of methanol and placed into the Spectra/Por 6 dialyse bag (1000 Da). The polymer solution was dialysed against water (18 MΩ.cm) for 48 hours. The obtained aqueous solution was used for further experiments.

3.2. Size exclusion chromatography (SEC)

A: Homopolymers

Size exclusion chromatography measurements were performed on an Agilent 1260-series HPLC system equipped with a 1260 online degasser, a 1260 ISO-pump, a 1260 automatic liquid sampler, a thermostatted column compartment at 50°C equipped with two PLgel 5 μm mixed-D columns and a mixed-D guard column in series, a 1260 diode array detector and a 1260 refractive index detector. Dimethylacetamide containing 50 mM of lithium chloride was used as eluent at an optimized flow rate of 0.593 ml/min. Chromatograms were analyzed using Agilent Chemstation software with SEC add-on. Number average molar mass (M_n) and dispersity ($Đ$) values were determined against poly(methyl methacrylate) standards from Polymer Standards Service, Germany.

B: Block copolymers (SEC-MALS)

Labio Biospher GMB100 7.5 mm x 300 mm, particle size 10 μm, size exclusion column, applicable in aqueous as well as in organic mobile phases, was used for the analysis of the poly(2-oxazoline)s using methanol as the mobile phase at 0.18 ml/min. The pump was a Shimadzu 20ADvp liquid chromatography pump (Shimadzu Corp, Kyoto, Japan). The vacuum degasser was a DeltaChrom TVD (Watrex, Prague, Czech Republic). The 40 mg/ml polymers solutions in methanol were injected manually using a six port PEEK injection valve equipped with a 50 μl sample loop (Upchurch Scientific, Oak Harbor, WA). A home made in-line 25 mm filter holder with a 0.02 μm Anodisc 25 membrane (Whatman, Maidstone, UK) was positioned between the pump and the injection valve.

The light scattering detector was a DAWN-DSP multi-angle light scattering instrument (Wyatt Technology, Santa Barbara, CA) and a Shodex RI-101 differential refractometer

(Showa Denko, Japan) served as the concentration detector. The signals from the detectors were collected and analysed using ASTRA for Windows 4.50 software (Wyatt Technology, Santa Barbara, CA). The angular dependence of the scattered light intensity was found to be negligible for all samples.

The refractive index increment of the poly(2-oxazoline)s in methanol was determined using a DnDc2010 differential refractometer (Polymer Standard Service, Germany) with 620 nm light source. The dn/dc values are presented in the Supporting Information of respective manuscripts.

It should be noted here that this two detector arrangement with both a DAWN-DSP light scattering unit as an absolute molecular weight detector and single refractive index detection SEC units does not require the use of polymer standards to determine the polymer molar mass and dispersity (Đ).

3.3. Pyrene fluorescence critical micellar concentration (CMC) measurements

The pyrene fluorescence method was used for the determination of the CMCs of the polymers. A pyrene in water/ethanol (80 µM, 12.8 µl) solution was added to the polymer solutions over a wide concentration range ($3.81 \cdot 10^{-5}$ – 5 mg/mL) in water. The resulting solutions were stirred for 1 hour. The fluorescence spectra were recorded using a fluorescence spectrometer (Jasco FP-6200, Japan). The intensity ratio I_{373}/I_{384} was calculated for each concentration, and the ratio was plotted as a function of the copolymer concentration in water. The CMC was determined at the intersection point (in the region of lower concentration) of the two regression lines.

3.4. Transmission Cryo-Electron Microscopy (Cryo-TEM)

A: *Charles University in Prague, First Faculty of Medicine, Institute of Cellular Biology and Pathology, Prague, Czech Republic*

Cryo-TEM measurements were carried out using a Tecnai G2Sphera 20 electron microscope (FEI Company, Hillsboro, OR, USA) equipped with a Gatan 626 cryo-specimen holder (Gatan, Pleasanton, CA, USA) and a LaB6 gun. The samples for cryo-TEM were prepared by plunge-freezing.[70] Briefly, 3 µL of the sample solution was applied to a copper electron microscopy grid covered with a perforated carbon film forming woven-mesh-like openings of different sizes and shapes (Lacey carbon grids #LC-200 Cu, Electron Microscopy Sciences, Hatfield, PA, USA), glow discharged for 40 s with a current of 5 mA. Most of the sample was removed by blotting (Whatman no. 1 filter paper) for approximately 1 s, and the grid was immediately plunged into liquid ethane held at −183 °C. The grid was then transferred without rewarming into the microscope. Images were recorded at the accelerating voltage of 120 kV and with magnifications ranging from 11500× to 50000× using a Gatan UltraScan 1000 slow scan CCD camera in the low-dose imaging mode, with the electron dose not exceeding 1500 electrons per nm^2. The magnifications resulted in final pixel sizes ranging from 1 to 0.2 nm, and the typical value of the applied underfocus ranged between 0.5 to

2.5μm. The applied blotting conditions resulted in the specimen thicknesses varying between 100 to ca. 300 nm. All cryo-TEM images were carefully inspected for possible artefacts such as radiation damage and ice crystals.

B: *Department of Chemical Engineering, Technion-Israel Institute of Technology, Haifa, Israel*

Specimens were prepared in a controlled environment vitrification system (CEVS) at 25 °C and 100 % relative humidity. A drop (about 3 μL) of the sample was pipetted onto a perforated carbon film-coated electron microscopy copper grid, blotted with filter paper, and plunged into liquid ethane at its freezing point. Such specimens were then transferred to a 626 Gatan cryo-holder and imaged at an acceleration voltage 200 kV in a FEI (Eindhoven, NL) Talos 200C high-resolution transmission electron microscope at about −175 °C, in the low-dose imaging mode to minimize electron-beam radiation-damage. Image contrast was enhanced by "phase-plates" of the Talos. Images were digitally recorded with an FEI I Falcon II direct-imaging 16-megapixel camera.

3.5. Small-angle X-ray scattering (SAXS)

SAXS experiments for samples prepared by direct dissolution were performed on the high brilliance beamline ID02 at ESRF (Grenoble, France). The SAXS setup utilizes a pinhole camera with a beam stop placed in front of a two-dimensional Frelon CCD detector. The X-ray scattering patterns were recorded for sample-to-detector distances of 2.5 and 31 m, using a monochromatic incident X-ray beam with an energy of $E = 12\ 460$ eV ($\lambda = 0.1$ nm). The available scattering vector range was $q = 0.001-2.76$ nm^{-1} ($q = 4\pi \sin \theta/\lambda$, where 2θ is the scattering angle). Online corrections were applied for the detector, and the sample-to-detector distance, transmission, and incident intensity were calibrated. The isotropic scattering was azimuthally regrouped to determine the dependence of the scattered intensity $I(q)$ on the scattering vector q in absolute units. The scattering from a capillary filled with Milli-Q water was measured as a background and subtracted from the scattering signals of the samples. Prior to the experiment, a representative sample was checked to ensure lack of radiation damage.

SAXS experiments for samples obtained through solvent exchange from methanol were performed at the beamline B21 (Diamond Light Source, Didcot, UK) using a pixel detector (2M PILATUS). The X-ray scattering images were recorded for a sample-to-detector distance of 3.9 m, using a monochromatic incident X-ray beam ($\lambda = 0.1$ nm) covering the range of scattering vector 0.025 nm$^{-1} < q < 4$ nm^{-1}. Most of the samples had no measurable radiation damage by the comparison of 20 successive time frames with 50 ms exposures. The two-dimensional scattering patterns were azimuthally averaged to yield the dependence of the scattered intensity $I(q)$ on the scattering vector q. Before fitting analysis, the solvent scattering has been subtracted.

3.6. Small-angle neutron scattering (SANS)

SANS experiments for samples prepared by direct dissolution were performed at CEA-Saclay on the spectrometer PAXY of the Laboratoire Leon-Brillouin. Measurements were performed with a 128×128 multidetector (pixel size 0.5 × 0.5 cm) using a monochromatic (wavelength λ set by a mechanical velocity selector) incident neutron beam collimated with circular apertures for two sample-to-detector distances, namely, 1 m (with λ=0.6 nm) and 7 m (with λ=0.8 nm). With such a setup, the investigated range of scattering vector is from 5×10^{-2} to 4×10^{-1} nm^{-1}. The two-dimensional scattering patterns were isotropic so that they were azimuthally averaged to yield the dependence of the scattered intensity $I(q)$ on the scattering vector q.

3.7. NMR Spectroscopy

^{19}F NMR Spectroscopy

The ^{19}F NMR spectra were measured at 11.7 T on a Bruker Avance III HD 500 US/WB NMR spectrometer (Karlsruhe, Germany, 2013) using a solid-state 4-mm CP/MAS probehead optimized for the measurement of ^{19}F nuclei. The Hahn-echo experiment was applied to suppress the probehead residual signal; the echo-delay was 10 ms; the duration of the 90° (^{19}F) pulse was 1.5 µs; the repetition delay was 2 s; and 512-1024 scans were accumulated for each spectrum. ^{19}F NMR chemical shift scale was calibrated using the PTFE the signal of which was set to -122 ppm. Chloroform was used as the solvent.

3.8. Synthesis

The synthesis of all monomers and polymers was described in detail in the attached publications.

4. OVERVIEW OF RESULTS

The results are presented and discussed as follows:

Section 1 includes overview of Manuscripts M1 and M2 and devoted to synthesis and characterization of model quasi-triblock poly(2-oxazoline)s: synthesis of hydrophobic monomer 2-*n*-octyl-2-oxazoline (OctOx), synthesis of hydrophilic-hydrophobic diblock copolymer and its functionalization by perfluoroalkyl fragments of different lengths during the termination step as well as self-assembly behaviour study of obtained copolymers using cryo-TEM, DLS, SAXS and SANS.

In this part I provided the synthesis of hydrophobic monomer as well as synthesis and characterization of quasi-triblock copolymers and model diblock copolymer. Also I carried out the DLS study of polymer solutions. The total contributions into Manuscripts M1 and M2 are approx. 90 % and 60 % respectively.

Section 2 includes design of the 2-fluoroalkyl-2-oxazoline monomers with increased reactivity in CROP (Manuscript M3): synthesis of new fluorine containing 2-oxazolines with methyl and ethyl hydrocarbon spacers and their polymerization kinetics study. A series of di- and triblock copolymers of low dispersity with polymerizable fluorophilic block was synthesized and their ability to self-assemble in aqueous solution was shown.

The 90 % of results presented in Manuscript M3 were done by myself: the synthesis and the kinetics study of CF$_3$MeOx and CF$_3$EtOx, synthesis of copolymers and their characterization, DLS study of self-assembly behaviour.

Section 3 is devoted to poly(2-oxazoline)s with high fluorine content (Manuscript M4). The synthesis and polymerization activity of 2-(1H,1H,2H,2H-perfluorooctyl)-2-oxazoline are described. A number of well-defined 2-oxazoline copolymers were synthesized using this monomer and their solution behaviour in wide range of the solvents is presented.

Within this part I carried out optimization of the fluorophilic monomer synthesis and polymerization kinetics study, as well as the synthesis and characterization of all copolymers. Also I characterized the solution behaviour of obtained polymers by DLS. The total contribution to Manuscript M4 is approx. 80 %.

4.1. Poly-2-oxazoline block copolymers with terminal perfluoroalkyl fragments (Manuscripts M1 and M2)

4.1.1. Quasi-triblock copolymers synthesis

Quasi-triblock copolymers were synthesized via subsequent CROP as follows. 2-Methyl-2-oxazoline and methyl *p*-toluenesulfonate (initiator) were dissolved in acetonitrile and stirred at 140 °C in a pressure reactor to form the first PMeOx block (Scheme 1). After cooling down the reaction mixture after the desired reaction time, the second monomer OctOx was added, and the mixture was stirred at 140 °C to form the PMeOx-*b*-POctOx block

copolymer. The perfluoroalkyl fragments were attached to copolymers by termination of polymerization mixture with corresponding perfluorinated carboxylic acids in the presence of triethylamine at 70 °C. To obtain the model PMeOx-*b*-POctOx diblock copolymer, the polymerization was quenched with 1M KOH in methanol.
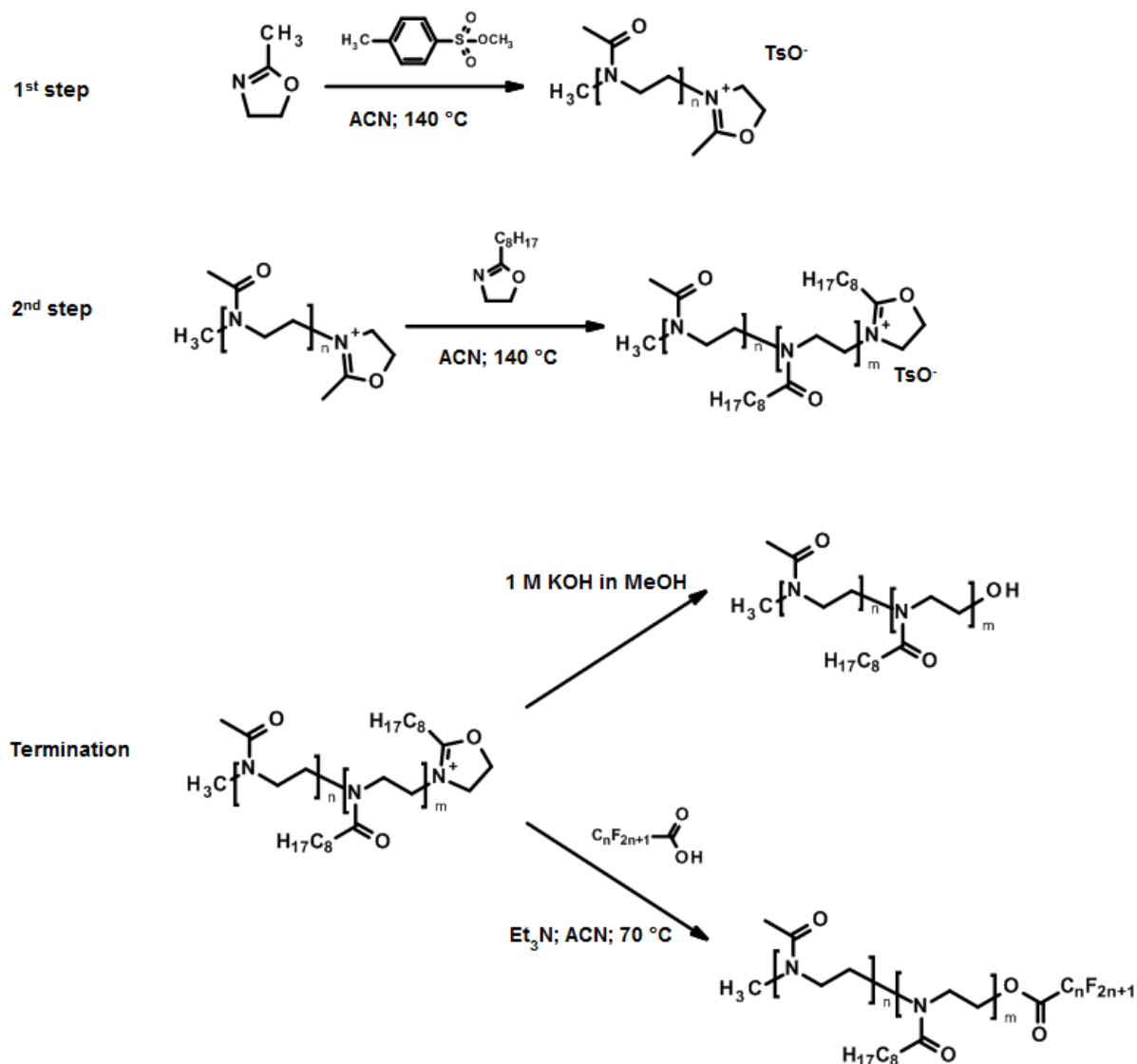
Scheme 1. Synthesis of di- and quasi-triblock copolymers.

^{1}H-NMR spectra of the polymers show the characteristic signals for protons belonging to the poly(2-oxazoline) backbone as well as PMeOx and POctOx side chains (see Figure 1 in Manuscript M1). Also, there are signals from the CH_2 group of the terminal 2-oxazoline repeat unit next to the ester group attached to the perfluorinated fragment. In the ^{19}F NMR spectra, typical resonances of CF_3 and CF_2 units of perfluorinated substituents were also clearly detected (Figure 14).
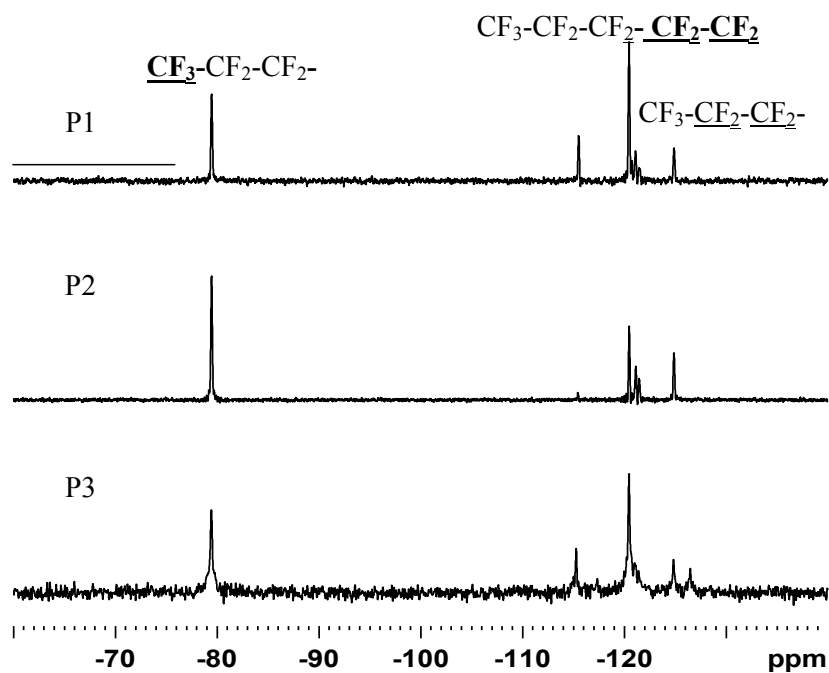
Figure 14. ^{19}F NMR spectra of the synthesized polymers P1, P2 and P3.

All of the synthesized polymers were characterized by SEC-MALS in methanol to determine their absolute number average molar mass M_n and Đ. The M_n of all of the copolymers is in the range of 5-6 KDa with typically narrow molar mass distributions (Table 1).

Table 1. Characteristics of fluorinated quasi-triblock poly(2-oxazolines) and reference nonfluorinated diblock copolymer.

Polymer	Composition	M_n, g/mol	Đ
P0	PMeOx$_{30}$-*b*-POctOx$_{20}$	6300	1.11
P1	PMeOx$_{30}$-*b*-POctOx$_{20}$-C$_8$F$_{17}$	6000	1.08
P2	PMeOx$_{30}$-*b*-POctOx$_{20}$-C$_{10}$F$_{21}$	5000	1.09
P3	PMeOx$_{30}$-*b*-POctOx$_{20}$-C$_{12}$F$_{25}$	5000	1.14

4.1.2. Quasi triblock copolymers self-assembly in water

4.1.2.1. Dynamic light scattering

Visual inspection and DLS shown that the synthesized polymers are dissolved as individual chains in a wide range of medium to high polarity solvents including methanol (MeOH), 1,1,1,3,3,3-hexafluoroisopropanol and dichloromethane, whereas they are insoluble in very low polarity solvents such as ethyl acetate and diethyl ether. The intensity distribution

functions of 10 mg/mL polymers solutions in MeOH revealed one peak with a D_h value of 1-2 nm (Figure 15 A) indicative of molecularly dissolved polymer chains.
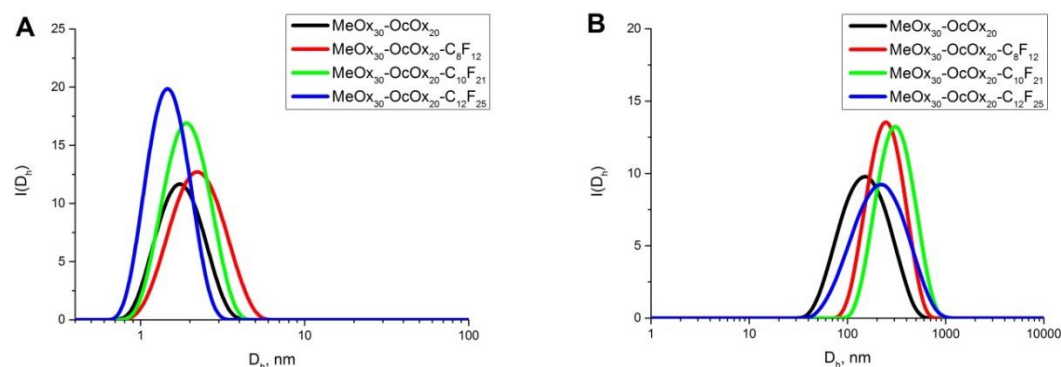
Figure 15. Distribution functions of D_h for 10 mg/ml polymer solutions in MeOH (A) and in water (B).

The DLS study also revealed peaks with D_h of 100-200 nm for all investigated polymers in aqueous solutions after direct dissolution of the polymers in water, which was attributed to nanoparticles (Figure 15 B).

The CMC values for synthesized copolymers in water are presented in Table 2. These CMC values are quite low, indicating a strong hydrophobic driving force for polymer assembly in water. However, there is no significant difference between the CMC values for the copolymers. It may be concluded that the long POctOx block dominates the hydrophobic self-assembly of the studied copolymers.

Table 2. The CMC values in water for the fluorine-containing quasi-triblock copolymers and non-fluorinated reference diblock copolymer.

Polymer	Composition	CMC, mg/mL
P0	PMeOx$_{30}$-*b*-POctOx$_{20}$	$1.6 \cdot 10^{-3}$
P1	PMeOx$_{30}$-*b*-POctOx$_{20}$-C$_8$F$_{17}$	$3.1 \cdot 10^{-3}$
P2	PMeOx$_{30}$-*b*-POctOx$_{20}$-C$_{10}$F$_{21}$	$4.0 \cdot 10^{-3}$
P3	PMeOx$_{30}$-*b*-POctOx$_{20}$-C$_{12}$F$_{25}$	$5.0 \cdot 10^{-3}$

4.1.2.2. Cryo-TEM study

Cryo-TEM analysis was performed of 10 mg/mL aqueous solutions of the investigated copolymers revealing the presence of aggregates of different morphologies, including mono- and multi-layered vesicles, isolated and aggregated rod-like micelles, for the different copolymers (see Figure 12 in Manuscript M1).

The P0 polymer that has no fluorinated tail formed primarily multi-layered vesicles, which is in agreement with the DLS result. In contrast, the cryo-TEM analysis of a P1 solution showed a mixture of aggregating rod-like micelles and little-populated single-layered vesicles. The copolymer P2 revealed a very similar behaviour to P1 with a mixture of vesicles and rod-like micelles However, the extension of the fluoroalkyl chain length further decreased the relative content of the vesicles. This trend is continued for copolymer P3 with the longest fluorinated alkyl chain, which only showed isolated rod-like micelles with a small fraction of agglomerates composed of rod-like micelles, while vesicles were no longer observed.

Based on the cryo-TEM investigations, it may be suggested that the insertion of a perfluorinated fragment as the end group of the PMeOx-*b*-POctOx copolymer introduces additional microphase separation of the perfluorinated fragment from the POctOx in the hydrophobic domains. Such microphase separation makes the energetic penalty to bend the copolymer bilayer too much. As a result, the formation of vesicles becomes less favourable and rod-like micelles are formed with the insertion of a short fluorinated block. The co-existence of rod-like micelles and vesicles could be due to the compositional polydispersity of the poly(MeOx)-*block*-poly(OctOx) copolymer. With the increasing length of the perfluorinated fragment in the case of P3 ($C_{12}F_{25}$), the elastic energy of bending becomes even higher so that vesicles could not be formed anymore and only rod-like micelles are observed (Figure 16).

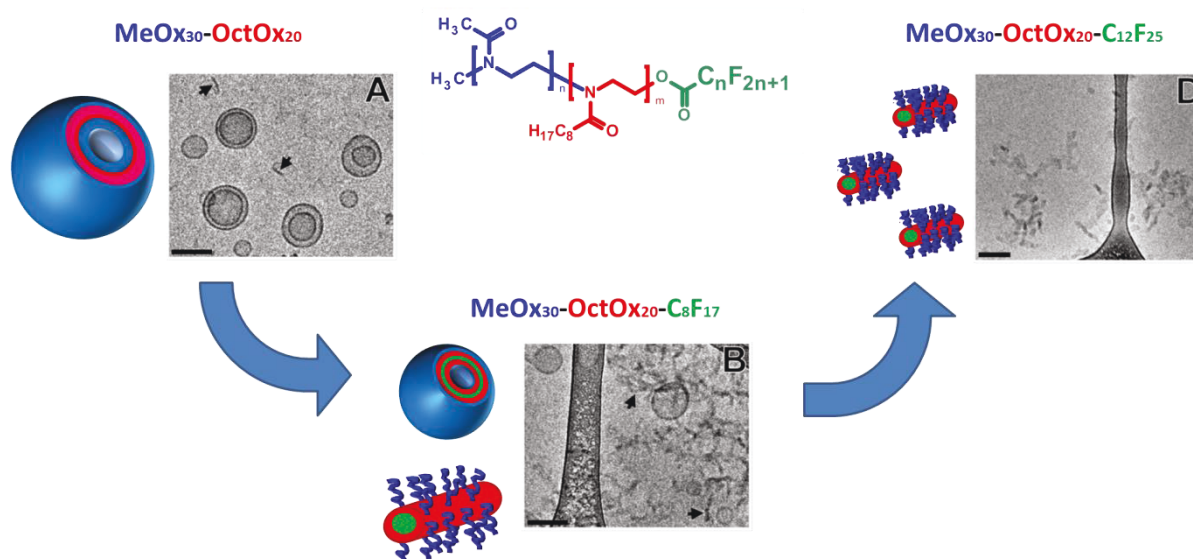*Figure 16. Phase sequence of poly(2-methyl-2-oxazoline)–block–poly(2-octyl-2-oxazoline) copolymer with increasing length of terminal perfluoroalkyl chain.*

4.1.2.3. Solvent exchange method for inducing the self-assembly of quasi-triblock copolymers

The preparation method of self-assembled structures can be of primary importance for the self-assembly of block copolymers as various kinetically trapped aggregates can be

obtained.[71–74] To study this effect, an aqueous solution of all of the block copolymers was prepared by solvent exchange from methanol where the polymers are unimolecularly dissolved in water by dialysis to induce self-assembly. The aqueous solution of quasi-triblock copolymers (1 wt. %) obtained by this solvent exchange method revealed one peak with D_h in the range of 20-40 nm in DLS. Cryo-TEM images also confirmed the presence of spherical micelles with diameters ranging from 15 to 20 nm. On the other hand, after solvent exchange, the model diblock copolymer forms particles with diameter of approximately 200 nm, which is close to the diameter of vesicles observed for that polymer after direct dissolution. We can conclude that due to the extreme hydrophobicity of the fluoroalkyl chain quasi-triblock copolymers are more able to form spherical micelles during solvent exchange. In the case of spherical micelles, the contact between the lipophilic and fluorophilic parts is minimized, and the perfluorinated core acts as an anchor that prevents further aggregation.

4.1.2.4. SAXS and SANS studies

4.1.2.4.1. Nanoparticles prepared by direct dissolution

For the in depth characterization of the internal structure of nanoparticles formed by fluorine-containing quasi-triblock copolymers and model diblock copolymer, the combination of small-angle X-ray and neutron scattering techniques was used.

The SANS and SAXS curves of all the copolymers at a concentration of 2 wt. % and 2.5 wt %, respectively, are presented in Figure 17a and Figure 17b.
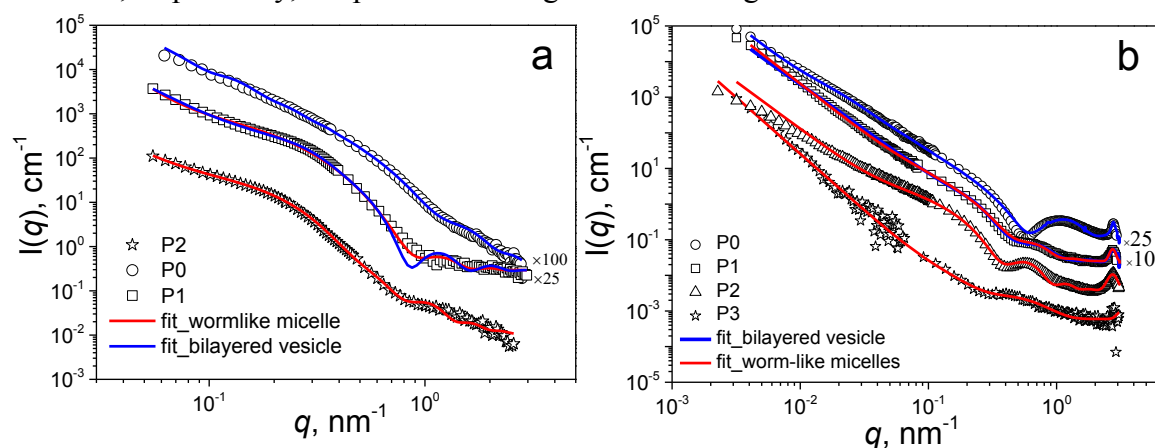
Figure 17. SANS (a) and SAXS (b) curves displayed by PMeOx₃₀-b-POctOx₂₀ (P0), PMeOx₃₀-b-POctOx₂₀-C₈F₁₇ (P1), PMeOx₃₀-b-POctOx₂₀-C₁₀F₂₁ (P2) and PMeOx₃₀-b-POctOx₂₀-C₁₂F₂₅ (P3) aqueous solutions prepared by direct dissolution.

The scattering data corresponding to the structures of the self-assembled diblock copolymers can be fitted using the bilayered vesicle form factor corrected with the Schultz−Zimm polydispersity over the radius of the vesicle interior R_a. Additionally, the contribution of large aggregates was added as background, which resulted in a good quality fit. The quantitative analysis of the SANS scattering data yields a R_a, consisting of solvent of 24.4 nm (Figure 18A) and a polydispersity value of 0.26. The hydrophobic layer thickness, t_i, of 1.6 nm consists of presumably the POctOx block, whereas the hydrophilic PMeOx layer

thickness, t_h, is 2.48 nm. The total radius of the vesicle is approximately 28.5 nm according to the SANS data.
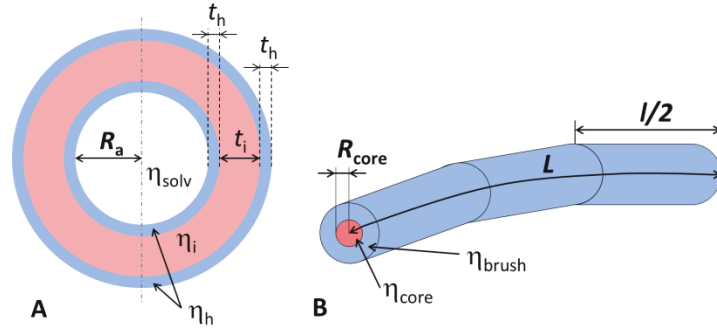
Figure 18. Scheme of bilayered vesicle (A), wormlike micelle (B). Here η_i, η_h, η_{solv}, η_{core}, η_{brush} are values of scattering length density (SLD) of corresponding aggregate fragments.

A similar scattering pattern was obtained by the SAXS measurements. However, the SAXS scattered intensity has a broad secondary maximum in the q-range from 0.7 to 2 nm^{-1}, that can be explained by the differences in scattering length density (SLD) values of the inner and outer bilayer parts on the solvent side. Values of the bilayer and outer layer thickness are in rather good agreement with those calculated from SANS data. At the highest q value, the scattering curves for higher concentrations of aqueous diblock copolymer solutions exhibit another peak located at $q = 2.75$ nm^{-1} (Figure 19b).

We utilized the bilayered vesicle model with Schultz−Zimm polydispersity and contribution from aggregates and in order to describe the small sharp peak at high q values the Voigt peak model was used (ref. [75]), which can be attributed to additional internal ordering. From the position of the peak the repeat distance can be calculated as $D = 2\pi / q$, being 2.27 nm, which can be explained by the crystallization of octyl chains within the inner part of the bilayered vesicle wall. The amplitude of the Voigt peak decreases with decreasing concentration (Figure 19a), indicating the decreasing packing density within the inner bilayer.
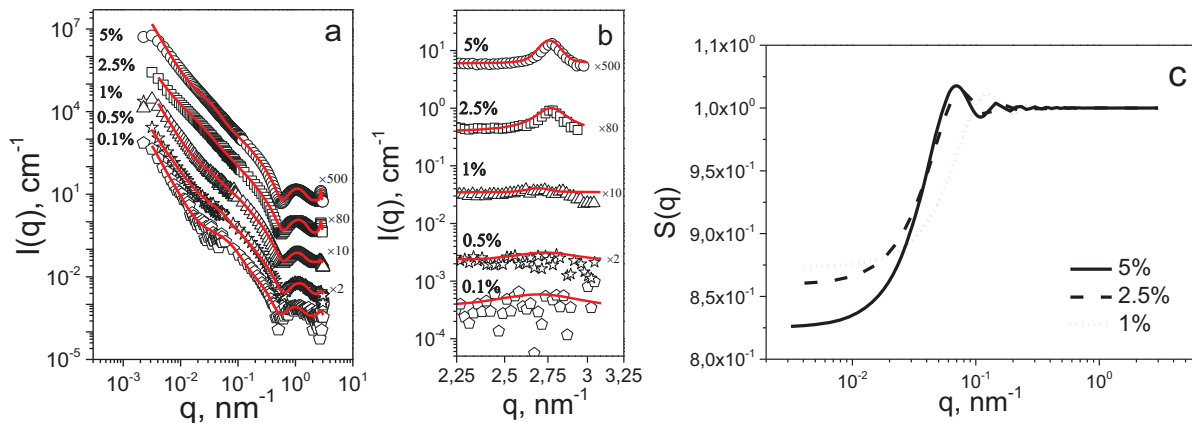
Figure 19. (a) SAXS data for 0.1, 0.5, 1, 2.5, 5 wt. % of PMeOx$_{30}$-b-POctOx$_{20}$ water solutions; (b) 2.25-3.25 nm^{-1} q-range of SAXS data for 0.1, 0.5, 1, 2.5, 5 wt. % of PMeOx$_{30}$-b-POctOx$_{20}$ water solutions; (c) structure factor, S(q), for 1, 2.5, 5% wt. % of PMeOx$_{30}$-b-POctOx$_{20}$ water solutions at 25 °C. Symbols are experimental scattering data. Solid lines are fits generated as described in the text.

In a subsequent step we evaluated the structural changes in nanoparticles assembled from the fluorinated copolymers. Cryo-TEM results revealed the presence of two types of self-assembled structures, namely bilayered vesicles and worm-like micelles. Therefore, we fitted the scattering curves by a combination of the worm-like micelles form factor (Figure 17B) and Schultz−Zimm polydispersity of a micelle core radius. Calculated radii of the wormlike micellar core are 8.2 nm from SAXS and 5.2 nm from SANS, again in good agreement with the values obtained from cryo-TEM (approximately 7.5 nm). From the calculated percentage of solvent inside of the wormlike micelles core of 0.03 from SAXS and 0.01 from SANS, one can assume that the core consists of the highly hydrophobic part of the polymer, probably a mixture of the POctOx and the perfluorinated chains, whereas the outer shell is formed mainly by the hydrophilic PMeOx part.

The sharp peak at high q values evidences an additional ordering of the octyl chains inside the hydrophobic micellar core as it was mentioned before for the bilayer vesicle structures. Besides, it is known that perfluorinated alkyl chains are quite rigid and also have a tendency to crystallize.[76–79] Based on this we can assume that there are maybe two types of ordering inside the nanoparticles: the ordering driven by perfluorinated alkyl chains which form the core of the worm-like micelle and the ordering of the POctOx chains in the first, hydrophobic, shell of the worm-like micelles.

In contrast to the polymer with the shortest perfluorinated fragment, the scattering curves for $PMeOx_{30}$-*b*-$POctOx_{20}$-$C_{10}F_{21}$ and $PMeOx_{30}$-*b*-$POctOx_{20}$-$C_{12}F_{25}$ solutions can satisfactorily be fitted with the wormlike micelles form factor only. As for the previous polymers, the final fit of the $PMeOx_{30}$-*b*-$POctOx_{20}$-$C_{10}F_{21}$ and $PMeOx_{30}$-*b*-$POctOx_{20}$-$C_{12}F_{25}$ scattering consists of a wormlike micelles form factor with contributions of large aggregates and of a Voigt peak.

Analysis of structural parameters obtained from the fitting procedures gives the possibility to establish the correlation between the length of fluorinated fragment of quasi-triblock poly(2-oxazoline)s, and morphology of nanoparticles obtained by their self-assembly in water solutions. Dependences of the main parameters on the length of fluorinated fragment in triblock poly-2-oxazolines solutions, prepared by direct dissolution, are presented in Figure 20.
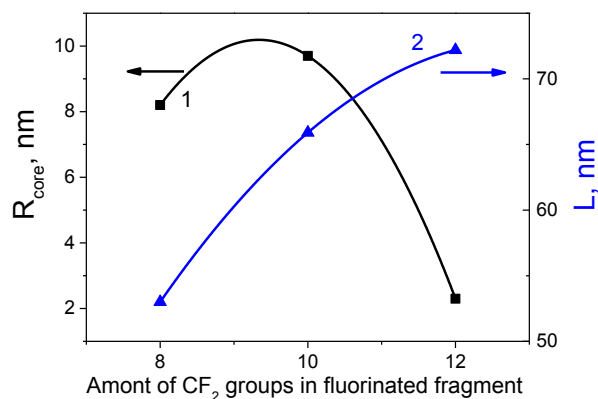
Figure 20. Dependence of the radius of the wormlike micelles core (1) and contour length of the wormlike micelle (2) as a function of the length of fluorinated fragment in triblock polyoxazolines (solutions prepared by direct dissolution).

The obvious changes in morphology are that: (1) the radius of the wormlike micelles core decrease from 8.2 to 2.3 nm and (2) the contour length of the wormlike micelle increases from 53 to 72.2 nm with the increasing of fluorinated fragment length, indicating that wormlike micelles become longer and thinner.

4.1.2.4.2. Nanoparticles prepared by solvent exchange method (dialysis)

As it was mentioned above, DLS and cryo-TEM studies of quasi-triblock copolymers aqueous solution prepared by solvent exchange method revealed the presence of spherical micelles with diameter 15-20 nm (see section 4.1.2.3.).

For all polymer solutions the SAXS curves are quite similar (Figure 21). There is no sign of aggregation of the self-assembled structures. For all obtained aqueous polymer solutions, the formed nanoparticles revealed a core-shell structure consisting of one or two layers with spherical symmetry. To fit the scattering data a model of sphere with two shells has been chosen (Figure 22).
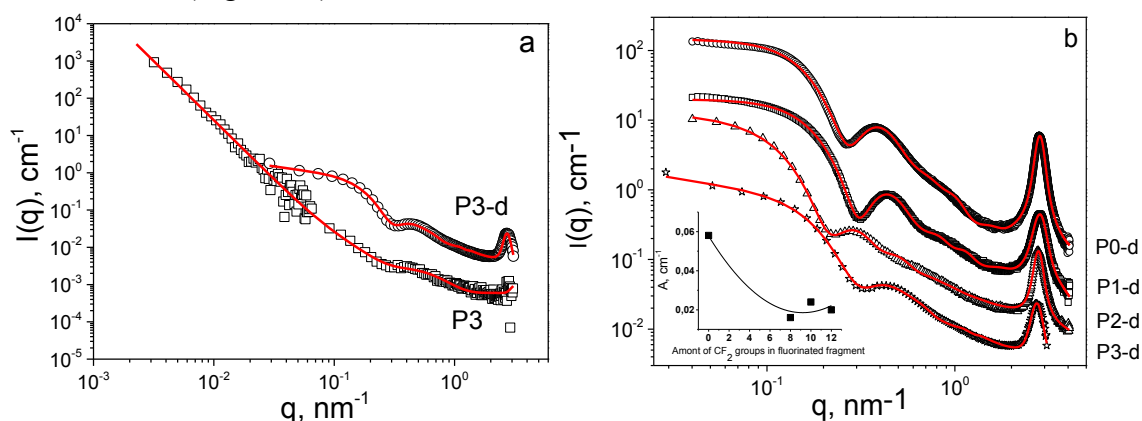
Figure 21. (a) Comparison of SAXS data for PMeOx$_{30}$-b-POctOx$_{20}$-C$_{12}$F$_{25}$ (P3) prepared by direct dissolution and by solvent exchange; (b) Comparison of SAXS data for all polymers prepared by solvent exchange and (b inset) dependence of maximum amplitude of Voigt peak (calculated by fitting procedure) on the length of fluorinated fragment for nanoparticles prepared by solvent exchange method.

Despite the fact that the diblock copolymer consists of two blocks, that can form a core with just one shell, the model of sphere with one shell did not fit correctly the scattering curve. We assume that the presence of a second shell (calculated from the fitting procedure) can be related to the inhomogeneously distributed density of the hydrophobic and hydrophilic parts of the micelle and that the indistinct border between the core and the shell can affect the values of the SLD. From the position of the first minimum on the scattering curve q_m, the radius of a sphere (R) with core-double shell structure could be determined to be approximately 15.2 nm using the following equation $q_m R = 4.493$.[80]
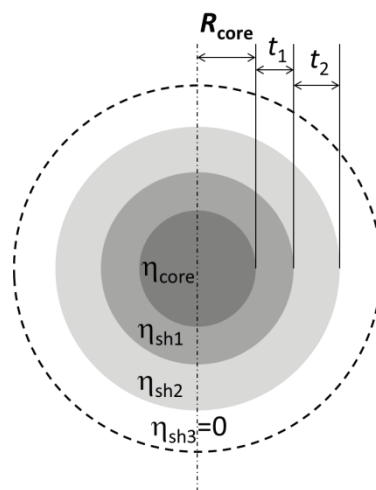
Figure 22. Scheme of sphere with two shells.

It is obvious from Figure 21b that the intensity of the peak at high q values decreases with increasing length of the fluorinated block. This feature may be related to the presence of two types of water-insoluble chains that both have a tendency to crystallize. While the POctOx segments form more strictly ordered structures due to the conditional homogeneity inside the core, the presence of fluorinated units penalize the homogeneity of the core and of one of the shells, thus reducing the ordering.

One can see that the thickness of the second shell, consisting of poly(2-methyl-2-oxazoline) block, varies only slightly, while the thickness of the first shell increases with the increasing of the length of fluorinated fragment (See Table 3 in Manuscript M2). At the same time the core radius decreases with the increasing of the fluorinated part length. It can be explained by the assumption that for copolymer $PMeOx_{30}$-b-$POctOx_{20}$-C_8F_{17} with the shortest fluorinated fragment, the poly(2-octyl-2-oxazoline) block is more hydrophobic then the fluorinated part. That is why the sphere core for $PMeOx_{30}$-b-$POctOx_{20}$-C_8F_{17} consists of the poly(2-octyl-2-oxazoline) block as it was for diblock copolymer. With increasing length of fluorinated fragment its hydrophobicity increases and for $PMeOx_{30}$-b-$POctOx_{20}$-$C_{10}F_{21}$ and $PMeOx_{30}$-b-$POctOx_{20}$-$C_{12}F_{25}$ the core is formed mainly by fluorinated groups. We can also assume that the first hydrophobic shell consists of poly(2-octyl-2-oxazoline) block with partially incorporated fluorinated fragment.

The proposed scheme of morphological transition observed in this study is presented in the Figure 23. It can be concluded from the comparison of the SAXS and SANS results as

well as of DLS and cryo-TEM results that the shape and inner structure of fluorinated quasi-triblock poly(2-oxazolines) can be easily controlled by changing the terminal fluorinated group as well as by the method of preparation.
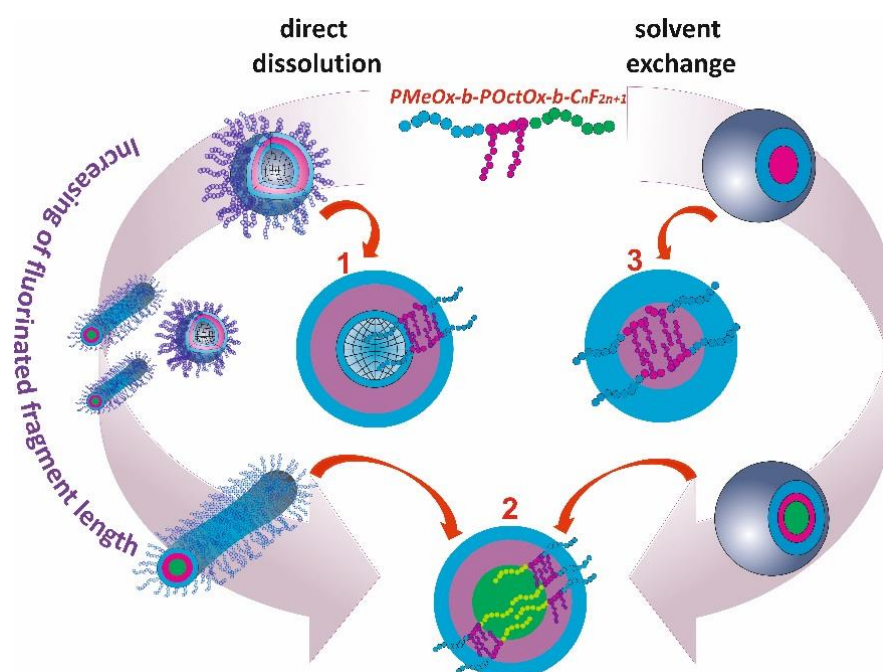
Figure 23. A proposed scheme of morphological transition of the fluorinated PMeOx$_{30}$-b-POctOx$_{20}$-C$_n$F$_{2n+1}$ nanoparticles (prepared by direct dissolution and by solvent exchange method) with increasing length of fluorinated fragment summarizing the SAXS and SANS results, where: 1- scheme of the inner structure of bilayered vesicle formed by PMeOx$_{30}$-b-POctOx$_{20}$ and PMeOx$_{30}$-b-POctOx$_{20}$-C$_{10}$F$_{21}$; 2 − scheme of the inner structure of worm-like micelle and core-shell-shell sphere formed by PMeOx$_{30}$-b-POctOx$_{20}$-C$_n$F$_{2n+1}$; 3 − scheme of the sphere with core-shell inner structure.

4.2. True triblock copolymers. Quest for fluorophilic monomer (Manuscript M3)

4.2.1. Fluorophilic monomers design

The next step of our research was the synthesis and investigation of triblock copolymers with polymerized fluorinated block (true triblock copolymers). As it was mentioned before, the polymerization of 2-perfluoroalkyl-2-oxazolines is associated with significant experimental difficulties (see Theoretical part, Section 1.3). The deceleration effect of perfluoroalkyl group could be decreased by distancing it from the 2-oxazoline ring using a carbohydrate spacer. To explore the spacer length effect on the polymerization activity three fluorine containing monomers were synthesized.

- I-effect of fluorine (arrows show shifting of electron density)

$\delta+ > \delta\delta+ > \delta\delta\delta+$
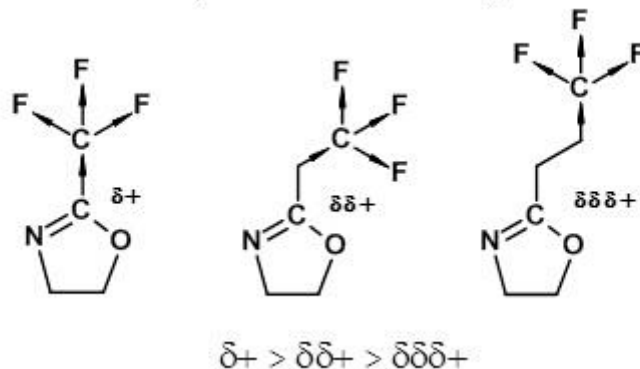
Figure 24. Structures of 2-oxazoline with directly attached CF₃-group and with spacers.

2-Trifluoromethyl-2-oxazoline was synthesized on the basis of a literature procedure.[81] According to this method *N*-(2-bromoethyl)trifluoroacetamide was obtained from ethyltrifluoroacetate by reaction with 2-bromoethylamine hydrobromide. The second step was ring-closure using sodium hydride as base yielding 2-trifluoromethyl-2-oxazoline (CF₃Ox).
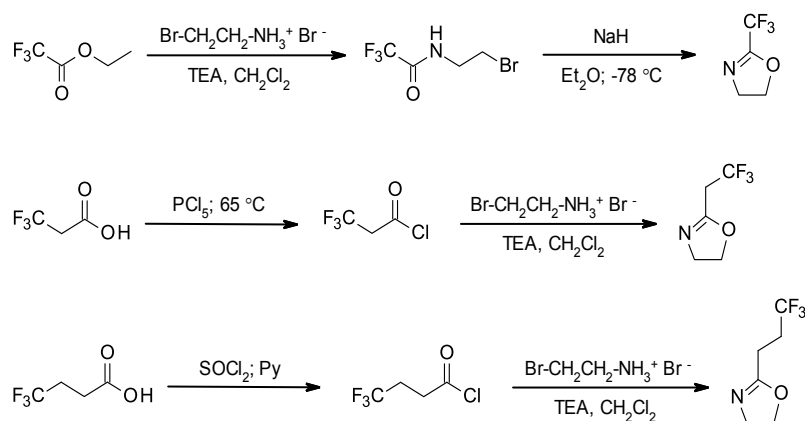
Scheme 2. Synthesis of the fluorinated 2-oxazoline monomers.

The synthesis of 2-(2,2,2-trifluoroethyl)-2-oxazoline (CF₃MeOx) and 2-(3,3,3-trifluoropropyl)-2-oxazoline (CF₃EtOx) was started from the corresponding carboxylic acids that were converted to the more reactive acid chloride. The amide formation was performed with 2-bromoethylamine in presence of excess of triethylamine, directly yielding the ring-closed 2-oxazoline monomers.

4.2.2. Kinetics of polymerization

The polymerization kinetics of the three monomers was studied at standard polymerization conditions of 140 °C in acetonitrile in a closed reaction vessel, at a monomer concentration of 1 M, with methyl *p*-toluenesulfonate (MeOTos) as initiator and a target degree of polymerization of 100.[82] The conversion of the monomer was determined by gas chromatography (GC), whereas molecular weights were analysed by size exclusion chromatography (SEC).

As it was expected, CF_3Ox revealed no noticeable conversion under these conditions after 24 hours. Variation of temperature (up to 180 °C when degradation occurs) and the use of another solvent/initiator system (dichlorobenzene/silver triflate + MeOTos) also gave no polymerization.

The polymerization of CF_3MeOx with a single methylene unit as spacer proceeds with acceptable rate and full monomer conversion was achieved after 2.5 hours under standard conditions (Figure 25a). However, the first order kinetic plot shows a continuous increase in slope indicative of slow initiation, *i.e.* during the polymerization more and more chains are initiated leading to faster monomer conversion, which can be ascribed to the low monomer nucleophilicity (Figure 25a). Due to this continuous initiation SEC revealed a very broad molar mass distribution that was not resolved from the system peak obstructing accurate integration (see Manuscript M3 Supporting information Figure S1).
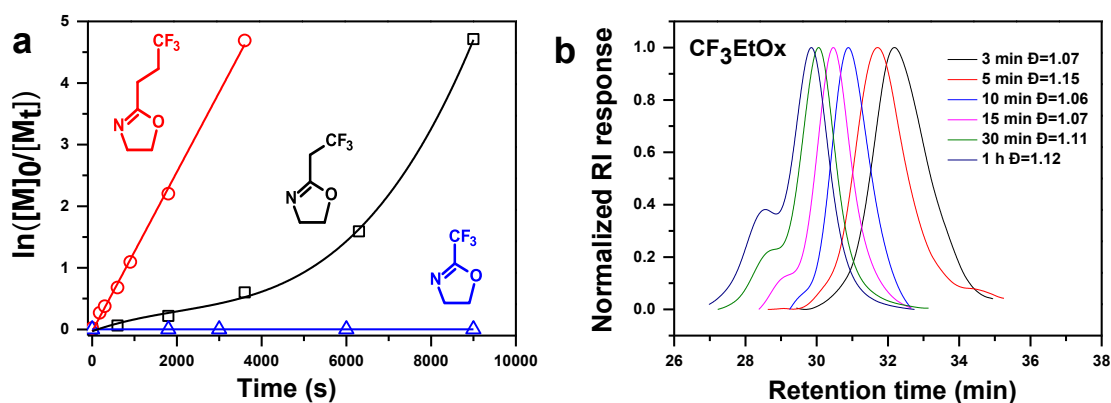
Figure 25. Kinetic plots for the cationic ring-opening polymerization (a) of CF_3Ox (blue), CF_3MeOx (black), CF_3EtOx (red), and the SEC data for CF_3EtOx (b). RI – Refractive Index.

Finally, the CF_3EtOx monomer with a double methylene spacer shows the linear first order kinetics, typical for living CROP (Figure 25a). The SEC traces at various conversions show a narrow molar mass distribution with dispersity (Đ) well below 1.2 (Figure 25b). The polymerization rate constant (k_p), calculated from the slope of the first order kinetic plot, was found to be $k_p = 129*10^{-3}$ L*mol^{-1}*s^{-1}, which is very similar to non-fluorinated 2-alkyl-2-oxazolines indicating that the electron-withdrawing effect of the CF_3-group on the 2-oxazoline ring is completely suppressed when introducing an ethyl spacer.[26] From these kinetic studies it can be concluded that only the CF_3EtOx is applicable for the synthesis of block copolymers.

4.2.3. Block copolymers synthesis and self-assembly studies

Next, we continued the preparation of a series of amphiphilic block copolymers by CROP with sequential monomer addition. More specifically, diblock copolymers were prepared by first polymerizing MeOx up to >98% conversion followed by addition of CF_3EtOx while triblock copolymers of MeOx, CF_3EtOx and 2-*n*-octyl-2-oxazoline were prepared by first polymerizing MeOx up to >98% conversion, followed by polymerization of the second monomer up to >98% conversion followed by addition of the third monomer and

polymerization up to >98% conversion. All polymerizations were terminated by the addition of 1 M KOH in methanol to the polymerization mixture. The structural details and characterization data of the synthesized diblock and triblock copolymers are summarized in Table 3 demonstrating that well defined polymers were obtained with $Đ$ < 1.4. Importantly, TB2 and TB3 have similar $Đ$ indicating that the order of addition of monomers does not make a difference, as anticipated based on their similar k_p.

Table 3. Characteristics of the synthesized block copolymers.

	Composition (NMR)	M_n, g/mol (SEC-MALS)	M_w, g/mol (SEC-MALS)	$Đ$ (SEC-MALS)	Monomer ratio (NMR)
DB1	$MeOx_{38}$-CF_3EtOx_{17}	6000	7200	1.20	2.2 : 1
DB2	$MeOx_{47}$-CF_3EtOx_{27}	8500	11000	1.30	1.7 : 1
DB3	$MeOx_{39}$-CF_3EtOx_{28}	7500	10300	1.37	1.4 : 1
DB4	$MeOx_{23}$-CF_3EtOx_{25}	6100	8100	1.33	0.9 : 1
TB1	$MeOx_{28}$-$OctOx_9$-CF_3EtOx_{12}	6300	8000	1.27	2.3 : 0.7 : 1
TB2	$MeOx_{49}$-$OctOx_{11}$-CF_3EtOx_{16}	9000	11800	1.31	3 : 0.7 : 1
TB3	$OctOx_{12}$-$MeOx_{52}$-CF_3EtOx_{18}	9700	13500	1.39	2.8 : 1 : 0.65

The aqueous solutions of block copolymers were prepared by using a solvent exchange method from methanol to water by dialysis. A DLS study of the obtained aqueous solutions of DB1-DB4 diblock copolymers revealed the presence of particles with hydrodynamic diameters in the range of 17-25 nm, attributed to micelles. The size of the aggregates resulting from the triblock copolymer is larger, up to 30-50 nm, and the appearance of a certain fraction of larger aggregates with a hydrodynamic diameter in the range of 150-300 nm was observed. In addition, the middle position of the hydrophilic block in the TB3 triblock caused the formation of larger aggregates compared to the same composition TB2 triblock with terminal hydrophilic block. On the cryo-TEM image of triblock TB1 (1 wt. %) (Figure 26), spherical aggregates with a mean diameter of 15 nm are observed representing the hydrophobic core of polymer micelles. A small population of large spherical objects was also found in the cryo-TEM image, which could correspond to the larger particles observed by DLS.
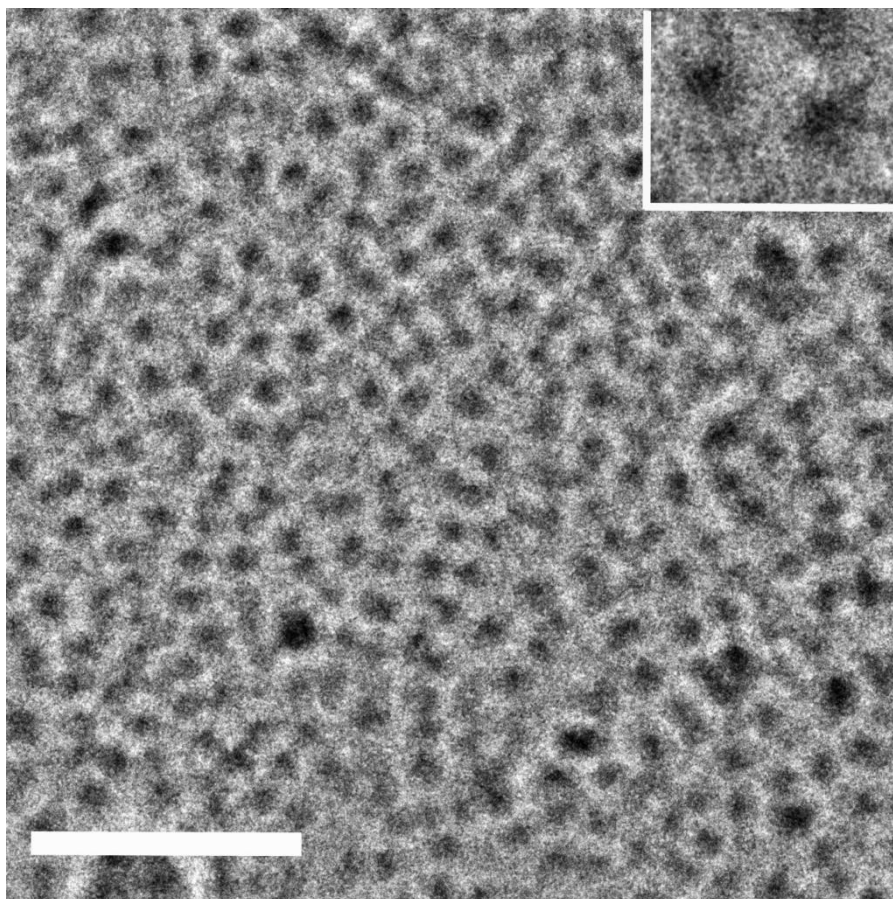
Figure 26. Cryo-TEM image micelles of triblock TB1. The scale bar equals 100 nm. The inset full width is 40 nm.

4.3. Poly-2-oxazoline triblock copolymers with highly fluorinated R_f^6EtOx (Manuscript M4)

4.3.1. Optimization of highly fluorinated monomer synthesis

Unlike to the used for the synthesis of CF$_3$EtOx 4,4,4-trifluorobutyl carboxylic acid, its analogues with longer perfluoroalkyl substituent are either not commercially available or very expensive. For this reason it was necessary to find an alternative procedure for the synthesis of highly fluorinated 2-oxazolines.

The applicability of several pathways for the synthesis of fluorophilic monomer was tested:

1) Witte–Seeliger synthesis of 2-oxazolines from nitriles[83] using 1H,1H,2H,2H-perfluorooctyl iodide

2) α-Deprotonation of 2-methyl-2-oxazoline (MeOx) + substitution reaction with an alkylbromide/iodide[84,85]

3) Wenker method of synthesis of 2-oxazolines from β-halo amides,[86] supplemented by the synthesis of 1H,1H,2H,2H-perfluorononanoic acid via Grignard reaction.

The first pathway was used before for the synthesis of fluorinated 2-oxazolines with a hydrocarbon spacer by Papadakis and co-workers. According to this procedure, the 2-oxazoline could be obtained by condensation between ethanolamine and fluorine containing nitrile, which was preliminarily obtained by a substitution reaction between 1H,1H,2H,2H-perfluoroalkyl iodide and sodium cyanide (Scheme 3). However, the corresponding nitrile was not obtained under the described conditions in case of 1H,1H,2H,2H-perfluorooctyl iodide. As the perfluoroalkyl chain length is extended compared to previous reports, the solubility of initial iodide and its derivatives is significantly reduced, which could complicate the synthesis.
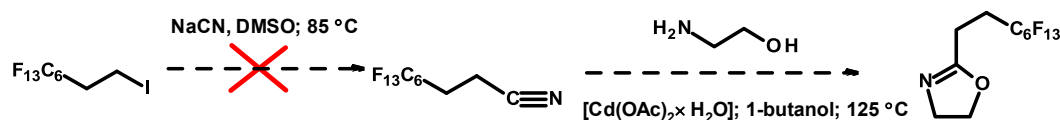
Scheme 3. Witte–Seeliger synthesis of 2-oxazolines.

The next try was one-step synthesis based on deprotonation of MeOx followed by a substitution reaction with an alkylbromide/iodide (Scheme 4).[30] According to this method, MeOx was deprotonated using n-butyllithium/tetramethylethylenediamine and the obtained carbanion then reacted with 1H,1H,2H,2H-perfluorooctylbromide to form 2-(1H,1H,2H,2H,3H,3H-perfluorononyl)-2-oxazoline. Unfortunately, the attempt to apply this procedure for the synthesis of fluorinated 2-oxazolines using 1H,1H,2H,2H-perfluorooctyl bromide failed. The usage of perfluorooctyl bromide and iodide made also no effect.
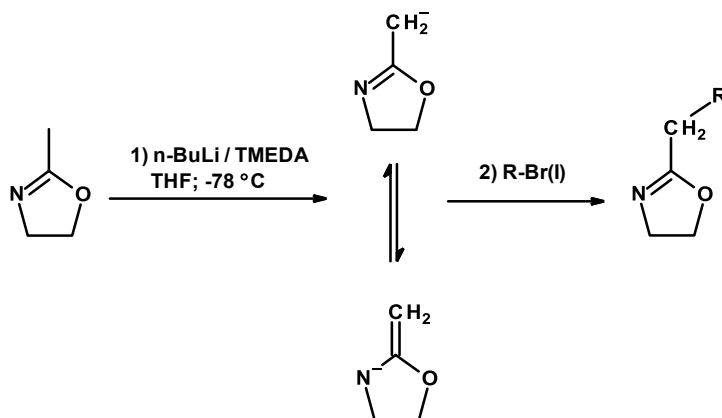
Scheme 4. Functionalization of 2-oxazolines by α-deprotonation of 2-methyl-2-oxazoline and imine-enamine equilibrium of the intermediate anion.

Our failure could be explained by the fact that the intermediate anion exists in the form of imine-enamine equilibrium (Scheme 4, middle). In case of soft leaving groups (according to HSAB theory), such as bromide or iodide, the substitution reaction via the α-position (imine form) is preferred. At the same time, the fluorine can act as a hard leaving group and the enamine form could be more active. The ^{1}H NMR specter of the product shows two peaks at 5.64 and 5.75 ppm, which could be attributed to enamine protons at double bond. However,

it could be concluded that this method is not applicable for functionalization of 2-oxazolines by fluorine containing alkyl bromides/iodides.

It was only the Wenker method that was successful for the synthesis of fluorophilic monomer. The appropriate carboxylic acid with -CH$_2$CH$_2$- spacer was synthesized by the reaction between 1H,1H,2H,2H-perfluorooctyl iodide and magnesium in a presence of iodine. The obtained Grignard reagent was treated with dry ice yielding target carboxylic acid with addition of iodide dimerization product (Scheme 5). The total yield of acid was 40-50 % which is in agreement with literature data.[87] Usage of 1H,1H,2H,2H-perfluorooctyl bromide decreases the amount of dimer and also increases the yield of the acid (up to 60 %).
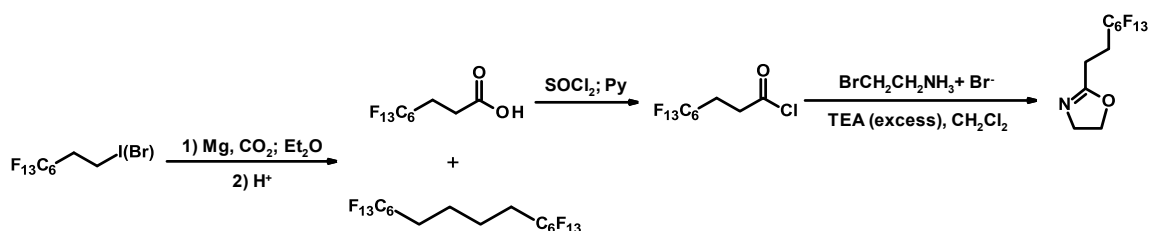
Scheme 5. Synthesis of 2-(1H,1H,2H,2H-perfluorooctyl)-2-oxazoline (R$_f^6$EtOx).

The obtained acid was converted to acid chloride by the reaction with thionyl chloride and then treated by 2-bromoethylamine hydrobromide in the presence of excess trimethylamine. The 2-(1H,1H,2H,2H-perfluorooctyl)-2-oxazoline (R$_f^6$EtOx) was isolated by distillation with total yield up to 50 % which is higher than that described by Jordan et al..[31] We conclude that Grignard reaction based procedure could be used as an alternative way for the synthesis of fluorine containing 2-oxazolines.

The polymerization kinetics of R$_f^6$EtOx was studied according to the standard procedure as it was described above for CF$_3$EtOx. The R$_f^6$EtOx monomer shows linear first order kinetics (Figure 27) and the k_p value calculated from the slope is $143*10^{-3}$ L*mol^{-1}*s^{-1}. The similarity of the k_p for R$_f^6$EtOx and CF$_3$EtOx (k_p=$129*10^{-3}$ L*mol^{-1}*s^{-1}) demonstrates that the length of the perfluoroalkyl substituent in 2-oxazolines with a double methylene spacer do not affect the k_p value.
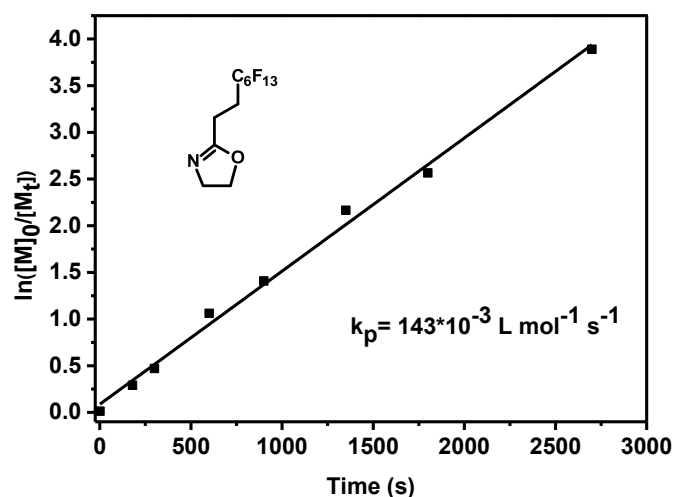
Figure 27. Kinetic plot for the cationic ring-opening polymerization of R_f^6EtOx (solvent – acetonitrile; monomer concentration - 1M; initiator – p-methyltoluenesulfonate (MeOTos); temperature – 140°C; targeted DP – 100).

4.3.2. Block copolymers synthesis

Having obtained the fluorinated monomer, we performed the synthesis of amphiphilic di- and triblock copolymers. 2-Methyl-2-oxazoline was used for the synthesis of hydrophilic block. The 2-*n*-octyl-2-oxazoline (OctOx) was chosen for hydrophobic block as nonfluorinated analogue of R_f^6EtOx.

To ensure water solubility of resulting copolymers, a high molar ratio of hydrophilic block was taken. Despite this, the wt. % of fluorophilic block in copolymer is quite high (due to high molecular weight of fluorophilic monomer (417 g/mol). With increasing of the fluorinated block length, the copolymers become insoluble even in methanol (polymers PD and PF), which could be attributed to high ability to crystallization of fluoroalkyl chains.

All polymers were characterized by SEC-MALS and ^{1}H NMR spectroscopy, and the results are presented in Table 4.

47

Table 4. Characteristics of synthesized poly-2-oxazolines.

	Composition (NMR)	M_n(SEC-MALS), g/mol	Đ (SEC-MALS)	Blocks ratio	
				mol. %	wt. %
P1	$MeOx_{55}$- $R_f^6EtOx_6$	7200	1.36	91 : 9	65 : 35
P2	$MeOx_{43}$- $R_f^6EtOx_5$	5700	1.34	89 : 11	63 : 37
P3	$MeOx_{38}$- $R_f^6EtOx_5$	5400	1.28	88 : 12	60 : 40
PD	$MeOx_{60}$- $R_f^6EtOx_{10}$*	-	-	85 : 15	55 : 45
PF	$MeOx_{40}$- $R_f^6EtOx_{10}$*	-	-	80 : 20	45 : 55
P4	$MeOx_{45}$-$OctOx_4$- $R_f^6EtOx_4$	5600	1.35	86 : 7 : 7	61 : 12 : 27
P5	$OctOx_7$-$MeOx_{41}$- $R_f^6EtOx_4$	6400	1.4	13 : 79 : 8	20 : 55 : 25
P6	$MeOx_{55}$-$OctOx_5$- $R_f^6EtOx_4$	7300	1.23	86 : 8 : 6	65 : 12 : 23

The proposed block ratios in polymers PD and PF was calculated from the initial monomer ratio.

4.3.3. Self-assembly study

Similarly to other obtained fluorine-containing poly-2-oxazolines, the copolymers P1-P6 were found to be molecularly dissolved in several solvents including methanol, ethanol, chloroform. The aqueous solutions were prepared using solvent exchange method and direct dissolving of copolymers in water.

The solutions of diblock copolymers prepared by solvent exchange contain mainly small particles of hydrodynamic diameter D_h of 20-40 nm with a minor fraction of large aggregates (see manuscript M4 Supporting Information Figure S3).

The preparation method has some impact on the fraction of large aggregates. The distribution functions for all diblock copolymers obtained by direct dissolving represent higher content of particles with mean D_h value of 150-300 nm. To have a deeper insight about each fraction observed by DLS study, Cryo-TEM experiments were conducted. The Cryo-TEM images of P2 copolymer in water show that the diameter of polymersomes depends on the preparation method (Figure 28 A and B).
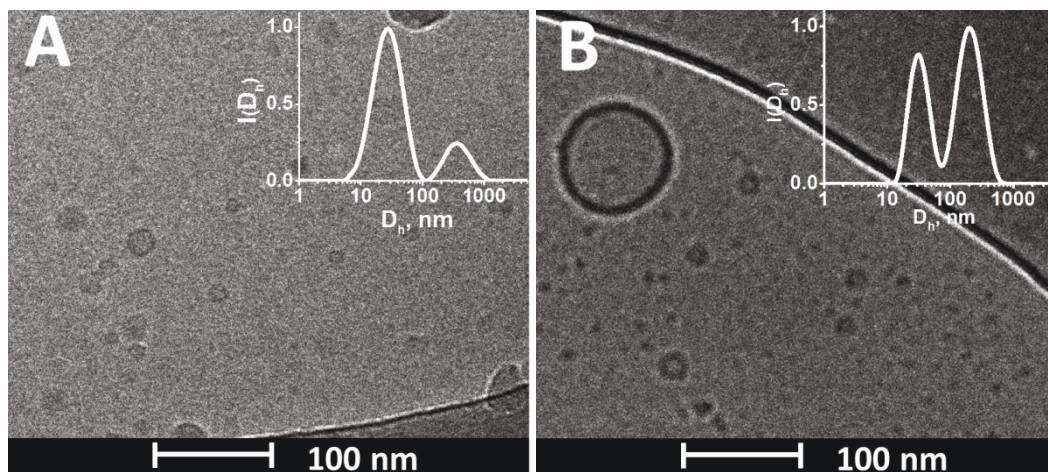
Figure 28. Cryo-TEM images of polymersomes in aqueos solutions of P2 (A – solvent exchange method, B – direct dissolving). The insets are DLS distribution functions of D_h for respective aqueous solutions.

Distribution functions for all three triblock copolymers in water prepared by solvent exchange method show one peak of approximately similar D_h value of 30 nm. The Cryo-TEM study of P4 and P5 confirms the presence of spherical micelles with diameter about 20 nm (Figure 29). At the same time, the presence of polymersomes in aqueous solution of triblock copolymers was not observed. It could be explained by the immiscibility of lipophilic and fluorophilic blocks, which makes the formation of complex hydrophobic polymersome layer (lipophilic-fluorophilic-lipophilic) thermodynamically unfavorable at a given blocks length, similarly like it was observed above for quasi-triblock copolymers.
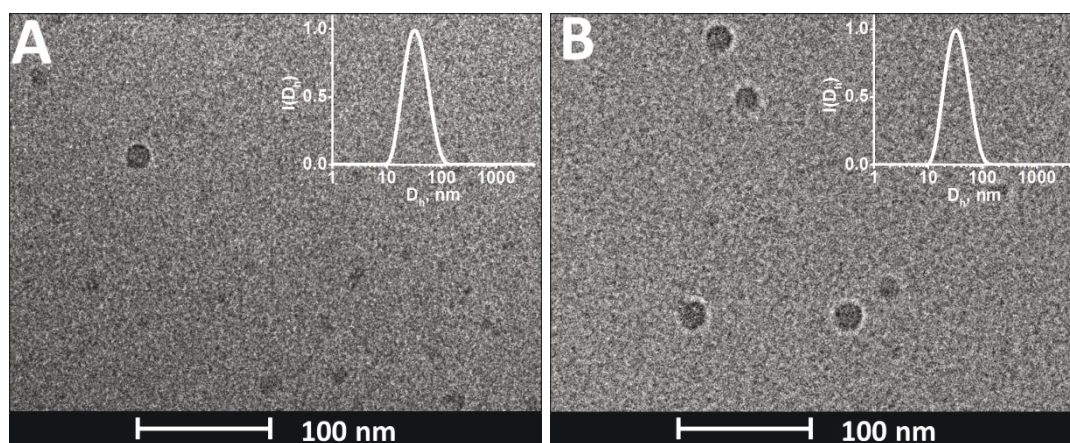
Figure 29. Cryo-TEM images of micelles formed by triblock copolymers P4 (A) and P5 (B) in aqueous solutions (solvent exchange). The insets are DLS distribution functions of D_h for respective aqueous solutions.

Although the obtained copolymers are molecularly soluble in a number of solvents, their self-assembly in non-aqueous solvents could be expected as well. It is known that polymers solubility is affected by many factors and it is essential to use a parameter that takes into account the contribution of different origin. For that reason the Hansen solubility

parameters were chosen. The total of Hansen solubility parameter δ_{total} consists of three components:

$$\delta_{\text{total}} = \sqrt{\delta_{\text{d}}^2 + \delta_{\text{p}}^2 + \delta_{\text{h}}^2} \tag{14}$$

where δ_{d}, δ_{p} and δ_{h} are components related to dispersion interactions, polarity and hydrogen bonding, respectively.[88] The Table 5 represents the literature data on Hansen parameters[88] for the solvents used in our study and the solution behavior of obtained copolymers. One can see that water has the highest value of δ_{p} and it could be hypothesized that self-assembly could be observed in solvent with polarity comparable to water.

Table 5. The solution behavior of di- and triblock copolymers (determined by DLS) and Hansen solubility parameters of respective solvents.

Solvent	Hansen solubility parameters				Behavior
	δ_{total}	δ_{d}	δ_{p}	δ_{h}	
Diethyl ether	15,40	14,50	2,90	4,60	Insoluble
Chloroform	18,70	17,80	3,10	5,70	Molecularly dissolved
Methylene chloride	20,20	17,00	7,30	7,10	Molecularly dissolved
Ethyl alcohol	26,20	15,80	8,80	19,40	Molecularly dissolved
Methyl alcohol	29,70	14,70	12,30	22,30	Molecularly dissolved
Water	48,00	15,50	16,00	42,30	Self-assembly

The additional DLS study of 10 mg/mL polymer solutions prepared via direct dissolving in a number of solvents was carried out (for the full list of used solvents see Manuscript M4 Supporting Information Table S1). It was found that the copolymers P1-P6 are molecularly soluble in solvents with the δ_{p} value below 14. At the same time, the DLS study of di- and triblock copolymers solutions in dimethyl sulphoxide (DMSO, δ_{p}=16.4) demonstrates unimodal distributions with a mean D_h value in a range of 150-200 nm (see Supporting Information Figure S4). This observation gives indirect support of our hypothesis that the polar contribution of Hansen solubility parameter is a keystone that controls the self-assembly of fluorinated polyoxazoline copolymers.

3.3 Nanoparticle morphology

Small Angle Neutron Scattering (SANS) in pure D$_2$O and DMSO-d6 was used to probe the nanoparticles architecture and determine their molecular parameters.
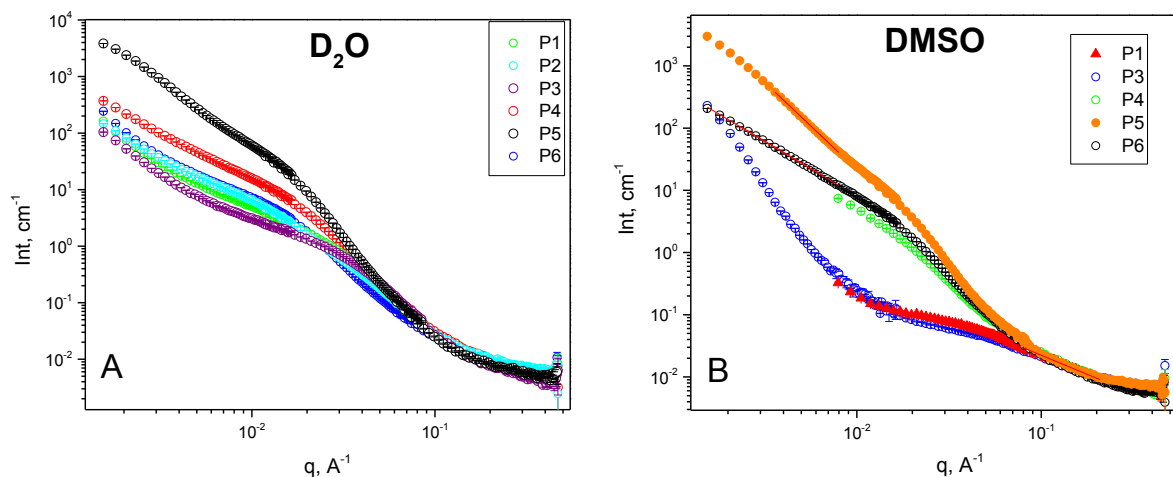
Figure 30. SANS curves for polymers P1-P6 in D₂O (A) and DMSO-d6 (B).

The scattering curves obtained for the D$_2$O solutions demonstrate similar shape (Figure 30 A) and can be well fitted with the "Sphere with attached Gaussian chain" model, assuming a Schulz-Zimm distribution for shell thickness σ (for the model description see Manuscript M4 chapter 2.4.6). Also, the contribution of large aggregates was added as a background to take into account the presence of polymersomes and increase the fit quality. The calculated structural parameters are presented in Table 6.

Table 6. Comparison of structural parameters obtained from samples P1-P6 in D₂O.

	Composition	R_{core} (nm)	N_{agg}	Chain	
				R_g, nm	σ
P1	$MeOx_{55}\text{-}R_f^6EtOx_6$	3.4	61	6.4	0.61
P2	$MeOx_{43}\text{-}R_f^6EtOx_5$	4.2	79	8.3	0.47
P3	$MeOx_{38}\text{-}R_f^6EtOx_5$	3.0	54	6.1	0.74
P4	$MeOx_{45}\text{-}OctOx_4\text{-}R_f^6EtOx_4$	6.1	103	6.4	0.27
P5	$OctOx_7\text{-}MeOx_{41}\text{-}R_f^6EtOx_4$	-	-	-	-
P6	$MeOx_{55}\text{-}OctOx_5\text{-}R_f^6EtOx_4$	6.0	55	6.0	0.34

The obtained value of core radii and shell thicknesses are in the range of 10-12 nm, which is in agreement with observations in DLS measurements and cryo-TEM. Unfortunately, the overall correlation between diblock structure parameters and polymer composition cannot be followed, mainly because of high polydispersity of the hydrophilic shell. Nevertheless, the significant increase of the mean micellar core radius with introduction of hydrophobic block can be observed (from 3.5 to 6 nm). This fact proves the coexistence of the lipophilic and fluorophilic fragments in the core.

Unlike to aqueous solutions, the diblock copolymers were found to be molecularly dissolved in DMSO-d6 (Figure 30 B). The disagreement between SANS and DLS data where peaks with 100-200 nm were only present on a distribution function is explained by the high

sensitivity of DLS to the presence of large aggregates, which obstruct the small particles detection. The successful fitting for copolymers P1 and P3 in DMSO-d6 was achieved using "Generalised Gaussian coil" model (Table 7) with a contribution of the large aggregates as a background (for the model description see Manuscript M4 chapter 2.4.6). It could be concluded from the high value of Flory parameter ν that DMSO is a "good solvent" for these polymers. The ν values of 0.75 and 0.93 imply that macromolecules exist in highly extended conformation that could be explained by intrinsic rigidity of fluorinated block.

Table 7. The structural parameters obtained for diblock copolymers P1 and P3 in DMSO-d6 using "Generalised Gaussian coil" model.

	Composition	R_g, nm	ν
P1	$MeOx_{55}\text{-}R_f^6EtOx_6$	4.4	0.74 ± 0.02
P3	$MeOx_{38}\text{-}R_f^6EtOx_5$	8	0.93 ± 0.05

In contrast, the shape of SANS curves of triblock copolymers P4-P6 indicates the presence of aggregates. This fact makes hydrophobic POctOx block exclusively responsible for self-assembly in DMSO. The scattering data was well fitted using monodisperse "Sphere with attached Gaussian chains" model (Table 8).

Table 8. The structural parameters obtained for triblock copolymers P4, P5 and P6 in DMSO-d6 using "Sphere with attached Gaussian chains" model.

	Composition	R_{core}, nm	R_g, nm	N_{agg}
P4	$MeOx_{45}\text{-}OctOx_4\text{-}R_f^6EtOx_4$	6.3	3.4	37
P5	$OctOx_7\text{-}MeOx_{41}\text{-}R_f^6EtOx_4$	7.5	4.7	100
P6	$MeOx_{55}\text{-}OctOx_5\text{-}R_f^6EtOx_4$	7.5	6.2	69

The mean aggregates radii in DMSO is 20-26 nm, which is of the same range as for D_2O solutions. It also can be seen that the change in the location of the hydrophobic block affects the size of the aggregates and the aggregation number: the P5 copolymer with lipophilic block on the side forms larger aggregates in comparison with P4 copolymer of similar composition with lipophilic block in the middle. Such effect of the block order was previously observed only for aqueous solutions. Also, the core radii of P4 and P6 aggregates have similar values in D_2O and in DMSO-d6. This fact allows proposing that in DMSO-d6 the core is also composed of lipophilic and fluorophilic blocks, despite the affinity of the last one to DMSO. Such ordering could be explained by the strong interactions between alkyl fragments in lipophilic layer and small length of fluorophilic block.

5. SUMMARY

In the framework of thesis an in-depth study of fluorine-containing polymers based on 2-oxazolines was carried out, and the following results were obtained:

1) A simple method for the insertion of perfluorinated fragments into the polymer by termination with a perfluorinated carboxylic acid was proposed. The rather broad range of available perfluorocarboxylic acids allows us to easily vary the length of the fluorophilic fragment. A series of well-defined block copolymers based on 2-methyl-2-oxazoline and 2-octyl-2-oxazolines with terminal perfluorocarbon alkyl fragments was synthesized.

2) The effect of the fluoroalkyl chain length on the aqueous self-assembly behaviour of the copolymers was studied by dynamic light scattering and cryo-TEM.

The tendency for hydrophobic self-assembly of all of the copolymers being dominated by the hydrophobic POctOx chains without any significant influence on the fluoroalkyl terminal chain was shown. On the other hand, cryo-TEM revealed that the structures and shapes of the resulting self-assembled structures are controlled by the presence and length of the perfluorinated fragment. The presence of single and multi-layer vesicles and rod-like micelles was visualized in aqueous solutions, and by increasing the content of the fluorinated alkyl chain, the ratio of vesicles to rod-like micellar aggregates was shifted towards the latter, whereby the longest $C_{12}F_{25}$-chain led to the exclusive formation of rod-like micellar aggregates. This shift in the formed self-assembled structures is ascribed to the formation of a fluorinated phase inside the aggregates, increasing the rigidity of the structure, which suppresses bending and, thus, vesicle formation.

It was shown that the preparation method is of prime importance to controlling the self-assembly process as the polymers with fluoroalkyl fragments self-assembled into spherical micelles when prepared by solvent exchange instead of direct dissolution.

3) The in-depth evaluation of the internal structure of resulting nanoparticles was performed by a combination of small-angle X-ray scattering (SAXS) and small-angle neutron scattering (SANS) experiments and a comparison with cryo-TEM data.

Nanoparticles formed by the reference diblock $PMeOx_{30}$-b-$POctOx_{20}$ without fluorinated segment could be described by a bilayered vesicle form factor. SANS and SAXS experiments revealed the morphological transition of micelles from bilayered vesicles to worm-like micelles with increasing length of the perfluorinated fragment of the quasi-triblock PAOx.

Additional ordering was identified within the inner layer of bilayered vesicles, the core of wormlike micelles as well as inside of the core of spheres, probably due to the crystallization of the POctOx and perfluorinated segments, and was described with a Voigt peak model.

It was further found that the preparation method influences the nanoparticles shape and internal structure: with solvent displacement it becomes independent of the fluorine content and the SAXS curves could be fitted with a core-shell-shell form factor.

5) A systematic study of the insertion of a spacer between the fluorinated fragment and the 2-oxazoline ring was reported revealing its effect on the monomer reactivity in CROP. Two new fluorinated 2-oxazoline monomers, namely CF$_3$MeOx and CF$_3$EtOx, were synthesized and characterized. The kinetic study showed a gradual increase of monomer reactivity in CROP with insertion of methylene spacers between the trifluoromethyl group and the 2-oxazoline ring. Insertion of two methylene groups allows complete suppression of the electron-withdrawing effect of the trifluoromethyl group, yielding similar reactivity as non-fluorinated 2-alkyl-2-oxazolines.

A set of di- and triblock copolymers with MeOx as hydrophilic block and a CF$_3$EtOx based fluorophilic block with polydispersity in the range of 1.2-1.4 was synthesized. The self-assembly potential of the synthesized block copolymers in aqueous solution was demonstrated by DLS. Cryo-TEM revealed the presence of micelles in aqueous solution based on the triphilic triblock copolymers.

6) The novel route of the synthesis of 2-oxazolines based on Grignard reaction was suggested. According to this approach highly fluorinated 2-(1H,1H,2H,2H-perfluorooctyl)-2-oxazoline monomer was synthesized.

A series of di- and triblock copolymers based on 2-(1H,1H,2H,2H-perfluorooctyl)-2-oxazoline, 2-methyl-2-oxazoline and 2-n-octyl-2-oxazoline was synthesized. Well-defined copolymers with M$_n$ in the range of 5300-7300 and Đ in the range of 1.2-1.4 were obtained. DLS study revealed the ability of the synthesized copolymers to self-assemble in aqueous milieu and in DMSO. The presence of micelle-like aggregates and polymersomes in aqueous solutions was confirmed by cryo-TEM.

Further investigation of the nanoparticle morphologies was done by SANS revealing that the presence of both the POctOx and the PR$_f^6$EtOx blocks results in the formation of nanoparticles with a core-shell structure in aqueous solutions of both di- and triblock copolymers, whereas in DMSO the presence of the POctOx block is required for the self-assembly. It was also found that in DMSO the block order has an influence on the aggregate size and structure in the same way as it was observed for aqueous solutions.

6. REFERENCES

(1)   Hamley, I. W. The Physics of Block Copolymers. 1998, p 424.

(2)   Wyman, I. W.; Liu, G. Micellar Structures of Linear Triblock Terpolymers: Three Blocks but Many Possibilities. *Polym. (United Kingdom)* **2013**, *54* (8), 1950–1978 DOI: 10.1016/j.polymer.2012.12.079.

(3)   Bae, S. J.; Suh, J. M.; Sohn, Y. S.; Bae, Y. H.; Kim, S. W.; Jeong, B. Thermogelling Poly(Caprolactone- *b* -Ethylene Glycol- *b* -Caprolactone) Aqueous Solutions. *Macromolecules* **2005**, *38* (12), 5260–5265 DOI: 10.1021/ma050489m.

(4)   Li, F.; Li, S.; El Ghzaoui, A.; Nouailhas, H.; Zhuo, R. Synthesis and Gelation Properties of PEG-PLA-PEG Triblock Copolymers Obtained by Coupling Monohydroxylated PEG-PLA with Adipoyl Chloride. *Langmuir* **2007**, *23* (5), 2778–2783 DOI: 10.1021/la0629025.

(5)   Huynh, D. P.; Shim, W. S.; Kim, J. H.; Lee, D. S. PH/Temperature Sensitive Poly(Ethylene Glycol)-Based Biodegradable Polyester Block Copolymer Hydrogels. *Polymer (Guildf).* **2006**, *47* (23), 7918–7926 DOI: 10.1016/j.polymer.2006.09.021.

(6)   Viegas, T. X.; Bentley, M. D.; Harris, J. M.; Fang, Z.; Yoon, K.; Dizman, B.; Weimer, R.; Mero, A.; Pasut, G.; Veronese, F. M. Polyoxazoline: Chemistry, Properties, and Applications in Drug Delivery. *Bioconjug. Chem.* **2011**, *22* (5), 976–986 DOI: 10.1021/bc200049d.

(7)   Woodle, M. C.; Engbers, C. M.; Zalipsky, S. New Amphipatic Polymer-Lipid Conjugates Forming Long-Circulating Reticuloendothelial System-Evading Liposomes. *Bioconjug. Chem.* **1994**, *5* (6), 493–496 DOI: 10.1021/bc00030a001.

(8)   Hrubý, M.; Filippov, S. K.; Štěpánek, P. Smart Polymers in Drug Delivery Systems on Crossroads: Which Way Deserves Following? *Eur. Polym. J.* **2015**, *65*, 82–97 DOI: 10.1016/j.eurpolymj.2015.01.016.

(9)   Hoogenboom, R.; Schlaad, H. Bioinspired Poly(2-Oxazoline)S. *Polymers (Basel).* **2011**, *3* (4), 467–488 DOI: 10.3390/polym3010467.

(10)   Hoogenboom, R. Poly(2-Oxazoline)s: A Polymer Class with Numerous Potential Applications. *Angew. Chemie - Int. Ed.* **2009**, *48* (43), 7978–7994 DOI: 10.1002/anie.200901607.

(11)   Schlaad, H.; Diehl, C.; Gress, A.; Meyer, M.; Levent Demirel, A.; Nur, Y.; Bertin, A. Poly(2-Oxazoline)s as Smart Bioinspired Polymers. *Macromol. Rapid Commun.* **2010**, *31* (6), 511–525 DOI: 10.1002/marc.200900683.

(12)   Woodle, M. C.; Engbers, C. M.; Zalipsky, S. New Amphipatic Polymer—Lipid Conjugates Forming Long-Circulating Reticuloendothelial System-Evading Liposomes. *Bioconjug. Chem.* **1994**, *5* (6), 493–496 DOI: 10.1021/bc00030a001.

(13)   Zalipsky, S.; Hansen, C. B.; Oaks, J. M.; Allen, T. M. Evaluation of Blood Clearance Rates and Biodistribution of Poly(2-Oxazoline)-Grafted Liposomes§. *J. Pharm. Sci.* **1996**, *85* (2), 133–137 DOI: 10.1021/js9504043.

(14)   Luxenhofer, R.; Han, Y.; Schulz, A.; Tong, J.; He, Z.; Kabanov, A. V; Jordan, R. Poly (2-Oxazoline)s as Polymer Therapeutics. *Macromol. Rapid Commun.* **2012**, *33*, 1613–1631 DOI: 10.1002/marc.201200354.

(15)   Guillerm, B.; Darcos, V.; Lapinte, V.; Monge, S.; Coudane, J.; Robin, J.-J. Synthesis and Evaluation of Triazole-Linked Poly(ε-Caprolactone)-Graft-Poly(2-Methyl-2-Oxazoline) Copolymers as Potential Drug Carriers. *Chem. Commun. (Camb).* **2012**, *48* (23), 2879–2881 DOI: 10.1039/c2cc30191a.

(16)   Hruby, M.; Filippov, S. K.; Panek, J.; Novakova, M.; Mackova, H.; Kucka, J.; Vetvicka, D.; Ulbrich, K. Polyoxazoline Thermoresponsive Micelles as Radionuclide Delivery Systemsa. *Macromol. Biosci.* **2010**, *10* (8), 916–924 DOI: 10.1002/mabi.201000034.

(17)   Hsiue, G.-H.; Chiang, H.-Z.; Wang, C.-H.; Juang, T.-M. Nonviral Gene Carriers Based on Diblock Copolymers of Poly(2-Ethyl-2-Oxazoline) and Linear Polyethylenimine. *Bioconjug. Chem.* **2006**, *17* (3), 781–786 DOI: 10.1021/bc050317u.

(18)   Pidhatika, B.; Rodenstein, M.; Chen, Y.; Rakhmatullina, E.; Muhlebach, A.; Acikgoz, C.; Textor, M.; Konradi, R. Comparative Stability Studies of Poly(2-Methyl-2-Oxazoline) and Poly(Ethylene Glycol) Brush Coatings. *Biointerphases* **2012**, *7* (1), 1 DOI: 10.1007/s13758-011-0001-y.

(19)   Kagiya, T.; Maeda, T.; Fukui, K.; Narisawa, S. Ring Opening Polymerization Of 2-Substituted 2-Oxazolines. *Polym. Lett.* **1966**, *4*, 441–445 DOI: 10.1002/pol.1966.110040701.

(20)   Seeliger, W.; Aufderhaar, E.; Diepers, W.; Feinauer, R.; Nehring, R.; Thier, W.;

Hellmann, H. Recent Syntheses and Reactions of Cyclic Imidic Esters. *Angew. Chemie Int. Ed. English* **1966**, *5* (10), 875–888 DOI: 10.1002/anie.196608751.

(21)   Tomalia, D. A.; Sheetz, D. P. Homopolymerization of 2-Alkyl- and 2-Aryl-2-Oxazolines. *J. Polym. Sci. Part A-1 Polym. Chem.* **1966**, *4* (9), 2253–2265 DOI: 10.1002/pol.1966.150040919.

(22)   Levy, A.; Litt, M. Polymerization of Cyclic Imino Ethers. II. Oxazines. *J. Polym. Sci. Part B Polym. Lett.* **1967**, *5* (9), 881–886 DOI: 10.1002/pol.1967.110050928.

(23)   Verbraeken, B.; Monnery, B. D.; Lava, K.; Hoogenboom, R. The Chemistry of Poly(2-Oxazoline)S. *Eur. Polym. J.* **2017**, *88*, 451–469 DOI: 10.1016/j.eurpolymj.2016.11.016.

(24)   Wiesbrock, F.; Hoogenboom, R.; Abeln, C. H.; Schubert, U. S. Single-Mode Microwave Ovens as New Reaction Devices: Accelerating the Living Polymerization of 2-Ethyl-2-Oxazoline. *Macromol. Rapid Commun.* **2004**, *25* (22), 1895–1899 DOI: 10.1002/marc.200400369.

(25)   Wiesbrock, F.; Hoogenboom, R.; Schubert, U. S. Microwave-Assisted Polymer Synthesis: State-of-the-Art and Future Perspectives. *Macromol. Rapid Commun.* **2004**, *25* (20), 1739–1764 DOI: 10.1002/marc.200400313.

(26)   Hoogenboom, R.; Fijten, M. W. M.; Thijs, H. M. L.; van Lankvelt, B. M.; Schubert, U. S. Microwave-Assisted Synthesis and Properties of a Series of Poly(2-Alkyl-2-Oxazoline)S. *Des. Monomers Polym.* **2005**, *8* (6), 659–671 DOI: 10.1163/156855505774597704.

(27)   Fijten, M. W. M.; Haensch, C.; Lankvelt, B. M. V.; Hoogenboom, R.; Schubert, U. S. Clickable Poly(2-Oxazoline)s as Versatile Building Blocks. *Macromol. Chem. Phys.* **2008**, *209* (18), 1887–1895 DOI: 10.1002/macp.200800226.

(28)   Brissault, B.; Guis, C.; Cheradame, H. Kinetic Study of Poly(Ethylene Oxide-b-2-Methyl-2-Oxazoline) Diblocs Synthesis from Poly(Ethylene Oxide) Macroinitiators. *Eur. Polym. J.* **2002**, *38* (2), 219–228 DOI: 10.1016/S0014-3057(01)00157-4.

(29)   Zahoranová, A.; Mrlík, M.; Tomanová, K.; Kronek, J.; Luxenhofer, R. ABA and BAB Triblock Copolymers Based on 2-Methyl-2-Oxazoline and 2-n-Propyl-2-Oxazoline: Synthesis and Thermoresponsive Behavior in Water. *Macromol. Chem. Phys.* **2017**, *1700031*, 1–12 DOI: 10.1002/macp.201700031.

(30) Taubmann, C.; Luxenhofer, R.; Cesana, S.; Jordan, R. First Aldehyde-Functionalized Poly(2-Oxazoline)s for Chemoselective Ligation. *Macromol. Biosci.* **2005**, *5* (7), 603–612 DOI: 10.1002/mabi.200500059.

(31) Ivanova, R.; Komenda, T.; Bonné, T. B.; Lüdtke, K.; Mortensen, K.; Pranzas, P. K.; Jordan, R.; Papadakis, C. M. Micellar Structures of Hydrophilic/Lipophilic and Hydrophilic/Fluorophilic Poly(2-Oxazoline) Diblock Copolymers in Water. *Macromol. Chem. Phys.* **2008**, *209* (21), 2248–2258 DOI: 10.1002/macp.200800232.

(32) Deslongchamps, P.; Dubé, S.; Lebreux, C.; Patterson, D. R.; Taillefer, R. J. The Hydrolysis of Imidate Salts. Stereoelectronic Control in the Cleavage of the Hemiorthoamide Tetrahedral Intermediate. *Can. J. Chem.* **1975**, *53* (18), 2791–2807 DOI: 10.1139/v75-394.

(33) Kobayashi, S.; Igarashi, T.; Moriuchi, Y.; Saegusa, T. Block Copolymers from Cyclic Imino Ethers: A New Class of Nonionic Polymer Surfactant. *Macromolecules* **1986**, *19* (3), 535–541 DOI: 10.1021/ma00157a006.

(34) De La Rosa, V. R. Poly(2-Oxazoline)s as Materials for Biomedical Applications. *J. Mater. Sci. Mater. Med.* **2014**, *25* (5), 1211–1225 DOI: 10.1007/s10856-013-5034-y.

(35) Luxenhofer, R.; Schulz, A.; Roques, C.; Li, S.; Bronich, T. K.; Batrakova, E. V.; Jordan, R.; Kabanov, A. V. Doubly Amphiphilic Poly(2-Oxazoline)s as High-Capacity Delivery Systems for Hydrophobic Drugs. *Biomaterials* **2010**, *31* (18), 4972–4979 DOI: 10.1016/j.biomaterials.2010.02.057.

(36) Binder, W. H.; Gruber, H. Block Copolymers Derived from Photoreactive 2-Oxazolines, 1 - Synthesis and Micellization Behavior. *Macromol. Chem. Phys.* **2000**, *201* (9), 949–957 DOI: 10.1002/1521-3935(20000601)201:9<949::AID-MACP949>3.0.CO;2-0.

(37) Lambermont-Thijs, H. M. L.; Hoogenboom, R.; Fustin, C.-A.; Bomal-D'Haese, C.; Gohy, J.-F.; Schubert, U. S. Solubility Behavior of Amphiphilic Block and Random Copolymers Based on 2-Ethyl-2-Oxazoline and 2-Nonyl-2-Oxazoline in Binary Water-Ethanol Mixtures. *J. Polym. Sci. Part A Polym. Chem.* **2009**, *47* (2), 515–522 DOI: 10.1002/pola.23168.

(38) Hoogenboom, R.; Wiesbrock, F.; Huang, H.; Leenen, M. A. M.; Thijs, H. M. L.; Van Nispen, S. F. G. M.; Van Der Loop, M.; Fustin, C. A.; Jonas, A. M.; Gohy, J. F.;

Schubert, U. S. Microwave-Assisted Cationic Ring-Opening Polymerization of 2-Oxazolines: A Powerful Method for the Synthesis of Amphiphilic Triblock Copolymers. *Macromolecules* **2006**, *39* (14), 4719–4725 DOI: 10.1021/ma060952a.

(39) Hoogenboom, R.; Wiesbrock, F.; Leenen, M. A. M.; Thijs, H. M. L.; Huang, H.; Fustin, C. A.; Guillet, P.; Gohy, J. F.; Schubert, U. S. Synthesis and Aqueous Micellization of Amphiphilic Tetrablock Terand Quarterpoly(2-Oxazoline)S. *Macromolecules* **2007**, *40* (8), 2837–2843 DOI: 10.1021/ma062725e.

(40) Jin, R. H. Controlled Location of Porphyrin in Aqueous Micelles Self-Assembled from Porphyrin Centered Amphiphilic Star Poly(Oxazolines). *Adv. Mater.* **2002**, *14* (12), 889–892 DOI: 10.1002/1521-4095(20020618)14:12<889::AID-ADMA889>3.0.CO;2-6.

(41) Volet, G.; Chanthavong, V.; Wintgens, V.; Amiel, C. Synthesis of Monoalkyl End-Capped Poly (2-Methyl-2-Oxazoline) and Its Micelle Formation in Aqueous Solution. *Macromolecules* **2005**, *38* (12), 5190–5197 DOI: 10.1021/ma050407u.

(42) Obeid, R.; Maltseva, E.; Thünemann, A. F.; Tanaka, F.; Winnik, F. M. Temperature Response of Self-Assembled Micelles of Telechelic Hydrophobically Modified Poly(2-Alkyl-2-Oxazoline)s in Water. *Macromolecules* **2009**, *42* (6), 2204–2214 DOI: 10.1021/ma802592f.

(43) Filippov, S. K.; Bogomolova, A.; Kaberov, L.; Velychkivska, N.; Starovoytova, L.; Cernochova, Z.; Rogers, S. E.; Lau, W. M.; Khutoryanskiy, V. V.; Cook, M. T. Internal Nanoparticle Structure of Temperature-Responsive Self-Assembled PNIPAM-b-PEG-b-PNIPAM Triblock Copolymers in Aqueous Solutions: NMR, SANS, and Light Scattering Studies. *Langmuir* **2016**, *32* (21), 5314–5323 DOI: 10.1021/acs.langmuir.6b00284.

(44) Filippov, S. K.; Verbraeken, B.; Konarev, P. V.; Svergun, D. I.; Angelov, B.; Vishnevetskaya, N. S.; Papadakis, C. M.; Rogers, S.; Radulescu, A.; Courtin, T.; Martins, J. C.; Starovoytova, L.; Hruby, M.; Stepanek, P.; Kravchenko, V. S.; Potemkin, I. I.; Hoogenboom, R. Block and Gradient Copoly(2-Oxazoline) Micelles: Strikingly Different on the Inside. *J. Phys. Chem. Lett.* **2017**, *8* (16), 3800–3804 DOI: 10.1021/acs.jpclett.7b01588.

(45) Vishnevetskaya, N. S.; Hildebrand, V.; Niebuur, B.-J.; Grillo, I.; Filippov, S. K.; Laschewsky, A.; Müller-Buschbaum, P.; Papadakis, C. M. Aggregation Behavior of

Doubly Thermoresponsive Polysulfobetaine- b -Poly(N -Isopropylacrylamide) Diblock Copolymers. *Macromolecules* **2016**, *49* (17), 6655–6668 DOI: 10.1021/acs.macromol.6b01186.

(46)   Vishnevetskaya, N. S.; Hildebrand, V.; Niebuur, B.-J.; Grillo, I.; Filippov, S. K.; Laschewsky, A.; Müller-Buschbaum, P.; Papadakis, C. M. "Schizophrenic" Micelles from Doubly Thermoresponsive Polysulfobetaine- b -Poly(N -Isopropylmethacrylamide) Diblock Copolymers. *Macromolecules* **2017**, *50* (10), 3985–3999 DOI: 10.1021/acs.macromol.7b00356.

(47)   Cook, M. T.; Filippov, S. K.; Khutoryanskiy, V. V. Synthesis and Solution Properties of a Temperature-Responsive PNIPAM–b-PDMS–b-PNIPAM Triblock Copolymer. *Colloid Polym. Sci.* **2017**, *295* (8), 1351–1358 DOI: 10.1007/s00396-017-4084-y.

(48)   Lowe, K. C. Fluorinated Blood Substitutes and Oxygen Carriers. *J. Fluor. Chem.* **2001**, *109* (1), 59–65 DOI: 10.1016/S0022-1139(01)00374-8.

(49)   Liu, W.; Frank, J. A. Detection and Quantification of Magnetically Labeled Cells by Cellular MRI. *Eur. J. Radiol.* **2009**, *70* (2), 258–264 DOI: 10.1016/j.ejrad.2008.09.021.

(50)   Boehm-Sturm, P.; Mengler, L.; Wecker, S.; Hoehn, M.; Kallur, T. In Vivo Tracking of Human Neural Stem Cells with 19F Magnetic Resonance Imaging. *PLoS One* **2011**, *6* (12) DOI: 10.1371/journal.pone.0029040.

(51)   Srinivas, M.; Heerschap, A.; Ahrens, E. T.; Figdor, C. G.; de Vries, I. J. M. 19F MRI for Quantitative in Vivo Cell Tracking. *Trends Biotechnol.* **2010**, *28* (7), 363–370 DOI: 10.1016/j.tibtech.2010.04.002.

(52)   Krafft, M. P.; Riess, J. G. Chemistry, Physical Chemistry, and Uses of Molecular Fluorocarbon- Hydrocarbon Diblocks, Triblocks, and Related Compounds-Unique "Apolar" Components for Self-Assembled Colloid and Interface Engineering. *Chem. Rev.* **2009**, *109* (5), 1714–1792 DOI: 10.1021/cr800260k.

(53)   Li, Z.; Kesselman, E.; Talmon, Y.; Hillmyer, M. A.; Lodge, T. P. Multicompartment Micelles from ABC Miktoarm Stars in Water. *Science (80-.).* **2004**, *306* (5693), 98–101 DOI: 10.1126/science.1103350.

(54)   Kubowicz, S.; Baussard, J. F.; Lutz, J. F.; Thünemann, A. F.; Von Berlepsch, H.; Laschewsky, A. Multicompartment Micelles Formed by Self-Assembly of Linear ABC Triblock Copolymers in Aqueous Medium. *Angew. Chemie - Int. Ed.* **2005**, *44* (33),

5262–5265 DOI: 10.1002/anie.200500584.

(55)   Kotzev, A.; Laschewsky, A.; Rakotoaly, R. H. Polymerizable Surfactants and Micellar Polymers Bearing Fluorocarbon Hydrophobic Chains Based on Styrene. *Macromol. Chem. Phys.* **2001**, *202* (17), 3257–3267 DOI: 10.1002/1521-3935(20011101)202:17<3257::AID-MACP3257>3.0.CO;2-P.

(56)   Berlepsch, H. V.; Böttcher, C.; Skrabania, K.; Laschewsky, A. Complex Domain Architecture of Multicompartment Micelles from a Linear ABC Triblock Copolymer Revealed by Cryogenic Electron Tomography. *Chem. Commun.* **2009**, No. 17, 2290 DOI: 10.1039/b903658j.

(57)   Laschewsky, A.; Marsat, J. N.; Skrabania, K.; Von Berlepsch, H.; Böttcher, C. Bioinspired Block Copolymers: Translating Structural Features from Proteins to Synthetic Polymers. *Macromol. Chem. Phys.* **2010**, *211* (2), 215–221 DOI: 10.1002/macp.200900378.

(58)   Skrabania, K.; Laschewsky, A.; Berlepsch, H. V.; Böttcher, C. Synthesis and Micellar Self-Assembly of Ternary Hydrophilic- Lipophilicfluorophilic Block Copolymers with a Linear PEO Chain. *Langmuir* **2009**, *25* (13), 7594–7601 DOI: 10.1021/la900253j.

(59)   Skrabania, K.; Berlepsch, H. V.; Böttcher, C.; Laschewsky, A. Synthesis of Ternary, Hydrophilic-Lipophilic-Fluorophilic Block Copolymers by Consecutive RAFT Polymerizations and Their Self-Assembly into Multicompartment Micelles. *Macromolecules* **2010**, *43* (1), 271–281 DOI: 10.1021/ma901913f.

(60)   Miyamoto, M.; Aoi, K.; Saegusa, T. Mechanisms of Ring-Qpening Polymerization of 2-(Perfluoroalkyl)-2-Oxazolines Initiated by Sulfonates: A Novel Covalent-Type Electrophilic Polymerization. *Macromolecules* **1988**, No. 21, 1880–1883.

(61)   Saegusa, T.; Chujo, Y.; Aoi, K.; Miyamoto, M. One-Shot Block Copolymerization. *Makromol. Chem., Macromol. Symp.* **1990**, No. 32, 1–10.

(62)   Miyamoto, M.; Aoi, K.; Saegusa, T. Novel Covalent-Type Electrophilic Polymerization of 2-(Perfluoroalkyl)-2-Oxazolines Initiated by Sulfonates. *Macromolecules* **1991**, *24* (1), 11–16 DOI: 10.1021/ma00001a002.

(63)   Lobert, M.; Köhn, U.; Hoogenboom, R.; Schubert, U. S. Synthesis and Microwave Assisted Polymerization of Fluorinated 2-Phenyl-2-Oxazolines: The Fastest 2-Oxazoline Monomer to Date. *Chem. Commun. (Camb).* **2008**, No. 12, 1458–1460 DOI:

10.1039/b717455a.

(64) Lobert, M.; Thijs, H. M. L.; Erdmenger, T.; Eckardt, R.; Ulbricht, C.; Hoogenboom, R.; Schubert, U. S. Synthesis, Microwave-Assisted Polymerization, and Polymer Properties of Fluorinated 2-Phenyl-2-Oxazolines: A Systematic Study. *Chem. - A Eur. J.* **2008**, *14* (33), 10396–10407 DOI: 10.1002/chem.200800671.

(65) Kempe, K.; Hoogenboom, R.; Hoeppener, S.; Fustin, C.-A.; Gohy, J.-F.; Schubert, U. S. Discovering New Block Terpolymer Micellar Morphologies. *Chem. Commun.* **2010**, *46* (35), 6455 DOI: 10.1039/c001629b.

(66) Brown, W. *Dynamic Light Scattering: The Method and Some Applications*; Oxford University Press, 1993.

(67) Linder, P.; Zemb, T. *Neutrons, X-Rays and Light: Scattering Methods Applied to Soft Condensed Matter*; Elsevier, 2002.

(68) Schnablegger, H.; Singh, Y. The SAXS Guide. *Ant. Paar* **2011**, 1–99.

(69) J. Kohlbrecher. User Guide for the SASfit Software Package SASfit : A Program for Fitting Simple Structural Models to Small Angle Scattering Data Joachim Kohlbrecher. **2013**, 1–420.

(70) Lepault, J.; Adrian, M.; Chang, J.-J.; Homo, J.-C.; Lepault, J.; McDowall, A. W.; Schultz, P. Cryoelectron Microscopy Of Vitrified Specimens - Study Of Rat Tail Tendon. *Q. Rev. Biophys.* **1988**, *2* (21), 129–228.

(71) Riess, G. Micellization of Block Copolymers. *Prog. Polym. Sci.* **2003**, *28* (7), 1107–1170 DOI: 10.1016/S0079-6700(03)00015-7.

(72) Mai, Y.; Eisenberg, A. Self-Assembly of Block Copolymers. *Chem. Soc. Rev.* **2012**, *41* (18), 5969 DOI: 10.1039/c2cs35115c.

(73) Pochan, D. J.; Chen, Z.; Cui, H.; Hales, K.; Qi, K.; Wooley, K. L. Toroidal Triblock Copolymer Assemblies. *Science (80-.).* **2004**, *306* (5693), 94–97 DOI: 10.1126/science.1102866.

(74) Fustin, C.-A.; Thijs-Lambermont, H. M. L.; Hoeppener, S.; Hoogenboom, R.; Schubert, U. S.; Gohy, J.-F. Multiple Micellar Morphologies from Tri- and Tetrablock Copoly(2-Oxazoline)s in Binary Water-Ethanol Mixtures. *J. Polym. Sci. Part A Polym. Chem.* **2010**, *48* (14), 3095–3102 DOI: 10.1002/pola.24089.

(75) Balzar, D.; Ledbetter, H. Voigt-Function Modeling in Fourier Analysis of Size- and Strain-Broadened X-Ray Diffraction Peaks. *J. Appl. Crystallogr.* **1993**, *26* (pt 1), 97–103 DOI: 10.1107/S0021889892008987.

(76) Wilson, L. M.; Griffin, A. C. Liquid Crystalline Fluorocarbon Side-Chain Polyesters. *Macromolecules* **1994**, *27* (7), 1928–1931 DOI: 10.1021/ma00085a041.

(77) Wilson, L. M.; Griffin, a. C. Liquid-Crystalline Behavior in a Series of Fluorocarbon Side-Chain Polyesters. 2. *Macromolecules* **1994**, *27* (16), 4611–4614 DOI: 10.1021/ma00094a027.

(78) Hirao, A.; Koide, G.; Sugiyama, K. Synthesis of Novel Well-Defined Chain-End- and in-Chain-Functionalized Polystyrenes with One, Two, Three, and Four Perfluorooctyl Groups and Their Surface Characterization. *Macromolecules* **2002**, *35* (20), 7642–7651 DOI: 10.1021/ma0203187.

(79) Volkov, V. V.; Platé, N. A.; Takahara, A.; Kajiyama, T.; Amaya, N.; Murata, Y. Aggregation State and Mesophase Structure of Comb-Shaped Polymers with Fluorocarbon Side Groups. *Polymer (Guildf).* **1992**, *33* (6), 1316–1320 DOI: 10.1016/0032-3861(92)90780-Z.

(80) *Small-Angle X-Ray Scattering*, Academic P.; Glatter, O., Kratky, O., Eds.; London, 1982.

(81) ISHIKAWA, N.; AKIRA, S. EP0151449 (A2) - Process for the Production of Fluorine Containing N-(Beta-Bromoethyl)Amide and of 2-(Perfluoroalkyl)-1,3-Oxazoline., 1985.

(82) Wiesbrock, F.; Hoogenboom, R.; Leenen, M. A. M.; Meier, M. A. R.; Schubert, U. S. Investigation of the Living Cationic Ring-Opening Polymerization of 2-Methyl-, 2-Ethyl-, 2-Nonyl-, and 2-Phenyl-2-Oxazoline in a Single-Mode Microwave Reactor. *Macromolecules* **2005**, *38* (12), 5025–5034 DOI: 10.1021/ma0474170.

(83) Witte, H.; Seeliger, W. Cyclische Imidsaureester Aus Nitrilen Und Aminoalkoholen. *Justus Liebigs Ann. Chem.* **1974**, *1974* (6), 996–1009 DOI: 10.1002/jlac.197419740615.

(84) Verbraeken, B.; Lava, K.; Hoogenboom, R. Poly (2-Oxazoline) S. *Encycl. Polym. Sci. Technol.* **2014**, No. 1, 1–51.

(85) Persigehl, P.; Jordan, R.; Nuyken, O. Functionalization of Amphiphilic Poly(2-

Oxazoline) Block Copolymers: A Novel Class of Macroligands for Micellar Catalysis. *Macromolecules* **2000**, *33* (19), 6977–6981 DOI: 10.1021/ma0007381.

(86) Wenker, H. The Synthesis of Δ2-Oxazolines and Δ2-Thiazolines from N-Acyl-2-Aminoethanols. *J. Am. Chem. Soc.* **1935**, *57* (6), 1079–1080 DOI: 10.1021/ja01309a034.

(87) Baker, R. J.; McCabe, T.; O'Brien, J. E.; Ogilvie, H. V. Thermomorphic Metal Scavengers: A Synthetic and Multinuclear NMR Study of Highly Fluorinated Ketones and Their Application in Heavy Metal Removal. *J. Fluor. Chem.* **2010**, *131* (5), 621–626 DOI: 10.1016/j.jfluchem.2010.02.004.

(88) Hansen, C. M. *Hansen Solubility Parameters A User's Handbook*; 2007.

APPENDIX

MANUSCRIPT M1

Kaberov L.I., Verbraeken B., Hruby M., Riabtseva A., Kovacik L., Kereïche S., Brus J., Stepanek P., Hoogenboom R., Filippov S.K.. Novel triphilic block copolymers based on poly(2-methyl-2-oxazoline)–*block*–poly(2-octyl-2-oxazoline) with different terminal perfluoroalkyl fragments: synthesis and self-assembly behaviour. *Eur. Polym. J.* **2017**, 88, 645–655. DOI: 10.1016/j.eurpolymj.2016.10.016.

Novel triphilic block copolymers based on poly(2-methyl-2-oxazoline)–*block*–poly(2-octyl-2-oxazoline) with different terminal perfluoroalkyl fragments: Synthesis and self-assembly behaviour

Leonid I. Kaberov [a], Bart Verbraeken [b], Martin Hruby [a], Anna Riabtseva [a], Lubomir Kovacik [c], Sami Kereïche [c], Jiri Brus [a], Petr Stepanek [a], Richard Hoogenboom [b], Sergey K. Filippov [a,*]

[a] Institute of Macromolecular Chemistry, Academy of Sciences of the Czech Republic, Heyrovský Sq. 2, 162 06 Prague 6, Czech Republic
[b] Supramolecular Chemistry Group, Department of Organic and Macromolecular Chemistry, Ghent University, Krijgslaan 281 S4, B-9000 Ghent, Belgium
[c] Charles University in Prague, First Faculty of Medicine, Institute of Cellular Biology and Pathology, Albertov 4, 12801 Prague 2, Czech Republic

A B S T R A C T

We report on the synthesis and solution properties of novel fluorine-containing copolymers. Our synthetic approach provides an easy way to attach a C_nF_{2n+1} perfluorinated terminal chain to a poly(2-methyl-2-oxazoline)–*block*–poly(2-octyl-2-oxazoline) copolymer and to combine hydrophilic, hydrophobic and fluorophilic moieties into one segmented polymer. A series of such quasi-triblock copolymers was prepared with variation of the length of the fluorinated chain end. Using a variety of experimental methods including dynamic light scattering and transmission cryo-electron microscopy, we prove that all of the synthesized copolymers self-assemble into nanostructures in aqueous milieu. The structures and shapes of the nanostructures are controlled by the length of the perfluoroalkyl chain. Single-layer and multi-layer vesicles as well as rod-like micelles are observed in aqueous solutions. The supramolecular structures described represent a potential platform for ^{19}F magnetic resonance imaging contrast agents.

© 2016 Elsevier Ltd. All rights reserved.

1. Introduction

Molecules composed of fragments with different natures are prospective substances for the formation of phase-separated materials with controlled properties. It was reported earlier that block copolymers based on hydrophilic and hydrophobic polymers are able to form self-assembled structures in aqueous solution. The morphology of these structures can be controlled by a number of factors: polymer composition, concentration, presence of additives and co-solvents, etc. [1,2]. Varying these parameters can lead to structures ranging from simple spherical and cylindrical micelles to more complex bicontinuous and bilayer (lamellae, vesicles) structures.

The main goal of contemporary research in this area is to develop combinations of different monomers, which enable the creation of a plethora of different self-assembled structures. The main criteria for such monomers are the simplicity of the synthesis, the ability to control polymerization with a narrow dispersity of the resulting polymers and the possibility for easy

---

* Corresponding author.
 E-mail address: filippov@imc.cas.cz (S.K. Filippov).

structure tuning. Poly(2-alkyl-2-oxazoline)s exhibit all of these characteristics, making them appealing candidates. It is known that poly(2-methyl-2-oxazoline) and poly(2-ethyl-2-oxazoline) exhibit "stealth" behaviour and possess excellent biocompatibility and non-immunogenicity, comparable with poly(ethylene oxide) [3,4], which could make them useful in medicine, for example, as nanocontainers for the targeted delivery of drugs [5–8]. It was shown that these polymers do not accumulate in body tissues [9–11].

Polymerization of 2-alkyl-2-oxazolines via the cationic ring-opening polymerization (CROP) mechanism was discovered in the 1960s [12–17]. This mechanism includes all of the common steps of chain-growth polymerization: initiation, propagation, and termination. In the absence of termination and chain transfer agents (first of all, moisture and other chain transfer inducing functional groups and impurities), the CROP of 2-oxazolines can proceed as living polymerization. The living CROP of 2-oxazolines is ideally suited for the preparation of amphiphilic block copolymers because both hydrophilic and hydrophobic poly(2-oxazoline)s are readily accessible by varying the side-chain substituent of the monomer [16] and block copolymers can be easily prepared by sequential addition of the second monomer after full conversion of the first monomer. Furthermore, functional groups can be introduced during initiation and termination [18]. For example, Binder and Gruber reported the synthesis of a series of block copolymers with poly(2-methyl-2-oxazoline) as the hydrophilic block combined with a variety of hydrophobic 2-oxazolines to form the hydrophobic block [19]. These amphiphilic copolymers self-assemble in aqueous solution, and with increasing molecular weight and mass fraction of the hydrophobic block, the size of the aggregates also increased. The insertion of long alkyl fragments by initiation and/or termination of the living CROP of 2-oxazolines also allows the preparation of amphiphilic structures that self-assemble into micelles. Volet and Amiel reported the self-assembly of poly(2-methyl-2-oxazoline)s synthesized with a lipophilic initiator [20]. Winnik et al. demonstrated the formation of micellar aggregates in aqueous solutions of a range of poly(2-ethyl-2-oxazoline)s and poly(2-isopropyl-2-oxazoline)s with terminal n-octadecyl chains and discussed their thermoresponsive behaviour [21]. Moreover, in studies of Tiller and co-workers, the antimicrobial activity of *N,N*-dimethyldodecylammonium-modified poly(2-oxazoline)s was shown [22].

Currently, considerable interest is paid to fluorinated substances. Perfluorohydrocarbons are components of many commercial intravascular oxygen carriers and tissue oxygenation fluids, such as Fluosol®, Perftoran®, Oxyfluor® [23], etc. One of the main upcoming applications of perfluorinated substances is as contrast agents in [19]F Magnetic Resonance Imaging (MRI). The ^{19}F atoms have 100% natural abundance, and their MR sensitivity is 83% that of ^{1}H atoms. Perfluorocarbons are immiscible with blood, but they could be injected as emulsions and since there are almost no endogenous fluorine atoms in body tissues (except bones and teeth) ^{19}F MRI allows imaging without significant background signal [24–26]. Perfluoroalkane chains are hydrophobic, but they are also lipophobic - alkanes and perfluoroalkanes are immiscible beginning from C_6. Moreover, perfluoroalkyl chains are much less flexible and polarizable in comparison to alkyl chains due to the larger fluorine atoms and high electron density, resulting in a greater ability to crystallize and form more ordered structures [27].

One can expect that the insertion of perfluorinated fragments into amphiphilic block copolymers will promote additional complexity and decrease critical micelle concentrations due to their strong hydrophobic character and immiscibility with hydrocarbon hydrophobic domains. Indeed, Laschewsky and co-workers reported that linear acrylic block copolymers with different side chains - hydrophilic, hydrophobic and fluorophilic - form micellar aggregates with complex phase-separated structure of the hydrophobic core in aqueous solution [28–30]. In the work of Hillmyer and Lodge, miktoarm star block copolymers with poly(ethylene oxide), polyethylene, and poly(perfluoropropylene oxide) arms were found to form multi-compartment micelles in dilute aqueous solution [31]. Depending on the relative lengths of the blocks, discrete multicompartment micelles or wormlike structures with segmented cores were observed.

The synthesis and polymerization of fluorinated 2-phenyl-2-oxazolines was studied in detail by Schubert et al. [32]. In later works, the synthesis of amphiphilic triblock poly(2-oxazoline)s with poly(2-(2,6-difluorophenyl)-2-oxazoline) fluorophilic block and the formation of multicompartment structures were demonstrated [33,34]. Jordan and co-workers reported the synthesis of amphiphilic block copolymers of 2-fluoroalkylethyl-2-oxazoline and 2-methyl-2-oxazoline [35]. It was shown by small-angle neutron scattering and TEM that these copolymers form elongated core–shell micelles in aqueous solution, which should be associated with the high stiffness and hydrophobicity of the perfluorinated chain. It was also shown that mixing this copolymer with a hydrophilic/lipophilic block copolymer leads to the coexistence of lyophilic and fluorophilic micelles rather than the formation of mixed micelles. Furthermore, Thünemann and colleagues reported the synthesis of poly(2-methyl-2-oxazoline) bearing a perfluoroalkyl chain at the α-terminus resulting from initiation and a regular alkyl chain at the ω-terminus resulting from end-capping [36]. It was demonstrated that these chain-end functionalized polymers self-assembled into cylindrical micelles, and it was speculated that the addition of a fluorinated dopant may lead to the formation of cylindrical micelles with a phase separated hydrophobic core.

In this study, we report the synthesis of poly(2-oxazoline) diblock copolymers with hydrophilic and hydrophobic blocks as well as terminal perfluoroalkyl chains of which the chain length is varied. We propose a simple method for the insertion of perfluorinated fragments into the polymer by termination with a perfluorinated carboxylic acid instead of making real triblock copolymers. The rather broad range of available perfluorocarboxylic acids allows us to easily vary the length of the fluorophilic fragment in contrast to polymerization of perfluorinated monomers. The effect of the fluoroalkyl chain length on the aqueous self-assembly behaviour of the copolymers was studied by a number of physico-chemical methods and will also be discussed.

2. Experimental section

2.1. Materials

2-Methyl-2-oxazoline (MeOx, 99%, Acros Organics) was dried over BaO and distilled before use. Triethylamine (TEA, >99%, Fisher Scientific) was dried over CaH$_2$ and distilled under reduced pressure. *n*-Nonanoic acid, 2-chloroethylamine hydrochloride, 18-crown-6 ether, thionyl chloride were purchased from Acros Organics and used as received. Perfluorinated acids (nonanoic, undecanoic, tridecanoic) and methyl tosylate were purchased from Sigma-Aldrich and used as received. Dichloromethane (DCM, Lachner) was dried by refluxing over phosphorus pentoxide and distilled before use. Tetrahydrofuran (THF, Lachner) was dried by refluxing over CaH$_2$ and distilled before use. Acetonitrile (ACN, Lachner) was dried by refluxing over BaO and distilled before use. Ethyl acetate (EtAc, Lachner) was dried over CaCl$_2$ and distilled before use. MilliQ water was prepared by MilliPore Milli-Q® Gradient installation. All other chemicals were used as received.

2.2. Synthesis of n-nonanoic acid chloride

n-Nonanoic acid (10 g, 0.063 mol) was dissolved in dry DCM (50 mL). The mixture was cooled down in an ice bath. After that, thionyl chloride (7 mL, 0.096 mol) was added dropwise. The mixture was stirred at 40 °C over night. Next, DCM and excess thionyl chloride were removed under reduced pressure. Yield = 11 g (98%). ^{1}H NMR (300 MHz, CDCl$_3$) δ 2.88 (t, *J* = 7.3 Hz, —**CH₂**—C(O)Cl, 2H), 1.69 (m, —**CH₂**—CH₂—C(O)Cl, 2H), 1.27 (m, CH$_3$(**CH₂**)$_5$—, 10H), 0.88 (t, *J* = 6.7 Hz, **CH₃**—, 3H).

2.3. Synthesis of n-(2-chloroethyl)nonyl amide

2-Chloroethylamine hydrochloride (11 g, 0.95 mol) was placed in a round-bottom flask. *n*-Nonanoic acid chloride (11 g, 0.057 mol) was dissolved in DCM (150 mL) and added to the same flask. The mixture was cooled in an ice bath. Then, triethylamine (30 mL, 0.216 mol) was added dropwise while stirring. The mixture was allowed to warm to room temperature and stirred overnight. The DCM was removed, and ethylacetate was added. The mixture was filtered to remove the triethylamine hydrochloride, and the filtrate was washed twice with 10% acetic acid solution, twice by saturated sodium bicarbonate, and twice by brine solution. The organic layer was dried over magnesium sulfate. Magnesium sulfate was filtered off, and the solvent was removed under reduced pressure, yielding the product as a white powder. Yield = 9.9 g (70%); ^{1}H NMR (300 MHz, CDCl$_3$) δ 6.04 (s (broad), —**NH**—CH₂—, 1H), 3.60 (m, —NH—**CH₂**—**CH₂**—Cl, 4H), 2.19 (m, —**CH₂**—C(O)—, 2H), 1.62 (m, —**CH₂**—CH₂—C(O)—, 2H), 1.25 (m, CH$_3$(**CH₂**)$_5$—, 10H), 0.86 (t, *J* = 6.7 Hz, **CH₃**—, 3H).

2.4. Synthesis of 2-(n-octyl)-2-oxazoline (OctOx)

N-(2-Chloroethyl)nonylamide (9.9 g, 0.045 mol) synthesized in the previous step was dissolved in dry THF (20 mL), and 18-crown-6 ether (0.595 g, 0.00225 mol) was added. The mixture was cooled in an ice bath and potassium hydroxide (7.56 g, 0.135 mol) was added. The mixture was allowed to warm to room temperature and stirred overnight. THF was removed under reduced pressure, and the residue was dispersed in water and extracted 3 times with DCM. The organic layers were combined and dried with magnesium sulfate. After filtration and removing the solvent under reduced pressure, the resulting oil was dried with barium oxide and distilled under reduced pressure yielding the product as a clear colourless liquid. Yield = 6.7 g (80%); T$_{boil}$ = 48 °C (0,9 mbar); ^{1}H NMR (300 MHz, CDCl$_3$) δ 4.22 (t, *C*—O—**CH₂**—CH₂—N═, 2H), 3.81(t, —C—O—**CH₂**—**CH₂**—N═, 2H), 2.26 (t, —**CH₂**—C(O)N—, 2H), 1.62 (m, —**CH₂**—CH₂—C(O)N—, 2H), 1.26 (m, CH$_3$(**CH₂**)$_5$—, 10H), 0.86 (t, *J* = 6.7 Hz, **CH₃**—, 3H).

2.5. Polymer synthesis

2-Methyl-2-oxazoline (0.204 g, 0.0024 mol) was dissolved in acetonitrile (6 mL), and methyl tosylate (0.015 g, 8 * 10^{-5} mol) was added as the initiator. The mixture was stirred 35 min at 140 °C in a pressure reactor. After cooling to room temperature, 2(*n*-octyl)-2-oxazoline (0.292 g, 0.0016 mol) was added, and the mixture was stirred again for 45 min at 140 °C. Next, a perfluorinated acid (perfluorononanoic acid C$_8$F$_{17}$COOH, perfluoroundecanoic acid C$_{10}$F$_{21}$COOH or perfluorotridecanoic acid C$_{12}$F$_{25}$COOH; 12 * 10^{-5} mol) and triethylamine (25 μl, 18 * 10^{-5} mol) were added after cooling the solution, and the resulting mixture was stirred at 70 °C overnight. A model diblock copolymer with terminal OH groups was also synthesized by quenching the polymerization via the addition of a 1 M KOH solution in MeOH. The polymer residue that was obtained after removing the solvent under reduced pressure was dissolved in DCM and washed with a NaCl solution (24 wt.%, 90% of saturated). The organic layer was dried over MgSO$_4$, and the solvent was evaporated. The residue was dispersed in ether and filtered, yielding the block copolymers.

2.6. Characterization techniques

2.6.1. Dynamic Light Scattering (DLS)
Dynamic Light Scattering (DLS) was performed to characterize the copolymers in dilute solutions. For this purpose, the hydrodynamic diameter of the particles, D_h, and the scattering intensity were measured at a scattering angle of θ = 173° with

a Zetasizer Nano-ZS instrument, model ZEN3600 (Malvern Instruments, UK). The DTS (Nano) program was used to evaluate the data. It provides intensity-, volume-, and number-weighted D_h distribution functions $I(D_h)$. The intensity-weighted value of the apparent D_h was chosen to characterize the dispersity of the solutions.

All solutions were prepared via the direct dissolution of the copolymers in water and via a solvent exchange method in which the polymer was molecularly dissolved in water and self-assembly was induced by dialysis against water.

2.6.2. SEC-MALS

Labio Biospher GMB100 7.5 mm × 300 mm, particle size 10 μm, size exclusion column, applicable in aqueous as well as in organic mobile phases, was used for the analysis of the poly(2-oxazoline)s using methanol as the mobile phase at 0.18 mL/min. The pump was a Shimadzu 20ADvp liquid chromatography pump (Shimadzu Corp, Kyoto, Japan). The vacuum degasser was a DeltaChrom TVD (Watrex, Prague, Czech Republic). The 40 mg/mL polymers solutions in methanol were injected manually using a six port PEEK injection valve equipped with a 50 μl sample loop (Upchurch Scientific, Oak Harbor, WA). A home made in-line 25 mm filter holder with a 0.02 μm Anodisc 25 membrane (Whatman, Maidstone, UK) was positioned between the pump and the injection valve.

The light scattering detector was a DAWN-DSP multi-angle light scattering instrument (Wyatt Technology, Santa Barbara, CA) and a Shodex RI-101 differential refractometer (Showa Denko, Japan) served as the concentration detector. The signals from the detectors were collected and analysed using ASTRA for Windows 4.50 software (Wyatt Technology, Santa Barbara, CA). The angular dependence of the scattered light intensity was found to be negligible for all samples.

The refractive index increment of the poly(2-oxazoline)s in methanol was determined using a Brookhaven BI-DNDC differential refractometer and BI-DNDCW software. The dn/dc values are presented in Table S1 (Supporting information).

It should be noted here that this two detector arrangement with both a DAWN-DSP light scattering unit as an absolute molecular weight detector and single RI detection SEC units does not require the use of polymer standards to determine the polymer molar mass and dispersity (Đ).

2.6.3. Critical micellar concentration (CMC) measurements

The pyrene fluorescence method was used for the determination of the CMCs of the polymers. A pyrene in water/ethanol (80 μM, 12.8 μl) solution was added to the polymer solutions over a wide concentration range ($3.81 \cdot 10^{-5}$–5 mg/mL) in water. The resulting solutions were stirred for 1 h. The fluorescence spectra were recorded using a fluorescence spectrometer (Jasco FP-6200, Japan) at an excitation wavelength of 332 nm and emission wavelengths of 373 and 384 nm. The intensity ratio I_{373}/I_{384} was calculated for each concentration, and the ratio was plotted as a function of the copolymer concentration in water. The CMC was determined at the intersection point (in the region of lower concentration) of the two regression lines.

2.6.4. Transmission Cryo-Electron Microscopy (Cryo-TEM)

Cryo-TEM measurements were carried out using a Tecnai G^{2}Sphera 20 electron microscope (FEI Company, Hillsboro, OR, USA) equipped with a Gatan 626 cryo-specimen holder (Gatan, Pleasanton, CA, USA) and a LaB$_6$ gun. The samples for cryo-TEM were prepared by plunge-freezing [37]. Briefly, 3 μL of the sample solution was applied to a copper electron microscopy grid covered with a perforated carbon film forming woven-mesh-like openings of different sizes and shapes (lacey carbon grids #LC-200 Cu, Electron Microscopy Sciences, Hatfield, PA, USA), glow discharged for 40 s with a current of 5 mA. Most of the sample was removed by blotting (Whatman No. 1 filter paper) for approximately 1 s, and the grid was immediately plunged into liquid ethane held at −183 °C. The grid was then transferred without rewarming into the microscope. Images were recorded at the accelerating voltage of 120 kV and with magnifications ranging from 11,500× to 50,000× using a Gatan UltraScan 1000 slow scan CCD camera in the low-dose imaging mode, with the electron dose not exceeding 1500 electrons per nm^2. The magnifications resulted in final pixel sizes ranging from 1 to 0.2 nm, and the typical value of the applied underfocus ranged between 0.5 and 2.5 μm. The applied blotting conditions resulted in the specimen thicknesses varying between 100 and ca. 300 nm. All cryo-TEM images were carefully inspected for possible artefacts such as radiation damage and ice crystals.

2.6.5. ^{19}F NMR Spectroscopy

The ^{19}F NMR spectra were measured at 11.7 T on a Bruker Avance III HD 500 US/WB NMR spectrometer (Karlsruhe, Germany, 2013) using a solid-state 4-mm CP/MAS probehead optimized for the measurement of ^{19}F nuclei. The Hahn-echo experiment was applied to suppress the probehead residual signal; the echo-delay was 10 ms; the duration of the 90°(^{19}F) pulse was 1.5 μs; the repetition delay was 2 s; and 512–1024 scans were accumulated for each spectrum. ^{19}F NMR chemical shift scale was calibrated using the PTFE the signal of which was set to −122 ppm. Chloroform was used as the solvent.

## 3. Results and discussion

3.1. Polymer synthesis

The hydrophobic 2-(n-octyl)-2-oxazoline (OctOx) monomer was synthesized via the well-known three-step synthesis method starting from the corresponding acid [17]. In the first step, n-nonanoic acid was first converted to n-nonanoic acid

chloride via reaction with thionyl chloride followed by reaction with (2-chloroethylamino) hydrochloride in the presence of trimethylamine as the base. Subsequent ring-closure to OctOx was performed in the presence of potassium hydroxide as the base and 18-crown-6 ether as the phase transfer catalyst under inert atmosphere (Scheme 1). Distillation over barium oxide yielded pure and dry OctOx for polymerization.

All polymers were synthesized via cationic ring-opening polymerization using methyl tosylate as the initiator. 2-Methyl-2-oxazoline and the initiator were dissolved in acetonitrile and stirred at 140 °C in a pressure reactor to form the first PMeOx block (Scheme 2). After cooling down the reaction mixture after the desired reaction time (35 min for ~98% of monomer
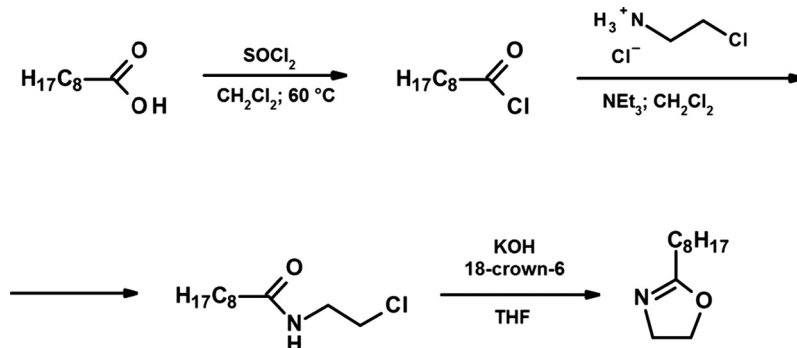
Scheme 1. Synthesis of 2-octyl-2-oxazoline.
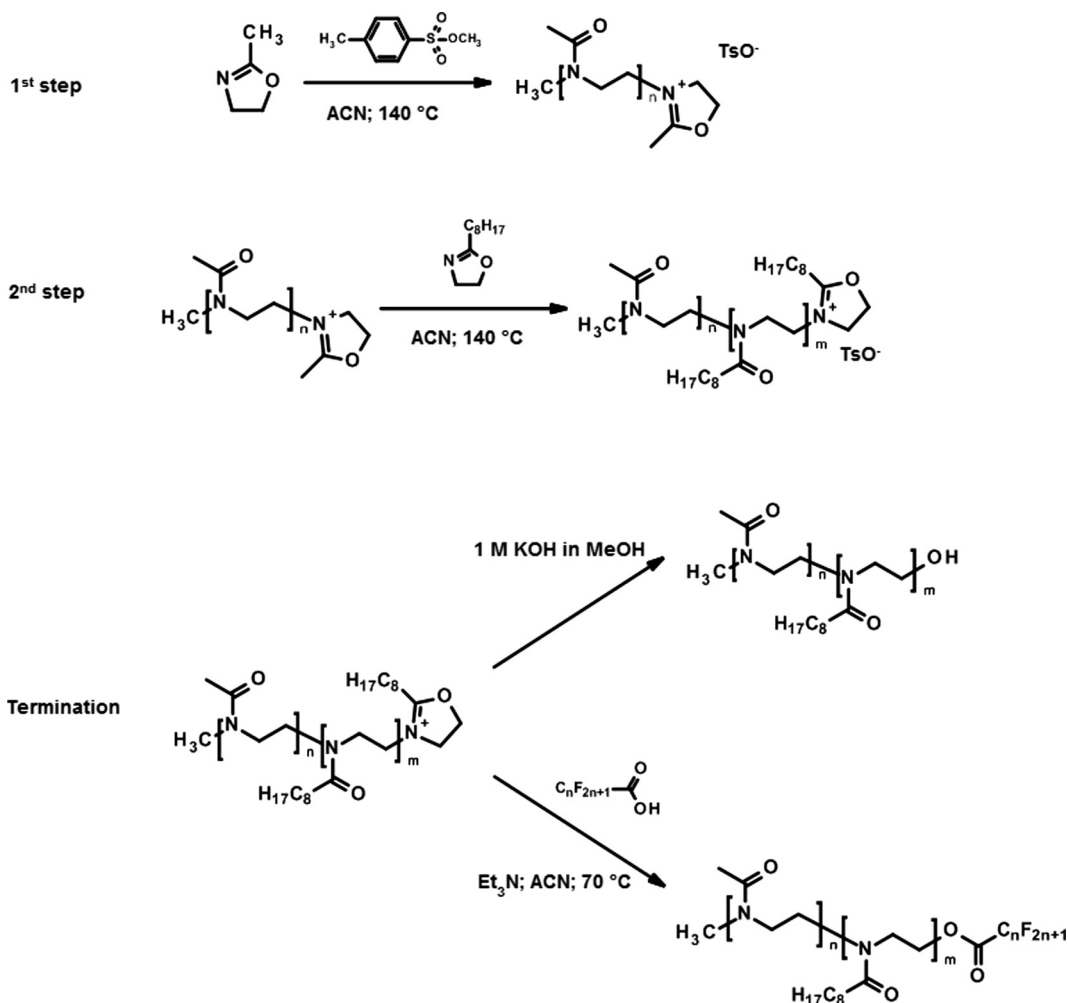
Scheme 2. Synthesis of di- and quasi-triblock copolymers.

conversion), the second OctOx monomer was added, and the mixture was stirred at 140 °C for another 45 min to form the PMEOx-*b*-POctOx block copolymer.

To attach the perfluorinated fragment, the living polymerization mixtures were terminated with different perfluorinated carboxylic acids in the presence of base (trimethylamine) at 70 °C [38]. In addition, we separately synthesized PMeOx-*b*-POctOx diblock copolymers with the same composition for comparative analysis. For this purpose, the polymerization was quenched with a 1 M KOH methanol solution (Scheme 2). ^{1}H NMR spectra of the polymers (Fig. 1) show the characteristic signals for protons belonging to the poly(2-oxazoline) backbone (a + b) as well as the signals from the methyl side chain of PMeOx (c) and the hydrophobic octyl side chain of POctOx (e, f, g, h). Moreover, there are signals from the initiating methyl group (d) as well as from the CH$_2$ group of the terminal 2-oxazoline repeat unit next to the ester group attached to the perfluorinated fragment (i). Unfortunately, it was not possible to quantify the end-group fidelity by ^{1}H NMR spectroscopy as the relative intensities of the signals vary in different solvents due to changes in the solvation and chain mobility of the poly(2-methyl-2-oxazoline) and the fluorinated alkyl tail.

To additionally prove the presence of the fluorinated moieties, ^{19}F NMR spectra were recorded. In the recorded ^{19}F NMR spectra, typical resonances of CF$_3$ and CF$_2$ units of perfluorinated substituents were clearly detected (Fig. 2). The terminal CF$_3$ unit resonates at −79.5 ppm, while the neighbouring CF$_2$ units can be found at ca. −125.0 ppm. The CF$_2$ groups in the central parts of substituents then exhibit resonance frequencies at ca. −120 ppm.
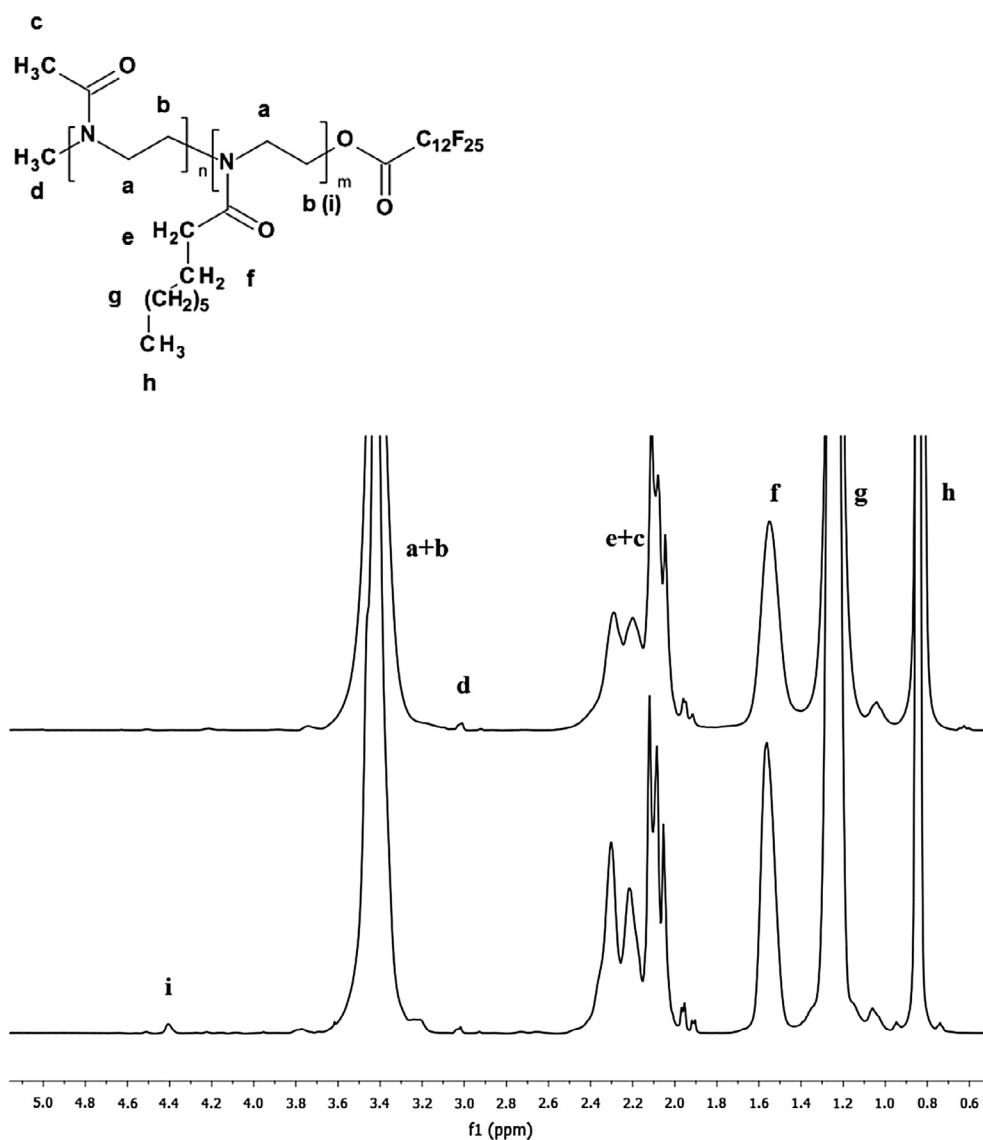

Fig. 1. ^{1}H NMR spectra of P0 without fluorinated end groups and P3 as a representative example of the polymers with fluorinated end groups (solvent - CDCl$_3$).
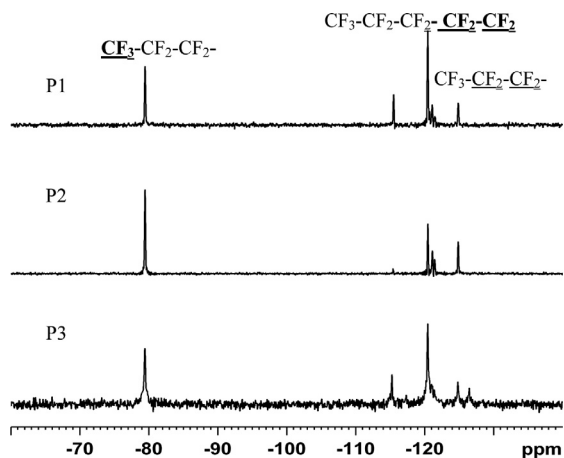
Fig. 2. ^{19}F NMR spectra of the synthesized polymers P1, P2 and P3 (Table S2).

All of the synthesized polymers were characterized by SEC-MALS in methanol to determine their absolute number average molar mass (M_n) and Đ. The M_n of all of the copolymers is in the range of 5–6 KDa (with a measurement accuracy of approximately 7–10%), and they revealed typically narrow molar mass distributions with Đ in a range of 1.08–1.14 (Table S2).

3.2. Polymer assembly in water

Visual inspection and DLS revealed that the synthesized polymers are dissolved as individual chains in a wide range of medium to high polarity solvents, such as dimethyl sulfoxide (DMSO), water, methanol (MeOH), 1,1,1,3,3,3-hexafluoroisopropanol (HFIP) and dichloromethane (DCM), whereas they are insoluble in very low polarity solvents such as ethyl acetate (AcOEt) and diethyl ether. DLS confirmed that the polymers were soluble at 10 mg/mL in MeOH solution (and the same in DMSO and HPIF) as only one peak was observed with a D_h value of 1–2 nm in the distribution functions (Fig. 3) indicative of molecularly dissolved polymer chains. Nonetheless, the difficulties in integration of the ^{1}H NMR spectra indicate that even though the polymers are present as individual chains, the fluoroalkyl tails are not solvated in all solvents and may be hidden inside the polymer globules.

The DLS study also revealed peaks with D_h of 100–200 nm for all investigated polymers in aqueous solutions after direct dissolution of the polymers in water, which was attributed to nanoparticles (Fig. 3). PDI values calculated from cumulant analysis for polymers P0-P3 were in the range of 0.2–0.3, which corresponds to a rather broad polydispersity of nanoparticles. Such polydispersity obscures the differences in size that could result from a variation of the perfluoroalkyl fragment length.

In a following step, the critical micellization concentrations (CMC) of the synthesized copolymers were studied in water to study the influence of the fluorinated tail. The CMC values for the poly(2-oxazoline)-based copolymers were determined from the I_{373}/I_{384} fluorescence intensity ratio of pyrene as a function of polymer concentration. This intensity ratio is a probe for the polarity of the local environment of pyrene, and an abrupt decrease indicates the presence of hydrophobic domains in
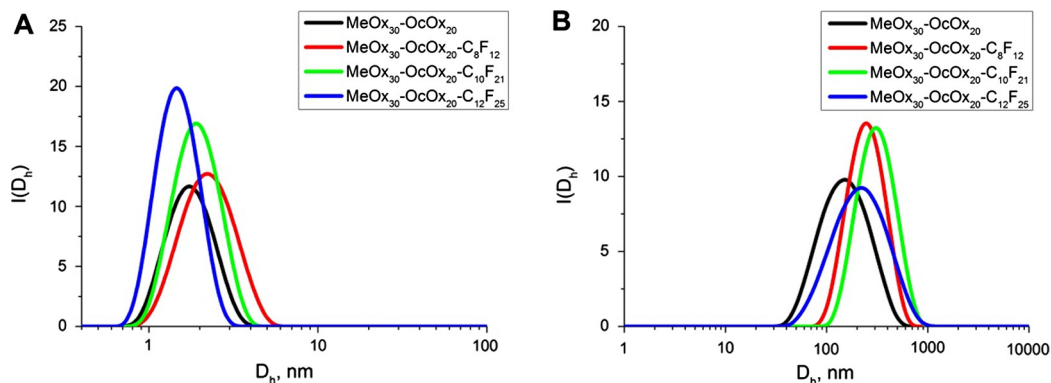

Fig. 3. Distribution functions of D_h for 10 mg/mL polymer solutions in MeOH (A) and in water (B).
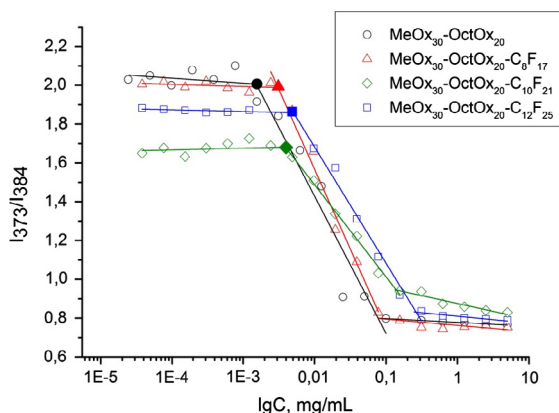
Fig. 4. Plot of the fluorescence intensity ratio of pyrene vs. the logarithm of the concentrations of the polymer solutions in water (mg/mL).

solution resulting from aggregation of the polymer chains [39–41]. The CMC values for the non-fluorinated PMeOx-*b*-POctOx diblock copolymer and the fluorinated quasi-triblock copolymers PMeOx-POctOx-C_8F_{17}, PMeOx-POctOx-$C_{10}F_{21}$, PMeOx-POctOx-$C_{12}F_{25}$ were determined to be $1.6 \cdot 10^{-3}$, $3.1 \cdot 10^{-3}$, $4.0 \cdot 10^{-3}$, $5.0 \cdot 10^{-3}$ mg/mL, respectively. These CMC values are quite low, indicating a strong hydrophobic driving force for polymer assembly in water. However, there is no significant difference between the CMC values for the different copolymers with introduction of the fluorinated alkyl chain or changing the length of the fluorinated fragment. As such, it may be concluded that the long POctOx block dominates the hydrophobic self-assembly of the studied copolymers (see Fig. 4).

Even though the DLS and CMC studies did not reveal significant differences between the four studied copolymers, we continued our endeavours to investigate whether there is an influence of the fluorinated alkyl chain end on the morphology of the self-assembled structures in water. Therefore, Cryo-TEM analysis was performed of 10 mg/mL aqueous solutions of the investigated copolymers revealing the presence of different (ratios) of aggregates of different morphologies, including mono- and multi-layered vesicles, isolated and aggregated rod-like micelles, for the different copolymers (Fig. 5).
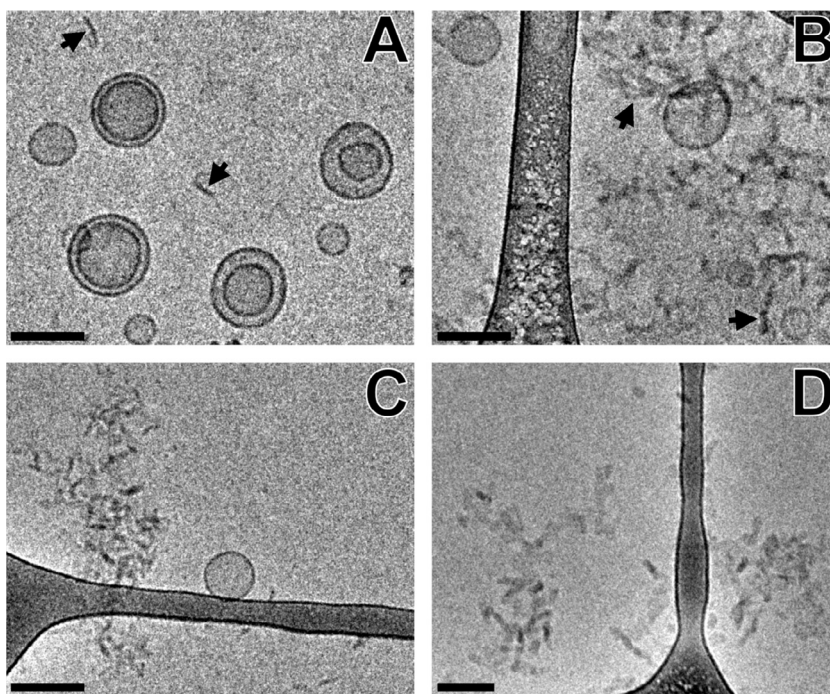

Fig. 5. Cryo-TEM images of the investigated polymers. (A) The P0 non-fluorinated diblock copolymer formed single- and multi-layered vesicles, together with short rod-like micelles. (B) The P1 (C_8F_{17}) and C) P2 ($C_{10}F_{21}$) copolymers formed single-layered vesicles and aggregates of rod-like micelles. (D) The P3 ($C_{12}F_{25}$) copolymer assembled into rod-like micelles only. Scale bars: 100 nm.
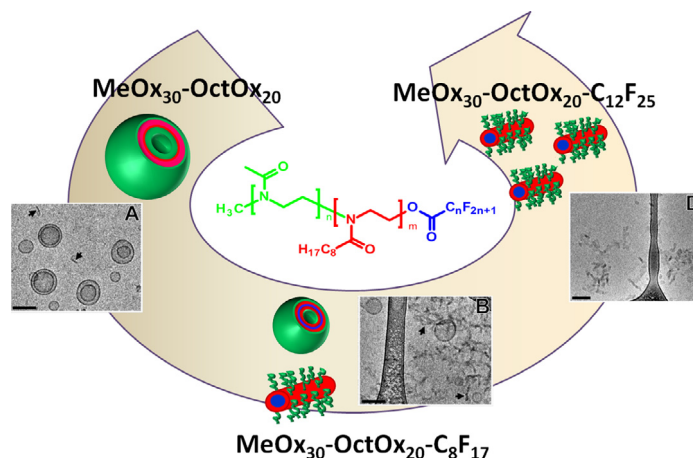
Fig. 6. Phase sequence of poly(2-methyl-2-oxazoline)–*block*–poly(2-octyl-2-oxazoline) copolymer with increasing the length of terminal perfluoroalkyl chain.

The P0 polymer that has no fluorinated tail formed primarily multi-layered vesicles with diameters ranging from 60 to 125 nm with ∼8 nm thick layers, which are typical for diblock copolymers with 59 wt.% hydrophobic content. The diameter of the observed entities is in agreement with the DLS result. In addition to these multi-layered vesicles, smaller single-layered vesicles with diameters between 36 nm and 46 nm and a few isolated rod-like micelles with lengths of 40–60 nm and diameters of 6–20 nm were also observed (Fig. 5A).

In contrast, the cryo-TEM analysis of a P1 solution showed a mixture of aggregating rod-like micelles approximately 5–15 nm in diameter and little-populated single-layered vesicles with a size range between 40 and 160 nm in diameter (Fig. 5B). The layer thickness of the vesicles is approximately 10 nm, clearly indicating that the fluorinated alkyl chain end has an influence on the self-assembly behaviour as the increase in the hydrophobic content is rather minor (from 59 wt.% for P0 to 62 wt.% for P1) and is not expected to cause a large difference in self-assembly behaviour.

The copolymer P2 revealed a very similar behaviour to P1 with a mixture of vesicles with diameters of approximately 60 nm with ∼8–10 nm thick layers and rod-like micelles with diameters of 10–20 nm and lengths of 50–100 nm (Fig. 5C). However, the extension of the fluoroalkyl chain length further decreased the relative content of the vesicles.

This trend is continued for copolymer P3 with the longest fluorinated alkyl chain, which only showed isolated rod-like micelles with a small fraction of agglomerates composed of rod-like micelles, while vesicles were no longer observed (Fig. 5D).

Based on the cryo-TEM investigations, which revealed an effect of the fluorinated alkyl chain length on the self-assembled structures that are formed, it may be suggested that the insertion of a perfluorinated fragment as the end group of the PMeOx-*b*-POctOx copolymer introduces additional microphase separation of the perfluorinated fragment from the POctOx in the hydrophobic domains. Such microphase separation makes the energetic penalty to bend the copolymer bilayer too high. As a result, the formation of vesicles becomes less favourable and rod-like micelles are formed with the insertion of a short fluorinated block (Fig. 6). The co-existence of rod-like micelles and vesicles could be due to the compositional polydispersity of the poly(MeOx)-*block*-poly(OctOx) copolymer. With the increasing length of the perfluorinated fragment in the case of P3 ($C_{12}F_{25}$), the elastic energy of bending becomes even higher so that vesicles could not be formed anymore and only rod-like micelles are observed (Fig. 6).

In addition to the copolymer composition, the preparation method of self-assembled structures can be of primary importance for the self-assembly of block copolymers as various kinetically trapped aggregates can be obtained [1,2,42,43]. To study the effect of the preparation method via the direct dissolution of the copolymers in water on the formed self-assembled structures, an aqueous solution of all of the block copolymers was prepared by solvent exchange from methanol where the polymer is unimolecularly dissolved in water by dialysis to induce self-assembly.

The aqueous solution of quasi-triblock copolymers (1 wt.%) obtained by this solvent exchange method revealed one peak with D_h in the range of 20–40 nm in DLS (Fig. 7) with a PDI of 0.3–0.1. Furthermore, cryo-TEM images (Fig. 8) confirmed the presence of spherical micelles with diameters ranging from 15 to 20 nm. This is in contrast to the previously described direct dissolution method, which led to the formation of rod-like micelles, thereby demonstrating the importance of the assembly method to controlling the self-assembled structures that are formed.

On the other hand, after solvent exchange, the model diblock copolymers form particles with diameters of approximately 200 nm, which is close to the diameters of vesicles observed for that polymer after direct dissolution. We can conclude that the extreme hydrophobicities of the fluoroalkyl chain quasi-triblock copolymers are more able to form spherical micelles during solvent exchange. In the case of spherical micelles, the contact between the lipophilic and fluorophilic parts is minimized, and the perfluorinated core acts as an anchor that prevents further aggregation.
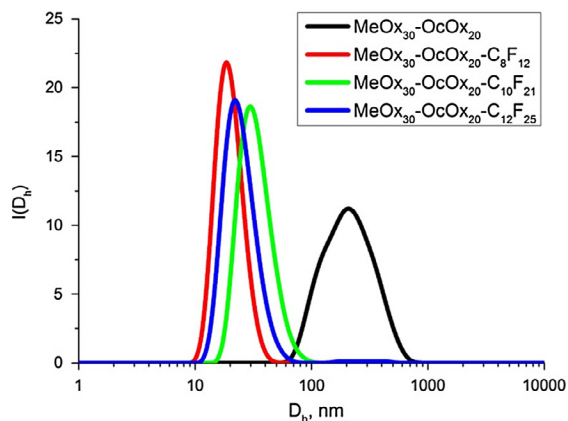
Fig. 7. Distribution functions of D_h for 10 mg/mL polymer solutions prepared by solvent exchange (from methanol to water).
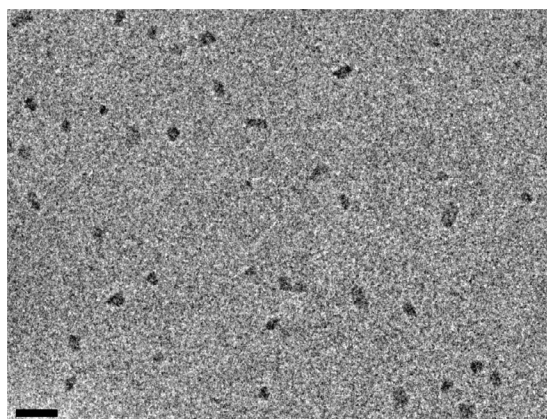

Fig. 8. Cryo-TEM image of copolymer P3 ($C_{12}F_{25}$) in water prepared by switching the solvent. Scale bar: 50 nm.

4. Conclusions

A series of block copolymers based on 2-methyl-2-oxazoline and 2-octyl-2-oxazolines with terminal perfluorocarbon alkyl fragments as well as a non-fluorinated reference diblock copolymer were synthesized by cationic ring opening polymerization. Well-defined copolymers with Đ in the range of 1.08–1.14 were obtained by sequential monomer addition followed by termination with perfluoroalkyl acids. It was shown by a combination of DLS and pyrene fluorescence that the tendency for hydrophobic self-assembly of all of the copolymers is dominated by the hydrophobic POctOx chains without any significant influence on the fluoroalkyl terminal chain. Nonetheless, cryo-TEM revealed that the structures and shapes of the resulting self-assembled structures are controlled by the presence and length of the perfluorinated fragment. The presence of single and multi-layer vesicles and rod-like micelles were visualized in aqueous solutions, and by increasing the content of the fluorinated alkyl chain, the ratio of vesicles to rod-like micellar aggregates was shifted towards the latter, whereby the longest $C_{12}F_{25}$ chain led to the exclusive formation of rod-like micellar aggregates. This shift in the formed self-assembled structures is ascribed to the formation of a fluorinated phase in the middle of the aggregates, increasing the rigidity of the structure, which suppresses bending and, thus, vesicle formation. Finally, it is shown that the preparation method is of prime importance to controlling the self-assembly process as the polymers with fluoroalkyl fragments self-assembled into spherical micelles when prepared by solvent exchange instead of direct dissolution.

Acknowledgements

Appendix A. Supplementary material

Supplementary data associated with this article can be found, in the online version, at http://dx.doi.org/10.1016/j.eur-polymj.2016.10.016.

References

[1] Y. Mai, A. Eisenberg, Chem. Soc. Rev. 41 (2012) 5969–5985.
[2] G. Riess, Prog. Polym. Sci. 28 (2003) 1107–1170.
[3] M.C. Woodle, C.M. Engbers, S. Zalipsky, Bioconjugate Chem. 5 (1994) 493–496.
[4] S. Zalipsky, C.B. Hansen, J.M. Oaks, T.M. Allen, J. Pharm. Sci. 85 (1996) 133–137.
[5] T.X. Viegas, M.D. Bentley, J.M. Harris, Z. Fang, K. Yoon, B. Dizman, R. Weimer, A. Mero, G. Pasut, F.M. Veronese, Bioconjugate Chem. 22 (2011) 976–986.
[6] O. Sedlacek, B.D. Monnery, S.K. Filippov, R. Hoogenboom, M. Hruby, Macromol. Rapid Commun. 33 (2012) 1648–1662.
[7] M. Barz, R. Luxenhofer, R. Zentelb, M.J. Vicenta, Polym. Chem. 2 (2011) 1900–1918.
[8] K. Knop, R. Hoogenboom, D. Fischer, U.S. Schubert, Angew. Chem. Int. Ed. 49 (2010) 6288–6308.
[9] P. Goddard, L.E. Hutchinson, J. Brown, L.J. Brookman, J. Controlled Release 10 (1989) 5–16.
[10] F.C. Gaertner, R. Luxenhofer, B. Blechert, R. Jordan, M. Essler, J. Controlled Release 119 (2007) 291–300.
[11] L. Wyffels, T. Verbrugghen, B.D. Monnery, M. Glassner, S. Stroobants, R. Hoogenboom, S. Staelens, J. Controlled Release 235 (2016) 63–71.
[12] D.A. Tomalia, D.P. Sheetz, J. Polym. Sci. Part A 4 (1966) 2253–2265.
[13] W. Seeliger, E. Aufderhaar, W. Diepers, R. Feinauer, R. Nehring, W. Thier, H. Hellmann, Angew. Chem. 78 (1966) 913–927. Angew. Chem. Int. Ed. Engl. 5 (1966) 875–888.
[14] T. Kagiya, S. Narisawa, T. Maeda, K. Fukui, J. Polym. Sci. Part B 4 (1966) 441–445.
[15] A. Levy, M. Litt, J. Polym. Sci. Part B 5 (1967) 871–879.
[16] R. Hoogenboom, Angew. Chem. Int. Ed. 48 (2009) 7978–7994.
[17] B. Verbraeken, K. Lava, R. Hoogenboom, Encyclopedia of Polymer Science and Technology, John Wiley & Sons Inc., 2014.
[18] K. Lava, B. Verbraeken, R. Hoogenboom, Eur. Polymer. J. 65 (2015) 98–111.
[19] W.H. Binder, H. Gruber, Macromol. Chem. Phys. 201 (2000) 949–957.
[20] G. Volet, V. Chanthavong, V. Wintgens, C. Amiel, Macromolecules 38 (2005) 5190–5197.
[21] R. Obeid, E. Matseva, A.F. Thunemann, F. Tanaka, F.M. Winnik, Macromolecules 42 (2009) 2204–2214.
[22] C.J. Waschinski, J.C. Tiller, Biomacromolecules 6 (2005) 235–243.
[23] K.C. Lowe, J. Fluorine Chem. 109 (2001) 59–65.
[24] W. Liu, J.A. Frank, Eur. J. Radiol. 70 (2009) 258–264.
[25] P. Boehm-Sturm, L. Mengler, S. Wecker, M. Hoehn, T. Kallur, PLoS ONE 6 (12) (2011) e29040.
[26] M. Srinivas, A. Heerschap, E.T. Ahrens, C.G. Figdor, I.J.M. de Vries, Trends Biotechnol. 28 (2010) 363–370.
[27] M.P. Krafft, J.G. Riess, Chem. Rev. 109 (2009) 1714–1792.
[28] H. Berlepsch, C. Bottcher, K. Skrabania, A. Laschewsky, Chem. Commun. 17 (2009) 2290–2292.
[29] K. Skrabania, H. Berlepsch, C. Bottcher, A. Laschewsky, Macromolecules 43 (2010) 271–281.
[30] K. Skrabania, A. Laschewsky, H. Berlepsch, C. Bottcher, Langmuir 25 (13) (2009) 7594–7601.
[31] Z. Li, E. Kesselman, Y. Talmon, M. Hillmyer, T. Lodge, Science 306 (2004) 98–101.
[32] M. Lobert, H.M.L. Thijs, T. Erdmenger, R. Eckardt, C. Ulbricht, R. Hoogenboom, U.S. Schubert, Chem. Eur. J. 14 (2008) 10396–10407.
[33] K. Kempe, A. Baumgaertel, R. Hoogenboom, U.S. Schubert, J. Polym. Sci. Part A 48 (2010) 5100–5108.
[34] K. Kempe, R. Hoogenboom, S. Hoeppener, C.-A. Fustin, J.-F. Gohy, U.S. Schubert, Chem. Commun. 46 (2010) 6455–6457.
[35] R. Ivanova, T. Komenda, T.B. Bonne, K. Ludtke, K. Mortenson, P.K. Pranzas, R. Jordan, C.M. Papdakis, Macromol. Chem. Phys. 209 (2008) 2248–2258.
[36] S. Kubowicz, A.F. Thünemann, R. Weberskirch, H. Möhwald, Langmuir 21 (16) (2005) 7214–7219.
[37] J. Dubochet, M. Adrian, J.-J. Chang, J.-C. Homo, J. Lepault, A.W. McDowall, P.Q. Schultz, Rev. Biophys. 21 (02) (1988) 129–228.
[38] A. Baumgaertela, C. Webera, N. Fritz, G. Festaga, E. Altuntas, K. Kempe, R. Hoogenboom, U.S. Schubert, J. Chromatogr. A 1218 (2011) 8370–8378.
[39] H. Ringsdorf, J. Venzmer, F.M. Winnik, Macromolecules 24 (1991) 1678–1686.
[40] T. Nivaggioli, P. Alexandridis, T.A. Hatton, A. Yekta, M.A. Winnik, Langmuir 11 (1995) 730–737.
[41] S.K. Filippov, A. Lezov, O. Sergeeva, A. Olifirenko, S. Lesnichin, N. Domnina, E. Komarova, M. Almgren, G. Karlsson, P. Štepanek, Eur. Polymer. J. 44 (10) (2008) 3361–3369.
[42] D.J. Pochan, Z. Chen, H. Cui, K. Hales, K. Qi, K.L. Wooley, Science 306 (2004) 94–97.
[43] C.-A. Fustin, H.M.L. Thijs-Lambermont, S. Hoeppener, R. Hoogenboom, U.S. Schubert, J.-F. Gohy, J. Polym. Sci. Part A 48 (2010) 3095–3102.

Novel triphilic block copolymers based on poly(2-methyl-2-oxazoline*)–block–* poly(2-octyl-2-oxazoline) with different terminal perfluoroalkyl fragments: synthesis and self-assembly behavior

Leonid I. Kaberov[a], Bart Verbraeken[b], Martin Hruby[a], Anna Riabtseva[a], Lubomir Kovacic[c], Sami Kereïche[c], Jiri Brus[a], Petr Stepanek[a], Richard Hoogenboom[b], Sergey K. Filippov[a,*]

Monomer synthesis

The hydrophobic 2-(n-octyl)-2-oxazoline (OctOx) monomer was synthesized by the well-known three-steps method starting from the corresponding acid [17]. In the first step, n-nonanoic acid was first converted to n-nonanoic acid chloride by reaction with thionyl chloride followed by reaction with (2-chloroethylamino) hydrochloride in presence of trimethylamine as base.
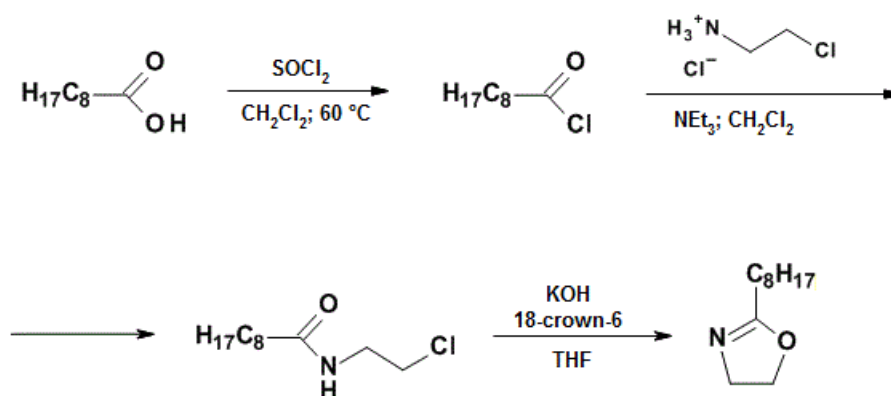
Fig. S1. Synthesis of 2-(n-octyl)-2-oxazoline.

It is important to mention that during first step we often obtained some amount of 2-oxazoline as a side product, which could be caused by heating during evaporation and a large excess of triethylamine. It is possible to wash it out by petroleum ether and get the main product in a pure form. However, only the resulting oxazoline was purified to prevent possible losses.

The ^{1}H NMR spectrum of purified N-(2-chloroethyl)nonanoyl amide was recorded and the assignment of different signals was determined (Figure S2). The group of signals in weak field is typical for hydrophobic fragment: δ=0.86 ppm from terminal CH_3-group, broad signal at δ=1.26 ppm from overlapping methylene groups $(CH_2)_5$-, δ=1.62 ppm and δ =2.19 ppm from β (-CH_2-CH$_2$-C(O)-) and α (-CH_2-C(O)-) methylene groups of alkyl fragment, respectively. The spectrum also shows overlapping signals from methylene groups of attached 2-chloroethylamine (-NH-CH_2-CH_2-Cl) at δ=3.66-3.58 ppm and broad singlet from amide proton δ=6.04 ppm (-NH-CH$_2$-). There are no signals from acid proton in strong field and no signals from α methylene group

1

from nonanoic acid (δ=2.35 ppm) and nonanoic acid chloride (δ=2.88 ppm) which indicates on purity of amide.
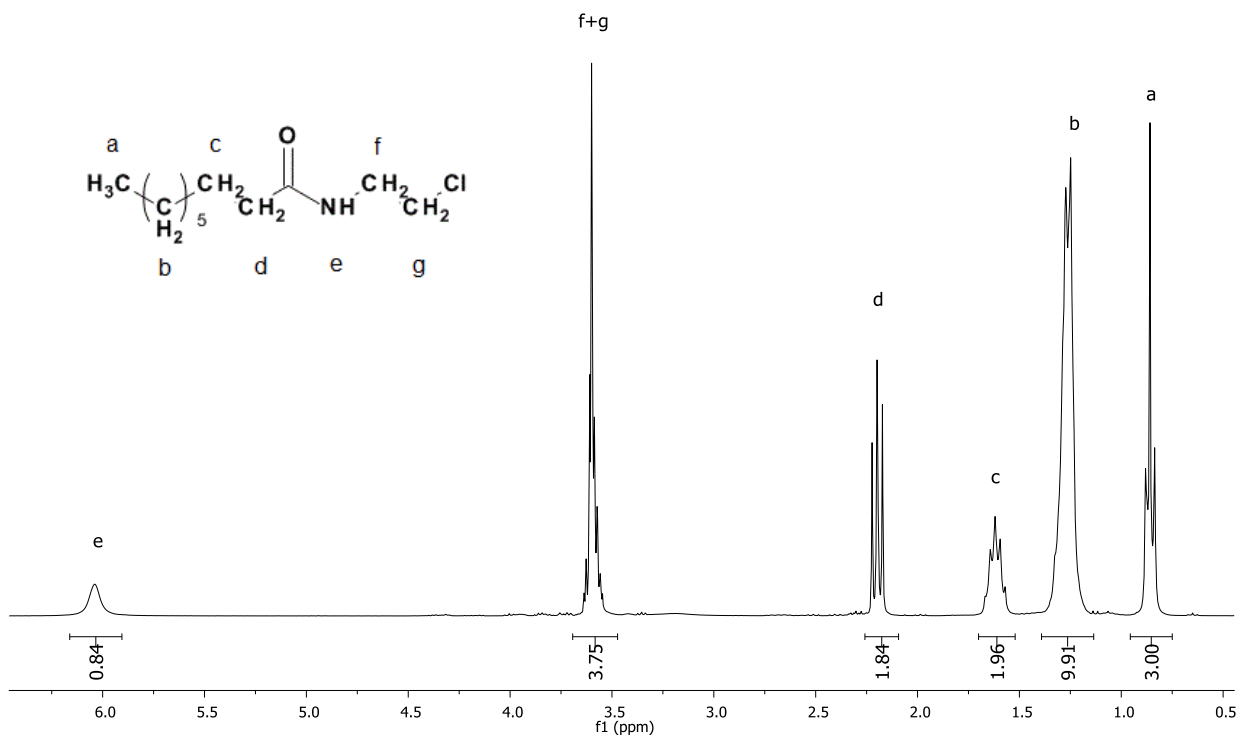
Fig. S2. NMR spectrum of N-(2-chloroethyl)nonanoyl amide.

The second step was the ring-closing reaction in presence of potassium hydroxide as a base and 18-crown-6 ether as a catalyst in inert atmosphere (Scheme 1). After distillation the product – colorless liquid – was characterized by ^{1}H NMR spectroscopy (Figure **S3**). In the spectrum we can see (as it was for amide) signals from alkyl chain: δ=0.86 ppm (**CH$_3$-**), δ=1.26 ppm (CH$_3$(**CH$_2$**)$_5$-), δ=1.62 ppm (-**CH$_2$**-CH$_2$-C(N)O-); the signal from α-CH$_2$ group (δ=2.26 ppm)is slightly shifted in comparison with signals from same groups in amide (δ=2.19 ppm) due to changes in electron density distribution. Also there are signals from 2-oxazoline ring at δ=4.22 ppm (-C-O-**CH$_2$**-CH$_2$-N=) and δ=3.81 ppm (-C-O-CH$_2$-**CH$_2$**-N=). The absence of signals at δ=2.19 ppm indicates that ring-closing reaction was completed.

2
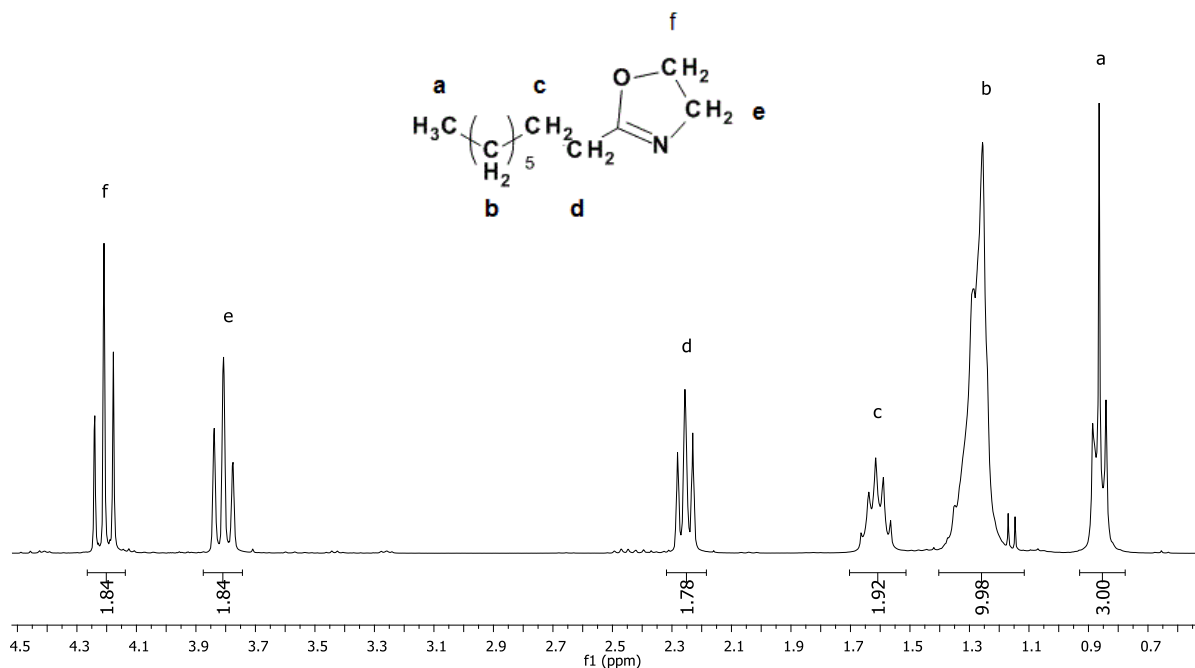
Fig. S3. ^{1}H NMR spectrum of 2-(n-octyl)-2-oxazoline (OctOx)

Table S1. Refractive index increment of poly(2-oxazolines) in methanol.

Polymer	Composition	dn/dc
P0	MeOx$_{30}$-OctOx$_{20}$	0.173±0.002
P1	MeOx$_{30}$-OctOx$_{20}$-C$_8$F$_{17}$	0.178±0.002
P2	MeOx$_{30}$-OctOx$_{20}$-C$_{10}$F$_{21}$	0.179±0.002
P3	MeOx$_{30}$-OctOx$_{20}$-C$_{12}$F$_{25}$	0.185±0.001

Table S2. Molar mass and dispersity of the synthesized polymers.

Polymer	Composition	M_n, g/mol	Đ
P0	MeOx$_{30}$-OctOx$_{20}$	6300	1.11
P1	MeOx$_{30}$-OctOx$_{20}$-C$_8$F$_{17}$	6000	1.08
P2	MeOx$_{30}$-OctOx$_{20}$-C$_{10}$F$_{21}$	5000	1.09
P3	MeOx$_{30}$-OctOx$_{20}$-C$_{12}$F$_{25}$	5000	1.14

3

MANUSCRIPT M2

Riabtseva A., <u>Kaberov L.I.</u>, Noirez L., Ryukhtin V., Nardin C., Verbraeken B., Hoogenboom R., Stepanek P., Filippov S.K.. Structural characterization of nanoparticles formed by fluorinated poly(2-oxazoline)-based polyphiles. *Eur. Polym. J.* **2018**, 99, 518-527. DOI: 10.1016/j.eurpolymj.2018.01.007.

Macromolecular Nanotechnology

Structural characterization of nanoparticles formed by fluorinated poly(2-oxazoline)-based polyphiles

Anna Riabtseva[a], Leonid I. Kaberov[a], Laurence Noirez[b], Vasyl Ryukhtin[c], Corinne Nardin[d], Bart Verbraeken[e], Richard Hoogenboom[e], Petr Stepanek[a], Sergey K. Filippov[a,*]

[a] Institute of Macromolecular Chemistry, Academy of Sciences of the Czech Republic, Heyrovský Sq. 2, 162 06 Prague 6, Czech Republic
[b] Laboratoire Léon Brillouin (CEA-CNRS), UMR12, Université Paris-Saclay, CEA-Saclay, F-91191 Gif-sur-Yvette, France
[c] Nuclear Physics Institute, ASCR, v.v.i., Husinec-Řež 250 68, Czech Republic
[d] Université de Pau et des Pays de l'Adour/CNRS, Institut des Sciences Analytiques et de Physico-chimie pour l'Environnement et les Matériaux, UMR5254, 64000 Pau, France
[e] Supramolecular Chemistry Group, Department of Organic and Macromolecular Chemistry, Ghent University, Krijgslaan 281 S4, B-9000 Ghent, Belgium

ABSTRACT

We report on the self-assembly behavior of poly(2-methyl-2-oxazoline)–block–poly(2-octyl-2-oxazoline) comprising different terminal perfluoroalkyl fragments in aqueous solutions. As reported previously [Kaberov et al. (2017)] such polyphiles can form a plethora of nanostructures depending of the composition and on the way of preparation. Here we report, for the first time, detailed information on the internal structure of the nanoparticles resulting from the self-assembly of these copolymers. Small-angle neutron and X-ray scattering (SANS/SAXS) experiments unambiguously prove the existence of polymersomes, wormlike micelles and their aggregates in aqueous solution. It is shown that increasing content of fluorine in the poly(2-oxazoline) copolymers results in a morphological transition from bilayered or multi-layered vesicles to wormlike micelles for solutions prepared by direct dissolution.

In contrast, nanoparticles prepared by dialysis of a polymer solution in a non-selective organic solvent against water are characterized by SAXS method. The internal structure of the nanoparticles could be assessed by fitting of the scattering data, revealing complex core-double shell architecture of spherical symmetry. Additionally, long range ordering is identified for all studied nanoparticles due to the crystallization of the poly(2-octyl-2-oxazoline) segments inside the nanoparticles.

1. Introduction

Owing to their versatile properties, poly(2-alkyl/aryl-2-oxazoline)s (PAOx) and their derivatives currently receiving significant scientific attention [1–3]. Due to their biocompatibility and nontoxicity, PAOx are widely studied as materials for biomedical applications such as drug, protein, radionuclide or gene delivery [4–7] as well as for the preparation of non-fouling surfaces that resist non-specific adsorption of proteins, bacteria, and higher organisms [8]. Living cationic ring-opening polymerization (CROP) is usually used for the synthesis of polyoxazolines [9,10] and allows not only controlling the molecular weight and dispersity of the resulting polymers but also to obtain PAOx of desired architecture. One can vary the nature and ratio of monomers, use different functional initiators or terminate agents thereby introducing fragments with different functionality and controlling the hydrophilic to hydrophobic balance [11–13].

Varying the ratio and the order of hydrophilic and hydrophobic blocks constituents of amphiphilic PAOx leads to a plethora of self-assembled structures such as spheres [14], vesicles [15], rod- or wormlike micelles, cylinders and corresponding aggregates in solution. Usually, poly(2-methyl-2-oxazoline) (MeOx) or poly(2-ethyl-2-oxazoline) (EtOx) are used to build hydrophilic blocks since these are biocompatible and reveal "stealth-like" behavior [16–18]. More complex structures, for example, multicompartment micelles, could be obtained upon self-assembly of triblock terpolymers in water or organic solvents [19,20]. Especially interesting are the so-called polyphiles - triblock copolymers that combine hydrophilic, hydrophobic and fluorophilic blocks [21–25]. Due to the immiscibility of the lipophilic and fluorophilic hydrophobic segments the resulting copolymers can form particles of complex morphologies depending on the polymer architecture and solvent [20,26,27]. Such nano- and microparticles containing fluorinated fragments are of high interest for potential application as

magnetic resonance imaging contrast agents [28,29].

While the synthesis and the self-assembly behavior of di- and tri-block PAOx containing hydrophilic and hydrophobic blocks were widely studied, there is not much information about triblock PAOx that contain fluorinated moieties. Schubert and co-authors reported on the investigation of nanostructures formed by triblock terpolymers consisting of poly[2-ethyl-2-oxazoline-block-2-(1-ethylpentyl)-2-oxazoline-block-2-(Xfluorophenyl)-2-oxazoline] (X = di, tri, tetra and penta). The authors studied the influence of the fluorination degree of these polymers on their self-assembly ability. A transition from rod-like micelles to highly complex round-shaped super-aggregates was observed by cryo-TEM with increasing fluorine content [30]. Water-soluble polymer surfactants based on 2-methyl-2-oxazoline with both fluorinated terminal group $C_8H_{17}CH_2CH_2$ (constant length) and hydrocarbon terminal group of different lengths C_nH_{2n+1} (n = 6,8,…,18) were synthesized by Nuyken and co-authors [31]. It was shown by the fluorescence spectroscopy of polymer solutions with solubilized pyrene that micelle core composition and first micellization point depends on the ratio between hydrophobic and fluorocarbon parts of polymer.

Recently we reported on the synthesis and solution properties of a novel quasi-triblock fluorine-containing copolymers based on 2-oxazolines [32]. Our synthetic approach provides an easy way to attach a C_nF_{2n+1} perfluorinated terminal chain to a poly(2-methyl-2-oxazoline)–block–poly(2-octyl-2-oxazoline) (PMeOx-b-POctOx) dilock copolymer through termination and to combine hydrophilic, hydrophobic and fluorophilic moieties along one polymer chain. Preliminary investigations of the self-assembly of the synthesized polymers in water using dynamic light scattering and cryo-TEM revealed the coexistence of bilayer and multi-layer vesicles as well as rod-like micelles. The shape and the size of the nanoparticles in solution could be controlled by the way of preparation. Spherical micelles with diameters ranging from 15 to 20 nm were observed in solution for the polymers assembled by solvent exchange. However, more detailed insights into the internal structure (size of the core and the shell thickness) of the formed nanoparticles and their dependence on the length of the fluorinated fragment or the method of preparation were not investigated.

Here, we report on the in depth evaluation of the internal structure of nanoparticles formed by the self-assembly of quasi-triblock fluorine-containing copolymers, namely PMeOx-POctOx-C_8F_{17}, PMeOx-POctOx-$C_{10}F_{21}$, PMeOx-POctOx-$C_{12}F_{25}$, as well as the non-fluorinated PMeOx-b-POctOx reference diblock copolymer. We describe the influence of the length of the perfluorinated terminal chain and of the preparation methods on the features of the self-assembled polymers. To achieve a comprehensive characterization of the morphology of the resulting nanoparticles, we combined both small-angle X-ray scattering (SAXS) and small-angle neutron scattering (SANS) experiments.

2. Experimental section

2.1. Materials

2-Methyl-2-oxazoline (MeOx, 99%, Acros Organics) was dried over BaO and distilled before use. 2-(n-octyl)-2-oxazoline (OctOx) was synthesized according to procedure described elsewhere [32]. Perfluorinated acids (nonanoic, undecanoic, tridecanoic) and p-toluenesulfonate were purchased from Sigma-Aldrich and used as received. Acetonitrile (ACN, Lachner) was dried by refluxing over BaO and distilled before use. Water was deionized with a MilliPore Milli-Q® gradient installation. All other chemicals were used as received.

2.2. Polymer synthesis

All copolymers were synthesized separately by the CROP. The detailed procedure was described in our previous work [32]. In brief, the first monomer MeOx and the initiator (p-toluenesulfonate) were dissolved in acetonitrile and stirred at 140 °C in pressure reactor under
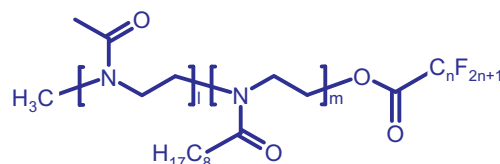
Scheme 1. Chemical structure of quasi-triblock copolymers, n = 8, 10 or 12.

Table 1
Composition and characteristics of fluorinated quasi-triblock poly(2-oxazolines) and reference nonfluorinated diblock copolymer.

Polymer	Composition	M_n, g/mol	Đ
P0	PMeOx$_{30}$-b-POctOx$_{20}$	6300	1.11
P1	PMeOx$_{30}$-b-POctOx$_{20}$-C$_8$F$_{17}$	6000	1.08
P2	PMeOx$_{30}$-b-POctOx$_{20}$-C$_{10}$F$_{21}$	5000	1.09
P3	PMeOx$_{30}$-b-POctOx$_{20}$-C$_{12}$F$_{25}$	5000	1.14

inert atmosphere for 35 min ($\approx$ 98% of conversion). After cooling down the reaction mixture, the second monomer OctOx was added and the mixture was stirred at 140 °C for another 45 min to form diblock copolymer.

The perfluoroalkyl fragments were attached to copolymers by termination of polymerization with corresponding perfluorinated carboxylic acids in the presence of triethylamine at 70 °C. To obtain the model PMeOx-b-POctOx diblock copolymer, the polymerization was quenched with 1 M KOH in methanol.

The chemical structures of the polymers are shown in Scheme 1. The molecular weights of the polymers range from 5 to 6 kDa, and the polydispersities of the samples according to the reference [32] in range from 1.08 to 1.14 (Table 1).

2.3. Preparation of samples

All solutions for SAXS experiments were prepared using deionized water in the range of concentrations from 0.1 to 5 wt%. All solutions for SANS experiments were prepared using D$_2$O (99.9%, Sigma-Aldrich) as solvent to reduce the incoherent scattering. The concentration of all SANS solutions was 2 wt%. Scattering from pure H$_2$O or D$_2$O was measured separately and subtracted from solution scattering data.

Samples for SAXS and SANS experiments were prepared in two ways: by direct dissolution in H$_2$O or D$_2$O or by solvent exchange.

2.3.1. Solvent exchange method

Briefly, 5 mL of 2.5 wt% polymer solution in methanol was placed in dialysis tubing with MWCO 3.5–5 kDa (Spectra/Por, Spectrum Laboratories, Inc.) and dialyzed against 5 L of deionized water with mild stirring at 25 °C. The deionized water was refreshed 5 times and the total dialysis time was 24 h. Samples were stored in sealed containers at 4 °C.

2.4. Small-angle X-ray scattering

SAXS experiments for samples prepared by direct dissolution were performed on the high brilliance beamline ID02 at ESRF (Grenoble, France). The SAXS setup utilizes a pinhole camera with a beam stop placed in front of a two-dimensional Frelon CCD detector. The X-ray scattering patterns were recorded for sample-to-detector distances of 2.5 and 31 m, using a monochromatic incident X- ray beam with an energy of E = 12 460 eV (λ = 0.1 nm). The available scattering vector range was q = 0.001–2.76 nm^{-1} (q = 4π sin θ/λ, where 2θ is the scattering angle). Online corrections were applied for the detector, and the sample-to-detector distance, center, transmission, and incident intensity were calibrated. The isotropic scattering was azimuthally regrouped to determine the dependence of the scattered intensity I(q) on
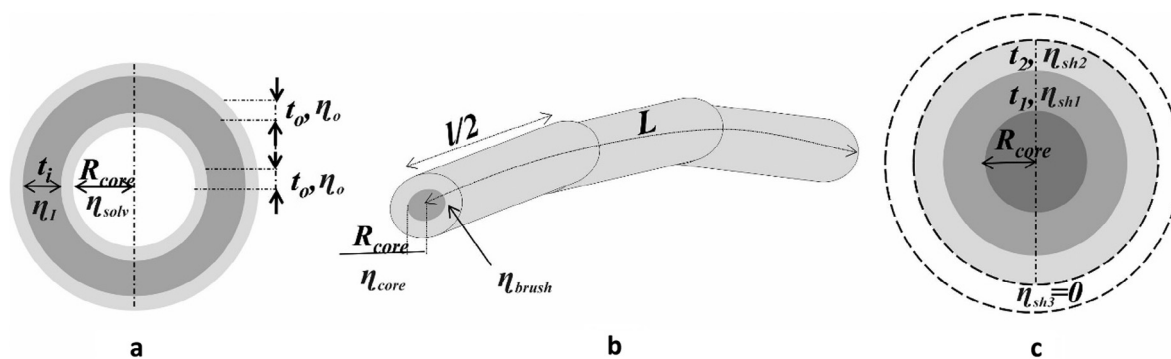
Fig. 1. Scheme of bilayered vesicle (a), wormlike micelle (b) and sphere with three shells (c).

the scattering vector q in absolute units. The scattering from a capillary filled with Milli-Q water was measured as a background and subtracted from the scattering signals of the samples. Prior to the experiment, a representative sample was checked to ensure lack of radiation damage.

SAXS experiments for samples obtained through solvent exchange from methanol were performed at the beamline B21 (Diamond Light Source, Didcot, UK) using a pixel detector (2M PILATUS). The X-ray scattering images were recorded for a sample-to-detector distance of 3.9 m, using a monochromatic incident X-ray beam ($\lambda = 0.1$ nm) covering the range of scattering vector $0.025\,\text{nm}^{-1} < q < 4\,\text{nm}^{-1}$. Most of the samples had no measurable radiation damage by the comparison of 20 successive time frames with 50 ms exposures. The two-dimensional scattering patterns were azimuthally averaged to yield the dependence of the scattered intensity $I(q)$ on the scattering vector q. Before fitting analysis, the solvent scattering has been subtracted.

2.5. Small-angle neutron scattering

SANS experiments for samples prepared by direct dissolution were performed at CEA-Saclay on the spectrometer PAXY of the Laboratoire Leon-Brillouin. Measurements were performed with a 128×128 multidetector (pixel size 0.5×0.5 cm) using a monochromatic (wavelength λ set by a mechanical velocity selector) incident neutron beam collimated with circular apertures for two sample-to-detector distances, namely, 1 m (with $\lambda = 0.6$ nm) and 7 m (with $\lambda = 0.8$ nm). With such a setup, the investigated range of scattering vector is from 5×10^{-2} to 4×10^{-1} nm^{-1}. The two-dimensional scattering patterns were isotropic so that they were azimuthally averaged to yield the dependence of the scattered intensity I(q) on the scattering vector q.

3. Data analysis

The SANS and SAXS data were fitted using several models implemented in the SASfit software [33] (http://kur.web.psi.ch/sans1/SANSSoft/sasfit.html). The curves were fitted using the following function:

$$I(q) = P(q)S_{HS}(q) + P_{Voigt}(q) + I_{bkg} \tag{1}$$

where $P(q)$ is the form factor of the scattering object, $S_{HS}(q)$ is the structure factor for hard sphere interaction (Percus–Yevick model), $P_{Voigt}(q)$ is Voigt peak form factor, which describes peaks in the high q range of scattering curves and I_{bkg} is the incoherent background.

Scattering length densities (SLDs) of polymeric parts for all implemented models (Tables S2 and S3) were freely fitted during the fitting procedure and compared to estimated values of SLD to decide whether the fit results were in agreement with theoretical ones (Table S1). SLD of D$_2$O and H$_2$O were fixed to the literature values of 6.33×10^{-4} nm^{-2} and 9.44×10^{-4} nm^{-2}, respectively.

3.1. Structure factor

To take into account the interactions between nanoparticles we used Perkus-Yevick structure factor for hard spheres $S_{HS}(q)$ [34]:

$$S_{HS}(q) = \frac{1}{1 + 24 f_{HS} G(2R_{HS}q)/(2R_{HS}q)}$$

where R_{HS} is radius of hard sphere and f_{HS} is hard-sphere volume fraction. The function $G(x)$ is given by:

$$G(x) = \gamma'\frac{\sin x - \cos x}{x^2} + \delta'\frac{2x\sin x + (2-x^2)\cos x - 2}{x^3}$$
$$+ \varepsilon'\frac{-x^4\cos x + 4(3x^2 - 6\cos x + (x^3 - 6x)\sin x + 6)}{x^5}$$

where $\gamma' = \frac{(1+2f_{HS})^2}{(1-f_{HS})^4}$, $\delta' = \frac{-6f_{HS}(1+f_{HS}/2)^2}{(1-f_{HS})^4}$, $\varepsilon' = \frac{\gamma f_{HS}}{2}$

3.2. Bilayered vesicle

The form factor of bilayered vesicle $P_{BLV}(q)$ was used for diblock copolymer PMeOx$_{30}$-b-POctOx$_{20}$ and as one of the possible form factors for triblock copolymer with the shortest perfluorinated fragment PMeOx$_{30}$-b-POctOx$_{20}$-b-C$_8$H$_{17}$:

$$P_{BLV}(q) = (K(q,R_{core},\eta_{solv}-\eta_i) + K(q,R_{core}+t_o,\eta_i-\eta_o) + K(q,R_{core}+t_i$$
$$+ t_o,\eta_o-\eta_i) + K(q,R_{core}+2t_i+t_o,\eta_i-\eta_{solv}))^2 \tag{2}$$

with

$$K(q,R,\Delta\eta) = \frac{4}{3}\pi R^3 \Delta\eta 3\frac{\sin qR - qR\cos qR}{(qR)^3} \tag{3}$$

where R_{core} is the radius of bilayered vesicles core, which consists of solvent, t_o is thickness of outer part of bilayer, t_i is thickness of inner part of bilayer. η_o, η_i, η_{solv}, are SLD of outer part of bilayer, inner part of bilayer and solvent, respectively. The scheme of bilayered vesicle model is shown on the Fig. 1a. To account for polydispersity, a Schulz-Zimm distribution of R_{core} was included.

For solutions with concentration below 1% no structure factor was needed and $S_{HS}(q)$ was set to 1.

3.3. Wormlike micelle

The overall scattering intensity of wormlike micelle with contour length L and Kuhn length l can be written as [35]

$$P_{wm} = N_{agg}^2\beta_{core}^2 P_{core}(q) + N_{agg}\beta_{brush}^2 P_{brush}(q) + 2N_{agg}^2\beta_{core}\beta_{brush}S_{brush-core}(q)$$
$$+ N_{agg}(N_{agg}-1)\beta_{brush}^2 S_{brush-brush}(q),$$

where $N_{agg}^2\beta_{core}^2 P_{core}(q)$ is self-correlation term of the core, $N_{agg}\beta_{brush}^2 P_{brush}(q)$ is self-correlation term of the chains, $2N_{agg}^2\beta_{core}\beta_{brush}S_{brush-core}(q)$ is the cross-term between the core and chains

and $N_{agg}(N_{agg}-1)\beta_{brush}^2 S_{brush-brush}(q)$ is the cross-term between different chains. N_{agg} is the aggregation number of polymers forming the micelle per surface area, $\beta_{brush} = V_{brush}(\eta_{brush}-\eta_{solv})$ and $\beta_{core} = V_{core}(\eta_{core}-\eta_{solv})$ are the excess scattering lengths of a block in the corona and in the core, respectively. V_{brush} and V_{core} are the total volume of a block in the corona and in the core, respectively. η_{brush} and η_{core} are the corresponding SLDs. $P_{core}(q)$ is scattering of wormlike core and can be written as the product of the scattering from the conformation of worm $P_{worm}(q,l,L)$ and the cross section scattering $P_{cs}(q,R_{core},d,R_g)$

$$P_{core}(q,R_{core},l,L) = P_{worm}(q,l,L)P_{cs}(q,R_{core},d,R_g)$$

,where R_{core} is radius of wormlike core with uniform scattering length density

$$R_{core} = \sqrt{\frac{N_{agg}V_{core}}{1-x_{solv,core}}\frac{1}{\pi L}},$$

where $x_{solv,core}$ is amount of solvent in the micellar core.

The contribution of wormlike conformation P_{worm} is described by the model from Kholodenkos approach [36]

$$P_{worm}(q,l,L) = \frac{2l}{3L}[I_1(x)-\frac{l}{3L}I_2(x)],$$

where $x = \frac{3L}{l}$

$$I_n(x) = \int_0^x f(z)z^{n-1}dz$$

$$f(z) = \begin{cases} \frac{1}{E}\frac{\sinh(Ez)}{\sinh z} & for q \leqslant \frac{3}{l} \\ \frac{1}{F}\frac{\sinh(Fz)}{\sinh z} & for q > \frac{3}{l} \end{cases},$$

where $E = \sqrt{1-\left(\frac{lq}{3}\right)^2}$ and $F = \sqrt{\left(\frac{lq}{3}\right)^2-1}$.

For the contribution of the cross section P_{cs} is given as

$$P_{cs}(q,R_{core},d,R_g) = \left[\frac{2J_1(qR_{core})}{qR_{core}}\right]^2,$$

where R_g is radius of gyration of the block unit in the corona, J_1 is the first order Bessel function of the first kind: $J(x) = (\sin x - x\cos x)/x^2$.

The scattering intensity for the brush of wormlike micelle is given by:

$$P_{brush}(q,R_g) = 2\frac{exp(-x)-1+x}{x^2},$$

where $x = R_g^2 q^2$.

The contribution of cross term between core and chains which form brush of wormlike micelle is calculated using equation:

$$S_{brush-core}(q,R_{core},l,L,R_g,d) = \psi(qR_g)\frac{2J_1(qR_{core})}{qR_{core}}J_0[q(R_{core} + dR_g)]P_{worm}(q,l,L)$$

The contribution of cross term between chains is calculated using equation:

$$S_{brush-brush}(q,R_{core},l,L,R_g,d) = \psi^2(qR_g)J_0^2[q(R_{core} + dR_g)]P_{worm}(q,l,L),$$

where $\psi(qR_g) = \frac{1 - exp(-x)}{x}$ is the form factor amplitude of the chain, J_0 is the zeroth order Bessel function of the first kind, d is parameter that accounts non-penetration of the chains into the core and should be mimicked by $d \sim 1$ for $R_{core} \gg R_g$.

To account for polydispersity, a Schulz-Zimm distribution of R_g was included. The structure factor $S(q)$ in the case of fitting with wormlike micelles model was set to 1. The model of wormlike micelle is presented on the Fig. 1b.

3.4. Sphere with three shells

The SAXS data obtained for dialyzed samples were fitted with a model 'Sphere with 3 shells' implemented in the SASFit software (Fig. 1c). To utilize this model for fitting SAXS curves of studied polymers the thickness of the third shell was set as 0 and its SLD was the same as SLD of H_2O. The scattering intensity for sphere with 3 shells, $P_{S3Shell}(q)$, is calculated based on the core-shell model [37] and is given by:

$$P_{S3Shell}(q) = (K(q,R_{core},\eta_{core}-\eta_{sh1}) + K(q,R_c + t_1,\eta_{sh2}-\eta_{sh1})$$
$$+ K(q,R_{core} + t_1 + t_2,\eta_{sh3}-\eta_{sh2}) + K(q,R_{core} + t_1 + t_2 + t_3,\eta_{sh3}$$
$$-\eta_{solv}))^2$$

were $K(q,R,\Delta\eta)$ is calculated using Eq. (2), t_1, t_2, t_3 are thicknesses of the first, second and third shell, η_{core}, η_{sh1}, η_{sh2}, η_{sh3} are SLDs of core and shells, respectively. To account for polydispersity, a Schulz-Zimm distribution of R_{core} was included.

3.5. Voigt peak

Voigt function was used to describe the shape of the peaks at high q range of scattering curves. The amplitude version of the Voigt peak is parameterized as

$$V_{Amplitude}(x|A,\sigma,\gamma) = A\frac{\int_{-\infty}^\infty \frac{exp(-u^2)}{\frac{\gamma^2}{2\sigma^2} + \left(\frac{x-x_c}{\sqrt{2}\sigma} - u\right)^2}du}{\int_{-\infty}^\infty \frac{exp(-u^2)}{\frac{\gamma^2}{2\sigma^2} + u}du} = A\frac{V(x,x_c|\sigma,\gamma)}{V(x_c,x_c|\sigma,\gamma)}$$

where A is an amplitude of the Voigt peak, x_c is location parameter, σ is width of Doppler contribution, γ is a width of Lorentzian contribution.

The modified Porod function was used to describe the contribution of large aggregates at the lowest q range: $C_0 + \frac{c_1}{q^\alpha}$, where α is modified Porod exponent.

4. Results and discussion

4.1. Nanoparticles prepared by direct dissolution

The SANS and SAXS curves of all the copolymers at a concentration of 2 wt% and 2.5 wt%, respectively, are presented in Fig. 2a and b.

For the reference PMeOx$_{30}$-b-POctOx$_{20}$ diblock copolymer at low q range the scattering intensity follow a power law of I $\sim q^{-2.53 \pm 0.02}$ for SANS and $q^{-2.25 \pm 0.01}$ for SAXS (Fig. 3a and b). Such scaling exponent implies planar like structure. In the middle q range, the scattered intensity is decreasing and obeys a power law of I $\sim q^{-4.38 \pm 0.08}$ that corresponds to the scattering of compact structures with a sharp interface. The SANS and SAXS data were quantitatively analyzed by fitting the scattering curves with an appropriate model as shown in Fig. 1. The fitting parameters are presented in Table 2 and explained above in Data analysis section.

The scattering data corresponding to the structures of the self-assembled diblock copolymer can be fitted using the bilayered vesicle form factor corrected with the Schultz–Zimm polydispersity over R_a. These findings are in agreement with previously reported cryo-TEM imaging of diblock copolymer PMeOx$_{30}$-b-POctOx$_{20}$, where bilayered vesicles were revealed [32]. Additionally, the contribution of large aggregates was added as background, which resulted in a good quality fit. The quantitative analysis of the SANS scattering data yields a radius of vesicle interior, R_a, consisting of solvent of 24.4 nm and a polydispersity value of 0.26. The hydrophobic layer, t_i, consists of presumably the POctOx block of 1.6 nm thickness, whereas the hydrophilic PMeOx layer thickness, t_h, is 2.48 nm. The total radius of the vesicle is approximately 28.5 nm according to the SANS data. These values are in agreement with Cryo-TEM images where polydispersed vesicles in the
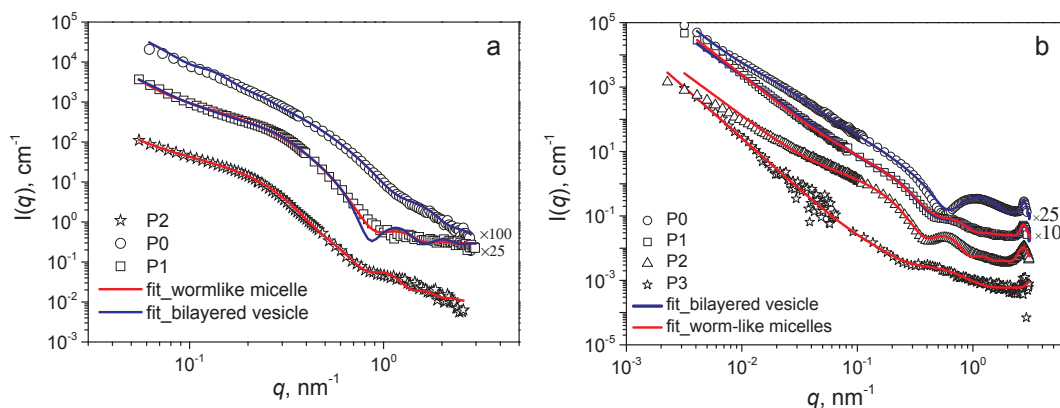
Fig. 2. SANS (a) and SAXS (b) curves displayed by PMeOx$_{30}$-b-POctOx$_{20}$ (P0), PMeOx$_{30}$-b-POctOx$_{20}$-C$_8$F$_{17}$ (P1), PMeOx$_{30}$-b-POctOx$_{20}$-C$_{10}$F$_{21}$ (P2) and PMeOx$_{30}$-b-POctOx$_{20}$-C$_{12}$F$_{25}$ (P3) aqueous solutions prepared by direct dissolution.

range 20–50 nm are observed.

A similar scattering pattern was obtained by the SAXS measurements (Fig. 3b). However, the SAXS scattered intensity has a broad secondary maximum in the q-range from 0.7 to 2 nm^{-1}, that can be explained by the differences in SLD values of the inner and outer bilayer parts on the solvent side. Such phenomenon was experimentally observed in a variety of other reported studies [38,39]. Values of the bilayer and outer layer thickness are in rather good agreement with those calculated from SANS data (Table 2). At the highest q value, the scattering curves for higher concentrations of aqueous diblock copolymer solutions exhibit another peak located at $q = 2.75$ nm^{-1} (Fig. 4a (inset)).

We utilized the bilayered vesicle model with Schultz − Zimm polydispersity and contribution from aggregates and in order to describe the small sharp peak at high q values the Voigt peak model was used (Ref. [40]), which can be attributed to additional internal ordering. From the position of the peak the repeat distance can be calculated as $D = 2\pi/q$, being 2.27 nm (Table 2). This ordering can be explained by the crystallization of octyl chains within the inner part of the bilayered vesicle wall. Such crystalline properties of self-assembled comb-like polymers were also described by Plate and Shibaev, who reported on the tendency for crystallization in the hexagonal crystal structure of polymers with long hydrocarbon side chains [41]. This assumption is further supported with copolymers of shorter hydrophobic block length for which no peak was observed by SAXS (data not shown). The amplitude of the Voigt peak decreases with decreasing concentration (Fig. 4a), indicating the decreasing packing density within the inner bilayer.

The scattering pattern is determined by nanoparticle form-factor

only for diluted solutions. However, with the increase of concentration, the interparticle scattering must also be taken into consideration [42]. To account for these interactions in the fitting model, the Percus-Yevik structure factor was applied for concentrations above 1 wt%. In Fig. 4c the structure factors, $S(q)$, for different concentrations of diblock copolymer are shown. The $S(q)$ at small q decreases with increasing concentration from 1 wt% to 5 wt%, indicating increasing repulsive interactions between the particles.

In a subsequent step we evaluated the structural changes in nanoparticles assembled from the fluorinated copolymers. One can see from the Fig. 2a that the SANS scattering curves are rather different from the curves obtained for the diblock copolymer P0 that does not contain a perfluorinated fragment.

For comparison, the SANS and SAXS scattering curves obtained for the polymer with the C$_8$F$_{17}$ perfluorinated alkyl chain was also fitted by a bilayered vesicle form factor. The final fit and all contributions are shown in Fig. 5a. While the fit of the SAXS data with a bilayered vesicle form factor is quite good, we could not obtain a satisfactory fit of the SANS data. The structural parameters calculated from SANS and SAXS data are presented in Table 2. One can see that the polydispersity over core radius of PMeOx$_{30}$-b-POctOx$_{20}$-C$_8$F$_{17}$ particles is high, which we explain by the presence of particles of different size and shape. Previous cryo-TEM results [32] indeed revealed the presence of two different species of self-assembled structures, namely bilayered vesicles and worm-like micelles. Therefore, we fitted the scattering curves by a combination of the wormlike micelles form factor and Schultz − Zimm polydispersity radius of a core. It can be seen on Fig. 5(b and d) that the wormlike micelles form factors fit well the scattering curves. Calculated radii of the wormlike micellar core are 8.2 nm from SAXS and 5.2 nm
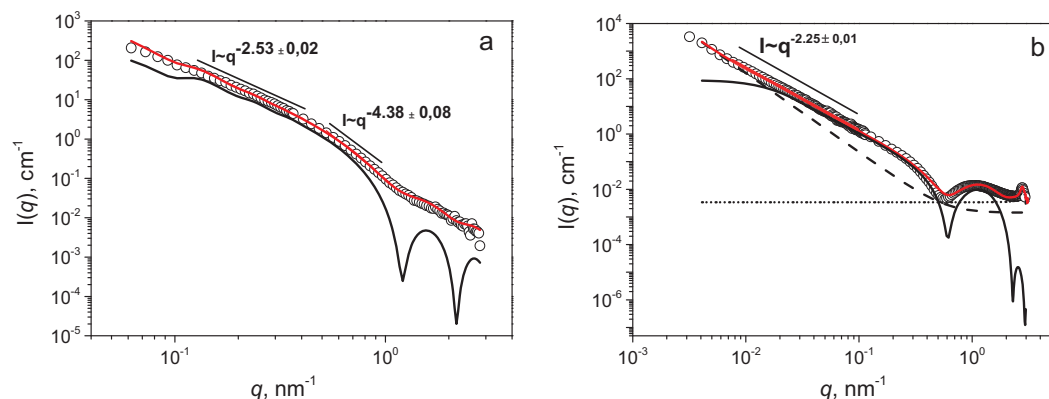

Fig. 3. SANS (a) and SAXS (b) curves of PMeOx$_{30}$-b-POctOx$_{20}$ solutions prepared by direct dissolution. Symbols are experimental scattering data, and red solid lines are fits generated as described in the text. The black solid lines are the form factors of bilayered vesicles, the black dashed lines are the form factors of large aggregates and the black short dotted lines describe the Voigt peak contribution. (For interpretation of the references to colour in this figure legend, the reader is referred to the web version of this article.)

Table 2

Comparison of structural parameters obtained from SAXS and SANS data for PMeOx$_{30}$-b-POctOx$_{20}$ (P0), PMeOx$_{30}$-b-POctOx$_{20}$-C$_8$F$_{17}$ (P1), PMeOx$_{30}$-b-POctOx$_{20}$-C$_{10}$F$_{21}$ (P2) and PMeOx$_{30}$-b-POctOx$_{20}$-C$_{12}$F$_{25}$ (P3). Concentrations are 2 wt% for SANS and 2.5 wt% for SAXS.

Fitting parameter	PMeOx$_{30}$OctOx$_{20}$		PMeOx$_{30}$OctOx$_{20}$-C$_8$H$_{17}$				PMeOx$_{30}$OctOx$_{20}$-C$_{10}$H$_{21}$		PMeOx$_{30}$OctOx$_{20}$-C$_{12}$H$_{25}$	
	Bilayered vesicle		Bilayered vesicle		Wormlike micelle		Wormlike micelle		Wormlike micelle	
	SAXS	SANS	SAXS	SANS	SAXS	SANS	SAXS	SANS	SAXS	SANS
R_{core} (nm)	25.4	24.4	38.9	16.6	8.2	5.2	9.7	–	2.3	4.9
Sig	0.82	0.26	0.78	0.71	0.12	0.3	–	–	–	–
t_o (nm)	2.2	1.6	5.5	3.0	–	–	–	–	–	–
t_i/^{a}V$_{brush}$ (nm)	2.2	2.5	0.8	1.4	14.4[a]	18.3[a]	15.2[a]	–	5.6[a]	8.7[a]
N_{agg}	–	–	–	–	0.12	0.16	0.2	–	0.19	0.24
$x_{solv,core}$	–	–	–	–	0.03	0.01	0.12	–	0.01	0.01
l (nm)	–	–	–	–	4	9.6	4	–	7	7
L (nm)	–	–	–	–	53.0	87.0	65.9	–	72.2	94.0
R_g (nm)	–	–	–	–	5.63	9.0	4.7	–	4.1	3.0
D (nm)	2.27	–	2.27	–	2.29	–	2.3	–	2.0	–
σ	$5*10^{-3}$	–	0.14	–	0.14	–	0.22	–	0.2	–
γ	0.1	–	$3*10^{-2}$	–	$3*10^{-2}$	–	$1.3*10^{-3}$	–	0.03	–
α	2.9	2.9	2.7	3	2.8	4	2.7	–	2.6	2.8

R_{core} – core radius, Sig – value of polydispersity, t_o – thickness of outer shell of bilayered vesicle, t_i – thickness of inner shell of bilayered vesicle, V_{core} – volume of a block in a core, V_{brush} – volume of a block in brush, N_{agg} – aggregation number per surface area, $x_{solv,core}$ – amount of solvent in the micellar core, l – Kuhn length, L – contour length, R_g – radius of gyration of the block unit in the corona, D – repeating distance, σ – width of Gaussian profile, γ – width of Lorentzian profile, α – modified Porod exponent.

[a] Shows values that correspond to the second parameter in the row.

from SANS, again in good agreement with the values obtained from cryo-TEM (approximately 7.5 nm) [32]. From the calculated percentage of solvent inside of the wormlike micelles core of 0.03% from SAXS and 0.01 from SANS ($x_{solv,core}$, Table 2), one can assume that the core consists of the highly hydrophobic part of the polymer, probably a mixture of the POctOx and the perfluorinated chains, whereas the outer shell is formed mainly by the hydrophilic PMeOx part. This conclusion is further supported by the fact that the fitted values of the SLD of the micellar core and shell are quite close to the theoretical ones estimated on a basis of their composition. However, the volume of the hydrophilic outer shell and the contour length calculated from the SANS and SAXS curves differs. This can be explained by the discrepancy of the SLD values of the core and the shell determined by SANS and SAXS as well as by the polydispersity of the system.

The polydispersity may also be explained by the fact that we applied only polydispersity over the core radius of the wormlike micelles that are also polydisperse in their contour length. Probably, the most proper way to fit these data is to combine bilayered vesicle and wormlike micelles form factors with several polydispersities in one fitting procedure, however we are not able to fit such a high number of fitting parameters.

The sharp peak at high q values evidences an additional ordering of

the octyl chains inside the hydrophobic micellar core as it was mentioned before for the bilayer vesicle structures. Besides, it is known that perfluorinated alkyl chains are quite rigid and also have a tendency to crystallize [43–46]. Based on this we can assume that there are may be two types of ordering inside the nanoparticles. The first one is ordering driven by perfluorinated alkyl chains which form the core of the wormlike micelle. The second one is ordering of the POctOx chains in the first, hydrophobic, shell of the wormlike micelles.

In contrast to the polymer with the shortest perfluorinated fragment, the scattering curves for PMeOx$_{30}$-b-POctOx$_{20}$-C$_{10}$F$_{21}$ and PMeOx$_{30}$-b-POctOx$_{20}$-C$_{12}$F$_{25}$ solutions can satisfactorily be fitted with the wormlike micelles form factor only. Scattering and fitting curves with all contributions for both polymers are presented in Fig. 6. As for the previous polymers, the final fit of the PMeOx$_{30}$-b-POctOx$_{20}$-C$_{10}$F$_{21}$ and PMeOx$_{30}$-b-POctOx$_{20}$-C$_{12}$F$_{25}$ scattering consists of a wormlike micelles form factor with contributions of large aggregates and of a Voigt peak.

The calculated structural parameters are shown in Table 2. The corona volume for the PMeOx$_{30}$-b-POctOx$_{20}$-C$_{10}$F$_{21}$ wormlike micelles has the highest value. The SLD of the core and the shell of the wormlike micelles formed by PMeOx$_{30}$-b-POctOx$_{20}$-C$_{10}$F$_{21}$ are almost the same (Table S2), which can mean that the core of micelle contains high

Fig. 4. (a) SAXS data for 0.1, 0.5, 1, 2.5, 5 wt% of PMeOx$_{30}$-b-POctOx$_{20}$ water solutions; (b) 2.25–3.25 nm^{-1} q-range of SAXS data for 0.1, 0.5, 1, 2.5, 5 wt% of PMeOx$_{30}$-b-POctOx$_{20}$ water solutions; (c) structure factor, S(q), for 1, 2.5, 5% wt% of PMeOx$_{30}$-b-POctOx$_{20}$ water solutions at 25 °C. Symbols are experimental scattering data. Solid lines are fits generated as described in the text.
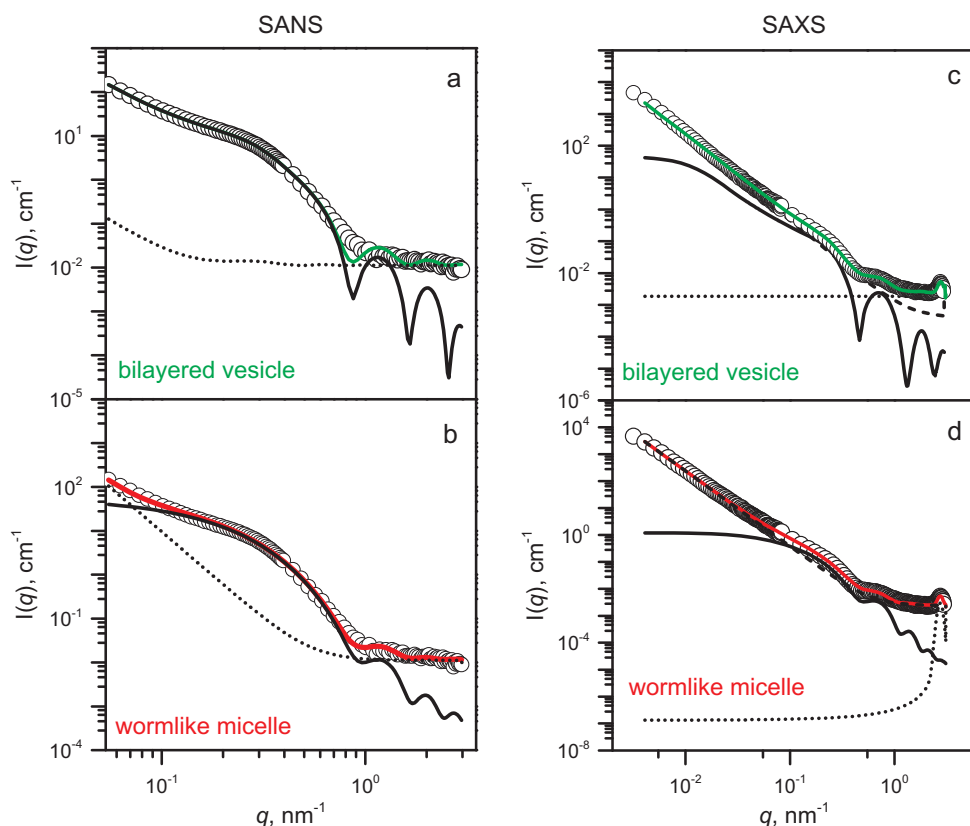
SANS

SAXS

amount of water and is rather loose. This is further supported by the amount of solvent in the core of 0.12 from SAXS ($x_{solv,core}$, Table 2) resulting from the fitting procedure. Similarly, the contour length of the wormlike micelles formed by PMeOx$_{30}$-b-POctOx$_{20}$-C$_{10}$F$_{21}$ is shorter compared to the polymer with the highest amount of fluorine: 65.9 nm for PMeOx$_{30}$-b-POctOx$_{20}$-C$_{10}$F$_{21}$ and 72.2 nm for PMeOx$_{30}$-b-POctOx$_{20}$-C$_{12}$F$_{25}$. This difference can be explained by the increase in stiffness of the wormlike micelles with increasing perfluorinated chain content.

Analysis of structural parameters obtained from the fitting procedures (Table 2) gives the possibility to establish the correlation between the length of fluorinated fragment of quasi-triblock poly(2-oxazolines), and morphology of nanoparticles obtained by their self-assembly in water solutions. Dependences of the main parameters on the length of fluorinated fragment in triblock polyoxazolines solutions, prepared by direct dissolution, are presented in Fig. 7.

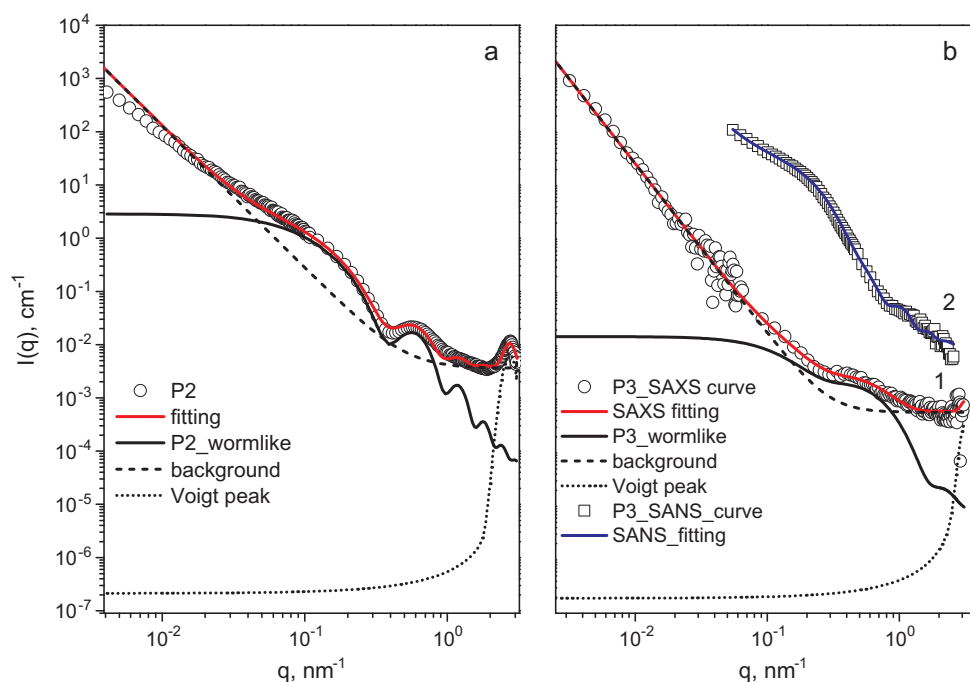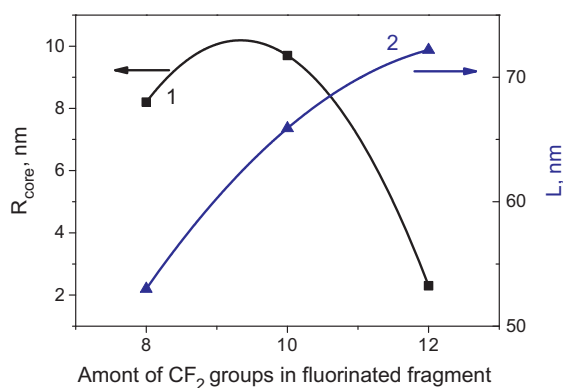The obvious changes in morphology are that: (1) the radius of the

Fig. 7. Dependence of the radius of the wormlike micelles core (1) and contour length of the wormlike micelle (2) as a function of the length of fluorinated fragment in triblock polyoxazolines (solutions prepared by direct dissolution).

wormlike micelles core decrease from 8.2 to 2.3 nm and (2) the contour length of the wormlike micelle increases from 53.0 to 72.2 nm with the increasing of fluorinated fragment length, indicating that wormlike micelles become more long and thin.

4.2. Nanoparticles prepared by solvent exchange method (dialysis)

In a second part of this work, the structures of nanoparticles prepared from the fluorinated quasi-triblock copolymers by solvent exchange (dialysis from methanol against water) are examined. According to the previous DLS results [32], studied polymers present in methanol solutions as individual chains and no self-assembly is observed. In contrast to the results obtained for polymer solutions prepared by direct dissolution method, DLS and cryo-TEM studies of aqueous solution of quasi-triblock copolymers prepared by solvent exchange method revealed the presence of spherical micelles with diameter 15–20 nm.

The obtained scattering curves are quite similar for all polymer water solutions (Fig. 8). There is no sign of aggregation of the self-assembled structures. For all obtained aqueous polymer solutions, the formed nanoparticles revealed a core–shell structure consisting of one or two layers with spherical symmetry. To fit the scattering data a model of sphere with two shells has, thus, been chosen.

Despite the fact that the diblock copolymer consists of two blocks, which can form a core with just one shell, the model of sphere with one shell did not fit correctly the scattering curve. We assume that the presence of a second shell (calculated from the fitting procedure) can be related to the inhomogeneously distributed density of the hydrophobic and hydrophilic parts of the micelle and that the indistinct border between the core and the shell can affect the values of the SLD. From the
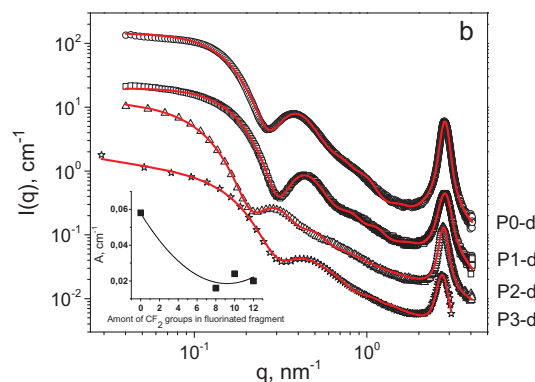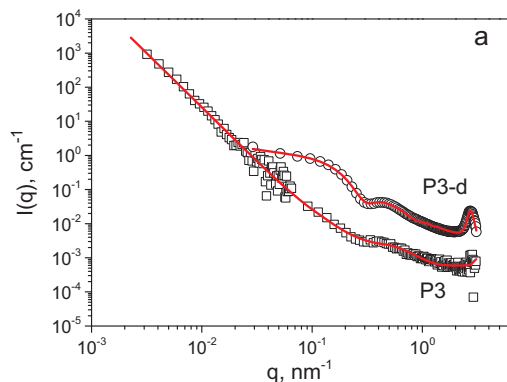
Table 3

Comparison of structural parameters obtained from all samples $PMeOx_{30}$-b-$POctOx_{20}$ (P0), $PMeOx_{30}$-b-$POctOx_{20}$-C_8F_{17} (P1), $PMeOx_{30}$-b-$POctOx_{20}$-$C_{10}F_{21}$ (P2) and $PMeOx_{30}$-b-$POctOx_{20}$-$C_{12}F_{25}$ (P3) prepared by solvent exchange by SAXS.

Fitting parameter	$PMeOx_{30}$-b-$POctOx_{20}$	$PMeOx$-b-$POctOx$-C_8F_{17}	$PMeOx$-b-$POctOx$-$C_{10}F_{21}$	$PMeOx$-b-$POctOx$-$C_{12}F_{25}$
R_{core} (nm)	5.19	4.72	3.7	3.76
sig	0.21	0.17	0.58	0.04
t_1	3.06	2.49	9.9	7.08
t_2	6.96	6.47	3.89	5.61
D (nm)	2.22	2.22	2.26	
σ	0.086	0.115	0.078	0.12
γ	0.1	0.145	0.108	0.09
α	1	1	1	1.13

R_{core} – core radius, Sig – value of polydispersity, t_1 – thickness of first shell of sphere, t_2 – thickness of second shell of sphere, D – repeat distance, σ – width of Gaussian (Doppler) profile, γ – width of Lorentzian profile, α – modified Porod exponent.
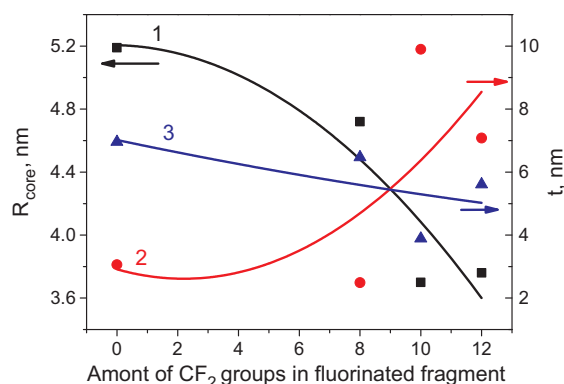
Fig. 9. Dependence of the core radius (R_{core}) (1), thickness (t) of the first (2) and second (3) shell on the length of fluorinated fragment of triblock polyoxazoline polymers (solutions prepared by solvent exchange method).

position of the first minimum in the scattering curve, the radius of a sphere (R) with core-double shell structure could be determined to be approximately 15.2 nm using the following equation qR = 4.493 [47].

It is obvious from Fig. 8b that the intensity of the peak at high q values decreases with increasing length of the fluorinated block. This feature may be related to the presence of two types of water-insoluble chains that both have a tendency to crystallize. While the POctOx segments form more strictly ordered structures due to the conditional homogeneity inside the core, the presence of fluorinated units penalize the homogeneity of the core and of one of the shells, thus reducing the ordering.

Fig. 8. (a) Comparison of SAXS data for $PMeOx_{30}$-b-$POctOx_{20}$-$C_{12}F_{25}$ (P3) prepared by direct dissolution and by solvent exchange; (b) Comparison of SAXS data for all polymers prepared by solvent exchange and (b inset) dependence of maximum amplitude of Voigt peak (calculated by fitting procedure) on the length of fluorinated fragment for nanoparticles prepared by solvent exchange method.

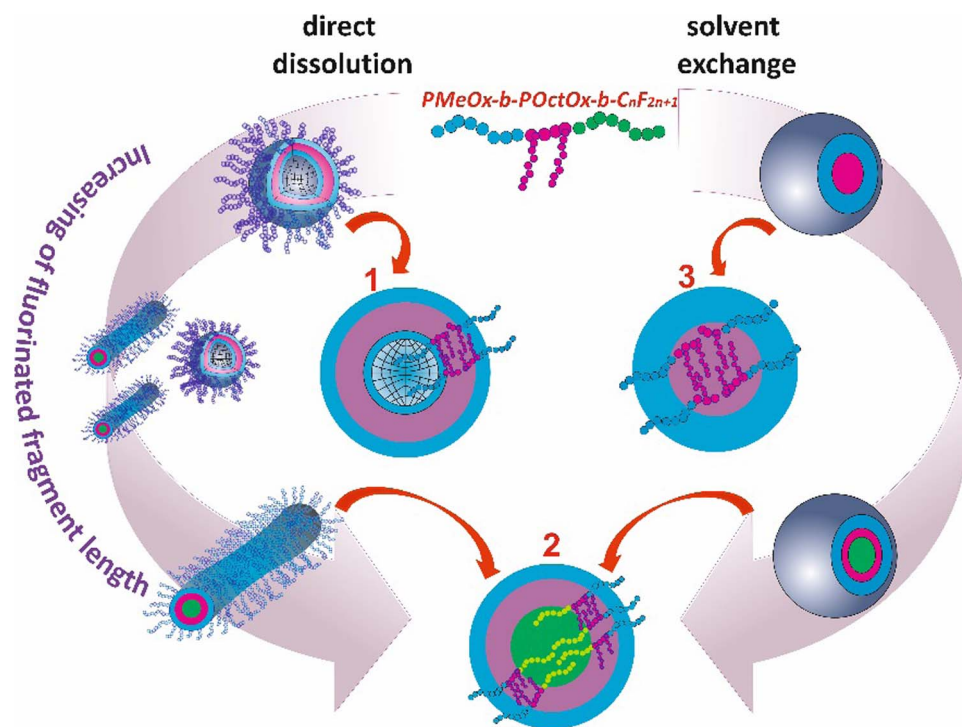**Fig. 10.** A proposed scheme of morphological transition of the fluorinated PMeOx$_{30}$-b-POctOx$_{20}$-C$_n$F$_{2n+1}$ nanoparticles (prepared by direct dissolution and by solvent exchange method) with increasing length of fluorinated fragment summarizing the SAXS and SANS results, where: 1 – scheme of the inner structure of bilayered vesicle formed by PMeOx$_{30}$-b-POctOx$_{20}$ and PMeOx$_{30}$-b-POctOx$_{20}$-C$_{10}$F$_{21}$; 2 – scheme of the inner structure of wormlike micelle and core-shell-shell sphere formed by PMeOx$_{30}$-b-POctOx$_{20}$-C$_n$F$_{2n+1}$; 3 – scheme of the sphere with core-shell inner structure.

Dependences of the main structural parameters (Table 3) obtained from the fitting procedure on the length of fluorinated fragment are presented in the Fig. 9.

One can see that the thickness of the second shell, consist of poly(2-methyl-2-oxazoline) block, varies only slightly, while thickness of the first shell increase with the increasing of the length of fluorinated fragment. At the same time core radius decreases with the increasing of the fluorinated part length. It can be explained by the assumption that for copolymer PMeOx30-b-POctOx20-C$_8$F$_{17}$ with the shortest fluorinated fragment poly(2-octyl-2-oxazoline) block is more hydrophobic then fluorinated part. That is why the core the sphere for PMeOx30-b-POctOx20-C$_8$F$_{17}$ consists of the poly(2-octyl-2-oxazoline) block as it was for diblock copolymer. With increasing of the length of fluorinated fragment its hydrophobicity increase and for PMeOx30-b-POctOx20-C$_{10}$F$_{21}$ and PMeOx30-b-POctOx20-C$_{12}$F$_{25}$ the core is formed mainly by fluorinated groups. We can also assume that the first hydrophobic shell consist of poly(2-octyl-2-oxazoline) block with partially involved fluorinated fragment.

The proposed scheme of morphological transition observed in this study is presented in the Fig. 10. It can be concluded from the comparison of the SAXS and SANS results as well as of DLS and cryo-TEM results presented recently [32] that shape and inner structure of fluorinated quasi-triblock poly(2-oxazolines) can be easily controlled by the changing of terminal fluorinated group as well as by the method of preparation.

5. Conclusions

Aqueous self-assembly of quasi-triblock copolymers composed of hydrophilic, hydrophobic and perfluorinated blocks was studied at room temperature using SAXS and SANS analysis. Detailed information about the shape and the internal structure of the self-assembled nanoparticles as function of their composition and fluorine content was obtained and compared with previously obtained cryo-TEM data. Nanoparticles formed by the reference diblock PMeOx$_{30}$-b-POctOx$_{20}$ without fluorinated segment could be described by a bilayered vesicle form factor in combination with a Percus-Yevick structure factor. SANS and SAXS experiments revealed the morphological transition of

micelles from bilayered vesicles to wormlike micelles with increasing length of the perfluorinated fragment of the quasi-triblock PAOx. It was further found that the preparation method influences the nanoparticles' shape and internal structure: with solvent displacement it becomes independent of the fluorine content and the SAXS curves could be fitted with a core–shell-shell form factor. Additional ordering was identified within the inner layer of bilayered vesicles, core of wormlike micelles as well as inside of the core of spheres, probably due to the crystallization of the POctOx and perfluorinated segments, and was described with a Voigt peak model.

Notes

Appendix A. Supplementary material

Supplementary data associated with this article can be found, in the online version, at http://dx.doi.org/10.1016/j.eurpolymj.2018.01.007.

References

[1] T.X. Viegas, M.D. Bentley, J.M. Harris, Z. Fang, K. Yoon, B. Dizman, R. Weimer, A. Mero, G. Pasut, F.M. Veronese, Polyoxazoline: chemistry, properties, and applications in drug delivery, Bioconjug. Chem. 22 (5) (2011) 976–986.
[2] M.C. Woodle, C.M. Engbers, S. Zalipsky, New amphipatic polymer-lipid conjugates forming long-circulating reticuloendothelial system-evading liposomes, Bioconjug.

Chem. 5 (1994) 493–496.

[3] M. Hrubý, S.K. Filippov, P. Štěpánek, Smart polymers in drug delivery systems on crossroads: which way deserves following? Eur. Polym. J. 65 (2015) 82–97.

[4] R. Luxenhofer, Y. Han, A. Schulz, J. Tong, Z. He, A.V. Kabanov, R. Jordan, Poly (2-oxazoline)s as polymer therapeutics, Macromol. Rapid Commun. 33 (2012) 1613–1631.

[5] B. Guillerm, V. Darcos, V. Lapinte, S. Monge, J. Coudane, J.-J. Robin, Synthesis and evaluation of triazole-linked poly(ε-caprolactone)-graft-poly(2-methyl-2-oxazoline) copolymers as potential drug carriers, Chem. Commun. 48 (2012) 2879–2881.

[6] M. Hruby, S.K. Filippov, J. Panek, M. Novakova, H. Mackova, J. Kucka, D. Vetvicka, K. Ulbrich, Polyoxazoline thermoresponsive micelles as radionuclide delivery systems, Macromol. Biosci. 10 (2010) 916–924.

[7] G.-H. Hsiue, H.-Z. Chiang, C.-H. Wang, T.-M. Juang, Nonviral gene carriers based on diblock copolymers of poly(2-ethyl-2-oxazoline) and linear polyethylenimine, Bioconjug. Chem. 17 (2006) 781–786.

[8] B. Pidhatika, M. Rodenstein, Y. Chen, E. Rakhmatullina, A. Muhlebach, C. Acikguz, M. Textor, R. Konradi, Comparative stability studies of poly(2-methyl-2-oxazoline) and poly(ethylene glycol) brush coatings, Biointerphases 7 (2012) 1–4.

[9] D.A. Tomalia, D.P. Sheetz, Homopolymerization of 2-alkyl- and 2-aryl-2-oxazolines, J. Polym. Sci. Part A-1 Polym. Chem. 4 (1966) 2253–2265.

[10] B. Verbraeken, B.D. Monnery, K. Lava, R. Hoogenboom, The Chemistry of poly(2-oxazoline)s, Eur. Polym. J. (2016).

[11] M.A. Tasdelen, M.U. Kahveci, Y. Yagci, Telechelic polymers by living and controlled/living polymerization methods, Prog. Polym. Sci. 36 (2011) 455–567.

[12] B. Guillerm, S. Monge, V. Lapinte, J.J. Robin, How to modulate the chemical structure of polyoxazolines by appropriate functionalization, Macromol. Commun. 33 (2012) 1600–1612.

[13] K. Lava, B. Verbraeken, R. Hoogenboom, Poly(2-Oxazoline)s and click chemistry: a versatile toolbox toward multi-functional polymers, Eur. Polym. J. 65 (2015) 98–111.

[14] B. Trzebicka, N. Koseva, V. Mitova, A. Dworak, Organization of poly(2-ethyl-2-oxazoline)-block-poly(2-phenyl-2-oxazoline) copolymers in water solution, Polymer (Guildf) 51 (2010) 2486–2493.

[15] J. Du, Polymer vesicles, Adv. Hierarchical Nanostruct. Mater. 967 (2002) 177–192.

[16] S. Zalipsky, C.B. Hansen, J.M. Oaks, T.M. Allen, Evaluation of blood clearance rates and biodistribution of poly(2-oxazoline)-grafted liposomes, J. Pharm. Sci. 85 (1996) 133–137.

[17] Y. Milonaki, E. Kaditi, S. Pispas, C. Demetzos, Amphiphilic gradient copolymers of 2-methyl- and 2-phenyl-2-oxazoline: self-organization in aqueous media and drug encapsulation, J. Polym. Sci. Part A Polym. Chem. 50 (2012) 1226–1237.

[18] R. Luxenhofer, A. Schulz, C. Roques, S. Li, T.K. Bronich, E.V. Batrakova, R. Jordan, A.V. Kabanov, Doubly amphiphilic poly(2-oxazoline)s as high-capacity delivery systems for hydrophobic drugs, Biomaterials 31 (2010) 4972–4979.

[19] A.O. Moughton, M.A. Hillmyer, T.P. Lodge, Multicompartment block polymer micelles, Macromolecules 45 (2012) 2–19.

[20] Z. Li, E. Kesselman, Y. Talmon, M.A. Hillmyer, T.P. Lodge, Multicompartment micelles from ABC Miktoarm stars in water, Science 306 (5693) (2004) 98–110.

[21] S. Kubowicz, J.F. Baussard, J.F. Lutz, A.F. Thünemann, H. Von Berlepsch, A. Laschewsky, Multicompartment micelles formed by self-assembly of linear ABC triblock copolymers in aqueous medium, Angew. Chemie - Int. Ed. 44 (33) (2005) 5262–5265.

[22] F. Tournilhac, L. Bosio, J.F. Nicoud, J. Simon, Polyphilic molecules: synthesis and mesomorphic properties of a four-block molecule, Chem. Phys. Lett. 145 (5) (1988) 452–454.

[23] L. Campo, T. Varslot, M.J. Moghaddam, J.J.K. Kirkensgaard, K. Mortensen, S.T. Hyde, A novel lyotropic liquid crystal formed by triphilic star-polyphiles: hydrophilic/oleophilic/fluorophilic rods arranged in a 12.6.4. tiling, Phys. Chem. Chem. Phys. 13 (2011) 3139–3152.

[24] S.T. Hyde, L. de Campo, C. Oguey, Tricontinuous mesophases of balanced three-arm "star Polyphiles", Soft Matter 5 (2009) 2782.

[25] G.F. von Rudorff, T. Watermann, X.-Y. Guo, D. Sebastiani, Conformational space of a polyphilic molecule with a fluorophilic side chain integrated in a DPPC bilayer, J.

Comput. Chem. 38 (9) (2017) 576–583.

[26] D.J. Pochan, Z. Chen, H. Cui, K. Hales, K. Qi, K.L. Wooley, Toroidal triblock copolymer assemblies, Science 306 (5693) (2004) 94–97.

[27] K. Kempe, R. Hoogenboom, S. Hoeppener, C.-A. Fustin, J.-F. Gohy, U.S. Schubert, Discovering new block terpolymer micellar morphologies, Chem. Commun. (Camb.) 46 (35) (2010) 6455–6457.

[28] H. Peng, I. Blakey, B. Dargaville, F. Rasoul, S. Rose, A.K. Whittaker, Synthesis and evaluation of partly fluorinated block copolymers as MRI imaging agents, Biomacromolecules 10 (2009) 374–381.

[29] K. Wang, H. Peng, K.J. Thurecht, S. Puttick, A.K. Whittaker, PH-responsive star polymer nanoparticles: potential 19F MRI contrast agents for tumour-selective imaging, Polym. Chem. 4 (16) (2013) 4480–4489.

[30] U. Mansfeld, S. Hoeppener, K. Kempe, J.-M. Schumers, J.-F. Gohy, U.S. Schubert, Tuning the morphology of triblock terpoly(2-oxazoline)s containing a 2-phenyl-2-oxazoline block with varying fluorine content, Soft Matter 9 (25) (2013) 5966.

[31] R. Weberskirch, J. Preuschen, H.W. Spiess, O. Nuyken, Design and synthesis of a two compartment micellar system based on the self-association behavior of poly(N-acylethyleneimine) end-capped with a fluorocarbon and a hydrocarbon chain, Macromol. Chem. Phys. 201 (10) (2000) 995–1007.

[32] L.I. Kaberov, B. Verbraeken, M. Hruby, A. Riabtseva, L. Kovacik, S. Kereïche, J. Brus, P. Stepanek, R. Hoogenboom, S.K. Filippov, Novel triphilic block copolymers based on poly(2-methyl-2-oxazoline)–block–poly(2-octyl-2-oxazoline) with different terminal perfluoroalkyl fragments: synthesis and self-assembly behaviour, Eur. Polym. J. 88 (2017) 645–655.

[33] I. Bressler, J. Kohlbrecher, A.F. Thanemann, SASfit: a tool for small-angle scattering data analysis using a library of analytical expressions, J. Appl. Crystallogr. 48 (2015) 1587–1598.

[34] J.K. Percus, G.J. Yevick, Analysis of classical statistical mechanics by means of collective coordinates, Phys. Rev. 110 (1958) 1–13.

[35] J.S. Pedersen, M.C. Gerstenberg, Scattering form factor of block copolymer micelles, Macromolecules 29 (1996) 1363–1365.

[36] A.L. Kholodenko, Analytical calculation of the scattering function for polymers of arbitrary flexibility using the dirac propagator, Macromolecules 26 (1993) 4179–4183.

[37] A. Guinier, G. Fournet, G. Fournet (Ed.), Small-Angle Scattering of X-Rays, John Wiley and Sons, New York, 1955.

[38] M.J. Derry, O.O. Mykhaylyk, S.P. Armes, A vesicle-to-worm transition provides a new high-temperature oil thickening mechanism, Angew. Chemie - Int. Ed. 56 (7) (2017) 1746–1750.

[39] N. Baccile, A.S. Cuvier, S. Provost, C.V. Stevens, E. Delbeke, J. Berton, W. Soetaert, I.N.A. Van Bogaert, S. Roelants, Self-assembly mechanism of pH-responsive glycolipids: micelles, fibers, vesicles, and bilayers, Langmuir 32 (2016) 10881–10894.

[40] D. Balzar, H. Ledbetter, Voigt-function modeling in fourier analysis of size- and strain-broadened X-ray diffraction peaks, J. Appl. Crystallogr. 26 (pt 1) (1993) 97–103.

[41] N.A. Plate, V.P. Shibaev, Comb-Shaped Polymers and Liquid Crystals, Plenum Press, New York, 1987.

[42] B. Weyerich, J. Brunner-Popela, O. Glatter, Small-angle scattering of interacting particles. II. Generalized indirect fourier transformation under consideration of the effective structure factor for polydisperse systems, J. Appl. Crystallogr. 32 (1999) 197–209.

[43] L.M. Wilson, A.C. Griffin, Liquid crystalline fluorocarbon side-chain polyesters, Macromolecules 27 (1994) 1928–1931.

[44] L.M. Wilson, A.C. Griffin, Liquid-crystalline behavior in a series of fluorocarbon side-chain polyesters. 2, Macromolecules 27 (1994) 4611–4614.

[45] A. Hirao, G. Koide, K. Sugiyama, Synthesis of novel well-defined chain-end- and in-chain-functionalized polystyrenes with one, two, three, and four perfluorooctyl groups and their surface characterization, Macromolecules 35 (2002) 7642–7651.

[46] V.V. Volkov, N.A. Plate, A. Takahara, T. Kajiyama, N. Amaya, Y. Murata, Aggregation state and mesophase structure of comb-shaped polymers with fluorocarbon side groups, Polymer (Guildf). 33 (1992) 1316–1320.

[47] O. Glatter, O. Kratky, Small-angle X-ray scattering, Academic Press, London, 1982.

Supporting Information

Structural characterization of nanoparticles formed by fluorinated poly(2-oxazoline)-based polyphiles

Anna Riabtseva[1], Leonid I. Kaberov[1], Laurence Noirez[2], Vasyl Ryukhtin[3], Corinne Nardin[4], Bart Veerbraeken[5], Richard Hoogenboom[5], Petr Stepanek[1], Sergey K. Filippov[1]

[1]Institute of Macromolecular Chemistry, Academy of Sciences of the Czech Republic, Heyrovský Sq. 2, 162 06 Prague 6, Czech Republic

[2]Laboratoire Léon Brillouin (CEA-CNRS), UMR12, Université Paris-Saclay, CEA-Saclay, F-91191 Gif-sur-Yvette, France

[3]Nuclear Physics Institute, ASCR, v.v.i., Husinec-Řež 250 68, Czech Republic

[4]Université de Pau et des Pays de l'Adour/CNRS, Institut des Sciences Analytiques et de Physico-chimie pour l'Environnement et les Matériaux, UMR5254, 64000, Pau, France

[5]Supramolecular Chemistry Group, Department of Organic and Macromolecular Chemistry, Ghent University, Krijgslaan 281 S4, B-9000 Ghent, Belgium

Table S1. Theoretical scattering length densities (SLD) for solvent and polymeric blocks calculated with SASfit software. Weight densities for calculation of SLD were taken from literature.

	SAXS $\times 10^{-4}$, nm^{-2}	SANS $\times 10^{-4}$, nm^{-2}
MeOx	9.65	1.16
OctOx	10.4	0.35
C_8F_{17}	8.99	2.36
$C_{10}F_{21}$	8.99	2.36
$C_{12}F_{25}$	8.99	2.37
water	9.44	6.33

Table S2. Scattering length densities (SLD) for aqueous solutions of polymer obtained by direct dissolution calculated by fitting procedure. All SLD values have units of nm^{-2}.

Fitting parameter	PMeOx$_{30}$OctOx$_{20}$		PMeOx$_{30}$OctOx$_{20}$-C$_8$F$_{17}$				PMeOx$_{30}$OctOx$_{20}$-C$_{10}$F$_{21}$		PMeOx$_{30}$OctOx$_{20}$-C$_{12}$F$_{25}$	
	Bilayered vesicle		Bilayered vesicle		Wormlike micelle		Wormlike micelle		Wormlike micelle	
	SAXS ×10^{-4}	SANS ×10^{-4}	SAXS ×10^{-4}	SANS ×10^{-4}	SAXS ×10^{-4}	SANS ×10^{-4}	SAXS ×10^{-4}	SANS ×10^{-4}	SAXS ×10^{-4}	SANS ×10^{-4}
η_o	10	1.59	9.27	1.59	-	-	-	-	-	-
η_i	8.9	0.18	9.65	0.35	-	-	-	-	-	-
η_{brush}	-	-	-	-	9.76	2.72	9.8	-	8.4	1.15
η_{core}	-	-	-	-	9.9	0.46	9.91	-	9.9	2.3

Table S3. Scattering length densities (SLD) for aqueous solutions of polymer obtained by solvent exchange calculated by fitting procedure.

Fitting parameter	PMeOx$_{30}$OctOx$_{20}$	PMeOx$_{30}$OctOx$_{20}$-C$_8$F$_{17}$	PMeOx$_{30}$OctOx$_{20}$-C$_{10}$F$_{21}$	PMeOx$_{30}$OctOx$_{20}$-C$_{12}$F$_{25}$
	SAXS ×10^{-4}, nm^{-2}	SAXS ×10^{-4}, nm^{-2}	SAXS ×10^{-4}, nm^{-2}	SAXS ×10^{-4}, nm^{-2}
η_{core}	8.93	9.0	9.50	5.69
η_{sh1}	9.82	9.83	9.45	1.08
η_{sh2}	9.50	9.51	9.52	9.72

MANUSCRIPT M3

Kaberov L.I., Verbraeken B., Riabtseva A., Brus J., Talmon Y., Stepanek P., Hoogenboom R., Filippov S.K.. Fluorinated 2-alkyl-2-oxazolines of high reactivity: Spacer-length induced acceleration for Cationic Ring-Opening polymerization as basis for triphilic block copolymer synthesis. *ACS Macro Lett.* **2018**, 7, 7−10. DOI: 10.1021/acsmacrolett.7b00954

Fluorinated 2-Alkyl-2-oxazolines of High Reactivity: Spacer-Length-Induced Acceleration for Cationic Ring-Opening Polymerization As a Basis for Triphilic Block Copolymer Synthesis

Leonid I. Kaberov,[†] Bart Verbraeken,[‡] Anna Riabtseva,[†] Jiri Brus,[†] Yeshayahu Talmon,[§] Petr Stepanek,[†] Richard Hoogenboom,[‡] and Sergey K. Filippov*,[†]

[†]Institute of Macromolecular Chemistry, Academy of Sciences of the Czech Republic, Heyrovský Sq. 2, 162 06 Prague 6, Czech Republic

[‡]Supramolecular Chemistry Group, Department of Organic and Macromolecular Chemistry, Ghent University, Krijgslaan 281 S4, B-9000 Ghent, Belgium

[§]Department of Chemical Engineering, Technion-Israel Institute of Technology, Haifa 3200003, Israel

S *Supporting Information*

ABSTRACT: The synthesis of defined triphilic terpolymers with hydrophilic, lyophilic, and fluorophilic blocks is an important challenge as a basis for the development of multicompartment self-assembled structures with potential for, e.g., cascade catalysis and multidrug loading. The synthesis of fluorophilic poly(2-oxazoline)s generally suffers from a very low reactivity of fluorinated 2-oxazoline monomers in cationic ring-opening polymerization (CROP). We report a systematic study on overcoming the extremely low reactivity of 2-perfluoroalkyl-2-oxazolines in CROP by the insertion of methyl and ethyl hydrocarbon spacers between the 2-oxazoline ring and the trifluoromethyl group. The kinetic studies showed the gradual increase of the rate of polymerization with increasing of the hydrocarbon spacer length. The monomer with an ethyl spacer was found to have similar reactivity as 2-alkyl-2-oxazolines and allowed the synthesis of defined triphilic triblock copolymers.
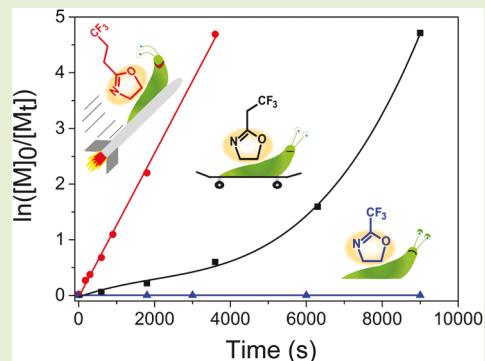
Poly(2-oxazoline)s are widely used in many medical and biological applications.[1,2] The cationic ring-opening polymerization (CROP) of 2-substituted 2-oxazolines can proceed at certain conditions in a living mode, which allows us to synthesize defined polymers with very low dispersity. In combination with a variety of commercially and synthetically available monomers, it makes 2-oxazolines very attractive candidates for the design of amphiphilic polymer systems with controlled properties.[3−5] The majority of these systems is amphiphilic AB block and ABA triblock copolymers. However, in recent years, the behavior of hydrophilic−hydrophobic−fluorophilic ABC triblock copolymers has attracted significant attention as they form more complex self-assembled structures than traditional AB copolymers due to mutual incompatibility of all three blocks.[6−9] Such multicompartment self-assembled structures are highly interesting as for developing cascade catalysis or multidrug drug delivery by encapsulation of incompatible catalysts or drugs into the separate compartments.

The development of triphilic poly(2-oxazoline)s is severely hampered by the extremely low reactivity of fluorinated 2-oxazolines in CROP, representing the main limitation and challenge for the synthesis of aliphatic fluorophilic poly(2-oxazoline)s. Usually, the CROP of 2-alkyl-2-oxazolines proceeds via ionic propagation centers.[10] However, the presence of a strong electron-withdrawing perfluoroalkyl

substituent in the 2-position of the 2-oxazoline ring extremely decreases the reactivity of the monomer and facilitates the transition of the active center into the less reactive covalent form.[11,12] The synthesis of such perfluoroalkyl poly(2-oxazoline)s with high degree of polymerization (more than 10 monomeric units) is associated with significant experimental difficulties (e.g., high temperature and long reaction times), making it practically impossible.[13]

To overcome this limitation, there is a need for novel fluorinated 2-oxazolines with higher reactivity. Recently, the polymerization of fluorinated 2-phenyl-2-oxazolines has been reported by Schubert et al., allowing the preparation of triblock copolymers and the formation of multicompartment micelles.[14,15] A few examples of fluorinated poly(2-oxazoline)s based on monomers with an ethyl spacer between the fluorinated segment and the 2-oxazoline ring were also reported in works of Papadakis[16] and Sogah,[17,18] where it was postulated that this decouples the fluorinated segment from the 2-oxazoline ring without providing kinetic evidence.

Here we present a detailed systematic study on increasing the reactivity of fluorinated 2-oxazoline monomers by insertion of

hydrocarbon spacers. Therefore, new fluorine-containing 2-alkyl-2-oxazolines were developed having methyl and ethyl spacers between the terminal CF_3 group and the 2-oxazoline ring. All fluorinated 2-oxazolines were synthesized by a standard method based on the synthesis of N-(β-haloethyl)amides followed by a ring-closing reaction to obtain the desired 2-oxazoline monomers.

2-Trifluoromethyl-2-oxazoline was synthesized on the basis of a literature procedure (Figure 1).[19] According to this method
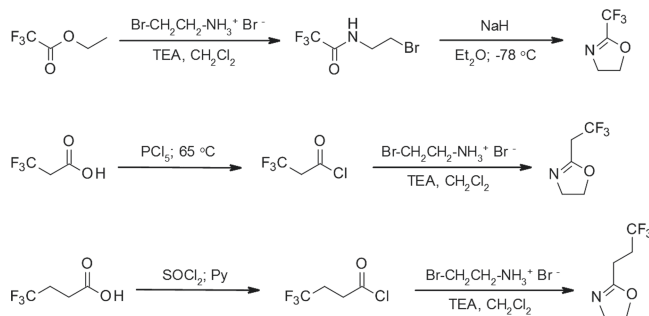

Figure 1. Synthesis scheme for the fluorinated 2-oxazoline monomers.

N-(2-bromoethyl)trifluoroacetamide was obtained from ethyl-trifluoroacetate by reaction with 2-bromoethylamine hydro-bromide. The second step was ring closure using sodium hydride as base yielding 2-trifluoromethyl-2-oxazoline (CF_3Ox).

The synthesis of 2-(2,2,2-trifluoroethyl)-2-oxazoline (CF_3MeOx, **a**) and 2-(3,3,3-trifluoropropyl)-2-oxazoline (CF_3EtOx, **b**) was started from the corresponding carboxylic acids that were converted to the more reactive acid chloride. The amide formation was performed with 2-bromoethylamine in the presence of excess of triethylamine, directly yielding the ring-closed 2-oxazoline monomers.

The polymerization kinetics of the three monomers was studied at standard polymerization conditions, being 140 °C in acetonitrile in a closed reaction vessel, at a monomer concentration of 1 M, with methyl p-toluenesulfonate (MeTos) as initiator and a target degree of polymerization of 100.[20] The conversion of the monomer was determined by gas chromatography (GC), whereas molecular weights were analyzed by size exclusion chromatography (SEC).

Under these conditions, CF_3Ox revealed no noticeable conversion after 24 h. Variation of temperature (up to 180 °C

when degradation occurs) and the use of another solvent/initiator system (dichlorobenzene/silver triflate (AgOTf) + MeTos) also gave no polymerization. This behavior can be ascribed to the strong electron-withdrawing effect of the trifluoromethyl group on the reactivity of the monomer and is in agreement with previous observations by Jordan and Papadakis for 2-perfluoroalkyl-2-oxazolines.[12]

The polymerization of CF_3MeOx with a single methylene unit as spacer proceeds with acceptable rate, and full monomer conversion was achieved after 2.5 h under standard conditions (Figure 2a). However, the first-order kinetic plot shows a continuous increase in slope indicative of slow initiation; i.e., during the polymerization more and more chains are initiated leading to faster monomer conversion, which can be ascribed to the low monomer nucleophilicity (Figure 2a). Due to this continuous initiation SEC revealed a very broad molar mass distribution that was not resolved from the system peak obstructing accurate integration (see Supporting Information Figure S1).

Finally, the CF_3EtOx monomer with a double methylene spacer shows the linear first-order kinetics, typical for living CROP (Figure 2a). The SEC traces at various conversions show a narrow molar mass distribution with dispersity ($Đ$) well below 1.2 (Figure 2b). The appearance of the double molar mass shoulder at higher conversion is due to unavoidable chain transfer reactions that result in enamine end-capped polymers. Toward the end of the reaction, these enamine functional polymers react with living polymer chains inducing higher molar mass branched structures.[10] This shoulder is resolved in the high-resolution SEC system but does not strongly influence the $Đ$. The polymerization rate constant (k_p), calculated from the slope of the first-order kinetic plot, was found to be $k_p = 129 \times 10^{-3}$ L mol^{-1} s^{-1}, which is very similar to nonfluorinated 2-alkyl-2-oxazolines indicating that the electron-withdrawing effect of the CF_3 group on the 2-oxazoline ring is completely suppressed when introducing an ethyl spacer.[21] From these kinetic studies it can be concluded that only the CF_3EtOx is applicable for the synthesis of block copolymers.

Next, we continued the preparation of a series of amphiphilic block copolymers by CROP with sequential monomer addition. More specifically, diblock copolymers were prepared by first polymerizing MeOx up to >98% conversion followed by addition of CF_3EtOx, while triblock copolymers of MeOx, CF_3EtOx, and 2-octyl-2-oxazoline (OctOx, chosen as hydro-phobic comonomer immiscible with CF_3EtOx) were prepared
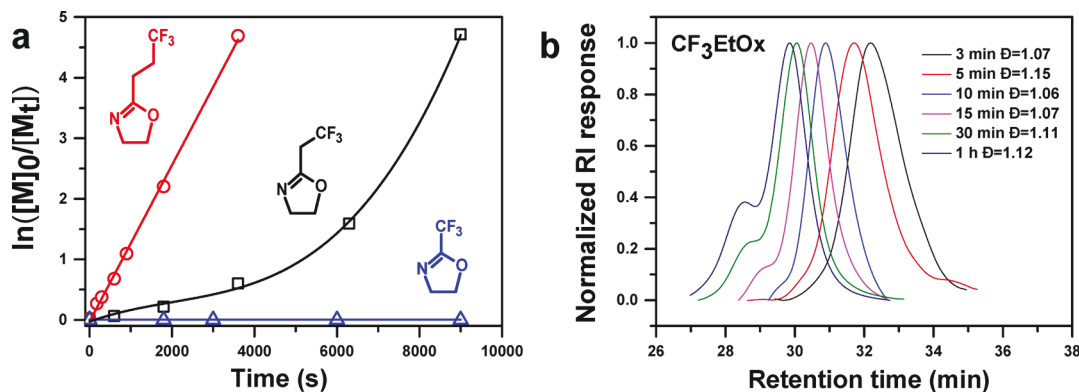

Figure 2. Kinetic plots for the cationic ring-opening polymerization (a) of CF_3Ox (blue), CF_3MeOx (black), CF_3EtOx (red), and the SEC data for CF_3EtOx (b). RI: Refractive Index.

Table 1. Characteristics of the Synthesized Block Copolymers

	composition (NMR)	M_n (SEC-MALS), g/mol	M_w (SEC-MALS), g/mol	Đ (SEC-MALS)	monomer ratio (NMR)
DB1	$MeOx_{38}\text{-}CF_3EtOx_{17}$	6000	7200	1.20	2.2:1
DB2	$MeOx_{47}\text{-}CF_3EtOx_{27}$	8500	11000	1.30	1.7:1
DB3	$MeOx_{39}\text{-}CF_3EtOx_{28}$	7500	10300	1.37	1.4:1
DB4	$MeOx_{23}\text{-}CF_3EtOx_{25}$	6100	8100	1.33	0.9:1
TB1	$MeOx_{28}\text{-}OctOx_9\text{-}CF_3EtOx_{12}$	6300	8000	1.27	2.3:0.7:1
TB2	$MeOx_{49}\text{-}OctOx_{11}\text{-}CF_3EtOx_{16}$	9000	11800	1.31	3:0.7:1
TB3	$OctOx_{12}\text{-}MeOx_{52}\text{-}CF_3EtOx_{18}$	9700	13500	1.39	0.65:2.8:1

by first polymerizing MeOx up to >98% conversion, followed by polymerization of the second monomer up to >98% conversion, followed by addition of the third monomer and polymerization up to >98% conversion. All polymerizations were terminated by the addition of 1 M KOH in methanol to the polymerization mixture. The structural details and characterization data of the synthesized diblock and triblock copolymers are summarized in Table 1, demonstrating that well-defined polymers were obtained with Đ < 1.4. Importantly, TB2 and TB3 have similar Đ indicating that the order of addition of monomers does not make a difference, as anticipated based on their similar k_p.

In the final part of this work, a preliminary evaluation of the self-assembly potential of the synthesized partially fluorinated block copolymers in water was performed. It was proven by dynamic light scattering (DLS) that all polymers can be molecularly dissolved in a number of common organic solvents, including methanol (Figure S2), ethanol, and chloroform. The aqueous solutions of block copolymers were prepared by using a solvent exchange method from methanol to water by dialysis. A DLS study of the obtained aqueous solutions of the MeOx-CF_3EtOx diblock copolymers revealed the presence of particles with hydrodynamic diameters in the range of 17−25 nm, attributed to micelles (see Supporting Information Figure S3). The size of the aggregates resulting from the triblock copolymer is larger, up to 30−50 nm, and the appearance of a certain fraction of larger aggregates with a hydrodynamic diameter in the range of 150−300 nm was observed (see Supporting Information Figure S4). In addition, the middle position of the hydrophilic block in the TB3 triblock caused the formation of larger aggregates compared to the same composition TB2 triblock with terminal hydrophilic block (see Supporting Information Figure S4). On the cryo-TEM image of triblock TB1 (1 wt %) (Figure 3), spherical aggregates with a mean diameter of 15 nm are observed representing the hydrophobic core of polymer micelles. A small population of large spherical objects was also found in the cryo-TEM image, which could correspond to the larger particles observed by DLS.

To conclude, a systematic study on the insertion of a spacer between the fluorinated fragment and the 2-oxazoline ring was reported revealing its effect on the monomer reactivity in CROP. Two new fluorinated 2-oxazoline monomers, namely, CF_3MeOx and CF_3EtOx, were synthesized and characterized. The kinetic study showed a gradual increase of monomer reactivity in CROP with insertion of methylene spacers between the trifluoromethyl group and the 2-oxazoline ring. Insertion of two methylene groups allows complete suppression of the electron-withdrawing effect of the trifluoromethyl group, yielding similar reactivity as nonfluorinated 2-alkyl-2-oxazolines. Subsequently, a set of di- and triblock copolymers with MeOx as hydrophilic block and a CF_3EtOx-based fluorophilic block
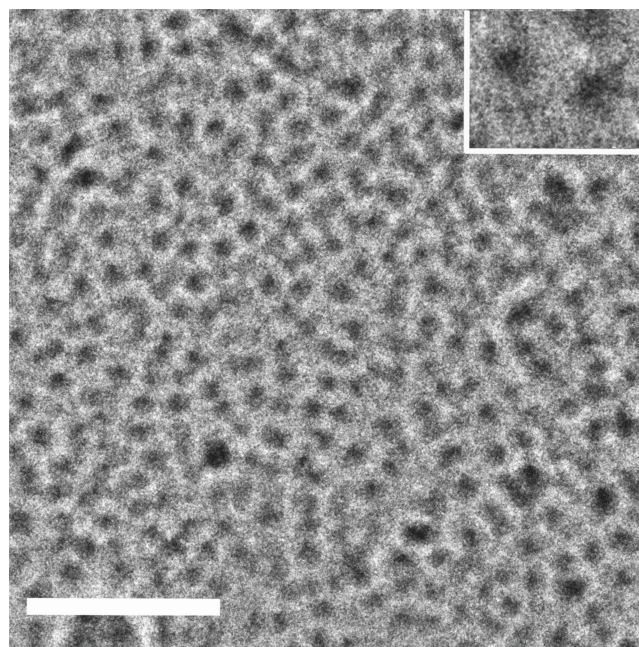

Figure 3. Cryo-TEM image micelles of triblock TB1. The scale bar equals 100 nm; the inset: full width is 40 nm.

with polydispersity in the range of 1.2−1.4 was synthesized. The self-assembly potential of the synthesized block copolymers in aqueous solution was demonstrated by DLS. Cryo-TEM revealed the presence of micelles in aqueous solution based on the triphilic triblock copolymers. Future work will focus on more in-depth studies on the self-assembly behavior of amphiphilic diblock and triblock copolymers based on CF_3EtOx.

■ ASSOCIATED CONTENT

Ⓢ Supporting Information

The Supporting Information is available free of charge on the ACS Publications website at DOI: 10.1021/acsmacro-lett.7b00954.

> Materials and methods, monomer synthesis, polymer synthesis, characterization techniques, and experimental data (PDF)

■ AUTHOR INFORMATION

Corresponding Author

*E-mail: filippov@imc.cas.cz.

ORCID Ⓞ

Jiri Brus: 0000-0003-2692-612X

Richard Hoogenboom: 0000-0001-7398-2058

Sergey K. Filippov: 0000-0002-4253-5076

Notes

The authors declare no competing financial interest.

REFERENCES

(1) Luxenhofer, R.; Schulz, A.; Roques, C.; Li, S.; Bronich, T. K.; Batrakova, E. V.; Jordan, R.; Kabanov, A. V. *Biomaterials* **2010**, *31* (18), 4972−4979.

(2) Luxenhofer, R.; Sahay, G.; Schulz, A.; Alakhova, D.; Bronich, T. K.; Jordan, R.; Kabanov, A. V. *J. Controlled Release* **2011**, *153* (1), 73−82.

(3) Hoogenboom, R.; Schlaad, H. *Polymers (Basel, Switz.)* **2011**, *3* (4), 467−488.

(4) Hoogenboom, R. *Angew. Chem., Int. Ed.* **2009**, *48* (43), 7978−7994.

(5) Schlaad, H.; Diehl, C.; Gress, A.; Meyer, M.; Levent Demirel, A.; Nur, Y.; Bertin, A. *Macromol. Rapid Commun.* **2010**, *31* (6), 511−525.

(6) Kubowicz, S.; Baussard, J. F.; Lutz, J. F.; Thünemann, A. F.; Von Berlepsch, H.; Laschewsky, A. *Angew. Chem., Int. Ed.* **2005**, *44* (33), 5262−5265.

(7) Moughton, A. O.; Hillmyer, M. A.; Lodge, T. P. *Macromolecules* **2012**, *45* (1), 2−19.

(8) Li, Z.; Kesselman, E.; Talmon, Y.; Hillmyer, M. A.; Lodge, T. P. *Science (Washington, DC, U. S.)* **2004**, *306* (5693), 98−101.

(9) Pochan, D. J.; Chen, Z.; Cui, H.; Hales, K.; Qi, K.; Wooley, K. L. *Science (Washington, DC, U. S.)* **2004**, *306* (5693), 94−97.

(10) Verbraeken, B.; Monnery, B. D.; Lava, K.; Hoogenboom, R. *Eur. Polym. J.* **2017**, *88*, 451−469.

(11) Miyamoto, M.; Aoi, K.; Saegusa, T. *Macromolecules* **1988**, *21*, 1880−1883.

(12) Saegusa, T.; Chujo, Y.; Aoi, K.; Miyamoto, M. *Makromol. Chem., Macromol. Symp.* **1990**, *32*, 1−10.

(13) Miyamoto, M.; Aoi, K.; Saegusa, T. *Macromolecules* **1991**, *24* (1), 11−16.

(14) Lobert, M.; Thijs, H. M. L.; Erdmenger, T.; Eckardt, R.; Ulbricht, C.; Hoogenboom, R.; Schubert, U. S. *Chem. - Eur. J.* **2008**, *14* (33), 10396−10407.

(15) Kempe, K.; Hoogenboom, R.; Hoeppener, S.; Fustin, C.-A.; Gohy, J.-F.; Schubert, U. S. *Chem. Commun.* **2010**, *46* (35), 6455.

(16) Ivanova, R.; Komenda, T.; Bonné, T. B.; Lüdtke, K.; Mortensen, K.; Pranzas, P. K.; Jordan, R.; Papadakis, C. M. *Macromol. Chem. Phys.* **2008**, *209* (21), 2248−2258.

(17) Kaku, M.; Grimminger, L. C.; Sogah, D. Y.; Haynie, S. I. *J. Polym. Sci., Part A: Polym. Chem.* **1994**, *32* (11), 2187−2192.

(18) Rodriguez-Parada, J. M.; Kaku, M.; Sogah, D. Y. *Macromolecules* **1994**, *27* (6), 1571−1577.

(19) Ishikawa, N.; Akira, S. EP0151449(A2) - Process for the production of fluorine containing N-(beta-bromoethyl)amide and of 2-(perfluoroalkyl)-1,3-oxazoline, 1985.

(20) Wiesbrock, F.; Hoogenboom, R.; Leenen, M. A. M.; Meier, M. A. R.; Schubert, U. S. *Macromolecules* **2005**, *38* (12), 5025−5034.

(21) Hoogenboom, R.; Fijten, M. W. M.; Thijs, H. M. L.; van Lankvelt, B. M.; Schubert, U. S. *Des. Monomers Polym.* **2005**, *8* (6), 659−671.

Fluorinated 2-alkyl-2-oxazolines of high reactivity: Spacer-length induced acceleration for Cationic Ring-Opening polymerization as basis for triphilic block copolymer synthesis

Leonid I. Kaberov[a], Bart Verbraeken[b], Anna Riabtseva[a], Jiri Brus[a], Yeshayahu Talmon[c], Petr Stepanek[a], Richard Hoogenboom[b], Sergey K. Filippov[a,*]

1. Materials and methods

2-Methyl-2-oxazoline (MeOx, 99 %, Acros Organics) was dried over BaO and distilled before use. Triethylamine (TEA, >99 %, Fisher Scientific) was dried over CaH_2 and distilled under reduced pressure. n-Nonanoic acid, 2-chloroethylamine hydrochloride, 18-crown-6 ether, thionyl chloride were purchased from Acros Organics and used as received. 2-bromoethylamine hydrochloride was purchased from Sigma-Aldrich and used as received. 4,4,4-trifluorobutyric acid and 3,3,3-trifluoropropionic acid were purchased from Fluorochem Limited and used as received. Dichloromethane (DCM, Lachner) was dried by refluxing over phosphorus pentoxide and distilled before use. Tetrahydrofuran (THF, Lachner) was dried by refluxing over CaH_2 and distilled before use. Acetonitrile (ACN, Lachner) was dried by refluxing over BaO and distilled before use. Ethyl acetate (EtAc, Lachner) was dried over $CaCl_2$ and distilled before use. MilliQ water was prepared by MilliPore Milli-Q® Gradient installation. All other chemicals were used as received.

2. Monomer synthesis

2.1. Synthesis of n-nonanoic acid chloride

n-Nonanoic acid (10 g, 0.063 mol) was dissolved in dry DCM (50 mL). The solution was cooled down in an ice bath. After that, thionyl chloride (7 mL, 0.096 mol) was added dropwise. The mixture was stirred at 40 °C overnight. Next, DCM and excess thionyl chloride were removed under reduced pressure. Yield=11 g (98 %). ^{1}H NMR (300 MHz, $CDCl_3$) δ 2.88 (t, J = 7.3 Hz, -C**H**$_2$-C(O)Cl, 2H), 1.69 (m, -C**H**$_2$-CH$_2$-C(O)Cl, 2H), 1.27 (m, CH$_3$(C**H**$_2$)$_5$-, 10H), 0.88 (t, J = 6.7 Hz, C**H**$_3$-, 3H).

2.2. Synthesis of N-(2-chloroethyl)nonyl amide

2-Chloroethylamine hydrochloride (11 g, 0.95 mol) was placed in a round-bottom flask. n-Nonanoic acid chloride (11 g, 0.057 mol) was dissolved in DCM (150 mL) and added to the same flask. The mixture was cooled in an ice bath. Then, triethylamine (30 mL, 0.216 mol) was added dropwise while stirring. The mixture was allowed to warm to room temperature and stirred overnight. The DCM was removed, and ethylacetate was added. The mixture was

filtered to remove the triethylamine hydrochloride, and the filtrate was washed twice with 10 % acetic acid solution, twice by saturated sodium bicarbonate, and twice by brine solution. The organic layer was dried over magnesium sulfate. Magnesium sulfate was filtered off, and the solvent was removed under reduced pressure, yielding the product as a white powder. Yield=9.9 g (70 %); ^{1}H NMR (300 MHz, CDCl$_3$) δ 6.04 (s (broad), -N**H**-CH$_2$-, 1H), 3.60 (m, -NH-**CH$_2$**-**CH$_2$**-Cl, 4H), 2.19 (m, -**CH$_2$**-C(O)-, 2H), 1.62 (m, -**CH$_2$**-CH$_2$-C(O)-, 2H), 1.25 (m, CH$_3$(**CH$_2$**)$_5$-, 10H), 0.86 (t, J = 6.7 Hz, **CH$_3$**-, 3H).

2.3. Synthesis of 2-(n-octyl)-2-oxazoline (OctOx)

N-(2-Chloroethyl)nonylamide (9.9 g, 0.045 mol) synthesized in the previous step was dissolved in dry THF (20 mL), and 18-crown-6 ether (0.595 g, 0.00225 mol) was added. The mixture was cooled in an ice bath and potassium hydroxide (7.56 g, 0.135 mol) was added. The mixture was allowed to warm to room temperature and stirred overnight. THF was removed under reduced pressure, and the residue was dispersed in water and extracted 3 times with DCM. The organic layers were combined and dried with magnesium sulfate. After filtration and removing the solvent under reduced pressure, the resulting oil was dried with barium oxide and distilled under reduced pressure yielding the product as a clear colourless liquid. Yield=6.7 g (80 %); T$_{boil}$=48 °C (0.9 mbar); ^{1}H NMR (300 MHz, CDCl$_3$) δ 4.22 (t, J=9.4 Hz, C-O-**CH$_2$**-CH$_2$-N=, 2H), 3.81 (t, J=9.5 Hz ,-C-O-CH$_2$-**CH$_2$**-N=, 2H), 2.26 (t, -**CH$_2$**-C(O)N-, 2H), 1.62 (m, -**CH$_2$**-CH$_2$-C(O)N-, 2H), 1.26 (m, CH$_3$(**CH$_2$**)$_5$-, 10H), 0.86 (t, J = 6.7 Hz, **CH$_3$**-, 3H).

2.4. 2-N-(2-bromoethyl)-2,2,2-trifluoroacetamide

2-Bromoethylamine hydrobromide (233.10 g, 1.137 mol) was dispersed in 1 L of dry diethyl ether and then TEA (124.72 g, 1.25 mol, 171.79 mL) was added. Mixture was stirred for 15 minutes and cooled on ice bath. To this cold solution ethyl trifluoroacetate (177.80 g, 1.25 mol, 149 mL) in 200 mL of diethyl ether was added drop-wise under stirring. The mixture was allowed to warm to room temperature and stirred overnight. The reaction mixture was filtered, removing the precipitate of trimethylamine hydrobromide. Then ether was removed and residue was recrystallized from *n*-hexane: DCM mixture (twice). Yield 92 %. ^{1}H NMR (300 MHz, CDCl$_3$) δ 6.73 (s (broad), -N**H**-, 1H), 3.80 (q, J = 3.7 Hz, CNH-**CH$_2$**-, 2H), 3.53 (t, J = 3.5 Hz, -CH$_2$-**CH$_2$**-Br, 2H)

2.5. 2-(trifluoromethyl)-2-oxazoline (CF$_3$Ox)

N-(2-bromoethyl)-2,2,2-trifluoroacetamide (219.89 g, 1 mol) was dissolved 1.5 L of dry diethyl ether and cooled down to -78°C under argon atmosphere. To the solution 42 g (1.05 mol) 60% dispersion of NaH in mineral oil was added portion wise. The reaction mixture was allowed to warm up to room temperature overnight. The complete mixture was directly distilled with a Vigreux column (6 plates), while both receiving flasks where cooled to -78°C. CF$_3$Ox was distilled a second time over BaO to dryness (T$_{boil}$ = 104-106°C). Yield 35 % ^{1}H NMR (300 MHz, CDCl$_3$) δ 4.52 (t, J = 4.5 Hz, =N-**CH$_2$**-, 2H), 4.00 (m, -O-**CH$_2$**-, 2H)

2.6. 4,4,4-trifluoromethylbutyric acid chloride

4,4,4-trifluoromethylbutyric acid (10 g, 0.07 mol) was dissolved in 15 mL of DCM, then thionyl chloride (11 g, 0.093 mol, 6.75 mL) and few drops of N,N-dimethylformamide as a catalyst were added. Mixture was stirred at 40 °C overnight. DCM and excess of thionyl chloride were removed at atmospheric pressure and the product was distilled in vacuum yielding colorless liquid. Yield=9.7 g (86 %) ^{1}H NMR (300 MHz, CDCl$_3$) δ 3.18 (t, J = 7.4 Hz, -CH$_2$-C(O)Cl, 2H), 2.53 (m, CF$_3$-CH$_2$-CH$_2$-, 2H);

2.7. 2-(3,3,3-trifluoropropyl)-2-oxazoline

2-Bromoethylamine hydrobromide (12.4 g, 0.06 mol) was dispersed in 100 mL of DCM and then TEA (18.18 g, 0.18 mol, 25 mL) was added. Mixture was stirred for 15 minutes and cooled on ice bath. In cold solution 4,4,4-trifluoromethylbutiric acid chloride (9.7 g, 0.06 mol) in 40 mL of DCM was added drop-wise under stirring. The mixture was allowed to warm to room temperature and stirred overnight. The solvent was removed in vacuum, residue was dispersed in ether and the precipitate of trimethylamine hydrobromide was filtered off. Then ether was removed and residue was distilled over BaO in vacuum yielding colorless liquid, which crystallizes at room temperature. Yield=40 %. ^{1}H NMR (300 MHz, CDCl$_3$) δ 4.19 (t, J=9.4 Hz, C-O-CH$_2$-CH$_2$-N=, 2H), 3.76 (t, J=9.4 Hz, -C-O-CH$_2$-CH$_2$-N=, 2H), 2.41 (m, CF$_3$-CH$_2$-CH$_2$-, 4H). ^{19}F NMR (3kHz, CDCl$_3$) δ -66.27 (s, -CF$_3$).

2.8. 3,3,3-trifluoropropionic acid chloride

10 g (0.078 mol) of 3,3,3-trifluoropropionic acid was added dropwise to 16.3 g (0.078 mol) of phosphorus pentachloride under cooling with an ice bath. Then the mixture was warmed up to 65 °C and stirred over night. The result mixture was slowly distilled yielding colorless liquid. Yield 9.3 g (85%) T$_{boil}$=70–75 °C. ^{1}H NMR (300 MHz, CDCl$_3$): δ 3.73 (q, J=9.1 Hz, CF$_3$-CH$_2$-COCl, 1H).

2.9. 2-(2,2,2-trifluoroethyl)-2-oxazoline

2-Bromoethylamine hydrobromide (7.62 g, 0.037 mol) was dispersed in 150 mL of DCM and then TEA (11.2 g, 0.108 mol, 15.44 mL) was added. Mixture was stirred for 15 minutes and cooled on ice bath. In cold solution 3,3,3-trifluoropropionic acid chloride (5 g, 0.036 mol) in 40 mL of DCM was added drop-wise under stirring. The mixture was allowed to warm to room temperature and stirred overnight. The solvent was removed in vacuum, residue was dispersed in ether and the precipitate of trimethylamine hydrobromide was filtered off. Then ether was removed and residue was distilled over BaO in vacuum yielding colorless liquid. ^{1}H NMR (300 MHz, CDCl$_3$) δ 4.32 (t, J=9.7 Hz, C-O-CH$_2$-CH$_2$-N=, 2H), 3.90 (t, J=9.6 Hz, -C-O-CH$_2$-CH$_2$-N=, 2H), 3.16 (qt, J$_{HH}$=10.1 Hz, J$_{HF}$=1.1 Hz, CF$_3$-CH$_2$-, 2H). ^{19}F NMR (3kHz, CDCl3) δ -62.92 (s, -CF$_3$)

3. Polymer synthesis

All block copolymers were synthesized by subsequent Cationic Ring-Opening Polymerization of monomers as follows (on example of TB14).

The first monomer (MeOx, 0.765 g, 9 mmol), solvent (acetonitrile, 5 mL) and initiator (MeTos, 27.9 mg, 0.15 mmol) was added to prepared pressure reactor under inert atmosphere. The reaction mixture was stirred at 140 °C for 20 minutes. The polymerization mixture was cooled and the second monomer (OctOx, 0.55 g, 3 mmol) was added under inert atmosphere and stirred at 140 °C for 25 minutes. After cooling, the third monomer (CF$_3$EtOx, 0.5 g, 3 mmol) was added and the polymerization mixture was stirred at 140 °C for another 20 minutes. After cooling polymerization was terminated by 1 M KOH in MeOH and stirred overnight. The polymer was isolated by precipitation in cold diethyl ether yielding white powder.
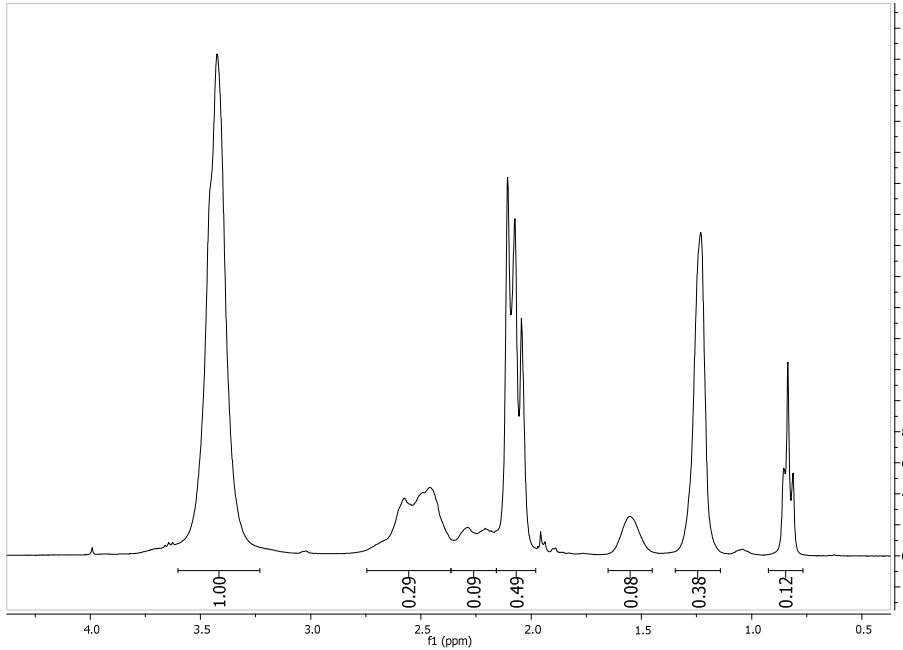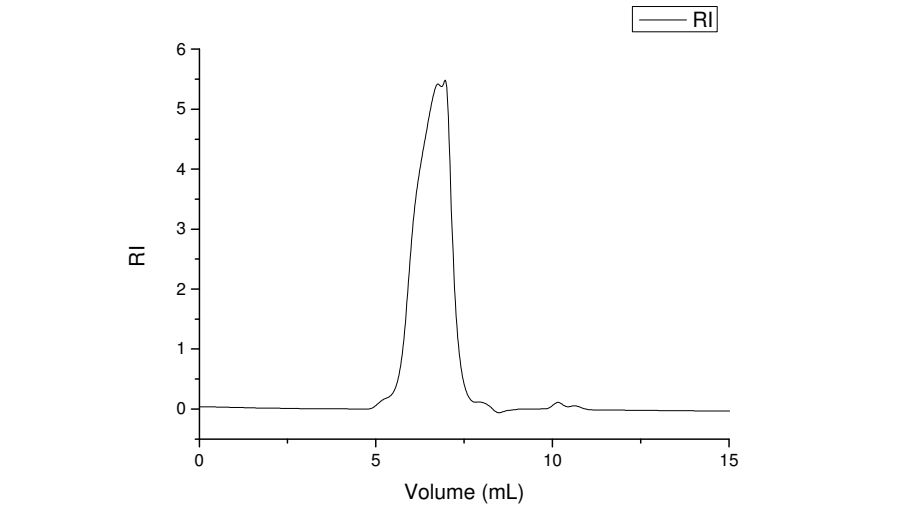
Polymer	REAGENTS	Name	mol	Mass, g	Volume, mL	Reaction time, min*
DB1	Initiator	MeOTs	0.00015	0.0279	0.0226	
	Solvent	ACN	-	-	5	
	Monomer 1	MeOx	0.009	0.765	0.765	19
	Monomer 2	CF_3EtOx	0.003	0.5	-	20
	Final composition	$MeOx_{38}-CF_3EtOx_{17}$				

NMR	

SEC	

Polymer	REAGENTS	Name	mol	Mass, g	Volume, mL	Reaction time, min
DB2	Initiator	MeOTs	0.00015	0.0279	0.0226	
	Solvent	AcN	-	-	5	19
	Monomer 1	MeOx	0.009	0.765	0.765	20
	Monomer 2	CF$_3$EtOx	0.0045	0.75	-	
	Final composition	MeOx$_{47}$-CF$_3$EtOx$_{27}$				
NMR						
SEC						

Polymer	REAGENTS	Name	mol	Mass, g	Volume, mL	Reaction time, min
DB3	Initiator	MeOTs	0.00009	0.0167	0.0136	
	Solvent	AcN	-	-	5	
	Monomer 1	MeOx	0.0054	0.458	0.458	31
	Monomer 2	CF$_3$EtOx	0.0036	0.6	-	35
	Final composition	MeOx$_{39}$-CF$_3$EtOx$_{28}$				
NMR						
SEC						

Polymer	REAGENTS	Name	mol	Mass, g	Volume, mL	Reaction time, min
DB4	Initiator	MeOTs	0.00006	0.0112	0.009	
	Solvent	AcN	-	-	5	
	Monomer 1	MeOx	0.0036	0.305	0.305	47
	Monomer 2	CF$_3$EtOx	0.0036	0.6	-	52
	Final composition	MeOx$_{23}$-CF$_3$EtOx$_{25}$				
	NMR					
	SEC					

Polymer	REAGENTS	Name	mol	Mass, g	Volume, mL	Reaction time, min
TB1	Initiator	MeOTs	0.00015	0.0279	0.0226	
	Solvent	AcN	-	-	5	
	Monomer 1	MeOx	0.009	0.765	0.765	20
	Monomer 2	OctOx	0.003	0.55	0.607	25
	Monomer 3	CF$_3$EtOx	0.003	0.5	-	20
	Final composition	MeOx$_{28}$-OctOx$_9$-CF$_3$EtOx$_{12}$				
NMR						
SEC						

Polymer	REAGENTS	Name	mol	Mass, g	Volume, mL	Reaction time, min
TB2	Initiator	MeOTs	0.0001	0.0186	0.0151	
	Solvent	AcN	-	-	4	
	Monomer 1	MeOx	0.006	0.51	0.51	27
	Monomer 2	OctOx	0.002	0.366	0.404	33
	Monomer 3	CF_3EtOx	0.003	0.5	-	25
	Final composition	$MeOx_{49}\text{-}OctOx_{11}\text{-}CF_3EtOx_{16}$				
NMR						
SEC						

Polymer	REAGENTS	Name	Mol	Mass, g	Volume, mL	Reaction time, min
TB3	Initiator	MeOTs	0.0001	0.0186	0.0151	
	Solvent	AcN	-	-	4	
	Monomer 1	OctOx	0.002	0.366	0.404	33
	Monomer 2	MeOx	0.006	0.51	0.51	27
	Monomer 3	CF$_3$EtOx	0.003	0.5	-	26
	Final composition	$OctOx_{12}$-$MeOx_{52}$-CF_3EtOx_{18}				

NMR	
SEC	

*The reaction time was calculated using the following equation[7]:

$$\ln([M]_0/[M]_t)=k_p*[I]_0*t$$

where $[M]_0$ and $[M]_t$ are monomer concentrations at the initial moment and t-moment, respectively (the meaning 4 of $\ln([M]_0/[M]_t)$ corresponds to 98 % conversion of the monomer), k_p – polymerization rate constant, $[I]_0$ – initial concentration of the initiator. The k_p-value was taken from the literature[7] and the kinetics study.

4. Characterisation techniques

4.1. Dynamic Light Scattering (DLS)

Dynamic Light Scattering (DLS) was performed to characterize the copolymers in dilute solutions. For this purpose, the hydrodynamic diameter of the particles, D_h, and the scattering intensity were measured at a scattering angle of $\vartheta = 173°$ with a Zetasizer Nano-ZS instrument, model ZEN3600 (Malvern Instruments, UK). The DTS (Nano) program was used to evaluate the data. It provides intensity-, volume-, and number-weighted D_h distribution functions $I(D_h)$.

All solutions were prepared via the direct dissolution of the copolymers in water and via a solvent exchange method in which the polymer was molecularly dissolved in methanol and self-assembly was induced by dialysis against water.

4.2. SEC (homopolymers)

Size exclusion chromatography (SEC) measurements were performed on an Agilent 1260-series HPLC system equipped with a 1260 online degasser, a 1260 ISO-pump, a 1260 automatic liquid sampler (ALS), a thermostatted column compartment (TCC) at 50°C equipped with two PLgel 5 µm mixed-D columns and a mixed-D guard column in series, a 1260 diode array detector (DAD) and a 1260 refractive index detector (RID). Dimethylacetamide (DMA) containing 50 mM of lithium chloride was used as eluent at an optimized flow rate of 0.593 ml/min. Chromatograms were analyzed using Agilent Chemstation software with SEC add-on. Number average molar mass (M_n) and dispersity (Đ) values were determined against poly(methyl methacrylate) (PMMA) standards from PSS (Polymer Standards Service, Germany).

4.3. SEC-MALS (block copolymers)

Labio Biospher GMB100 7.5 mm x 300 mm, particle size 10 µm, size exclusion column, applicable in aqueous as well as in organic mobile phases, was used for the analysis of the poly(2-oxazoline)s using methanol as the mobile phase at 0.18 ml/min. The pump was a Shimadzu 20ADvp liquid chromatography pump (Shimadzu Corp, Kyoto, Japan). The vacuum

degasser was a DeltaChrom TVD (Watrex, Prague, Czech Republic). The 40 mg/ml polymers solutions in methanol were injected manually using a six port PEEK injection valve equipped with a 50 µl sample loop (Upchurch Scientific, Oak Harbor, WA). A home made in-line 25 mm filter holder with a 0.02 µm Anodisc 25 membrane (Whatman, Maidstone, UK) was positioned between the pump and the injection valve.

The light scattering detector was a DAWN-DSP multi-angle light scattering instrument (Wyatt Technology, Santa Barbara, CA) and a Shodex RI-101 differential refractometer (Showa Denko, Japan) served as the concentration detector. The signals from the detectors were collected and analysed using ASTRA for Windows 4.50 software (Wyatt Technology, Santa Barbara, CA). The angular dependence of the scattered light intensity was found to be negligible for all samples.

The refractive index increment of the poly(2-oxazoline)s in methanol was determined using a Brookhaven BI-DNDC differential refractometer and BI-DNDCW software.

It should be noted here that this two detector arrangement with both a DAWN-DSP light scattering unit as an absolute molecular weight detector and single RI detection SEC units does not require the use of polymer standards to determine the polymer molar mass and dispersity (Đ).

4.4. ^{19}F NMR Spectroscopy

The ^{19}F NMR spectra were measured at 11.7 T on a Bruker Avance III HD 500 US/WB NMR spectrometer (Karlsruhe, Germany, 2013) using a solid-state 4-mm CP/MAS probe head optimized for the measurement of ^{19}F nuclei. The Hahn-echo experiment was applied to suppress the probe head residual signal; the echo-delay was 10 ms; the duration of the 90°(^{19}F) pulse was 1.5 µs; the repetition delay was 2 s; and 512-1024 scans were accumulated for each spectrum. ^{19}F NMR chemical shift scale was calibrated using the PTFE the signal of which was set to -122 ppm. Chloroform was used as the solvent.

4.5 Cryo-TEM

Specimens were prepared in a controlled environment vitrification system (CEVS) at 25 °C and 100 % relative humidity. A drop (about 3 µL) of the sample was pipetted onto a perforated carbon film-coated electron microscopy copper grid, blotted with filter paper, and plunged into liquid ethane at its freezing point. Such specimens were then transferred to a 626 Gatan cryo-holder and imaged at an acceleration voltage 200 kV in an FEI (Eindhoven, NL) Talos 200C high-resolution transmission electron microscope at about −175 °C, in the low-dose imaging mode to minimize electron-beam radiation-damage. Image contrast was enhanced by "phase-plates" of the Talos. Images were digitally recorded with eithers with an FEI I Falcon II direct-imaging 16-megapixel camera.

5. Experimental data

Table S1. Refractive index increment of poly(2-oxazolines) in methanol.

Polymer	Composition	dn/dc
DB1	MeOx$_{38}$-CF$_3$EtOx$_{17}$	0.148±0.002
DB2	MeOx$_{47}$-CF$_3$EtOx$_{27}$	0.121±0.002
DB3	MeOx$_{39}$-CF$_3$EtOx$_{28}$	0.129±0.002
DB4	MeOx$_{23}$-CF$_3$EtOx$_{25}$	0.115±0.001
TB1	MeOx$_{28}$-OctOx$_9$-CF$_3$EtOx$_{12}$	0.169±0.002
TB2	MeOx$_{49}$-OctOx$_{11}$-CF$_3$EtOx$_{16}$	0.149±0.001
TB3	OctOx$_{12}$-MeOx$_{52}$-CF$_3$EtOx$_{18}$	0.141±0.001

Table S2. CF$_3$EtOx kinetic data

Reaction time, min	monomer convertion, %	M_n (SEC), kDa	$Đ$ (SEC)
3	23.7	7.50	1.07
5	31.3	8.40	1.15
10	49.3	12.50	1.06
15	66.5	14.70	1.07
30	88.9	17.60	1.11
60	99.1	20.20	1.12

Table S3. Characteristics of the synthesized block copolymers (addition to Tab.1.).

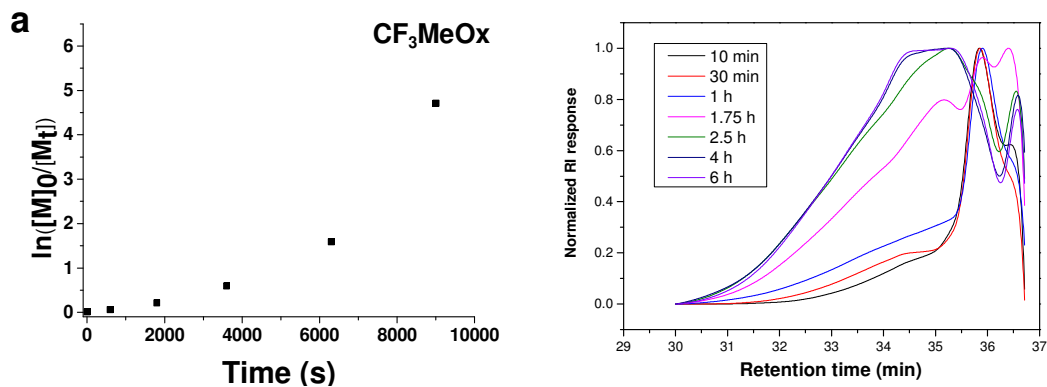|	Composition (NMR)	M_w (SEC-MALS), g/mol	M_w (RI), g/mol
DB1	MeOx$_{38}$-CF$_3$EtOx$_{17}$	7200	7300
DB2	MeOx$_{47}$-CF$_3$EtOx$_{27}$	11000	11900
DB3	MeOx$_{39}$-CF$_3$EtOx$_{28}$	10300	11200
DB4	MeOx$_{23}$-CF$_3$EtOx$_{25}$	8100	9000
TB1	MeOx$_{28}$-OctOx$_9$-CF$_3$EtOx$_{12}$	8000	8400
TB2	MeOx$_{49}$-OctOx$_{11}$-CF$_3$EtOx$_{16}$	11800	12800
TB3	OctOx$_{12}$-MeOx$_{52}$-CF$_3$EtOx$_{18}$	13500	15000

Figure S1. Kinetic plots for the cationic ring-opening polymerization (a) and SEC data (b) of CF$_3$MeOx. RI – Refractive index.
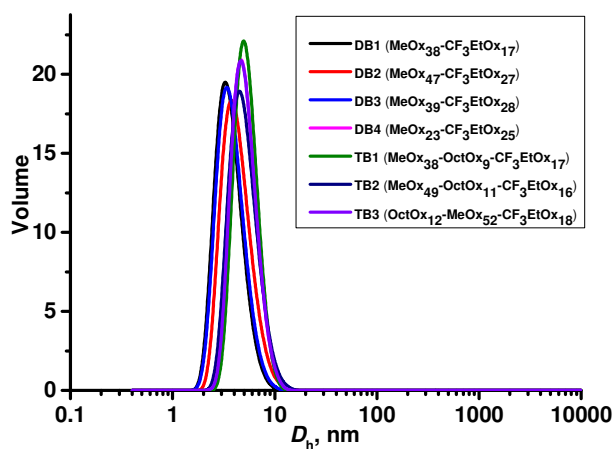

Figure S2. Hydrodynamic diameter distribution of di- and triblock copolymers in methanol
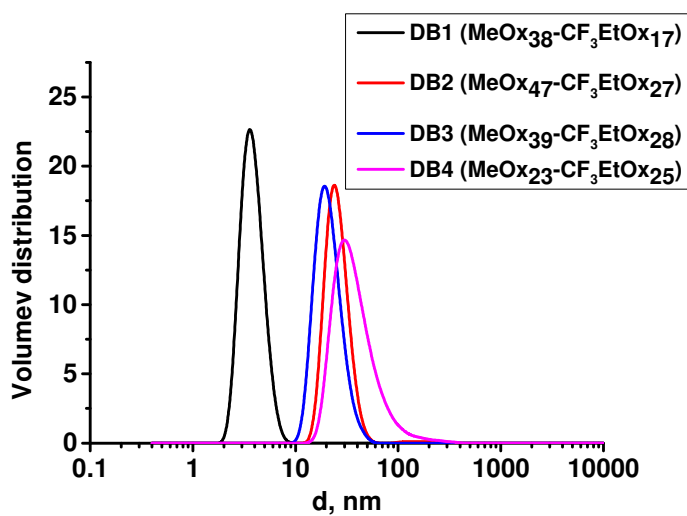

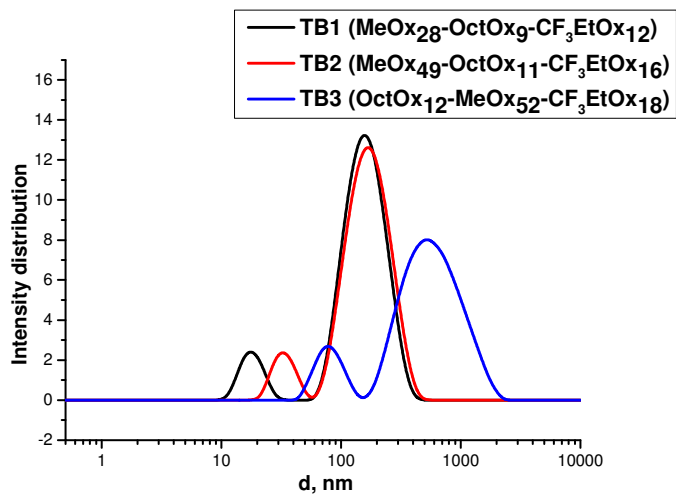Figure S3. Hydrodynamic diameter distribution of diblock copolymers in water

Figure S4. Hydrodynamic diameter distribution of triblock copolymers in water
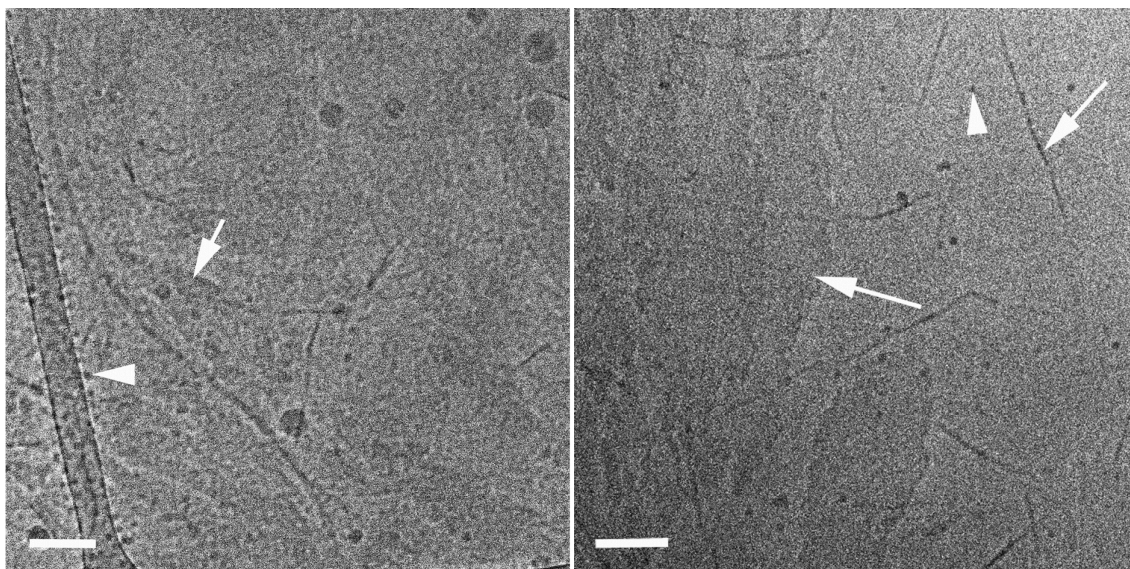

Figure S5. Cryo-TEM image of aqueous solution of polymer 10, containing small particles with affinity to support film (arrowheads). Also small population of large aggregates (white arrows) are observed. Bars equal 100 nm.

MANUSCRIPT M4

Kaberov L.I., Verbraeken B., Riabtseva A., Brus J., Radulescu A., Talmon Y., Stepanek P., Hoogenboom R., Filippov S.K.. Fluorophilic-lipophilic-hydrophilic poly-2-oxazolines block copolymers: from synthesis to self-assembly. (**Submitted to *ACS Macromolecules*, 05.2018**)

Fluorophilic-lipophilic-hydrophilic poly-2-oxazolines block copolymers as MRI contrast agents: from synthesis to self-assembly

Journal:	*Macromolecules*
Manuscript ID	ma-2018-009573
Manuscript Type:	Article
Date Submitted by the Author:	04-May-2018
Complete List of Authors:	Kaberov, Leonid; Institute of Macromolecular Chemistry AS CR, v.v.i., Verbraeken, Bart; Ghent University, Supramolecular Chemistry Group Riabtseva, Anna; National University of Lviv, Department of Physics Brus, Jiří; Institute of Macromolecular Chemistry , Academy of Sciences of the Czech Republic, Department of NMR Spectroscopy Radulescu, Aurel; Forscungszentrum Juelich, Juelich Centre for Neutron Science Talmon, Yeshayahu; Technion-Israel Institute of Technology, Department of Chemical Engineering Stepanek, Petr; Institute of Macromolecular Chemistry, Hoogenboom, Richard; Ghent University, Supramolecular Chemistry Group Filippov, Sergey; Institute of Macromolecular Chemistry,

SCHOLARONE™
Manuscripts

Fluorophilic-lipophilic-hydrophilic poly-2-oxazolines block copolymers as MRI contrast agents: from synthesis to self-assembly

Leonid I. Kaberov[1], Bart Verbraeken[2], Anna Riabtseva[1], Jiri Brus[1], Aurel Radulescu[3], Yeshayahu Talmon[4], Petr Stepanek[1], Richard Hoogenboom[2], Sergey K. Filippov[1*]

[1]*Institute of Macromolecular Chemistry, Academy of Sciences of the Czech Republic, Heyrovský Sq. 2, 162 06 Prague 6, Czech Republic*

[2]*Supramolecular Chemistry Group, Centre of Macromolecular Chemistry (CMaC), Department of Organic and Macromolecular Chemistry, Ghent University, Krijgslaan 281 S4, B-9000 Ghent, Belgium*

[3]*Forschungszentrum Jülich GmbH, Jülich Centre for Neutron Science JCNS, Outstation at Heinz Maier-Leibnitz Zentrum, Lichtenbergstraße 1, 85748 Garching, Germany*

[4]*Department of Chemical Engineering, Technion-Israel Institute of Technology, Haifa 3200003, Israel*

*e-mail: filippov@imc.cas.cz

ABSTRACT

This work focused on the synthesis and self-assembly of triphilic poly(2-oxazoline) triblock copolymers with high fluorine content towards our future aim of developing poly(2-oxazoline) MRI contrast agents. A highly fluorinated 2-substituted-2-oxazoline monomer, namely 2-(1H,1H,2H,2H-perfluorooctyl)-2-oxazoline was synthesized using the Grignard reaction. The polymerization kinetics of the synthesized monomer was studied and it was used for the preparation of triblock copolymers with hydrophilic 2-methyl-2-oxazoline, hydrophobic 2-octyl-2-oxazoline and fluorophilic blocks by Cationic Ring-Opening Polymerization yielding polymer with low relatively dispersity (1.2-1.4). The presence of the blocks with the different nature in one copolymer structure facilitated self-assembly of the copolymers in water and dimethylsulfoxide as observed by dynamic light scattering, cryo-transmition electron microscopy, and small-angle neutron scattering. The nanoparticle morphology is strongly influenced by the order and length of each block and the nature of solvent, leading to nanoparticles with core-shell structure as confirmed by small angle neutron scattering. The reported poly(2-oxazoline) block copolymers with high fluorine content have high potential for future development of MRI contrast agents.

1
2
3
4
5
6
7
8
9
10
11
12
13
14
15
16
17
18
19
20
21
22
23
24
25
26
27
28
29
30
31
32
33
34
35
36
37
38
39
40
41
42
43
44
45
46
47
48
49
50
51
52
53
54
55
56
57
58
59
60

Key-words: poly(2-oxazoline)s, fluorine, Grignard reaction, self-assembly, DLS, SANS, Cryo-TEM, MRI

1. INTRODUCTION

Since the first time that the cationic ring-opening polymerization (CROP) of 2-oxazolines was described in 1966,[1–4] this method became a popular approach for the controlled synthesis of self-assembling polymer systems. Under appropriate conditions the CROP proceeds in a living mode, which makes it very useful for the synthesis of block copolymers. Although it requires extreme purity of all components (lack of moisture and any nucleophilic impurities), the CROP of 2-oxazolines allows to obtain polymers with very low dispersity. By variation of the 2-oxazoline substituent one can obtain hydrophilic, hydrophobic, fluorophilic and various stimuli-responsive polymers (or blocks).[5] The application of the microwave synthesis significantly simplified the polymerization of 2-oxazolines and gave a new impetus for their development,[6–8] further stimulated by their potential for biomedical applications.

The self-assembly of hydrophilic-hydrophobic block copolymers in solutions is already studied in detail.[9–12] Nowadays there is a continuous quest for block copolymers that contain two immiscible hydrophobic moieties to further sophisticate their self-assembly. One of the options is to combine lipophilic and fluorophilic fragments in one polymer. Despite their similar structure, alkyl chains and their fluorinated analogues possess quite different behavior in terms of solubility, flexibility, and polarizability.[13] Also fluorinated substances are promising as contrast agents in ^{19}F magnetic resonance imaging (MRI). Fluorine atoms have high MR sensitivity and ^{19}F MRI has virtually no background signal since the fluorine in body occurs almost exclusively in bones.[14–16]

The additional ordering of polymers containing more than two thermodynamically incompatible blocks in aqueous solutions was nicely demonstrated by Hilmyer, Lodge and co-workers.[17] The investigation of multicompartment micelles formed by linear styrene-based ABC-triblock copolymers have been also reported by Laschewsky et.al..[18,19] The majority of fluorine-containing polymers reported in literature is based on poly(meth)acrylates.[20–26]

2

The synthesis of poly-2-oxazolines with fluorophilic blocks suffers from the difficulties of synthesis and polymerization of fluorophilic monomers. The deceleration effect of the perfluoroalkyl substituent in 2-substituted-2-oxazoline was described by Saegusa and co-workers.[27] The polymerization of these monomers is time-consuming and requires high temperatures leading to poor control.[27–29]

Nevertheless, several examples of other fluorine containing 2-oxazoline based polymers are known. Perfluoroalkyl fragments could be incorporated during initiation or termination of CROP. The synthesis of PMeOx-based polymeric surfactants with $C_8F_{17}CH_2CH_2$ terminal group using initiator-based modification was described for the first time by Nuyken and co-workers.[30] Later this method was used for the synthesis of ABC triblock copolymers end-capped with perfluoroalkyl and regular alkyl chains by initiation and termination respectively.[31] The small-angle X-ray scattering study had shown that these chain-end functionalized polymers self-assembled into cylindrical micelles with hypothetical multicompartment structure of the micellar core. Another approach for functionalization of poly(2-oxazoline)s by CROP termination with perfluorocarboxylic acids was described by Kaberov et.al.[32]

A detailed study of the polymerization kinetics of fluorinated 2-phenyl-2-oxazolines was reported by Schubert.[33] The ABC triblock copolymers with 2-difluorophenyl-2-oxazoline block was found to form aggregates of unique rolled-up cylindrical morphology in aqueous milieu.[34] The synthesis of amphiphilic block copolymers of 2-1H,1H,2H,2H-perfluorohexyl-2-oxazoline and 2-methyl-2-oxazoline was provided by Jordan and co-workers.[28] Small-angle neutron scattering and Transmission Electron Microscopy (TEM) study proved the formation of elongated micelles in aqueous solution for these copolymers. Recently, we reported a detailed study of increasing the polymerization reactivity of fluorophilic 2-oxazolines by the insertion of alkyl spacers between a fluorinated substituent and the 2-oxazoline ring.[35] By this approach we suggested a new platform for the synthesis of a variety of triblock copoly(2-oxazoline)s with fluorinated blocks.

In the current work we tested the classical approaches for the synthesis of the highly fluorinated 2-(1H,1H,2H,2H-perfluorooctyl)-2-oxazoline (R_f^6EtOx) monomer. On the basis of these unsuccessful attempts, we suggest an alternative pathway for the synthesis of this monomer based on a Grignard reaction step to make the perfluoralkyl acid and studied its polymerization kinetics. The insertion of a double methylene spacer significantly increases

the monomer reactivity in the polymerization reaction. Further, we describe the synthesis of new poly(2-oxazoline) di- and triblock copolymers with mutually immiscible hydrophilic, hydrophobic and fluorophilic blocks. In the last part of the paper we present the self-assembly behaviour of the copolymers by Dynamic Light Scattering (DLS), Small-angle Neutron Scattering (SANS), and Cryo-Transmission Electron Microscopy (Cryo-TEM).

2. **MATERIALS AND METHODS**

2.1. Materials

2-Methyl-2-oxazoline (MeOx, 99 %, Acros Organics) was dried over BaO and distilled before use. Triethylamine (TEA, >99 %, Fisher Scientific) was dried over CaH_2 and distilled under reduced pressure. n-Nonanoic acid, 2-chloroethylamine hydrochloride, 18-crown-6-ether, and thionyl chloride were purchased from Acros Organics and used as received. 2-Bromoethylamine hydrobromide was purchased from Sigma-Aldrich and used as received. Methyl p-toluenesulfonate (Sigma-Aldrich) was distilled under reduced pressure before use. 1H,1H,2H,2H-perfluorooctyl iodide was purchased from Fluorochem Limited and used as received. Dichloromethane (DCM, Lachner) was dried by refluxing over phosphorus pentoxide and distilled before use. Tetrahydrofuran (THF, Lachner) was dried by refluxing over CaH_2 and distilled before use. Acetonitrile (ACN, Lachner) was dried by refluxing over BaO and distilled before use. Ethyl acetate (EtAc, Lachner) was dried over $CaCl_2$ and distilled before use. MilliQ water was prepared by MilliPore Milli-Q® Gradient installation. All other chemicals were used as received.

2.2. Monomer synthesis

2.2.1. Synthesis of n-nonanoic acid chloride

n-Nonanoic acid (10 g, 0.063 mol) was dissolved in dry DCM (50 ml). The mixture was cooled down in an ice bath. After that, thionyl chloride (7 ml, 0.096 mol) was added dropwise. The mixture was stirred at 40 °C overnight. Next, DCM and excess thionyl chloride were removed under reduced pressure. The residue was distilled under reduced pressure yielding pure product as a colourless liquid. Yield=11 g (98 %). ^{1}H NMR (300 MHz, CDCl$_3$) δ 2.88 (t, J = 7.3 Hz, -C**H**$_2$-C(O)Cl,2H), 1.69 (m, -C**H**$_2$-CH$_2$-C(O)Cl, 2H), 1.27 (m, CH$_3$(C**H**$_2$)$_5$-, 10H), 0.88 (t, J = 6.7 Hz,C**H**$_3$-, 3H).

2.2.2. Synthesis of N-(2-chloroethyl)nonyl amide

2-Chloroethylamine hydrochloride (11 g, 0.95 mol) was placed in a round-bottom flask. n-Nonanoic acid chloride (11 g, 0.057 mol) was dissolved in DCM (150 ml) and added to the same flask. The mixture was cooled in an ice bath. Then, triethylamine (30 ml, 0.216 mol) was added dropwise while stirring. The mixture was allowed to warm to room temperature and stirred overnight. The DCM was removed, and ethylacetate was added. The mixture was filtered to remove the triethylamine hydrochloride, and the filtrate was washed twice with 10 % acetic acid solution, twice with saturated sodium bicarbonate, and twice with brine solution. The organic layer was dried over magnesium sulfate. Magnesium sulfate was filtered off, and the solvent was removed under reduced pressure, yielding the product as a white powder. Yield=9.9 g (70 %); ^{1}H NMR (300 MHz, CDCl$_3$) δ 6.04 (s (broad), -N**H**-CH$_2$-, 1H), 3.60 (m, -NH-C**H**$_2$-C**H**$_2$-Cl, 4H), 2.19 (m, -C**H**$_2$-C(O)-, 2H), 1.62 (m, -C**H**$_2$-CH$_2$-C(O)-, 2H), 1.25 (m, CH$_3$(C**H**$_2$)$_5$-, 10H), 0.86 (t, J = 6.7 Hz,C**H**$_3$-, 3H).

2.2.3. *Synthesis of 2-(n-octyl)-2-oxazoline (OctOx)*

N-(2-Chloroethyl)nonylamide (9.9 g, 0.045 mol) synthesized in the previous step was dissolved in dry THF (20 ml), and 18-crown-6-ether (0.595 g, 0.00225 mol) was added. The mixture was cooled in an ice bath and potassium hydroxide (7.56 g, 0.135 mol) was added. The mixture was allowed to warm to room temperature and stirred overnight. THF was removed under reduced pressure, and the residue was dispersed in water and extracted 3 times with DCM. The organic layers were combined and dried with magnesium sulfate. After filtration and removing the solvent under reduced pressure, the resulting oil was dried with barium oxide and distilled under reduced pressure yielding the product as a clear colourless liquid. Yield=6.7 g (80 %); T$_{boil}$=48 °C (0,9 mbar); ^{1}H NMR (300 MHz, CDCl$_3$) δ 4.22 (t, C-O-C**H**$_2$-CH$_2$-N=, 2H), 3.81(t, -C-O-CH$_2$-C**H**$_2$-N=, 2H), 2.26 (t, -C**H**$_2$-C(O)N-, 2H), 1.62 (m, -C**H**$_2$-CH$_2$-C(O)N-, 2H), 1.26 (m, CH$_3$(C**H**$_2$)$_5$-, 10H), 0.86 (t, J = 6.7 Hz, C**H**$_3$-, 3H).

2.2.4. Synthesis of 1H,1H,2H,2H-perfluorononanoic acid[36]

The 1H,1H,2H,2H-perfluorooctyl iodide (12 g, 6,2 mL, 0.025 mol) was dissolved in 6 mL of diethyl ether and the first portion of this mixture (1-2 mL) was added to a suspension of 0.6 g (0.025 mol) magnesium in 100 mL of freshly distilled diethyl ether with the addition of a few crystals of iodine. The mixture was stirred at 37 °C until the reaction started (20-30 minutes). Subsequently, the rest of the solution of 1H,1H,2H,2H-perfluorooctyl iodide was added dropwise during 1.5-2 hours and then stirring was continued for another 3 hours. The mixture was cooled on an ice bath and then 15 g of dry ice were added slowly. The mixture was

stirred for another 20 minutes before 25 mL of 20 % H_2SO_4 was added. The organic layer was separated, washed with saturated NaCl solution and dried over magnesium sulfate. The solvent was removed under reduced pressure and the residue was recrystallized from DCM. The resulting white crystals also contained the side product of iodide dimerization - 1,1,1,2,2,3,3,4,4,5,5,6,6,11,11,12,12,13,13,14,14,15,15,16,16,16-hexacosafluorohexadecane.

2.2.5. Purification of 1H,1H,2H,2H-perfluorononanoic acid

The obtained acid (colorless crystals) was dispersed in concentrated NaOH solution and stirred under heating. The precipitate was separated by decantation, the solution was neutralized by addition of 20 % H_2SO_4 and extracted 3 times with diethyl ether. The organic layers were combined, washed with saturated NaCl solution and dried over $MgSO_4$. The solvent was removed in vacuum yielding the pure product as white crystals. Yield = 5 g (50 %). ^{1}H NMR (300 MHz, $CDCl_3$) δ 9.17 (s (wide), -COO**H**, 1H), 2.71 (t, -C**H**$_2$-COOH, 2H), 2.48 (m, -CF$_2$-C**H**$_2$-, 2H).

2.2.6. Synthesis of 1H,1H,2H,2H-perfluorononanoic acid chloride

The acid synthesized in the previous step (5 g, 0.013 mol) was mixed with thionyl chloride 2.83 mL (4.64 g, 0.039 mol) and few drops of pyridine were added as a catalyst. The mixture was stirred at 50 °C overnight. The excess of thionyl chloride was removed under reduced pressure and the residue was distilled under reduced pressure. The product was used in the next reaction without further purification. Yield = 5 g (94 %). ^{1}H NMR (300 MHz, $CDCl_3$) δ 3.24 (t, -C**H**$_2$-C(O)Cl, 2H), 2.53 (m, -CF$_2$-C**H**$_2$-, 2H).

2.2.7. Synthesis of 2-(1H,1H,2H,2H-perfluorooctyl)-2-oxazoline (R_f^6EtOx)

2-Bromoethylamine hydrobromide (4.92 g, 0.024 mol) was dispersed in 50 mL of DCM, Then, 5 mL of triethylamine (3.64 g, 0.036 mol) was added and the mixture was stirred for 15-20 minutes. The reaction mixture was cooled on an ice/NaCl bath. 1H,1H,2H,2H-Perfluorononanoic acid chloride (5 g, 0.012 mol) was mixed with the same volume of DCM and added drop-wise under stirring and cooling. The mixture was allowed to warm to room temperature and stirred over 2 days. The solution was washed twice with water and saturated NaCl solution and dried over $MgSO_4$. The solvent was removed under reduced pressure and the oily residue was distilled over BaO yielding the product as a colorless liquid. Yield = 4.5 g (90 %). ^{1}H NMR (300 MHz, $CDCl_3$) δ 4.27 (t, C-O-C**H**$_2$-CH$_2$-N=, 2H), 3.84 (t, -C-O-CH$_2$-C**H**$_2$-N=, 2H), 2.63-2.37 (m, C_6F_{13}-C**H**$_2$-C**H**$_2$-, 4H).

2.3. Polymer synthesis

The synthesis of all polymers was performed in a pressure reactor (Ace pressure tube, Ace Glass, Inc.) under argon atmosphere using freshly distilled and dried monomers and solvents. The general procedure was as follows:

R_f^6EtOx (0.3 g, $7.2*10^{-4}$ mol) was dissolved in acetonitrile (3.2 ml), and methyl tosylate (0.0134 g, $7.2*10^{-5}$ mol) was added as the initiator. The mixture was stirred for 22 minutes at 140 °C in a pressure reactor. After cooling to room temperature, the second monomer - 2-(n-octyl)-2-oxazoline (0.264 g, $14.4*10^{-4}$ mol) - was added, and the mixture was stirred again for 31 minutes at 140 °C. Next, 2-methyl-2-oxazoline (0.612 g, 0.072 mol) was added and the polymerization mixture was stirred for 27 minutes at 140 °C. The mixture was cooled to room temperature and the polymerization was quenched by the addition of 0.3 mL of 1 M KOH (0.0168 g, $3*10^{-4}$ mol) solution in MeOH and stirred overnight. The polymer was isolated by precipitation in cold diethyl ether yielding the triblock copolymer as a white powder.

2.4. Methods

2.4.1.   Dynamic Light Scattering (DLS)

Dynamic Light Scattering (DLS) was performed to characterize the copolymers in dilute solutions. For this purpose, the hydrodynamic diameter of the particles, D_h, and the scattering intensity were measured at a scattering angle of θ = 173° with a Zetasizer Nano-ZS instrument, model ZEN3600 (Malvern Instruments, UK). The DTS (Nano) program was used to evaluate the data. The intensity-weighted value of the apparent D_h and Polydispersity Index PDI were chosen to characterize the dispersity of the solutions. For clarity, distribution functions were normalized by the amplitude of the peak of the highest intensity.

All solutions were prepared via the direct dissolution of the copolymers in water or dimethylsulphoxide as well as via a solvent exchange method (for aqueous solutions only) in which the polymer was molecularly dissolved in methanol and self-assembly was induced by dialysis against water.[37,38]

2.4.2.   Size Exclusion Chromatography – Multi-Angle Light Scattering (SEC-MALS)

Labio Biospher GMB100 7.5 mm x 300 mm, particle size 10 µm, size exclusion column, applicable in aqueous as well as in organic mobile phases, was used for the analysis of the poly(2-oxazoline)s using methanol as the mobile phase at 0.18 ml/min. The pump was a

Shimadzu 20ADvp liquid chromatography pump (Shimadzu Corp, Kyoto, Japan). The vacuum degasser was a DeltaChrom TVD (Watrex, Prague, Czech Republic). The 40 mg/ml polymer solutions in methanol were injected manually using a six port PEEK injection valve equipped with a 50 µl sample loop (Upchurch Scientific, Oak Harbor, WA). A home made in-line 25 mm filter holder with a 0.02 µm Anodisc 25 membrane (Whatman, Maidstone, UK) was positioned between the pump and the injection valve.

The light scattering detector was a DAWN-DSP multi-angle light scattering instrument (Wyatt Technology, Santa Barbara, CA) and a Shodex RI-101 differential refractometer (Showa Denko, Japan) served as the concentration detector. The signals from the detectors were collected and analysed using ASTRA for Windows 4.50 software (Wyatt Technology, Santa Barbara, CA). The angular dependence of the scattered light intensity was found to be negligible for all samples.

The refractive index increment of the poly(2-oxazoline)s in methanol was determined using a Brookhaven BI-DNDC differential refractometer and BI-DNDCW software.

It should be noted here that this two detector arrangement with both a DAWN-DSP light scattering unit as an absolute molecular weight detector and single RI detection SEC units does not require the use of polymer standards to determine the polymer molar mass and dispersity ($Đ$).

2.4.3. Transmission Cryo-Electron Microscopy (Cryo-TEM)

Specimens were prepared in a controlled environment vitrification system (CEVS) at 25 °C and 100 % relative humidity. A drop (about 3 µL) of the sample was pipetted onto a perforated carbon film-coated electron microscopy copper grid, blotted with filter paper, and plunged into liquid ethane at its freezing point. Such specimens were then transferred to a Gatan 626 cryo-holder and imaged at an acceleration voltage 200 kV in an FEI (Eindhoven, NL) Talos 200C high-resolution transmission electron microscope at about −175 °C, in the low-dose imaging mode to minimize electron-beam radiation-damage. Image contrast was enhanced by "phase-plates" of the Talos. Images were digitally recorded with an FEI I Falcon II direct-imaging 16-megapixel camera.

2.4.4. ^{19}F Nuclear Magnetic Resonance (NMR) Spectroscopy

The ^{19}F NMR spectra were measured at 11.7 T on a Bruker Avance III HD 500 US/WB NMR spectrometer (Karlsruhe, Germany, 2013) using a solid-state 4-mm CP/MAS probehead optimized for the measurement of ^{19}F nuclei. The Hahn-echo experiment was applied to suppress the probehead residual signal; the echo-delay was 10 ms; the duration of the 90°(19F) pulse was 1.5 µs; the repetition delay was 2 s; and 512-1024 scans were accumulated for each spectrum. ^{19}F NMR chemical shift scale was calibrated using PTFE for which the signal was set to -122 ppm. Chloroform was used as the solvent.

2.4.5. Small-Angle Neutron Scattering (SANS) experiments were performed at FRM II, Garching, Germany on the KWS-2 instrument.[39] Measurements were made on a 128 x 128 ^{3}He tubes array detector (pixel size 8 mm) using a non-polarized, monochromatic (wavelength λ set by a velocity selector) incident neutron beam collimated with rectangular apertures for two sample-to-detector distances, namely 2, 8, and 20 m (λ = 0.6 nm). With this setup, the investigated q-range was 0.015 nm^{-1} to 4.6 nm^{-1}. In all cases, the two-dimensional scattering patterns were isotropic and were azimuthally averaged, resulting in the dependence of the scattered intensity $I_s(q)$ on the momentum transfer $q = 4\pi\sin\theta/\lambda$, where 2θ is the scattering angle. The curves were corrected for background scattering from the empty cell and for detector efficiency. Helma quartz cells 1 and 2 mm thick were used for experiments. SANS Experiments were performed in D$_2$O and DMSO-d6. The buffer was measured and proper subtracted.

2.4.6. SANS data fitting

The scattered intensity curves were fitted using the sphere with attached Gaussian chain model implemented in SASFit software.[40]

The scattering curves in D$_2$O and partially in DMSO-d6 were fitted using the following function:

$$I(q) = P_{sgc}(q) + P_{agg}(q) \tag{1}$$

The overall scattering intensity of the sphere with attached Gaussian chain written as:

$$P_{sgc} = N_{agg}^2\beta_{core}^2 P_{core}(q) + N_{agg}\beta_{brush}^2 P_{brush}(q) + 2N_{agg}^2\beta_{core}\beta_{brush}S_{brush-core}(q) +$$

$$N_{agg}(N_{agg} - 1)\beta_{brush}^2 S_{brush-brush}(q), \tag{2}$$

where $N_{agg}^2 \beta_{core}^2 P_{core}(q)$ is self-correlation term of the core, $N_{agg} \beta_{brush}^2 P_{brush}(q)$ is self-correlation term of the chains, $2N_{agg}^2 \beta_{core} \beta_{brush} S_{brush-core}(q)$ is the cross-term between the core and chains and $N_{agg}(N_{agg} - 1)\beta_{brush}^2 S_{brush-brush}(q)$ is the cross-term between different chains. N_{agg} is the aggregation number of polymers forming the nanoparticle per surface area, $\beta_{brush} = V_{brush}(\eta_{brush} - \eta_{solv})$ and $\beta_{core} = V_{core}(\eta_{core} - \eta_{solv})$ are the excess scattering lengths of a block in the corona and in the core, respectively. V_{brush} and V_{core} are the total volume of a block in the corona and in the core, respectively. η_{brush} and η_{core} are the corresponding SLDs. $P_{core}(q)$ is scattering of spherical core

$$P_{core}(q,R) = \frac{(\sin(qR) - qR\cos(qR))}{(qR)^3}$$

The scattering intensity for the brush of is given by:

$$P_{brush}(q, R_g) = 2\frac{exp(-x) - 1 + x}{x^2}, \quad \text{where } x = R_g^2 q^2$$

The modified Porod function was used to describe the contribution of large aggregates (P_{agg}) at the lowest q range: $C_0 + \frac{C_1}{q^\alpha}$, where α is modified Porod exponent.

Excess scattering lengths of polymeric shell and a core were fixed during the fitting procedure.

The scattering curves from diblock copolymers in DMSO-d6 were fitted using the following function:

$$I(q) = P_{ggc}(q) + P_{agg}(q)$$

where P_{ggc} describes the form factor of Generalized Gaussian coil:

$$P_{ggc}(q) = I_0^c \frac{U^{\frac{1}{2\nu}}\Gamma\left(\frac{1}{2\nu}\right) - \Gamma\left(\frac{1}{\nu}\right) - U^{\frac{1}{2\nu}}\Gamma\left(\frac{1}{2\nu}, U\right) + \Gamma\left(\frac{1}{\nu}, U\right)}{\nu U^{1/\nu}}$$

here, $U = (2\nu + 1)(2\nu + 2)\frac{q^2 R_g^2}{6}$, and $\Gamma\left(\frac{1}{2\nu}\right)$ – Gamma function.

3. RESULTS AND DISCUSSIONS

3.1. Monomer synthesis

The synthesis of the hydrophobic 2-octyl-2-oxazoline monomer was performed as described in our previous work.[32] Subsequently, several pathways were tested for the synthesis of the 2-1H,1H,2H,2H-perfluorooctyl-2-oxazoline fluorophilic monomer. This monomer was chosen to have a strong fluorophilic character while the ethyl spacer ensures similar reactivity compared to 2-alkyl-2-oxazolines as we previously determined for 2-trifluoromethylethyl-2-oxazoline.[35]

As the perfluoroalkyl chain length is extended compared to previous reports by Jordan,[28] the solubility is significantly reduced in common organic solvents complicating its synthesis. Nonetheless, we first attempted to form the 1H,1H,2H,2H-perfluorooctylcyanide by reaction of the 1H,1H,2H,2H-perfluorooctyliodide with sodium cyanide, in analogy to the report of Jordan[28] for the preparation of the 2-(1H,1H,2H,2H-perfluorohexyl)-2-oxazoline via the Witte–Seeliger synthesis of 2-oxazolines from nitriles (Scheme 1).[41] Unfortunately, the corresponding nitrile was not obtained under the described conditions in the case of 1H,1H,2H,2H-perfluorooctyl iodide, probably because of the lower solubility of the iodide.
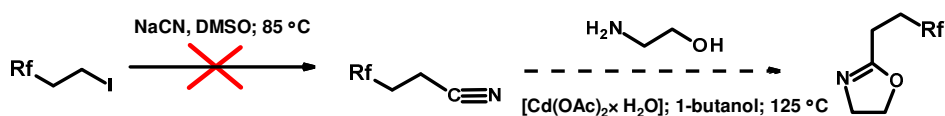
**Scheme 1.** Attempted Witte–Seeliger synthesis of 2-(1H,1H,2H,2H-perfluorohexyl)-2-oxazoline.

Subsequently, we attempted the α-deprotonation of 2-methyl-2-oxazoline (MeOx) followed by a substitution reaction with an alkylbromide/iodide.[42,43] More specifically, MeOx was deprotonated using n-butyllithium/tetramethylethylenediamine[44] and the obtained carbanion was then reacted with 1H,1H,2H,2H-perfluorooctylbromide to form 2-(1H,1H,2H,2H,3H,3H-perfluorononyl)-2-oxazoline (Scheme 2). Unfortunately, the attempt to apply this procedure for the synthesis of fluorinated 2-oxazolines failed and the usage of perfluorooctyl iodide was unsuccessful too.
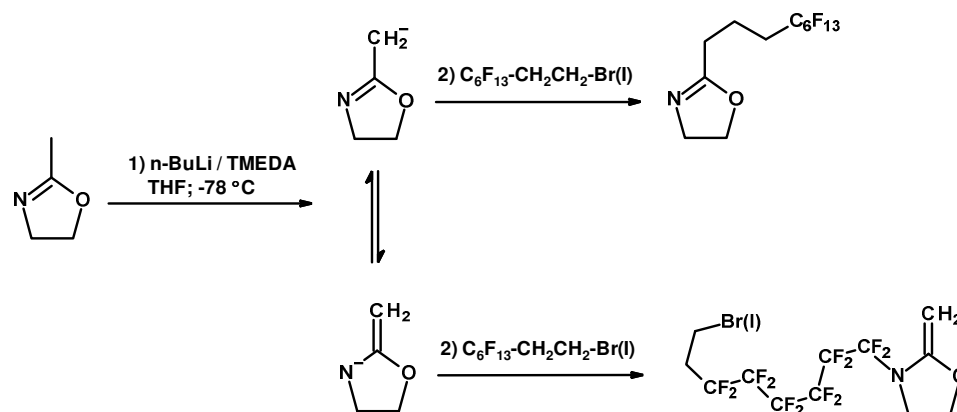
Scheme 2. Functionalization of 2-oxazolines by α-deprotonation of 2-methyl-2-oxazoline and imine-enamine equilibrium of the intermediate anion.

Our failure can be explained as follows. The intermediate anion exists in the form of imine-enamine equilibrium (Scheme 2, middle). In case of soft leaving groups (according to hard and soft Lewis acids and bases theory), such as bromide or iodide, the substitution reaction via the α-position (imine form) is preferred. At the same time, the fluorine can act as a hard leaving group and the enamine form will be more active. The ^{1}H NMR proves the presence of enamine in the reaction product: the signals from the protons at the double bond were observed at 5.64 and 5.75 ppm. Thus, it could be concluded that this method is not applicable for functionalization of 2-oxazolines by fluorine containing alkyl bromides/iodides.

In our third and successful attempt, we adopted the Wenker method for the synthesis of 2-oxazolines from β-halo amides,[45] supplemented by the synthesis of 1H,1H,2H,2H-perfluorononanoic acid via Grignard reaction as previously reported by Baker et al.[36] The required carboxylic acid with the ethyl spacer was synthesized starting from 1H,1H,2H,2H-perfluorooctyl iodide and magnesium in presence of iodine. The obtained Grignard reagent was then treated with dry ice yielding the target carboxylic acid, together with some unwanted iodide dimerization product (Scheme 3). The total yield of the desired acid was 40-50 %, which is in agreement with literature data.[36] The use of 1H,1H,2H,2H-perfluorooctyl bromide decreased the amount of dimer formation and also increased the yield of the acid (up to 60 %).
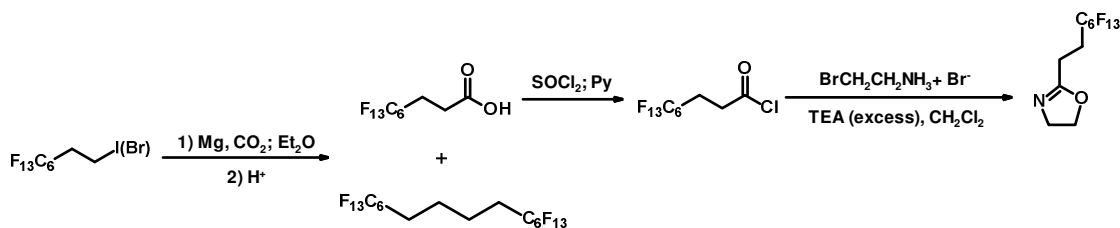
Scheme 3. Successful synthesis of 2-(1H,1H,2H,2H-perfluorooctyl)-2-oxazoline (R_f^6EtOx) via the Wenker method.

Subsequently, the obtained 1H,1H,2H,2H-perfluorooctyl carboxylic acid was converted to the acid chloride by the reaction with thionyl chloride, followed by reaction with 2-bromoethylamine hydrobromide in the presence of excess trimethylamine inducing in situ ring-closure of the formed amidoethylbromide to the 2-oxazoline ring. The R_f^6EtOx was isolated by distillation with a total yield up to 50 % which is higher than the one described by Jordan et al..[28] We conclude that the Grignard reaction based procedure could be used as an alternative way for the synthesis of fluorine containing 2-oxazolines.

The polymerization kinetics of R_f^6EtOx was studied according to the standard procedure, being polymerization at 140 ^{o}C in acetonitrile with methyl tosylate (MeOTs) as initiator.[46] The conversion of the monomer was followed by gas chromatography, which is plotted in a first order kinetic plot in Figure 1. The R_f^6EtOx monomer shows linear first order kinetics, which is typical for living CROP. The k_p value calculated from the slope is $143*10^{-3}$ L*mol^{-1}*s^{-1}, which is very similar to the k_p of 2-methyl-2-oxazoline ($146*10^{-3}$ L*mol^{-1}*s^{-1}). [47] Also, the similarity of the k_p for R_f^6EtOx and for obtained earlier 2-(3,3,3-trifluoropropyl)-2-oxazoline (CF$_3$EtOx, k_p=$129*10^{-3}$ L*mol^{-1}*s^{-1})[35] demonstrates that the length of the perfluoroalkyl substituent in 2-oxazolines with a double methylene spacer do not affect the k_p value. Even at low DP, poly-2-(1H,1H,2H,2H-perfluorooctyl)-2-oxazolines (polyR$_f^6$EtOx) was found to be insoluble at room temperature, thereby obstructing the analysis of its M$_n$ and dispersity.
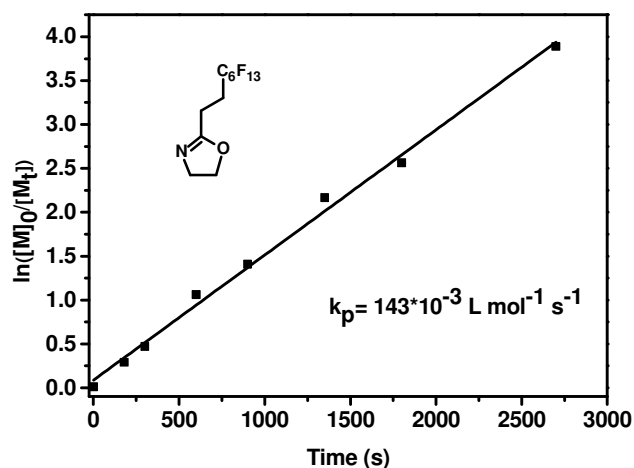
Figure 1. First order kinetic plot for the cationic ring-opening polymerization of R_f^6EtOx (solvent – acetonitrile; monomer concentration - 1M; initiator – p-methyltoluenesulfonate (MeOTos); temperature – 140°C; targeted DP – 100).

3.2. Block Copolymer synthesis

Having obtained the fluorinated monomer, we performed the synthesis of amphiphilic di- and triblock copolymers. 2-Methyl-2-oxazoline was used for the synthesis of the hydrophilic block and 2-*n*-octyl-2-oxazoline (OctOx) was chosen for the hydrophobic block as nonfluorinated analogue of R_f^6EtOx (Figure 2). It was also proposed that combination of long fluorinated and non-fluorinated fragments will promote the formation of multicompartment micelles in solution.
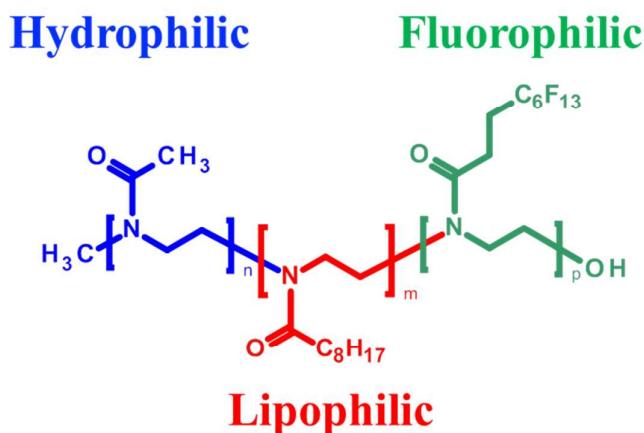

Figure 2. The common structure of investigated fluorophilic-lipophilic-hydrophilic copoly(2-oxazoline)s.

All polymers were synthesized via CROP in acetonitrile using MeOTos as the initiator. The monomers were polymerized subsequently, whereby the next monomer was added after a full conversion of the previous one. The full conversion time was calculated by following formula:

$$t = \ln\left(\frac{[M]_0}{[M]_t}\right) / (k_p * [I]_0)$$

using literature data[47] and the previously discussed kinetic study of R_f^6EtOx monomer. Here, *[M]$_0$* and *[M]$_t$* are monomer concentrations at the initial time and t stands for reaction time, respectively, k_p is the polymerization rate constant and *[I]$_0$* the initial concentration of the initiator.[47] The time to reach a value of 4 for *ln([M]$_0$/[M]$_t$)* was calculated corresponding to 98 % conversion of the monomer.

To ensure the water solubility of the resulting copolymers, a high molar ratio of the hydrophilic block was taken. Despite this, the wt. % of fluorophilic block in the copolymers is quite high due to high molecular weight of fluorophilic monomer of 417 g/mol. With increasing of the fluorinated block length, the copolymers become insoluble even in methanol (e.g. polymers PD and PF in Table 1), which may be attributed to the high crystallization tendency of fluoroalkyl chains.

All polymers were characterized by SEC-MALS and ^{1}H NMR spectroscopy, and the results are presented in Table 1.

Table 1. Characteristics of the synthesized block copoly(2-oxazoline)s.

	Composition (NMR)	M$_n$(SEC-MALS), g/mol	Đ (SEC-MALS)	Block ratios	
				mol. %	wt. %
P1	MeOx$_{55}$-R$_f^6$EtOx$_6$	7200	1.36	91 : 9	65 : 35
P2	MeOx$_{43}$-R$_f^6$EtOx$_5$	5700	1.34	89 : 11	63 : 37
P3	MeOx$_{38}$-R$_f^6$EtOx$_5$	5400	1.28	88 : 12	60 : 40
PD	MeOx$_{60}$-R$_f^6$EtOx$_{10}$*	-	-	85 : 15	55 : 45
PF	MeOx$_{40}$-R$_f^6$EtOx$_{10}$*	-	-	80 : 20	45 : 55

P4	$MeOx_{45}-OctOx_4-R_f^6EtOx_4$	6200	1.35	86 : 7 : 7	61 : 12 : 27
P5	$OctOx_7-MeOx_{41}-R_f^6EtOx_4$	6400	1.4	13 : 79 : 8	20 : 55 : 25
P6	$MeOx_{55}-OctOx_5-R_f^6EtOx_4$	7300	1.23	86 : 8 : 6	65 : 12 : 23

The proposed block ratios in polymers PD and PF was calculated from the initial monomer ratio.

3.3. Self-assembly study

The copolymers P1-P6 were found to be molecularly dissolved in several solvents including methanol, ethanol, chloroform, similarly to our previous studies on fluorinated poly(2-oxazoline)s.[32,35]

The aqueous solutions of the copolymers were prepared using two procedures. In the first case the polymers were first dissolved in methanol and then dialyzed against water. The alternative procedure was direct dissolution of the copolymers in water.

According to the DLS results, the solutions of diblock copolymers that were prepared by dialysis contained mainly small particles with a hydrodynamic diameter D_h of 20-40 nm and a minor fraction of larger aggregates (See Supporting Information Figure S3).

The preparation method has some impact on the fraction of large aggregates. The distribution functions for all diblock copolymers obtained by direct dissolution have a higher content of particles with mean D_h value of 150-300 nm. To gain deeper insights on each fraction that was observed in the DLS study, cryo-TEM experiments were conducted. The cryo-TEM images of the P2 copolymer in water shows that polymersomes are formed in both cases, whereby their diameter depends on the preparation method (Figure 3 A and B).
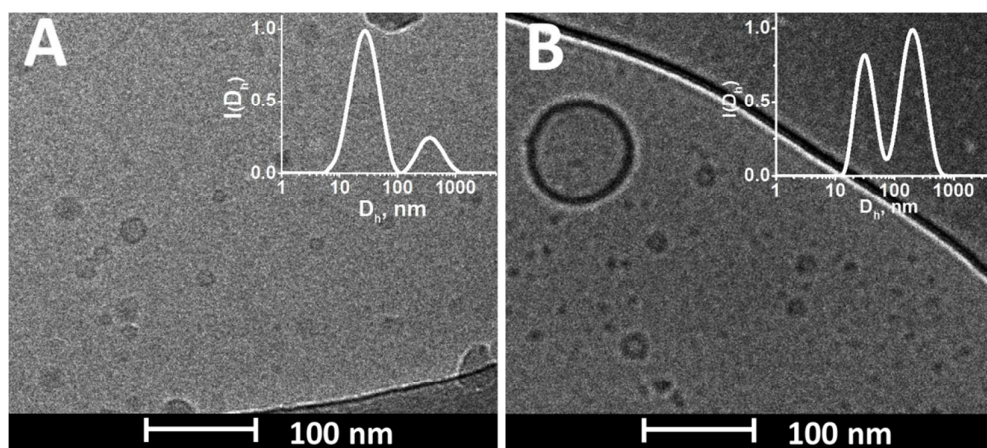
Figure 3. Cryo-TEM images of polymersomes in aqueous solutions of P2 (A – solvent exchange method, B – direct dissolution). The insets are DLS distribution functions of D_h for respective aqueous solutions.

The distribution functions for all three triblock copolymers in water obtained by solvent exchange show one peak of an approximately similar D_h value of 30 nm. The Cryo-TEM study of P4 and P5 revealed the presence of solid spheres with diameter about 20 nm that can be attributed to spherical micelles (Figure 4). At the same time, the presence of polymersomes in aqueous solution of triblock copolymers was not observed. It could be explained by the immiscibility of lipophilic and fluorophilic blocks, which makes the formation of complex hydrophobic polymersome layer (lipophilic-fluorophilic-lipophilic) thermodynamically unfavorable at a given blocks length. Similar effect was observed earlier for MeOx-b-OctOx copolymers with terminal perfluoroalkyl chains.[32]
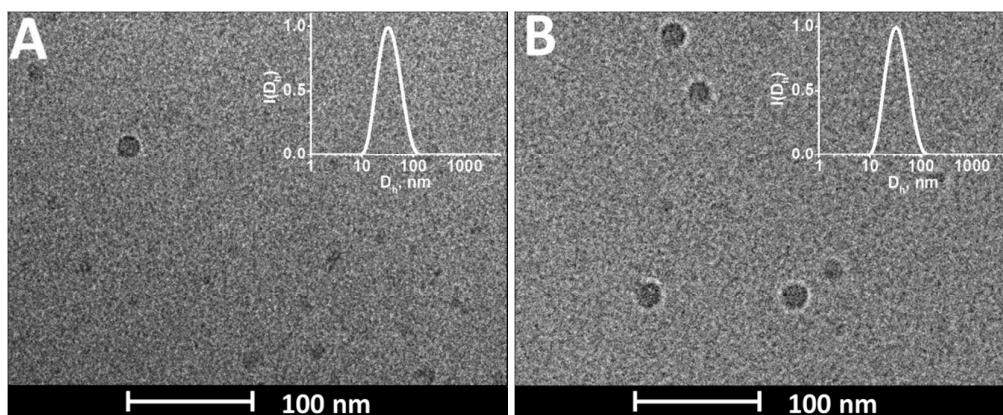

17

Figure 4. Cryo-TEM images of spherical micelles formed by triblock copolymers P4 (A) and P5 (B) in aqueous solutions (solvent exchange). The insets are DLS distribution functions of D_h for respective aqueous solutions.

Although the obtained copolymers are molecularly soluble in a number of solvents, their self-assembly in non-aqueous solvents could be expected as well. It is known that polymers solubility is affected by many factors and it is essential to use a parameter that takes into account the contribution of different origin. For that reason the Hansen solubility parameters were chosen. The total of Hansen solubility parameter δ_{total} consists of three components:

$$\delta_{total} = \sqrt{\delta_d^2 + \delta_p^2 + \delta_h^2}$$

where δ_d, δ_p and δ_h are components related to dispersion interactions, polarity and hydrogen bonding, respectively.[48] The Table 2 represents the literature data[48] on Hansen parameters for the solvents used in our study and the solution behavior of obtained copolymers. One can see that water has the highest value of δ_p and it could be hypothesized that self-assembly could be observed in solvent with polarity comparable to water.

Table 2. The solution behavior of di- and triblock copolymers (determined by DLS) and Hansen solubility parameters of respective solvents.

Solvent	Hansen solubility parameters				Behavior
	δ_{total}	δ_d	δ_p	δ_h	
Diethyl ether	15,40	14,50	2,90	4,60	Insoluble
Chloroform	18,70	17,80	3,10	5,70	Molecularly dissolved
Methylene chloride	20,20	17,00	7,30	7,10	Molecularly dissolved
Ethyl alcohol	26,20	15,80	8,80	19,40	Molecularly dissolved
Methyl alcohol	29,70	14,70	12,30	22,30	Molecularly dissolved
Water	48,00	15,50	16,00	42,30	Self-assembly

The additional DLS study of 10 mg/mL polymer solutions prepared via direct dissolving in a number of solvents was carried out (for the full list of used solvents see Supporting Information Table S1). It was found that the copolymers P1-P6 are molecularly soluble in

solvents with the δ_p value below 14. At the same time, the DLS study of di- and triblock copolymers solutions in dimethyl sulphoxide (DMSO, δ_p=16.4) demonstrates unimodal distributions with a mean D_h value in a range of 150-200 nm (see Supporting Information Figure S4). This observation gives indirect support of our hypothesis that the polar contribution of Hansen solubility parameter is a keystone that controls the self-assembly of fluorinated poly-2-oxazoline copolymers.

3.3 Nanoparticle morphology

Small Angle Neutron Scattering (SANS) was used to probe the nanoparticles architecture and determine their molecular parameters. The use of SANS allows to get more information about small particles compared with DLS method.
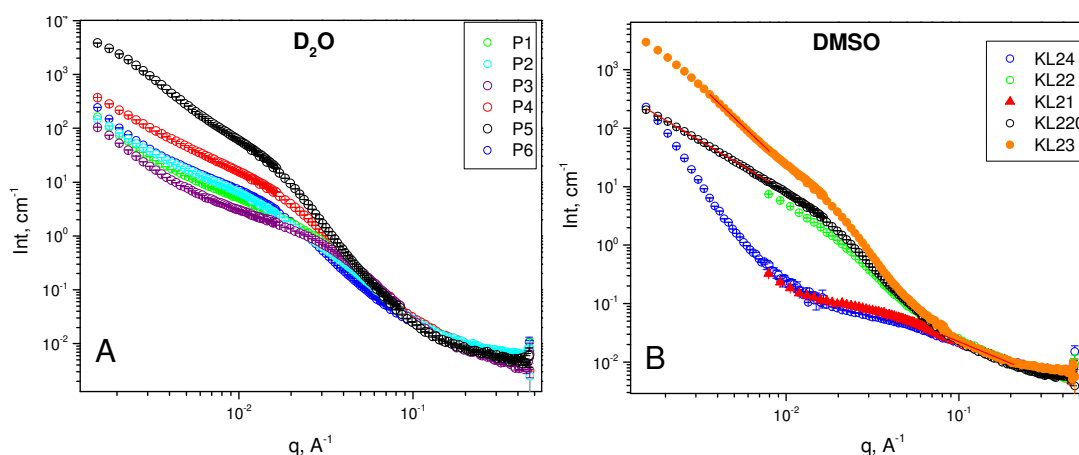

Figure 5. SANS curves for obtained polymers in D_2O (A) and DMSO-d6 (B).

The copolymers solutions were prepared by direct dissolution in pure D_2O and DMSO-d6. Under these conditions, the scattering from both core and shell is obtained as they are not matched with a particular solvent. The small q value data for polymers P1 and P4 were not measured because of their similarity at middle and high q ranges to P3 and P6 polymers, respectively.

The scattering curves obtained for the D_2O solutions demonstrate similar shape and can be well fitted with the "Sphere with attached Gaussian chain" model, assuming a Schulz-Zimm distribution for shell thickness (Figure S5 in Supporting Information). Also, the contribution of large aggregates was added as a background to take into account the presence of polymersomes and increase the fit quality. The calculated structural parameters are presented in Table 3.

Table 3. Comparison of structural parameters obtained from samples P1-P6 in D_2O

	Composition	R_{core} (nm)	N_{agg}	Chain	
				R_g, nm	σ
P1	MeOx$_{55}$-R$_f^6$EtOx$_6$	3.4	61	6.4	0.61
P2	MeOx$_{43}$-R$_f^6$EtOx$_5$	4.2	79	8.3	0.47
P3	MeOx$_{38}$-R$_f^6$EtOx$_5$	3.0	54	6.1	0.74
P4	MeOx$_{45}$-OctOx$_4$-R$_f^6$EtOx$_4$	6.1	103	6.4	0.27
P5	OctOx$_7$-MeOx$_{41}$-R$_f^6$EtOx$_4$*	-	-	-	-
P6	MeOx$_{55}$-OctOx$_5$-R$_f^6$EtOx$_4$	6.0	55	6.0	0.34

** P5 copolymer with inverse blocks order was fitted with the model of sphere with a radial profile
since attempts to fit SANS data for P5 by "Sphere with attached Gaussian chain" model failed.*

The obtained value of the core radii and shell thickness are in the range of 18-24 nm, which is
in agreement with the R_h as observed in the DLS measurements and cryo-TEM.
Unfortunately, the overall correlation between the diblock copolymer structural parameters
and the polymer composition could not be achieved, mainly because of high polydispersity of
the hydrophilic shell. Nevertheless, the significant increase of the mean micellar core radius
with introduction of the OctOx hydrophobic block can be observed (from 3.5 to 6 nm). This
observation indicates the coexistence of the lipophilic and fluorophilic fragments in the core.

Unlike to aqueous solutions, the MeOx-R$_f^6$EtOx diblock copolymers were found to be
molecularly dissolved in DMSO-d6 (Figure 5 B). The disagreement between SANS and DLS
data where peaks with 100-200 nm were only present on a distribution function is explained
by the high sensitivity of DLS to the presence of large aggregates, which obstruct the small
particles detection. The successful fitting for copolymers P1 and P3 in DMSO-d6 was
achieved using "Generalised Gaussian coil" model (Table 4) with a contribution of the large
aggregates as a background. It could be concluded from the high value of the Flory parameter
ν that DMSO is a "good solvent" for these polymers. The ν values of 0.75 and 0.93 imply that
macromolecules exist in highly extended conformation that could be explained by the
intrinsic rigidity of the fluorinated block.

Table 4. The structural parameters obtained for diblock copolymers P1 and P3 in DMSO-d6 using the "Generalised Gaussian coil" model.

	Composition	R_g, nm	ν
P1	$MeOx_{55}-R_f^6EtOx_6$	4.4	0.74±0.02
P3	$MeOx_{38}-R_f^6EtOx_5$	8	0.93±0.05

In contrast, the shape of the SANS curves of the triblock copolymers P4-P6 in DMSO-d6 indicates the presence of aggregates (Figure 5B). This observation implies that the hydrophobic POctOx block is mainly responsible for the self-assembly in DMSO. The scattering data could well be fitted using the monodisperse "Sphere with attached Gaussian chains" model (Table 5).

Table 5. The structural parameters obtained for triblock copolymers P4, P5 and P6 in DMSO-d6 using "Sphere with attached Gaussian chains" model.

	Composition	R_{core}, nm	R_g, nm	N_{agg}
P4	$MeOx_{45}-OctOx_4-R_f^6EtOx_4$	6.3	3.4	37
P5	$OctOx_7-MeOx_{41}-R_f^6EtOx_4$	7.5	4.7	100
P6	$MeOx_{55}-OctOx_5-R_f^6EtOx_4$	7.5	6.2	69

The mean aggregates radii in DMSO is 20-26 nm, which is in the same range as in D_2O solutions. It also can be seen that the change in the location of the hydrophobic block affects the size of the aggregates: the P5 copolymer with lipophilic end block forms larger aggregates than the P4 copolymer of similar composition with lipophilic block in the middle. Such effect of the block order was previously observed only for aqueous solutions.[49]

The core radii of P4 and P6 aggregates also have the similar values in D_2O and in DMSO-d6. Therefore it is proposed that in DMSO-d6 the core is also composed of both lipophilic and fluorophilic blocks, despite the affinity of the last one to DMSO. Such ordering could be explained by the strong interactions between alkyl fragments in lipophilic layer and short length of the fluorophilic block.

The difference in solution behavior of polymers P1-P6 in water and DMSO could be explained by comparison of their Hansen polarity (δ_p) and hydrogen bonds (δ_h) contributions. Indeed, MeOx has the highest polarity, while OctOx is almost nonpolar. The presence of these blocks in one macromolecule produces high non-homogeneity in polarity and facilitates self-assembly in polar water and DMSO. Also, this contrast is enhanced by the difference in ability to H-bonding, which is much stronger for PMeOx then for POctOx. At the same time, PR_f^6EtOx possesses noticeable polarity due to its structure, but still has low ability to form H-bonds.[13] Therefore, we can assume that PMeOx-*b*-PR_f^6EtOx diblock copolymers form micelles in aqueous solution, whereas in DMSO, where H-bonding effect is much lower; they are molecularly dissolved.

Conclusion

In this paper we tested a several approaches for the synthesis of highly fluorinated 2-oxazolines. The only successful route was the Wanker method supplemented by the Grignard synthesis of fluorinated carboxylic acid. According to this approach 2-(1H,1H,2H,2H-perfluorooctyl)-2-oxazoline monomer was synthesized. The polymerization kinetics study demonstrated the complete suppression of deceleration effect of perfluoroalkyl group by the insertion of double methylene spacer leading to good monomer reactivity in the Cationic Ring-Opening Polymerization.

A series of di- and triblock copolymers based on 2-(1H,1H,2H,2H-perfluorooctyl)-2-oxazoline, 2-methyl-2-oxazoline and 2-*n*-octyl-2-oxazoline were synthesized. Well-defined copolymers with M_n in the range of 5300-7300 and Đ in the range of 1.2-1.4 were obtained. DLS revealed the ability of the synthesized copolymers to self-assemble in aqueous milieu and in DMSO. The presence of micelle-like aggregates and polymersomes in aqueous solutions was visualized by Cryo-TEM.

Further investigation of the nanoparticle morphologies was done by SANS revealing that the presence of both the POctOx and the PR_f^6EtOx blocks results in the formation of nanoparticles with a core-shell structure in aqueous solutions of both di- and triblock copolymers, whereas in DMSO the presence of the POctOx block is required for the self-assembly. It was also found that in DMSO the block order has an influence on the aggregate size and structure in the same way as it was observed for aqueous solutions. The importance of Hansen polarity contribution is revealed for self-assembly of these fluorinated copolymers.

The obtained polymers represent a potential platform for application as ^{19}F magnetic resonance imaging contrast agents, which will be the focus of our future work.

Acknowledgment

References

(1)   Kagiya, T.; Maeda, T.; Fukui, K.; Narisawa, S. Ring Opening Polymerization Of 2-
        Substituted 2-Oxazolines. *Polym. Lett.* **1966**, *4*, 441–445 DOI:
        10.1002/pol.1966.110040701.

(2)   Seeliger, W.; Aufderhaar, E.; Diepers, W.; Feinauer, R.; Nehring, R.; Thier, W.;
        Hellmann, H. Recent Syntheses and Reactions of Cyclic Imidic Esters. *Angew. Chemie
        Int. Ed. English* **1966**, *5* (10), 875–888 DOI: 10.1002/anie.196608751.

(3)   Tomalia, D. A.; Sheetz, D. P. Homopolymerization of 2-Alkyl- and 2-Aryl-2-
        Oxazolines. *J. Polym. Sci. Part A-1 Polym. Chem.* **1966**, *4* (9), 2253–2265 DOI:
        10.1002/pol.1966.150040919.

(4) Levy, A.; Litt, M. Polymerization of Cyclic Imino Ethers. II. Oxazines. *J. Polym. Sci. Part B Polym. Lett.* **1967**, *5* (9), 881–886 DOI: 10.1002/pol.1967.110050928.

(5) Luxenhofer, R.; Schulz, A.; Roques, C.; Li, S.; Bronich, T. K.; Batrakova, E. V.; Jordan, R.; Kabanov, A. V. Doubly Amphiphilic poly(2-Oxazoline)s as High-Capacity Delivery Systems for Hydrophobic Drugs. *Biomaterials* **2010**, *31* (18), 4972–4979 DOI: 10.1016/j.biomaterials.2010.02.057.

(6) Wiesbrock, F.; Hoogenboom, R.; Abeln, C. H.; Schubert, U. S. Single-Mode Microwave Ovens as New Reaction Devices: Accelerating the Living Polymerization of 2-Ethyl-2-Oxazoline. *Macromol. Rapid Commun.* **2004**, *25* (22), 1895–1899 DOI: 10.1002/marc.200400369.

(7) Wiesbrock, F.; Hoogenboom, R.; Schubert, U. S. Microwave-Assisted Polymer Synthesis: State-of-the-Art and Future Perspectives. *Macromol. Rapid Commun.* **2004**, *25* (20), 1739–1764 DOI: 10.1002/marc.200400313.

(8) Hoogenboom, R.; Fijten, M. W. M.; Thijs, H. M. L.; van Lankvelt, B. M.; Schubert, U. S. Microwave-Assisted Synthesis and Properties of a Series of poly(2-Alkyl-2-Oxazoline)s. *Des. Monomers Polym.* **2005**, *8* (6), 659–671 DOI: 10.1163/156855505774597704.

(9) Filippov, S. K.; Bogomolova, A.; Kaberov, L.; Velychkivska, N.; Starovoytova, L.; Cernochova, Z.; Rogers, S. E.; Lau, W. M.; Khutoryanskiy, V. V.; Cook, M. T. Internal Nanoparticle Structure of Temperature-Responsive Self-Assembled PNIPAM-B-PEG-B-PNIPAM Triblock Copolymers in Aqueous Solutions: NMR, SANS, and Light Scattering Studies. *Langmuir* **2016**, *32* (21), 5314–5323 DOI: 10.1021/acs.langmuir.6b00284.

(10) Vishnevetskaya, N. S.; Hildebrand, V.; Niebuur, B.-J.; Grillo, I.; Filippov, S. K.; Laschewsky, A.; Müller-Buschbaum, P.; Papadakis, C. M. Aggregation Behavior of Doubly Thermoresponsive Polysulfobetaine- B -Poly(N -Isopropylacrylamide) Diblock Copolymers. *Macromolecules* **2016**, *49* (17), 6655–6668 DOI: 10.1021/acs.macromol.6b01186.

(11) Filippov, S. K.; Verbraeken, B.; Konarev, P. V.; Svergun, D. I.; Angelov, B.; Vishnevetskaya, N. S.; Papadakis, C. M.; Rogers, S.; Radulescu, A.; Courtin, T.;

Martins, J. C.; Starovoytova, L.; Hruby, M.; Stepanek, P.; Kravchenko, V. S.; Potemkin, I. I.; Hoogenboom, R. Block and Gradient Copoly(2-Oxazoline) Micelles: Strikingly Different on the Inside. *J. Phys. Chem. Lett.* **2017**, *8* (16), 3800–3804 DOI: 10.1021/acs.jpclett.7b01588.

(12)   Filippov, S. K.; Starovoytova, L.; Koňák, Č.; Hrubý, M.; MacKová, H.; Karlsson, G.; Štěpánek, P. PH Sensitive Polymer Nanoparticles: Effect of Hydrophobicity on Self-Assembly. *Langmuir* **2010**, *26* (18), 14450–14457 DOI: 10.1021/la1018778.

(13)   Krafft, M. P.; Riess, J. G. Chemistry, Physical Chemistry, and Uses of Molecular Fluorocarbon- Hydrocarbon Diblocks, Triblocks, and Related Compounds-Unique "apolar" components for Self-Assembled Colloid and Interface Engineering. *Chem. Rev.* **2009**, *109* (5), 1714–1792 DOI: 10.1021/cr800260k.

(14)   Liu, W.; Frank, J. A. Detection and Quantification of Magnetically Labeled Cells by Cellular MRI. *Eur. J. Radiol.* **2009**, *70* (2), 258–264 DOI: 10.1016/j.ejrad.2008.09.021.

(15)   Boehm-Sturm, P.; Mengler, L.; Wecker, S.; Hoehn, M.; Kallur, T. In Vivo Tracking of Human Neural Stem Cells with 19F Magnetic Resonance Imaging. *PLoS One* **2011**, *6* (12) DOI: 10.1371/journal.pone.0029040.

(16)   Srinivas, M.; Heerschap, A.; Ahrens, E. T.; Figdor, C. G.; de Vries, I. J. M. 19F MRI for Quantitative in Vivo Cell Tracking. *Trends Biotechnol.* **2010**, *28* (7), 363–370 DOI: 10.1016/j.tibtech.2010.04.002.

(17)   Li, Z.; Kesselman, E.; Talmon, Y.; Hillmyer, M. A.; Lodge, T. P. Multicompartment Micelles from ABC Miktoarm Stars in Water. *Science (80-.).* **2004**, *306* (5693), 98–101 DOI: 10.1126/science.1103350.

(18)   Kubowicz, S.; Baussard, J. F.; Lutz, J. F.; Thünemann, A. F.; Von Berlepsch, H.; Laschewsky, A. Multicompartment Micelles Formed by Self-Assembly of Linear ABC Triblock Copolymers in Aqueous Medium. *Angew. Chemie - Int. Ed.* **2005**, *44* (33), 5262–5265 DOI: 10.1002/anie.200500584.

(19)   Kotzev, A.; Laschewsky, A.; Rakotoaly, R. H. Polymerizable Surfactants and Micellar Polymers Bearing Fluorocarbon Hydrophobic Chains Based on Styrene. *Macromol. Chem. Phys.* **2001**, *202* (17), 3257–3267 DOI: 10.1002/1521-3935(20011101)202:17<3257::AID-MACP3257>3.0.CO;2-P.

25

(20)   Berlepsch, H. v.; Böttcher, C.; Skrabania, K.; Laschewsky, A. Complex Domain
       Architecture of Multicompartment Micelles from a Linear ABC Triblock Copolymer
       Revealed by Cryogenic Electron Tomography. *Chem. Commun.* **2009**, No. 17, 2290
       DOI: 10.1039/b903658j.

(21)   Laschewsky, A.; Marsat, J. N.; Skrabania, K.; Von Berlepsch, H.; Böttcher, C.
       Bioinspired Block Copolymers: Translating Structural Features from Proteins to
       Synthetic Polymers. *Macromol. Chem. Phys.* **2010**, *211* (2), 215–221 DOI:
       10.1002/macp.200900378.

(22)   Skrabania, K.; Laschewsky, A.; Berlepsch, H. V.; Böttcher, C. Synthesis and Micellar
       Self-Assembly of Ternary Hydrophilic- Lipophilicfluorophilic Block Copolymers with
       a Linear PEO Chain. *Langmuir* **2009**, *25* (13), 7594–7601 DOI: 10.1021/la900253j.

(23)   Skrabania, K.; Berlepsch, H. V.; Böttcher, C.; Laschewsky, A. Synthesis of Ternary,
       Hydrophilic-Lipophilic-Fluorophilic Block Copolymers by Consecutive RAFT
       Polymerizations and Their Self-Assembly into Multicompartment Micelles.
       Macromolecules **2010**, *43* (1), 271–281 DOI: 10.1021/ma901913f.

(24)   Matsumoto, K.; Nishimura, R.; Mazaki, H.; Matsuoka, H.; Yamaoka, H. Synthesis and
       Hydrogel Formation of Fluorine-Containing Amphiphilic ABA Triblock Copolymers.
       J. Polym. Sci. Part A Polym. Chem. **2001**, *39* (21), 3751–3760 DOI:
       10.1002/pola.10011.

(25)   Guo, W.; Tang, X.; Xu, J.; Wang, X.; Chen, Y.; Yu, F.; Pei, M. Synthesis,
       Characterization, and Property of Amphiphilic Fluorinated ABC-Type Triblock
       Copolymers. *J. Polym. Sci. Part A Polym. Chem.* **2011**, *49* (7), 1528–1534 DOI:
       10.1002/pola.24573.

(26)   Chen, J.; Li, J. J.; Luo, Z. H. Synthesis, Surface Property, Micellization and pH
       Responsivity of Fluorinated Gradient Copolymers. *J. Polym. Sci. Part A Polym. Chem.*
       2013, *51* (5), 1107–1117 DOI: 10.1002/pola.26473.

(27)   Miyamoto, M.; Aoi, K.; Saegusa, T. Novel Covalent-Type Electrophilic
       Polymerization of 2-(Perfluoroalkyl)-2-Oxazolines Initiated by Sulfonates.
       Macromolecules **1991**, *24* (1), 11–16 DOI: 10.1021/ma00001a002.

(28)   Ivanova, R.; Komenda, T.; Bonné, T. B.; Lüdtke, K.; Mortensen, K.; Pranzas, P. K.;

26

Jordan, R.; Papadakis, C. M. Micellar Structures of Hydrophilic/lipophilic and Hydrophilic/fluorophilic poly(2-Oxazoline) Diblock Copolymers in Water. *Macromol. Chem. Phys.* **2008**, *209* (21), 2248–2258 DOI: 10.1002/macp.200800232.

(29)   Miyamoto, M.; Aoi, K.; Saegusa, T. Poly[(acylimino)alkylene] Block Copolymers Having Perfluoroalkyl Hydrophobic Blocks. Synthesis and Surfactant Properties. *Macromolecules* **1989**, *22* (9), 3540–3543 DOI: 10.1021/ma00199a007.

(30)   Weberskirch, R.; Preuschen, J.; Spiess, H. W.; Nuyken, O. Design and Synthesis of a Two Compartment Micellar System Based on the Self-Association Behavior of poly(N-Acylethyleneimine) End-Capped with a Fluorocarbon and a Hydrocarbon Chain. *Macromol.Chem.Phys.* **2000**, *201* (10), 995–1007 DOI: 10.1002/1521-3935(20000601)201:10<995::AID-MACP995>3.0.CO;2-T.

(31)   Imine, E. P. N.; Kubowicz, S.; Thu, A. F.; Weberskirch, R. Cylindrical Micelles of R - Fluorocarbon- ω -Hydrocarbon. **2005**, No. 4, 7214–7219.

(32)   Kaberov, L. I.; Verbraeken, B.; Hruby, M.; Riabtseva, A.; Kovacik, L.; Kereiche, S.; Brus, J.; Stepanek, P.; Hoogenboom, R.; Filippov, S. K. Novel Triphilic Block Copolymers Based on poly(2-Methyl-2-Oxazoline)-Block-poly(2-Octyl-2-Oxazoline) with Different Terminal Perfluoroalkyl Fragments: Synthesis and Self-Assembly Behaviour. *Eur. Polym. J.* **2017**, *88*, 645–655 DOI: 10.1016/j.eurpolymj.2016.10.016.

(33)   Lobert, M.; Thijs, H. M. L.; Erdmenger, T.; Eckardt, R.; Ulbricht, C.; Hoogenboom, R.; Schubert, U. S. Synthesis, Microwave-Assisted Polymerization, and Polymer Properties of Fluorinated 2-Phenyl-2-Oxazolines: A Systematic Study. *Chem. - A Eur. J.* **2008**, *14* (33), 10396–10407 DOI: 10.1002/chem.200800671.

(34)   Kempe, K.; Hoogenboom, R.; Hoeppener, S.; Fustin, C.-A.; Gohy, J.-F.; Schubert, U. S. Discovering New Block Terpolymer Micellar Morphologies. *Chem. Commun.* **2010**, *46* (35), 6455 DOI: 10.1039/c001629b.

(35)   Kaberov, L. I.; Verbraeken, B.; Riabtseva, A.; Brus, J.; Talmon, Y.; Stepanek, P.; Hoogenboom, R.; Filippov, S. K. Fluorinated 2-Alkyl-2-Oxazolines of High Reactivity: Spacer-Length-Induced Acceleration for Cationic Ring-Opening Polymerization As a Basis for Triphilic Block Copolymer Synthesis. *ACS Macro Lett.* **2017**, 7–10 DOI: 10.1021/acsmacrolett.7b00954.

(36) Baker, R. J.; McCabe, T.; O'Brien, J. E.; Ogilvie, H. V. Thermomorphic Metal
Scavengers: A Synthetic and Multinuclear NMR Study of Highly Fluorinated Ketones
and Their Application in Heavy Metal Removal. *J. Fluor. Chem.* **2010**, *131* (5), 621–
626 DOI: 10.1016/j.jfluchem.2010.02.004.

(37) Petrova, S.; Klepac, D.; Konefał, R.; Kereïche, S.; Kováčik, L.; Filippov, S. K.
Synthesis and Solution Properties of PCL-B-PHPMA Diblock Copolymers Containing
Stable Nitroxyl Radicals. *Macromolecules* **2016**, *49* (15), 5407–5417 DOI:
10.1021/acs.macromol.6b01187.

(38) Trousil, J.; Filippov, S. K.; Hrubý, M.; Mazel, T.; Syrová, Z.; Cmarko, D.; Svidenská,
S.; Matějková, J.; Kováčik, L.; Porsch, B.; Konefał, R.; Lund, R.; Nyström, B.; Raška,
I.; Štěpánek, P. System with Embedded Drug Release and Nanoparticle Degradation
Sensor Showing Efficient Rifampicin Delivery into Macrophages. *Nanomedicine
Nanotechnology, Biol. Med.* **2017**, *13* (1), 307–315 DOI: 10.1016/j.nano.2016.08.031.

(39) Radulescu, A.; Szekely, N. K.; Appavou, M.-S. KWS-2: Small Angle Scattering
Diffractometer. *J. large-scale Res. Facil. JLSRF* **2015**, *1*, A29 DOI: 10.17815/jlsrf-1-
27.

(40) Breßler, I.; Kohlbrecher, J.; Thünemann, A. F. SASfit: A Tool for Small-Angle
Scattering Data Analysis Using a Library of Analytical Expressions. *J. Appl.
Crystallogr.* **2015**, *48*, 1587–1598 DOI: 10.1107/S1600576715016544.

(41) Witte, H.; Seeliger, W. Cyclische Imidsaureester Aus Nitrilen Und Aminoalkoholen.
Justus Liebigs Ann. Chem. **1974**, *1974* (6), 996–1009 DOI:
10.1002/jlac.197419740615.

(42) Verbraeken, B.; Lava, K.; Hoogenboom, R. Poly (2-Oxazoline) S. *Encycl. Polym. Sci.
Technol.* **2014**, No. 1, 1–51.

(43) Persigehl, P.; Jordan, R.; Nuyken, O. Functionalization of Amphiphilic poly(2-
Oxazoline) Block Copolymers: A Novel Class of Macroligands for Micellar Catalysis.
Macromolecules **2000**, *33* (19), 6977–6981 DOI: 10.1021/ma0007381.

(44) Taubmann, C.; Luxenhofer, R.; Cesana, S.; Jordan, R. First Aldehyde-Functionalized
poly(2-Oxazoline)s for Chemoselective Ligation. *Macromol. Biosci.* **2005**, *5* (7), 603–
612 DOI: 10.1002/mabi.200500059.

(45)   Wenker, H. The Synthesis of Δ2-Oxazolines and Δ2-Thiazolines from N-Acyl-2-
        Aminoethanols. *J. Am. Chem. Soc.* **1935**, *57* (6), 1079–1080 DOI:
        10.1021/ja01309a034.

(46)   Wiesbrock, F.; Hoogenboom, R.; Leenen, M. A. M.; Meier, M. A. R.; Schubert, U. S.
        Investigation of the Living Cationic Ring-Opening Polymerization of 2-Methyl-, 2-
        Ethyl-, 2-Nonyl-, and 2-Phenyl-2-Oxazoline in a Single-Mode Microwave Reactor.
        Macromolecules **2005**, *38* (12), 5025–5034 DOI: 10.1021/ma0474170.

(47)   Verbraeken, B.; Monnery, B. D.; Lava, K.; Hoogenboom, R. The Chemistry of poly(2-
        Oxazoline)s. *Eur. Polym. J.* **2017**, *88*, 451–469 DOI: 10.1016/j.eurpolymj.2016.11.016.

(48)   Hansen, C. M. *Hansen Solubility Parameters A User's Handbook*; 2007.

(49)   Hoogenboom, R.; Wiesbrock, F.; Huang, H.; Leenen, M. A. M.; Thijs, H. M. L.; Van
        Nispen, S. F. G. M.; Van Der Loop, M.; Fustin, C. A.; Jonas, A. M.; Gohy, J. F.;
        Schubert, U. S. Microwave-Assisted Cationic Ring-Opening Polymerization of 2-
        Oxazolines: A Powerful Method for the Synthesis of Amphiphilic Triblock
        Copolymers. *Macromolecules* **2006**, *39* (14), 4719–4725 DOI: 10.1021/ma060952a.

Fluorophilic-lipophilic-hydrophilic poly-2-oxazolines block copolymers as MRI contrast agents: from synthesis to self-assembly

Leonid I. Kaberov[1], Bart Verbraeken[2], Anna Riabtseva[1], Jiri Brus[1], Aurel Radulescu[3], Yeshayahu Talmon[4], Petr Stepanek[1], Richard Hoogenboom[2], Sergey K. Filippov[1*]
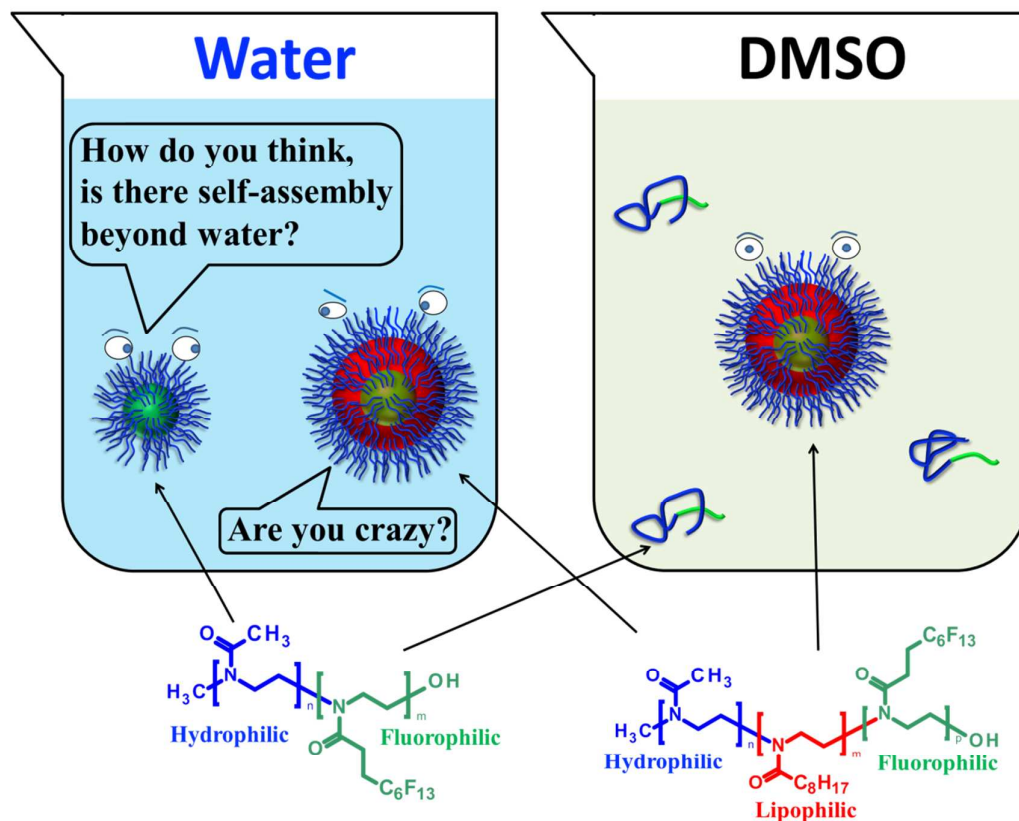
[1]*Institute of Macromolecular Chemistry, Academy of Sciences of the Czech Republic, Heyrovský Sq. 2, 162 06 Prague 6, Czech Republic*
[2]*Supramolecular Chemistry Group, Centre of Macromolecular Chemistry (CMaC), Department of Organic and Macromolecular Chemistry, Ghent University, Krijgslaan 281 S4, B-9000 Ghent, Belgium*
[3]*Forschungszentrum Jülich GmbH, Jülich Centre for Neutron Science JCNS, Outstation at Heinz Maier-Leibnitz Zentrum, Lichtenbergstraße 1, 85748 Garching, Germany*
[4]*Department of Chemical Engineering, Technion-Israel Institute of Technology, Haifa 3200003, Israel*
*e-mail: filippov@imc.cas.cz

Supporting Information

Fluorophilic-lipophilic-hydrophilic poly-2-oxazolines block copolymers as MRI contrast agents: from synthesis to self-assembly

Leonid I. Kaberov[1], Bart Verbraeken[2], Anna Riabtseva[1], Jiri Brus[1], Aurel Radulescu[3], Yeshayahu Talmon[4], Petr Stepanek[1], Richard Hoogenboom[2], Sergey K. Filippov[1*]

[1]*Institute of Macromolecular Chemistry, Academy of Sciences of the Czech Republic, Heyrovský Sq. 2, 162 06 Prague 6, Czech Republic*
[2]*Supramolecular Chemistry Group, Centre of Macromolecular Chemistry (CMaC), Department of Organic and Macromolecular Chemistry, Ghent University, Krijgslaan 281 S4, B-9000 Ghent, Belgium*
[3]*Forschungszentrum Jülich GmbH, Jülich Centre for Neutron Science JCNS, Outstation at Heinz Maier-Leibnitz Zentrum, Lichtenbergstraße 1, 85748 Garching, Germany*
[4]*Department of Chemical Engineering, Technion-Israel Institute of Technology, Haifa 3200003, Israel*

*e-mail: filippov@imc.cas.cz

S1: Synthesis of fluorinated 2-oxazolines by Witte-Seeliger method

The attempt to obtain highly fluorinated 2-oxazoline using Witte-Seeliger synthesis was carried out according to procedure described by Papadakis et.al. (ref. 28 in the main text) as follows.

Sodium cyanide (1.24 g, 0.0252 mol) was dissolved in 40 mL of DMSO at 85 °C. After that 1H,1H,2H,2H-perfluorooctyliodide (10 g, 5.17 mL) was added dropwise. After few drops solution became deep purple (almost black). The reaction mixture was stirred over 24 h at 85 °C and then cooled to a room temperature and added to an ice/potassium carbonate mixture. The product was extracted three times by diethyl ether, the organic layers were combined and dried over $MgSO_4$. The ether was removed under reduced pressure. The product was obtained as deep purple liquid with the yield of 1.2 g (15 %). The ^1H NMR does not show the expected signals from the protons for 1H,1H,2H,2H-perfluorooctyl cyanide. The signal from CN-group in ^{13}C NMR also was not observed.

S2: Synthesis of fluorinated 2-oxazolines via α-deprotonation of MeOx followed by nucleophilic substitution reaction with 1H,1H,2H,2H-perfluorooctyliodide

Diisopropylamine (2.66 mL, 0.019 mol) was dissolved in 20 mL of THF and cooled down using i-PrOH/dry ice bath (–89 °C) under an argon atmosphere. After cooling n-BuLi (7.6 mL of 2.5 M solution in hexane, 0.019 mol) was added dropwise during 0.5 h and the reaction mixture was stirred under for 1 h. After that MeOx (1.7 mL, 0.02 mol) was added dropwise during 0.5 h and stirred for 1 h. Afterwards, 1H,1H,2H,2H-perfluorooctyliodide (4.42 mL, 0.018 mol) was dissolved in 5 mL of hexane and added dropwise to reaction mixture during 0.5 h and solution was allowed to warm to room temperature overnight. The reaction was terminated by 10 mL of MeOH and the solvents were removed under reduced pressure. The residue was dissolved in dichloromethane, washed subsequently by water and brine and dried over $MgSO_4$. After drying the solvent was removed under reduced pressure and residue was distilled in vacuum yielding a product as a colourless liquid. Yield ~ 1.5 g (18%). According to ^{1}H NMR spectra, the signal from MeOx CH_3-group was not observed. On the over hand, there are signals at 5.64 and 5.75 ppm, which were attributed to protons from the C=C double bond. These observations indicate that the reaction proceeds via enamine form of intermediate anion.

S3: DLS

Table S1. The solution behavior of di- and triblock copolymers (determined by DLS) and Hansen solubility parameters of respective solvents.

| Solvent	Hansen solubility parameters				Behavior
	delta-(SI)	Dispersion	Polar	H-bonding	
n-Hexane	*14,90*	*14,90*	*0,00*	*0,00*	*Insoluble*
Diethyl ether	*15,40*	*14,50*	*2,90*	*4,60*	*Insoluble*
Ethyl acetate	*18,20*	*15,80*	*5,30*	*7,20*	*Insoluble*
Toluene	*18,30*	*18,00*	*1,40*	*2,00*	*Insoluble*
Tetrahydrofuran	*18,50*	*16,80*	*5,70*	*8,00*	*Insoluble*
Chloroform	18,70	17,80	3,10	5,70	Molecularly dissolved
Methylene chloride	20,20	17,00	7,30	7,10	Molecularly dissolved
Dimethylacetamide	22,50	7,90	11,50	10,20	Molecularly dissolved
HFIP	23,00	17,20	4,50	14,70	Molecularly dissolved
Dimethylformamide	24,70	17,40	13,70	11,30	Molecularly dissolved
i-Propyl alcohol	24,90	15,50	6,60	17,00	Molecularly dissolved
Ethyl alcohol	26,20	15,80	8,80	19,40	Molecularly dissolved
Dimethyl sulphoxide	**26,40**	**18,40**	**16,40**	**10,20**	**Self-assembly**
Methyl alcohol	29,70	14,70	12,30	22,30	Molecularly dissolved
Water	**48,00**	**15,50**	**16,00**	**42,30**	**Self-assembly**
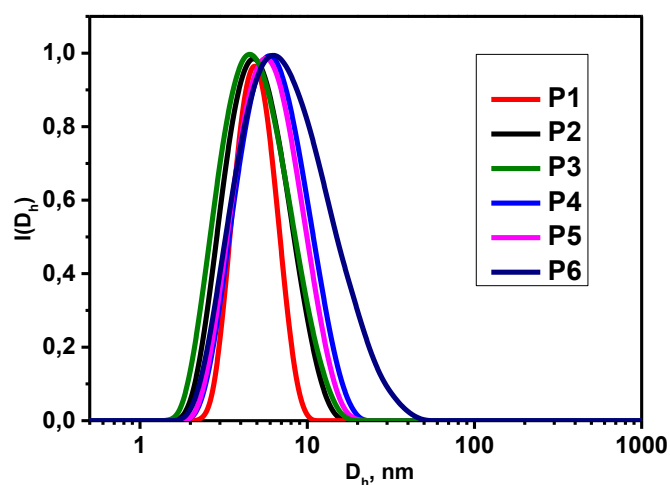
Figure S1. Distribution functions of D_h for 10 mg/ml polymer solutions in ethanol.
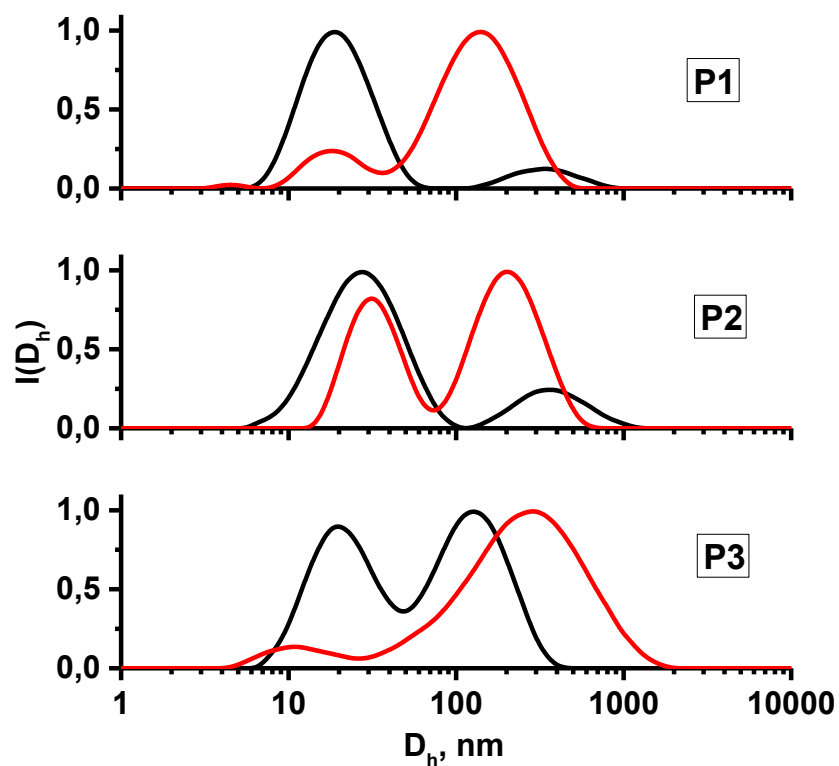
Figure S2. Distribution functions of D_h for 10 mg/ml diblock copolymers solutions in water prepared by solvent exchange method (black) and direct dissolving (red)
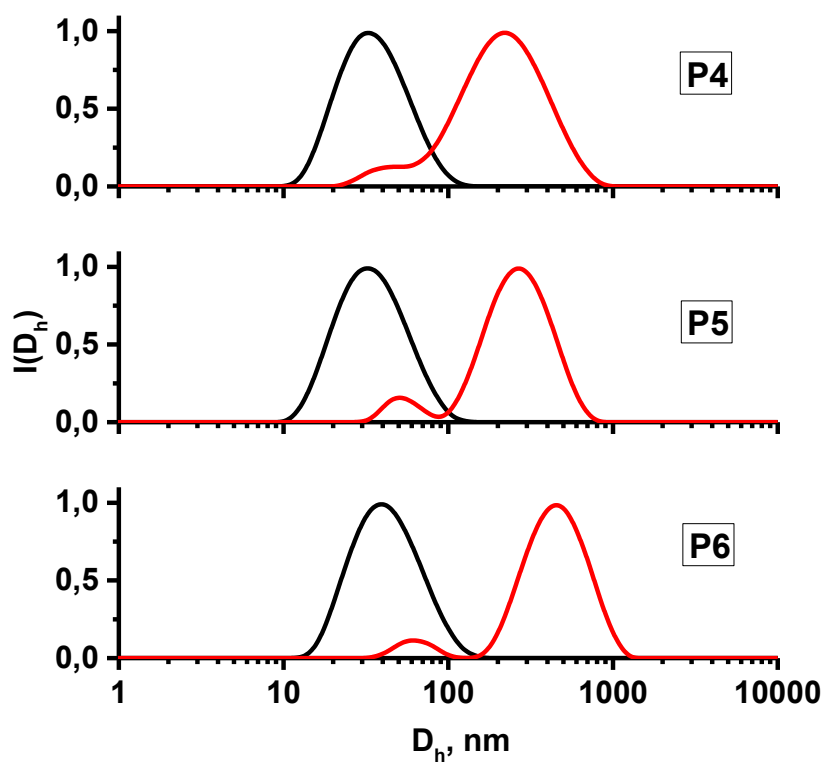
Figure S3. Distribution functions of D_h for 10 mg/ml triblock copolymers solutions in water prepared by solvent exchange method (black) and direct dissolving (red)
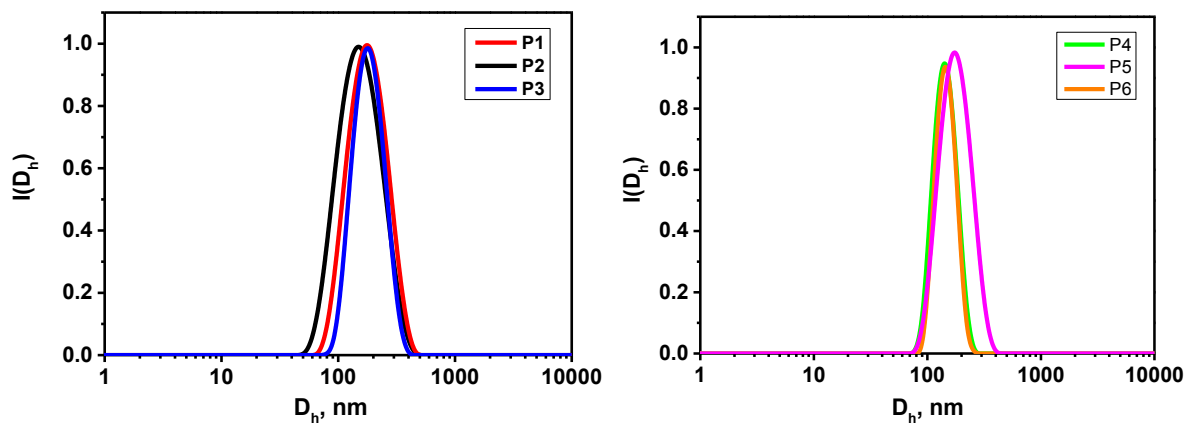

Figure S4. Distribution functions of D_h for 10 mg/ml polymer solutions in DMSO